Monitoring the Pulse Arrival Time Using Optical Fibre Sensors

Wan Suhaimizan Wan Zaki

Thesis submitted to the University of Nottingham for the degree of Doctor of Philosophy

JUNE 2020

Abstract

The plastic optical fibre (POF) is widely explored in various sensor applications. The non-toxic and biochemical inertness properties of the material make it safe to be applied on the human skin and hence opens up a wealth of wearable opportunities. To date, no one has investigated the combination of POFs and textile electrodes that are well suited to smart textile applications. Therefore, in this thesis, POFs were explored as an extrinsic sensor for the measurement of photoplethysmogram (PPG) on the human body. Further, a conductive textile electrode was utilized for Electrocardiogram (ECG) measurement. The ECG and the PPG signals were synchronized using a Nexus-10 MK II data acquisition device along with Matlab software for subsequent analysis.

In this study, the delay time between the ECG and PPG are calculated and denoted as pulse arrival time (PAT). The PAT is grouped into three categories which depend on the position of the PPG signal measured at the finger (PPTf), wrist (PATw) and underfoot (PATt). A relationship between mean PAT (15 beats) and instantaneous PAT (a single beat) with blood pressure (BP) was investigated on thirteen healthy male volunteers (aged between 17 to 42 years) through a pedal exercise. A linear regression model was applied to mean/instantaneous PAT-BP data and the absolute correlation coefficient, l*r*l was determined on each volunteer. The results show that the PAT is well correlated with systolic BP, especially for PATf (instantaneous and mean PAT), with 100% of volunteers achieving l*r*l > 0.5. For PAT and diastolic BP correlation, majority of volunteers achieving l*r*l < 0.5 for all categories, PATf, PATw and PATt (instantaneous and mean PAT).

Next, a new one-step calibration method and a pedal exercise calibration method were evaluated to estimate systolic BP during a tilt table experiment. The results show that the one-step calibration method at the finger show a marginally better correlation coefficient, (r = 0.65) compared to the pedal exercise calibration method (r = 0.45), when estimating systolic BP. Advantageously, the one-step calibration method is simple and time-saving because it only required one measurement of BP using a cuff-based BP monitor as a reference.

Lastly, a tubular cardiovascular phantom system was proposed and developed to simulate the PDT measurement in a controlled environment. The results of the phantom study showed a similar pattern to the PTT in human model, thus indicating that the system is able to simulate the PDT for sensor validation purposes.

Author’s published research papers

1. Wan Suhaimizan Wan Zaki, Ricardo Correia, Serhiy Korposh, Barrie R. Hayes-Gill, and Stephen P. Morgan. "Cuff-Less Continuous Blood Pressure Monitoring System Using Pulse Transit Time Techniques", International Journal of Integrated Engineering, volume 8, no. 1, (2016), pp. 51-57.

2. Wan Suhaimizan Wan Zaki, Ricardo Correia, Serhiy Korposh, Barrie R. Hayes-Gill, and Stephen P. Morgan. “Development of Tubular Cardiovascular Phantom System for Pulse Transit Time Simulation”, International Journal of Recent Technology and Engineering (IJRTE), volume 8, no. 2S2, (2019), pp. 291-296.

3. Wan Suhaimizan Wan Zaki, Ricardo Correia, Serhiy Korposh, Barrie R. Hayes-Gill, and Stephen P. Morgan. “Development of Wearable Optical-based Fibre Sensor System for Pulse Transit Time Measurement”. Proceeding of the 2nd International Conference on Applied Photonics and Electronics (InCAPE 2019), paper ID 20 (accepted manuscript).

Acknowledgement

First of all, I would like to express my sincere gratitude to all my supervisors, Professor Steve Morgan, Professor Barrie Hayes-Gill, Dr Serhiy Korposh, and Dr Ricardo Correia, for their encouragement and guidance. Their valuable support and advice were the greatest factor that enabled me to complete my research work and write this thesis. I would like to thank all my colleagues, especially the Optics and Photonics Research Group members for their useful advice and moral support throughout my time at the laboratory. I would also like to thank the Ministry of Higher Education Malaysia (MOHE) and Universiti Tun Hussein Onn Malaysia for the financial support during my studies at the University of Nottingham, UK. Last but not least, would like to thank my family for their love, constant advice and encouragement for me to succeed. Thanks to all of you.

Table of Contents

Abstract i

Author's published research papers iii

Acknowledgements iv

Table of Contents v

List of Figures ix

List of Tables xviii

List of Abbreviations xx

Chapter 1 Introduction 1

1.1 Project Background 1

1.2 Project Motivation and Objectives 6

1.3 Research Questions 8

1.4 Thesis Outline 9

Chapter 2 Literature Review 11

2.1 Introduction 11

2.2 Human Cardiovascular System 11

2.3 Blood Pressure 13

2.4 Blood Pressure Measurement 15

2.4.1 Auscultatory Method 16

2.4.2 Oscillometric Method 19

2.4.3 Tonometry Method 21
2.4.4 Volume Clamp Method 22
2.4.5 Pulse Arrival Time Method 24
2.5 Overview of Pulse Arrival Time (PAT) Measurement 27
2.5.1 PAT Measurement: ECG to PPG 29
2.5.2 PTT Measurement: PPG to PPG 35
2.5.3 PAT Measurement: BCG 36
2.5.4 PAT Measurement: Calibration Protocol 38
2.6 Optical Fibre Sensors (OFS) 43
2.6.1 OFS Measurement System 44
2.6.2 OFS for BP Measurement 45
2.6.3 Overview of Plastic Optical Fibre (POF) 48
2.7 Overview of Previous Cardiovascular Phantoms 49
2.8 Summary of PAT Measurement 51

Chapter 3 Design and Development of Wearable PAT Device 56
3.1 Introduction 56
3.2 Development of POF for PPG Measurement 58
3.2.1 Light Source: Green LEDs 61
3.2.2 Photodetector Module 63
3.2.3 PPG Amplifier Circuit 66
3.3 ECG Measurement 68
3.4 BP Measurement 70
3.4.1 Evaluated Ostar BP Monitor using NIBP Analyser 71

3.4.2 Ostar BP Waveform Measurement using Pressure Sensor 73
3.5 Nexus-10 Mark II Data Acquisition Device 74
3.6 MATLAB Software for Signal Analysis 81
3.6.1 Denoising and Filtering of ECG and PPG Signals 82
3.6.2 Signal Normalization 85
3.6.3 Thresholding and Peak Detection Algorithm 87
3.6.4 PAT Calculation 89
3.7 PAT Measurement System 91
3.8 Summary 92

Chapter 4 Development of Tubular Cardiovascular Pulse Delay Time Phantom System 93
4.1 Introduction 93
4.2 The Design of a Tubular Cardiovascular Phantom System 94
4.2.1 Water Pump 95
4.2.2 PendoTECH pressure sensor 96
4.2.3 Reservoir 1 106
4.2.4 One Way Valve 108
4.2.5 Flexible Silicone Tube 109
4.2.6 Resistance (Rotary valve) 112
4.2.7 Reservoir 2 114
4.3 Pulse Delay Time Phantom System – Experimental Set 114

4.4 Result and Discussion 119
4.4.1 Pulse Delay Time with Pump Voltage 119
4.4.2 Pulse Delay Time Measurement with Pulse Rate 123
4.4.3 Pulse Delay Time Measurement with Diastolic Basal Pressure 126
4.4.4 Pulse Delay Time Measurement with Pulse Pressure ... 129
4.5 Conclusion 133

Chapter 5 Verification and Validation of the Cuffless Blood Pressure Monitoring System 135
5.1 Introduction 135
5.2 Experimental Setup 136
5.2.1 Sensors Positions 137
5.2.2 Measurement on Volunteers 139
5.3 First Experiment: Pedal Exercise 141
5.3.1 Blood Pressure Cuff Waveform: Mean and Instantaneous PAT 145
5.3.2 PAT Measurement for Calibration Curve 148
5.3.3 The result on Pedal Exercise: Mean PAT 149
5.3.4 Mean and Instantaneous PAT 153
5.3.5 PAT-SBP Calibration Curve Based on Pedal Exercise .. 160
5.3.1 Comparison between instantaneous and mean PAT calibration equation on estimated SBP 165
5.4 Second Experiment: Tilt Table 170
5.4.1 One-Step Calibration Based on BP Cuff Oscillation Waveform 172

5.4.2 PAT Measurement on Tilt Table 178

5.4.3 Comparison between Exercise and BP Cuff Calibration on ESBP (Tilt Table) 183

5.5 Summary 189

Chapter 6 Conclusion and Future Work 191

6.1 Conclusion 191

6.2 Future Work 196

References 201

Appendices 231

List of Figures

Figure 2.1: The human circulatory system [37] 12

Figure 2.2: SBP and DBP determined based on K-Sound [68] 18

Figure 2.3: Estimation of SBP, MAP and DBP from the oscillometric cuff pressure waveform [73] 20

Figure 2.4: Tonometry method for recording the arterial pulse wave [79] 22

Figure 2.5: The working principle of the volume clamp method [59] 23

Figure 2.6: ECG and PPG waveforms for PAT measurement, I_H refers to the PPG peak, and I_L refers to PPG foot [84] 24

Figure 2.7: The illustration of light intensity measurement inside the tissues and the resulting PPG signal [90] 28

Figure 2.8: Illustration of Sotera Visi Mobile device attached to a patient [99] 32

Figure 2.9: Typical cross section of optical fibre [128] 43

Figure 2.10. A typical setup of an OFS system [132] 44

Figure 2.11: The operation of an FBG sensor [137] 46

Figure 3.1: System block diagram of wearable PAT device 56

Figure 3.2: (a) Illustration of POF probe with SMA connector (b) Photograph of POF PPG probe 58

Figure 3.3: (a) The position of POF PPG probe under the finger, (b) The illustration of the light out at the 45-degree tip of the transmitter and the receiver fibre 59

Figure 3.4: Polishing machine 60

Figure 3.5: LED attached to the heat sink. The size of the main components is stated in the figure 62

Figure 3.6: LED driver circuit 62

Figure 3.7: Phototransistor module for PPG measurement 64

Figure 3.8: Schematic of common collector phototransistor circuit..... 65

Figure 3.9: Schematic of PPG amplifier..... 67

Figure 3.10: PPG amplifier circuit with soldering components on the project board. The casing size is 6 cm x 10 cm (length x width)..... 68

Figure 3.11: (a) The surface electrode and fabric electrode for ECG measurement, (b) Wave of typical lead II ECG signal [173] 69

Figure 3.12: BP monitor (Ostar P2) 70

Figure 3.13: Measurement setup for NIBP analyser and BP monitor .. 71

Figure 3.14: Ostar BP monitor with a pressure sensor 73

Figure 3.15: a) Nexus device (NeXus 10 Mark-II) b) Front channel view with input channels as per show in Figure 3.1 75

Figure 3.16: ECG Measurement Cable (a) NX1-EXG2-snap cable (b) NX-EXG-Ref1-snap cable 78

Figure 3.17: Lemo connector (a) 6-pins, (b) 5-pins..... 78

Figure 3.18: Flow Chart of the algorithm to detect signal peaks and determine PAT..... 81

Figure 3.19: (a) Filtered and unfiltered (a) PPG signals 83

Figure 3.20: Normalization process (a) PPG signals 86

Figure 3.21: Thresholding and peak detection (a) PPG signals (b) ECG signals 88

Figure 3.22: A graphical representative of PAT (the delay time is calculated from the peak of R-wave ECG signal to the peak of PPG signal in one cardiac cycle) 90

Figure 3.23: PAT measurement system 91

Figure 4.1: Schematic of the designed pulse delay time tubular cardiovascular phantom system 95

Figure 4.2: The pump and the trigger control circuit 96

Figure 4.3: PendoTECH pressure sensor (PREPS-N-025); (a) Sensor attachment to the tube (b) Internal sensor illustration 97

Figure 4.4: Pressure sensor and difference amplifier circuit 99

Figure 4.5: Calibration setup for PendoTech pressure sensor 100

Figure 4.6: The response of PendoTech pressure sensor. Note that the error bars are smaller than the size of the symbols 101

Figure 4.7: The response of pulse pressure measured by the pressure sensor 1 (PS1) according to the setting (a) The duty cycle = 90%, (b) The duty cycle = 80% and (c) The duty cycle = 60% 103

Figure 4.8: (a) Pulse pressure signal when the duty cycle is set to 90%,(b) A typical PPG signal measured at the wrist 105

Figure 4.9: (a) The design of reservoir 1, (b) Illustration diagram of reservoir 1 107

Figure 4.10: (a) One-way valve (b) Schematic illustration of the internal structure of one-way valve. The valve size is 53 mm x 15 mm (length x width), and the valve is compatible with a tube of 4 mm inner diameter 108

Figure 4.11: Experiment Setup for tube flexibility measurement 109

Figure 4.12: Image of a flexible tube filled with water (a) Initial tube condition (b) Region of interest for tube expansion calculation between the upper line (UL) and lower line (LL). d1, d2 d3 are the distances between UL and LL at specific positions to calculate tube's diameter110

Figure 4.13: Flexible tube expansion measurement with static water pressure for two different wall thicknesses (WT). The error bar represents the standard deviation at three different tube positions while converting the mean number of pixels to the distance 111

Figure 4.14: (a) Rotary valve deployed in Figure 4.1; (b) Illustration of the internal structure of the rotary valve. The dimension of the rotary valve is 54.4 mm x 26.5 mm x 36.3 mm (length x width x height) and the diameter of the port connection (both side) is 6 mm. The diameter for the nozzle is 1 mm..... 113

Figure 4.15: Reservoir 2 with inflation bulb connected at the top. The size of reservoir 2 is 10 x 10 x 10 cm (length x width x height) 114

Figure 4.16: Photograph of the tubular cardiovascular pulse delay time phantom system. PS1 and PS2 are the pressure sensor 1 and pressure sensor 2, FT1 and FT2 are the flexible tube 1 and flexible tube 2, Re1 and Re2 are reservoir 1 and reservoir 2, MC is a microcontroller and RV is a rotary valve 115

Figure 4.17: (a) The position of POF probe for optical pulse measurement, (b) Illustration of the POF under the flexible tube. The two fibres in

between the transmitters were the receivers, with the gap between each fibre was 1 mm 116

Figure 4.18: Block diagram of pulse measurement on a tubular cardiovascular phantom system 117

Figure 4.19: Typical pressure sensor signals (PS1 and PS2 top trace) and resulting plastic optical fibre sensors (POF1 and POF2 lower trace) when the diaphragm pump power supply was set at 6V, the pulse rate was set at 60 pulses/minute and the water level inside reservoir 1 was set at 25 ml 120

Figure 4.20: Pulse delay time measurement (mean ± SD of 15 pulses) between PS1 and PS2 as well as POF1 to POF2 for varying pump supplied voltage from 6 V to 12 V. The pulse rate was set at 60 pulses/minute and the water level inside reservoir one was set at 25 ml 121

Figure 4.21: Pulse waveform measured by both PS (upper trace) and POF (lower trace) when the pump power supply was set at 10 V and the pulse rate was set at 160 pulses/minute 124

Figure 4.22: The pulse delay time (mean ± SD of 15 pulses) with increasing pulse rate with the pump power supply set at 10 V 125

Figure 4.23: Pulse measurement with two different PS2 basal pressures with the pump power supply set at 10 V and the pulse rate was set at 60 pulse/min 128

Figure 4.24: The pulse delay time (mean ± SD of 15 pulses) with the PS2 basal pressure. The pump power supply set at 10 V and the pulse rate was set at 60 pulse/min 129

Figure 4.25: Typical pressure sensor signals (PS1 and PS2 top trace) and resulting plastic optical fibre sensors (POF1 and POF2 lower trace)

when the pump power supply was set at 10 V, pulse rate set at 60 pulse/min and water level at reservoir 1 set to 60 ml 130

Figure 4.26: Pulse delay time measurement on PS and POF (mean ± SD of 15 pulses) with an increase of pulse pressure at PS2 with the power supply set at 10 V and pulse rate set at 60 pulse/min 132

Figure 5.1: Sensor placement on the volunteer. ECG surface electrodes and ECG fabric electrodes on the chest, POF on the wrist (right arm) and underfoot (right leg), Blood Volume Pulse sensor on the index finger (right arm) and Ostar BP on the left arm..... 137

Figure 5.2: The position of PPG sensors; (a) at the index finger (Blood Volume Pulse (BVP) sensor, NX-BVP1A, (b) at the wrist (POF), and (c) under the foot (POF)..... 138

Figure 5.3: Experimental setup for pedal exercise (a) Exercise bike, Domyos VM740, (b) Setting programmed for the exercise work rate level and (c) Volunteer position on an exercise bike for PAT and BP measurement..... 142

Figure 5.4: Test protocol for the pedal exercise using exercise bike (Domyos VM740)..... 143

Figure 5.5: A measurement setup to measure the pressure inside the BP cuff..... 144

Figure 5.6: BP cuff pressure waveform for volunteer 1 (Volunteer code: 1001) 146

Figure 5.7: Instantaneous PAT measurement for SBP (PATsys) and DBP (PATdia). The black trace represents the deflation of the BP curve (BP Cuff), the blue trace represents the ECG measured using surface electrode (ECG Nex) and the red trace represents the PPG on the fingertip measured by the BVP sensor (PPG Nex) 147

Figure 5.8: PAT measurement according to the spatial position of the PPG signal measured; (a) at the finger, (b) at the wrist and (c) under the foot 148

Figure 5.9: The relationship between (a) PAT and SBP (b) PAT and DBP measurement. The PPGs signals were measured at a finger (red trace), wrist (blue trace) and underfoot (black trace) on volunteer 1 (volunteer code: 1001). The PATs data is plotted based on the mean ± SD of 15 pulses of PPG signals 150

Figure 5.10: Mean PAT and instantaneous (Ins.) PAT measured at different spatial positions (a) PATf (finger), (b) PATw (wrist), and (c) PATt (underfoot) 154

Figure 5.11: Exercise calibration curve at the finger (PATf-SBP) and at the wrist (PATw-SBP). The PATf (red marker) and PATw (blue marker) is plotted based on mean ± SD of 15 pulses 161

Figure 5.12: The distribution of (a) gradient (m) and (b) Y-intercept for calibration equation in Table 5.5 and Table 5.6. Mean Finger and Mean_Wrist represents the calibration equation for mean PAT-SBP at finger and wrist respectively. Ins_Finger and Ins_Wrist represents the calibration equation for instantaneous PAT-SBP at finger and wrist respectively 164

Figure 5.13: The estimated systolic blood pressure (ESBP) based on mean PAT (blue marker) and instantaneous PAT (red marker) (a) at the finger and (b) at the wrist. The R-squared value for ESBP-SBP at finger is higher than R-squared ESBP-SBP at wrist indicated that the strong relationship between ESBP-SBP at the finger compared to the wrist 166

Figure 5.14: The Bland-Altman plot for ESBP using calibration equation (a) at the finger and (b) at the wrist..... 169

Figure 5.15: Experiment setup for tilt table (a) Volunteer on the tilt table in the supine position (0°), (b) Illustration of a volunteer on tilt table moving from supine position to tilt-up position (0° to 70°)..... 171

Figure 5.16: PATcuff measurement on volunteer 1 (Vol1, volunteer code: 1001). The ECG signals are represented in red (ECG Nex) and the BP cuff oscillation during deflation are represented in blue (BP Cuff) 173

Figure 5.17: PAT and BP cuff pressure response on three volunteers (Vol1, Vol2 and Vol3)..... 174

Figure 5.18: A calibration curve on volunteer 1 (Vol1) based on PATcuff–cuff pressure relation (blue trace). One-step calibration curve for PATf (red trace) and PATw (black trace) obtained by shifting the PATcuff regression line (blue trace) to the PATf position (red marker) and to the PATw position (black marker) respectively..... 175

Figure 5.19: PAT measurement during the tilt table experiment on eleven volunteers. The y-axis on the left side refers to PAT measurement, and the x-axis refers to the tilt table position with the number 1,2, and 3 refers to supine position, 4,5 and 6 refers to tilt-up position (70° degree) and 7,8, and 9 refers to tilt-down (supine) position. (a) The PATf refers to the delay time between ECG to PPG at the finger, (b) The PATw refers to the delay time between ECG to PPG on the wrist, and (c) The PATt refers to the delay time between ECG to PPG underfoot 180

Figure 5.20: (a) The SBP measurement and (b) The DBP measurement recorded on eleven volunteers according to the tilt table position; 1,2, and 3 refers to supine position, 4,5 and 6 refers to tilt-up position (70° degree) and 7,8, and 9 refers to tilt-down (supine) position..... 182

Figure 5.21: The correlation of ESBP with SBP during the tilt table experiment based on PAT measurement (a) at the finger (PATf) and (b) at the wrist (PATw). The ESBP calculated based on exercise calibration

equation (ExerCal. PAT, blue marker) and one-step calibration equation (OneCal. PAT, red marker)..... 184

Figure 5.22: Bland-Altman plot for ESBP and SBP with PAT measurement (a) at the finger and (b) at the wrist. The ESBP calculated based on pedal exercise calibration equation (ExerCal. PAT, blue marker) and one-step calibration equation (OneCal. PAT, red marker)..... 187

List of Tables

Table 2.1: Classification of BP level according to ESH/ESC [51] 15

Table 2.2: Summary of the relevant research study for PAT measurement for cuff-less BP 40

Table 3.1: Electrical characteristic of green LED 61

Table 3.2: Electrical characteristic of phototransistor (TEMT 6000) 64

Table 3.3: Ostar BP monitor specification 70

Table 3.4: Validation result on Ostar BP monitor 72

Table 3.5: Bipolar channel specification 76

Table 3.6: Auxiliary channel specification 77

Table 3.7: List of input channels 80

Table 4.1: Pressure sensor (PendoTECH, PREPS-N-025) specifications 98

Table 4.2: The pulse timing specification 102

Table 4.3. The high-speed camera Optronis CL600x2 specification . 110

Table 4.4: The pulse waveform data obtained using pressure sensors PS1 and PS2 in the tubular phantom. 122

Table 4.5: Pulse rate setting parameters 123

Table 4.6: Pulse delay time measurement with increased of PS2 basal pressure 127

Table 4.7: Pulse amplitude measurement by PS by varying reservoir 1 water level 131

Table 5.1: Volunteers physical information 140

Table 5.2: Absolute correlation coefficient (Irl) of mean and instantaneous PAT for (a) SBP and (b) DBP. The Irl values less than 0.5 are written in red colour and the number is highlighted with a yellow colour if Irl for the instantaneous PAT is greater than Irl for the mean PAT 156

Table 5.3: Absolute correlation coefficient (Irl) of mean and instantaneous PAT for DBP. The Irl < 0.5 is labelled red whilst yellow indicates instantaneous PAT “Irl” is more correlated than the mean PAT 157

Table 5.4: The numbers of data Irl > 0.5 and Irl < 0.5 in PAT-SBP and PAT-DBP for proportions Z-test 159

Table 5.5: Calibration equation on each volunteer based on mean PAT with SBP. Y represents the PAT and X represents blood pressure in mmHg 162

Table 5.6: Calibration equation on each volunteer based on instantaneous (Ins.) PAT with SBP. Y represents the PAT and X represents blood pressure in mmHg 163

Table 5.7: Correlation coefficient, r and RMSE for mean and instantaneous PAT at finger and wrist 167

Table 5.8: One-step calibration equation for all volunteers based on PATf-SBP and PATw-SBP with y1 is PATf, y2 is PATw and x1 is SBP 178

Table 5.9: Coefficient correlation, r and RMSE for ESBP-SBP relationship 185

List of Abbreviations

AAMI	American Association for the Advancement of Medical Instrumentation
ABPM	Ambulatory Blood Pressure Monitor
AC	Alternating Current
ADC	Analogue to Digital Converter
ATP	Adenosine Triphosphate
BCG	Ballistocardiography
BP	Blood Pressure
BPM	Beats Per Minute
BVP	Blood Volume Pulse
Ch	Channel
cm	Centimetre
CO	Cardiac Output
Co	Compliance
CuffCal	One-Step Calibration
CWT	Continuous Wavelet Transform
d	distance
DBP	Diastolic Blood Pressure
DC	Direct Current

DuCy	Duty Cycle
ECG	Electrocardiogram
ECG Fab	ECG Fabric
ECG Nex	ECG Nexus
ECGfe	Conductive Fabric Electrode
ECGs	ECG Surface Electrode
EEG	Electroencephalogram
EMG	Electromyography
ESBP	Estimated Systolic Blood Pressure
ESC	European Society of Cardiology
ESH	European Society of Hypertension
ExerCal	Exercise Calibration
FBG	Fibre Bragg Grating
FT	Flexible Tube
H_0	Null Hypothesis
HR	Heart Rate
I_b	Base Current
I_c	Collector Current
ID	Internal Diameter
Ins	Instantaneous

IoT	Internet of Things
Kg	Kilogram
k-sound	Korotkoff Sound
LED	Light-Emitting Diode
LL	Lower Line
lx	Lux
m	Metre
MAA	Maximum Amplitude Algorithm
MAE	Mean Absolute Error
MAP	Mean Arterial Pressure
MEMS	Micro-Electromechanical System
MIMIC	Multi-Parameter Intelligent Monitoring For Intensive Care
ml	Millilitres
mmHg	Millimetres of Mercury
MOHE	Ministry of Higher Education Malaysia
ms	Millisecond
NO	Normally Open
OCD	Obsessive-Compulsive Disorder
OH	Orthostatic Hypotension
PEP	Pre-Ejection Period

PLSR	Partial Least Squares Regression
PMMA	Poly-Methyl-Methacrylate
POF	Plastic Optical Fibre
PPG	Photoplethysmogram
PPGNex	Photoplethysmogram Nexus
PS	Pressure Sensor
PAT	Pulse Arrival Time
PATcuff	Pulse Arrival Time Cuff
PATdia	Pulse Arrival Time Diastolic
PATf	Pulse Arrival Time Finger
PATsys	Pulse Arrival Time Systolic
PATt	Pulse Arrival Time Underfoot
PATw	Pulse Arrival Time Wrist
PDT	Pulse Delay Time
PTT	Pulse Transit Time
PWV	Pulse Wave Velocity
R	Resistance
Re	Reservoir
RV	Rotary Valve
s	Second

SBP	Systolic Blood Pressure
SD	Standard Deviation
SMA	Subminiature Assembly
SpO_2	Oxygen Saturation
SV	Stroke Volume
TH	Thresholding
UL	Upper Line
USB	Universal Serial Bus
V	Voltage
V_{out}	Voltage output
Vol1, Vol2, Vol3	Volunteer 1, Volunteer 2, Volunteer 3
WBSN	Wireless Body Sensor Network
WT	Wall Thickness

Chapter 1 Introduction

1.1 Project Background

Hypertension is a major public health issue, especially in developing countries [1] and known as a “silent killer” because it has no symptoms [2]. According to the World Health Organization’s report in 2013, approximately 17 million deaths per year occur due to cardiovascular disease, out of which complications of hypertension accounts for 9.4 million deaths [3]. The report stated that the number of people with hypertension is increasing in low and middle income countries due to the weakness of their health system in terms of hypertension awareness, treatment, and control.

Untreated hypertension can potentially cause serious and fatal diseases such as heart attack, stroke and renal failure [4]. High blood pressure puts additional strain on blood vessels and can lead to atherosclerosis of the artery walls that can cause a heart attack and a stroke. Damage to blood vessels and filters in the kidney results in less blood travelling to the kidney, and the process of removing waste from the body thereby becomes more difficult.

Generally, high blood pressure falls into the category of hypertension when the systolic blood pressure (BP) is greater than 140 millimetres of mercury (mmHg), and the diastolic BP is greater than 90 mmHg. Hypertension screening is performed by monitoring blood pressure over 24 hours periods using an Ambulatory Blood Pressure Monitor (ABPM) over typically seven days, usually during activities of daily life. This method reduces the number of misdiagnoses of hypertension by

mitigating the white-coat effect [5]. The white-coat effect refers to higher blood pressure readings being obtained by being taken in a clinical setting when compared to those registered at home or other natural environments [6]. This effect is a result of stress and anxiety brought about by visiting the doctor or a hospital setting. An individual with white coat hypertension can be identified by recording multiple BP measurements away from the medical environment using an ABPM.

An ABPM is a small digital blood pressure device that is wearable with a cuff is connected on the upper arm. It operates by inflating the cuff to a certain pressure to temporary block the blood flow through the arteries. Pressure sensors connected to the cuff monitor the pressure changes and allow blood pressure to be measured using an oscillometric technique. The cuff pressure is then slowly released, and the systolic pressure and diastolic pressure are determined according to the algorithm built into the measuring device. The cycle is repeated and the results are stored in the device to be analysed by the doctor, who observes the variability of the blood pressure throughout the day.

Generally, the ABPM is sold with an individual software package for the visualization of blood pressure versus time during day and night time. At least 85 % of BP measurement during 24 h recording should be available in order to have reliable analysis in diagnosing hypertension [5]. The patient is required to stay still and take note of any activity before the BP recorded by the ABPM. The BP reading may not be accurate during exercise, movement, or driving or when the cardiac rhythm is irregular. Through 24 hours of BP recording, a medical practitioner is able to evaluate BP for patient’s health assessment. The American Heart Association Council on High Blood Pressure Research recommended that the mean normal daytime ABPM reading is less than 135/80 mmHg, and the mean normal night time is less than 120/70 mmHg [7]. In addition, the BP recorded during night time provides information on the dipping

pattern of BP. BP falling by <10% during night time is defined as non-dipping, and this is associated with increased risk of stroke, end-organ damage, congestive heart failure and cardiac death[5]. Moreover, morning BP surge can be evaluated based on the data recorded by the ABPM. The morning surge can be calculated based on the difference in BP recorded 2 hours after rising with the mean of BP during sleep. The normal BP surge reported is in the range of 14 mmHg to 30 mmHg for systolic BP and 12 mmHg to 23 mmHg for diastolic BP in a hypertensive patient [8]. Excessive morning BP surge is a cardiovascular risk [9].

A patient wearing an ABPM may feel uncomfortable because they need to wear it for a long time and may feel distracted, especially when the device starts to inflate the cuff tightens around the arm [10]. They may get anxious because of the noise of its pump and possibly feeling pain when the cuff squeezes the arm for a BP measurement. Consequently, these physiological conditions may affect BP measurement. Furthermore, the cuff-based blood pressure device only provides intermittent BP values and cannot perform continuous measurements [11]. Patients with haemodynamic instability or who are undergoing high-risk surgeries are recommended to have their BP continuously monitored [12]. In practice, an intra-arterial catheter is used to monitor continuous BP, but this method accrues a distinct disadvantage due to its invasive nature [13]. Patients with an arterial catheter device may experience complications such as bleeding, haematoma, thrombosis and the formation of pseudo aneurysms [14].

A substantial effort has been made by researchers towards developing a non-invasive, continuous and cuff-less BP monitor [15]–[17]. One of the most promising methods for cuff-less continuous BP monitoring is based on the pulse arrival time (PAT) technique. PAT is a delay time between two physiological signals related to the blood flow, namely the Electrocardiogram (ECG) and Photoplethysmogram (PPG) [18] and is

inversely related to BP [19]. The estimation of BP based on PAT values can be obtained by using linear or non-linear regression model. A linear model is derived according to Moens-Kortweg's equation by assuming there is a negligible change in the arterial thickness and diameter with pressure variations, thus the BP and the PAT can be linearly related [20]. Some researchers considered the nonlinearity of the elastic property of the vascular wall and established non-linear models to evaluate the relationship between PAT and BP [21]. A study by Wibmer et al. shows that there are slightly better limits of agreements on the Bland-Altman plots of systolic BP for the non-linear model (–10.9 mmHg to 10.9 mmHg) than for the linear model (−13.2 mmHg to 13.1 mmHg) [22]. However, the results of the linear regression model produced a significant, strong negative correlation (r) between PAT and SBP in all of the volunteers ($r^2 >$ 0.85).

Typically, the ECG signal is acquired on the chest and the PPG signal detected at the finger for pulse arrival time [23]–[26]. This arrangement has received great attention due to ready availability of the measurement devices and the possibility of minimising error in the time domain due to the relatively large distance between the heart and the finger. Furthermore, these two signals are often simultaneously recorded by patient monitors in the hospital and can be accessed through a patient's database system for PAT analysis [27].

A wide variety of studies have been conducted to improve the correlation between PAT and BP in terms of signal processing, calibration and improved sensing mechanisms. The mechanism in PAT measurement is simple thus it gained popularity for wearable monitoring purposes. There are several commercial PAT devices available on the market, such as Sotera ViSi Mobile and Somnotouch-NIBP [15]. Both devices calculate PAT based on the delay time between ECG on the chest and PPG on the finger. Although these devices have shown promise, there is still

room for improvement in terms of the flexibility and wearability of the device. A high degree of flexibility would mean that the device is easy to handle, and a high degree of wearability would mean that the device is comfortable to wear and does not restrict daily activities for the wearer.

Recent years have seen rapid development in flexible and wearable sensing devices, especially those with healthcare and biomedical applications. One of the attractive sensing platforms is a plastic optical fibre (POF). The POF is superior to standard electronic sensors in terms of flexibility, robustness and immunity to electromagnetic fields [28]. The sensing mechanism for the POF can be divided into two categories: intrinsic and extrinsic sensors. The intrinsic sensor refers to the fibre optic constituting the sensing element itself whilst an extrinsic sensor refers to fibre optics deployed as a medium to transport light. In this research, the POF will be explored as an extrinsic sensor for measuring PPG on the human body. Furthermore, a wearable PAT device has been developed based on a conductive textile ECG electrode and a POF. The performance of the developed device for detecting PAT will be evaluated and compared with a commercial BP device.

The novelty of the developed system lies in the miniaturization of the POF system for PPG measurement. The system consists of a light-emitting diode (LED) as a light source and photodetector circuit for the detection system. The flexibility of POFs makes it suitable to be embedded into textiles, thus enhancing the comfort and mobility for a user wearing the sensor for a long period. In order to realize a wearable textile based PAT measurement, the ECG signal was acquired by using a conductive fabric electrode.

The second novelty of the system is on the interfacing technique applied for PAT measurement. The NeXus-10 device was explored to acquire a signal from the ECG fabric electrode and POF simultaneously. The

BioTrace+ software from MindMedia (Nexus) was programmed to record beat to beat ECG and PPG signals from the developed and commercial sensors. In addition, an oscillometric blood pressure waveform was recorded by the external pressure sensor for calibration process of PAT with BP. The multiple input configuration of the NeXus-10 device allows the system to perform simultaneous PAT measurement between the developed sensor and a commercial sensor for benchmarking purposes.

Lastly, the novelty of this research is the development of a tubular cardiovascular phantom system for evaluation of the POF in pulse measurements. The system was developed with cost-effective components and is able to simulate pulse delay time (PDT) measurements. Furthermore, the system is able to generate low perfusion pulses that mimic the BP of newborn, making it very useful in PPG sensor evaluation.

1.2 Project Motivation and Objectives

Contemporary advances in sensor technology have led to increased interest in wearable device applications. A wearable device refers to a device that is attached to a body part for tracking a user's vital signs or gathering data related to health. Textile based wearable sensors enable monitoring of physiological parameters, such as ECG [29], EMG [30] and body movement [31] in a natural setting. Additionally, devices that incorporate thermocouples into fabrics can be used for sensing temperature [32], and likewise when coupled with a light source could be used for heart rate and SpO_2 measurement [33]. The aim of this research is to integrate conductive fabrics and POF sensors into textiles for cuff-less continuous BP monitoring, based on PAT measurement. Conductive fabrics will be used as an ECG electrode, and the POF will be used as a

medium to transfer and receive light from the skin for PPG detection. There are five objectives that need to be accomplished in order to fulfil the aim of the proposed research:

1. To measure multichannel PPG signals using the POF and acquire the ECG signal using a conductive fabric electrode. The PPGs will be measured at two different parts of the body; on the wrist and under the foot. The POF has been chosen as a sensor platform because of its ability to withstand a robust environment (underfoot). The ECG signals will be measured on the chest. Both of the sensors can be attached to a fabric for wearable purposes.

2. To develop an interfacing system for transferring the ECG and PPG signals simultaneously to a computer using a NeXus-10 Mark II data acquisition system.

3. To develop a Matlab script for the determination and analysis of PAT measurements. The delay times between the ECG and PPG signals will be computed and correlated with an oscillometric BP measurement.

4. To develop a tubular cardiovascular phantom system to verify the performance of sensors for pulse delay time measurement.

5. To conduct experiments on volunteers for evaluating the performance of the developed device for estimating systolic blood pressure (SBP).

1.3 Research Questions

The main contribution of this thesis is the development of a wearable PAT measurement device comprised of a conductive fabric based ECG electrode for ECG measurement and POF for PPG measurement. The device will be tested, and the results will be analysed to answer each of the following research questions:

1. **How can the reflected light be transferred and collected to/from the skin through a POF for PPG measurement?** In this research, the diameter size of the POF is 500µm. At this size, it will be a significant challenge to couple the LED light efficiently into the fibre. Furthermore, the reflected light that is transferred to the photodiode is also limited by the fibre diameter. Therefore, the design of the POF sensor will be investigated for PPG detection.

2. **How will the sensors' performance be validated for pulse delay time measurement?** The pulse transit time (PTT) is defined as a delay time between two pulse signals for one cardiac cycle. In the human body, the delay time between two PPG pulses varies due to variability in blood pressure making it difficult to verify the performance of a POF sensor on the human body. A proposed solution is to develop a phantom system that can vary pressure and the pulse delay time. The phantom acts as a simulator and the performance of the POF sensors will be evaluated in this setting.

3. **How should benchmarks be applied for comparing a developed wearable PAT device against standard devices?** The most common way to measure BP is by using an oscillometric BP monitor. As we shall see the BP device needs at least 30 seconds to estimate a value of both systolic and diastolic BP. Alternatively, the PAT

measurement gives beat-to-beat readings, which will give potentially a slightly different BP measurement every beat due to the natural variability in BP. Therefore, the correlation of mean PAT with corresponding BP – measured using the Ostar BP monitor – will be investigated and compared with the instantaneous PAT. The performance of the developed sensors will be compared to the commercial sensors (Nexus-10 Mark II device).

4. **How can an individual's calibration curve for estimating BP be determined?** A stand-alone PAT device is able to estimate BP by referring to the individual calibration curve. Mostly, a calibration curve is obtained by varying the BP and PAT through exercise. In reality, this method is not practical and an alternative method should be considered for estimating BP. In this research, a one-step calibration method to estimate SBP will be proposed based on the delay time between the peak of ECG and the peak of BP cuff oscillation waveforms. A comparison will be made between the two calibration methods (pedal exercise and one-step) and the results will be presented in terms of accuracy in estimating the SBP.

1.4 Thesis Outline

This thesis is divided into 6 chapters as follows:

Chapter 1 provides a brief description of the project's background, aim, motivation, as well as stating the objectives and the research question to be addressed in this work.

Chapter 2 provides relevant background regarding the blood pressure devices and principles of blood pressure measurement. This chapter also

covers the basic principles of operation of the ECG and the PPG measurement. A comprehensive review of PAT techniques will be presented and the gaps in research for this area are outlined.

Chapter 3 elaborates on the research methodology of the development of a wearable PAT measurement device using a conductive ECG electrode and the POF. The electronic design and the data acquisition unit deployed in this thesis will be explained in detail. At the end of the chapter, a brief description of the software used to record and analyse the signal is provided.

Chapter 4 elaborates on the successful development of a phantom system for pulse delay time measurement. The materials and methods used to create the pulsatile waveform is described. The result and analysis of the pressure and the pulse delay time will also be presented.

Chapter 5 covers the details of the experimental setup and protocol used for the healthy volunteer study. The results from this study are analysed, and comparison made between the developed sensors and commercial sensors in terms of PAT accuracy in estimating BP.

Chapter 6 will cover the final discussion and conclusion for this work and will describe the further work that is proposed for other workers to follow.

Chapter 2 Literature Review

2.1 Introduction

In this chapter, the physiology of the cardiovascular system is described to provide a better understanding of how the human body functions in regulating blood pressure (BP). The principles of non-invasive BP measurement are also explained. A detailed discussion on Pulse Arrival Time techniques for BP measurement is presented. The gaps in the development of cuffless BP measurement are highlighted, and a proposed system is briefly described.

2.2 Human Cardiovascular System

The function of the human circulatory system is to deliver nutrients and oxygen to all cells in the body and to remove waste products from tissue cells. This process is vital to the body to maintain cellular function in order to produce Adenosine Triphosphate (ATP) molecules as an energy source. In addition, the circulatory system helps the body to maintain and balance its internal condition such as temperature and pH by a homeostatic mechanism. Figure 2.1 shows the diagram of the circulatory system with the oxygenated blood shown in red and deoxygenated blood in blue.

The circulatory system consists of the heart and blood vessels. The muscular organ of the heart consists of two atria and two ventricles [34]. The right atrium receives deoxygenated blood from the vena cava and transports it to the right ventricle. The right ventricle pumps the

deoxygenated blood to the lungs. In the lungs, the blood flows through the capillaries to release carbon dioxide and collects oxygen during respiration. The oxygenated blood returns to the left side of the heart from the lungs via the pulmonary veins. The blood flows to the left atrium and then enters the left ventricle. The left ventricle then ejects the oxygenated blood into the arterial system through the aorta. The circulation of deoxygenated blood from the heart to the lungs and returns of oxygenated blood to the heart is called "*pulmonary circulation*" [35].

The oxygenated blood from the aorta travels to the upper and lower body. Through the upper body path, the aorta leads the blood to the arms via subclavian arteries and to the head via the carotid artery. For the lower body path, the aorta leads the blood to the liver via the hepatic artery, to the small intestine via the mesenteric arteries, to the kidney via the renal arteries and to the legs via the iliac arteries [36].

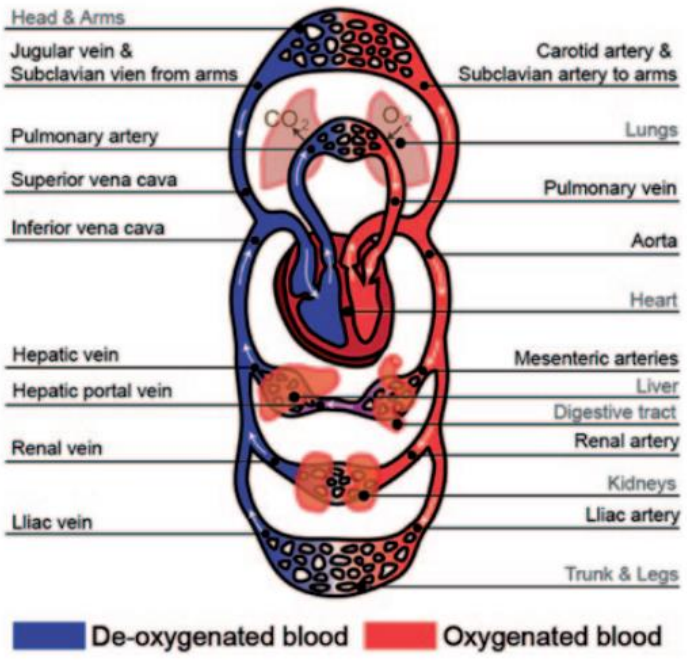


Figure 2.1: The human circulatory system [37]

The blood flows from the arteries to the veins through the capillaries. In the capillaries network, the blood releases oxygen, nutrients and other important substances and takes on carbon dioxide and waste substances through the diffusion process. The deoxygenated blood is collected by the veins and is then returned to the right side of the heart. The circulation of oxygenated blood that is moving away from the heart to the body and returning deoxygenated blood to the heart is called *"systemic circulation"*.

2.3 Blood Pressure

The heart pumps oxygenated blood to the organs and tissues in the human body via the arteries. In the arteries, the hydrostatic pressure near the heart is very high compared to the pressure at the arterioles (small arteries) [38]. This allows the blood to move from areas of high to low hydrostatic pressure. As the blood moves and builds up in volume, it pushes against the sides of the blood vessels. The strength of this pushing is called BP [39] and the average pressure throughout the cardiac cycle called mean arterial pressure (MAP) [40]. The unit of BP is generally stated in millimetres of mercury (mmHg). There are two main parameters associated with the BP and these are the systolic pressure and the diastolic pressure. Systolic pressure is defined as the peak pressure in the arteries during the cardiac cycle, and the diastolic pressure is the lowest pressure at the resting phase of the cardiac cycle [34]. A normal healthy adult BP reading is typically 120/80 mmHg, where 120 mmHg refers to the systole and an 80 mmHg for the diastole [41].

The BP has an ultra-short-term, short term variation and a long term variation. Ultra-short-term refers to beat-to-beat variability, and it is affected by neurohormonal factors like baroreceptor reflex and

sympathetic outflow [42]. Olbers et al. invasively measured and quantified beat-to-beat BP variability in patients with sinus rhythm and reported that the mean systolic and diastolic BP variability (15 beats) at the brachial artery was 2.4 mmHg and 1.1 mmHg respectively [43]. Short term variation refers to the BP change over 24 hours due to the day-night changes and the variability of heart rate throughout the day. This BP variation changes in response to physical activity, sleep, emotional stimuli, and influences of baroreflex [44]. The Baroreflex is responsible to stabilize BP through a feedback regulation mechanism to the autonomous nervous system (ANS) [45]. As an example, the baroreceptors sense the BP changes (increase) and this causes a signal to be sent to the ANS to reduce heart rate in order to stabilize the BP

A study conducted by Mancia et al. demonstrated that the variability of blood pressure is significantly in patients with hypertension than in healthy people [46]. They reported that the 24-hour mean SBP was 112.9 ± 2.1 mmHg in the normotensive and 159.4 ± 5.7 mmHg in the hypertensive group. For the long term variation, the variations of BP are over a much longer period such as days, months and seasons and is also due to age-related changes in arterial and arteriolar stiffness [47]. As the age increases, the wall of large conduit arteries, especially aorta, thicken and lose elasticity results in an increase in systolic BP [48]. Also, an individual's BP shows changes over time due to a change in diet, reduction in exercise and an increase in stress levels [47].

The body regulates BP in response to the cardiac output (CO). Cardiac output is defined as the "*volume of blood pumped by the heart per minute*" [49]. It can be calculated by multiplying the stroke volume (SV) measured in millilitres (ml) with the heart rate (HR) in beats per minute (BPM) [50]. During exercise, the increased heart rate will increase the cardiac output, thus changing the BP. The classification of BP level according to the European Society of Hypertension (ESH) and of the European Society of

Cardiology (ESC) for adults aged 18 or older is shown in Table 2.1 [51]. The Normal BP readings are between 120 mmHg to 129 mmHg for systolic and 80 mmHg to 84 mmHg for diastolic BP. The hypertension category, also known as high BP, occurs when the systolic reading is greater than 140 mmHg and the diastolic is greater than 90 mmHg.

Table 2.1: Classification of BP level according to ESH/ESC [51]

Category	**Systolic BP (mmHg)**	**Diastolic BP (mmHg)**
Hypotension	<90	<60
Optimal	<120	<80
Normal	120 - 129	80 - 84
High Normal	130 - 139	85 - 89
Grade I Hypertension	140 - 159	90 - 99
Grade II Hypertension	160 - 179	100 - 109
Grade III Hypertension	>180	>110

2.4 Blood Pressure Measurement

The BP can be measured by a direct or an indirect method. The direct method measures BP continuously and accurately [52], but it is a complex technique and requires trained medical staff to perform this procedure. This technique directly measures arterial pressure by placing a cannula needle into an artery. The cannula is connected to a fluid-filled system which is connected to a patient monitor for monitoring the BP on a beat to beat basis [53]. This technique is commonly used in intensive care units and operating theatres for intra-arterial BP monitoring [54]. The major drawback from this technique is that it is invasive and has potential risks to patients such as infection, site bleeding, arterial obstruction and distal limb ischemia [55]. Alternatively, indirect and non-invasive BP

monitoring has fewer risks and is less painful for the patient [56], and the measurement setup is much easier and quicker than the direct method. In the indirect method, a BP measurement can be performed by using a device equipped with a cuff or without a cuff. This method is also known as a non-invasive measurement because no contact is made with the blood. A non-invasive BP measurement can be classified according to its ability to measure BP intermittently or continuously [57]. Generally, intermittent BP measurement is performed by auscultatory or oscillometry methods with an interval of 3–5 min. Continuous BP is measured beat to beat and can be monitored by arterial tonometry [58] and the volume clamp method [59].

2.4.1 Auscultatory Method

In the auscultatory method, a cuff is placed on the upper arm, and a stethoscope is used to listen to the blood flow through the brachial artery. The BP is measured on the left arm at the brachial artery because it is closer to the heart, and the route from the aorta to the brachial artery is not as complicated [60]. The upper arm from which blood pressure is measured should be placed at the same level as the heart for the measurement. The arm positions below heart level lead to an overestimation of systolic and diastolic pressures and raising the arm above heart level leads to underestimation [61]. For the BP measurement, the cuff is manually inflated until the artery collapses, and no tapping sound is heard by the stethoscope. Next, the cuff pressure gradually decreases and as soon as the blood starts to flow into the previously collapsed artery, a series of sounds associated with each heartbeat will become audible through the stethoscope [62]. These sounds appear due to turbulent flow in the artery and are named as the Korotkoff sounds [63].

The first of the Korotkoff sounds indicates the first movement of blood flow through the constricted artery and the pressure at this moment is called the systolic BP [2]. The diastolic BP is determined when the sound disappears, which indicated that the blood flow has returned to its normal condition [64]. The auscultatory BP kit is simple, only requires a stethoscope and sphygmomanometer to perform the BP measurement. However, the observer must be trained to recognize the Korotkoff sounds to determine the SBP and DBP values [65]. There will always be measurement error due to user dependence in assessing BP, but this method is still recognized as the gold standard in non-invasive BP measurement in a clinical setting [66]. Computer-aided systems have been developed to provide the observer with more valuable objective information and to reduce the subjective influence of the observer in the audible BP measurement technique [67]. Figure 2.2 shows the recording of Korotkoff sound (k-sound) detected by a piezoelectric type microphone for SBP and DBP assessment [68].

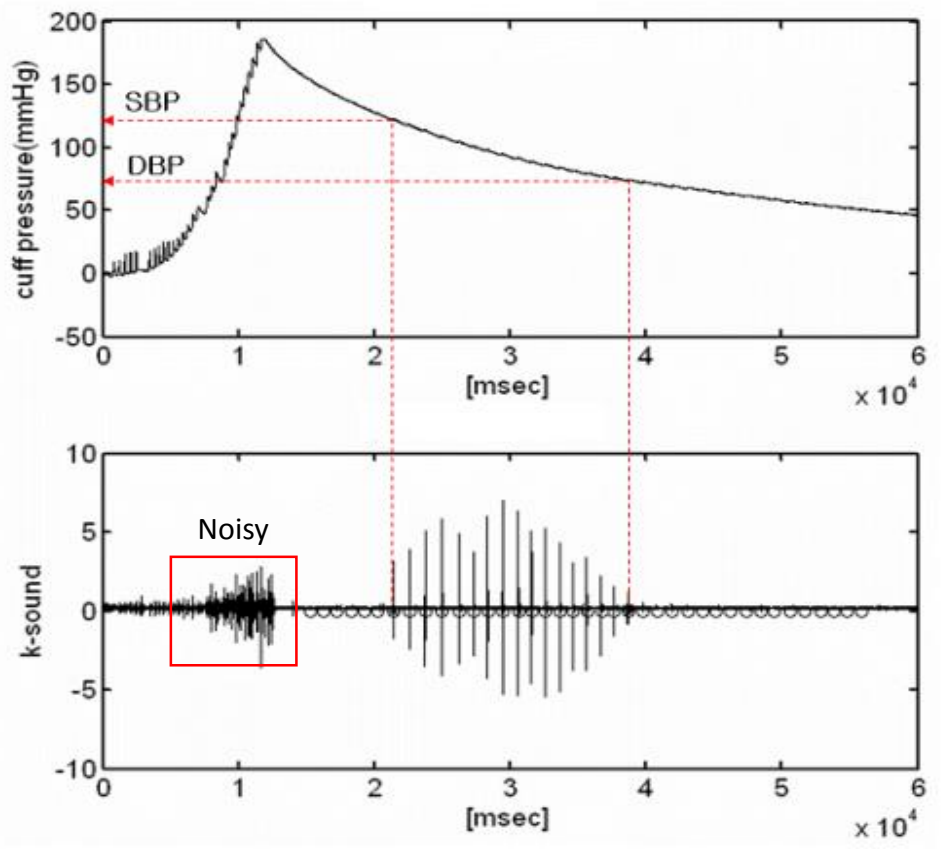


Figure 2.2: SBP and DBP determined based on K-Sound [68]

As shown in Figure 2.2, during the cuff inflation cycle, a noisy signal (marked with a red box) appeared on the k-sound due to air turbulence and electrical signal noise generated from the air pumping motor [69]. During the cuff deflation cycle, the SBP is determined based on the first k-sound detection, and the DBP determined when this k-sound disappears. The integration of a real-time visual display of the audio sounds, cuff pressure and pulsatile signals combined with advanced signal processing methods has led to more accurate BP measurement [70]. Recently, a hybrid sphygmomanometer has been introduced to replace the mercury-based sphygmomanometer due to environmental concerns. Mercury-based devices are no longer permitted in hospitals in certain countries due to its toxicity to the environment and the individual

[71]. In a hybrid sphygmomanometer, the technique applied to measure BP is the same as a normal sphygmomanometer except the mercury column is replaced by an electronic pressure gauge. Innovative products at this type are commercially available such as the Accoson Greenlight 300, Heine Gamma G7, and Welch-Allyn Maxi Stabil 3 [72].

2.4.2 Oscillometric Method

An alternative to automatic BP measurement with less opportunity for human error is the oscillometric method. This method is similar to the auscultatory method except that small fluctuations in the cuff are measured rather than listening to the Korotkoff sounds. The pressure cuff is automatically inflated above systolic BP and gradually deflated to a level below diastolic BP. The sensor picks up the oscillations from the artery near the surface, just below the compression cuff. The air pressure pulses during cuff deflation will be detected by the pressure sensor and analysed by the microprocessor. A high pass filter is used to extract the signals to obtain the oscillometric waveform. The waveforms are enveloped, and an algorithm such as the maximum amplitude algorithm (MAA) is applied to determine the BP [65]. In the MAA method, the peak of the waveform corresponds to the mean arterial pressure (MAP). Based on the MAP, the empirical coefficients are calculated and then used on the cuff pressure and pulse amplitude mapping to estimate systolic and diastolic BP. Conventionally, fixed ratios were performed to determine the SBP and DBP as shown in Figure 2.3 [73].

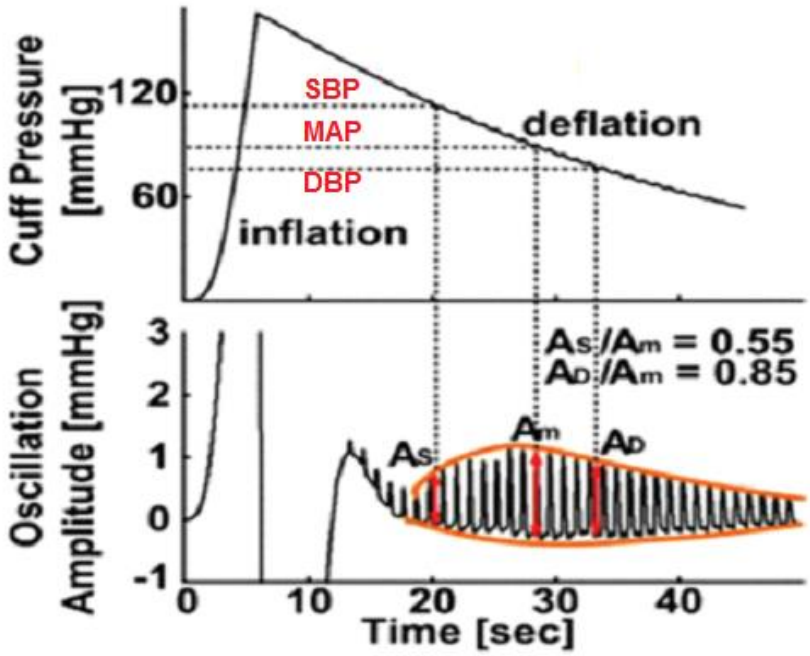


Figure 2.3: Estimation of SBP, MAP and DBP from the oscillometric cuff pressure waveform [73]

As shown in Figure 2.3, the systolic and diastolic coefficients were determined based on an amplitude ratio of 0.55 and 0.85 respectively. The ratios varied according to the device's manufacturer with the systolic coefficient ranging from 0.45 to 0.73, and the diastolic coefficient ranging from 0.69 to 0.83 [65]. The empirically derived coefficient methods were based on population means, thus limiting the device's accuracy to subjects with normal BP level only [74]. Patients with arrhythmia such as atrial fibrillation may give irregular oscillometric pulses resulting in errors in the BP reading [61]. Furthermore, the BP device may give unreliable results due to outlier points on the oscillation waveform caused by movement artefact [75]. As a result, numerous algorithms have been deployed to improve the estimation of BP and therefore reduce measurement errors [65].

Auscultatory and oscillometric methods are the most widely used methods for non-invasive BP measurements. Both methods use a cuff to block the blood flow by pressurising the upper arm to determine SBP and DBP. Patients may feel slight discomfort and inconvenience due to the increased strain applied to their brachial artery (the major blood vessel in the upper arm) during BP measurement. Since this method gives an intermittent BP reading, it cannot be used for cases such as high-risk surgical procedures which require continuous measurement. During the surgery operation, the intermittent BP measurement may leave BP fluctuations undetected or may lead to late recognition and delayed corrective procedures [76]. Therefore, a continuous BP measurement is desirable for applications such as in some cases during caesarean section surgery [77] and for assessing orthostatic hypotension [78]. Several methods have been deployed to measure BP continuously, such as tonometry, volume clamp and pulse arrival time. These are discussed individually in the next three sub-sections.

2.4.3 Tonometry Method

In the tonometry method, a pressure transducer is placed on the skin surface with the presence of a group of a blood vessel under it, as shown in Figure 2.4 [79]. The transducer is maintained at this position with moderate pressure applied on the arterial wall to sense the pulse pressure. The force changes with the pressure wave is often detected by a fully automated system, resulting in a continuous BP signal.

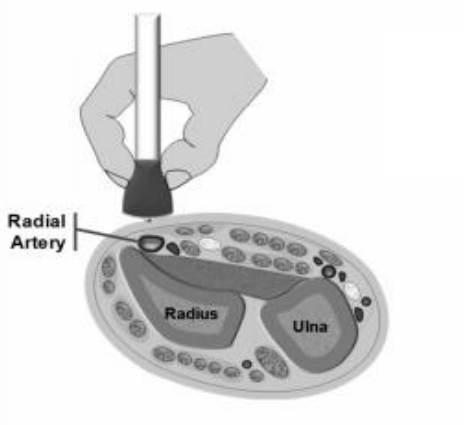


Figure 2.4: Tonometry method for recording the arterial pulse wave [79]

The force applied to the sensor probe on the skin can influence the BP reading. Also, misalignment of the sensor and improper pressurization may give rise to errors. One of the solutions is to introduce a micro triaxial force sensor to monitor the sensor alignment and the contact pressure [80]. This method can reduce the error in BP measurement compared to the device that only uses a pressure sensor. Commercially, some of the devices developed based on the tonometry method are The T-line (Tensys Medical Inc., San Diego, CA, USA); and the BPro (Center for Hearts, Canada) [59].

2.4.4 Volume Clamp Method

In the volume clamp method, the BP is measured based on volume changes in the finger. This method was described by a Czech medical doctor Jan Penaz in 1973 [81]. In this method, an inflatable finger cuff with built-in photoplethysmogram (PPG) sensor was used to measure the BP. A pressure control unit is used to control the counter pressure inside the alterable cuff to keep the blood flow constant. There is no

pulsation on the arterial wall as the blood volume in the vessel under the cuff is held constant. At this moment, the transmural pressure of the arterial wall is supposed to be zero so that the external pressure can represent the internal arterial pressure [81]. Therefore, the continuous pressure, which is applied from the outside of the finger, corresponds to the intra-arterial pressure and this pressure is proportional to the continuous arterial BP. Figure 2.5 shows an illustration of the working principle of the volume clamp method [59].

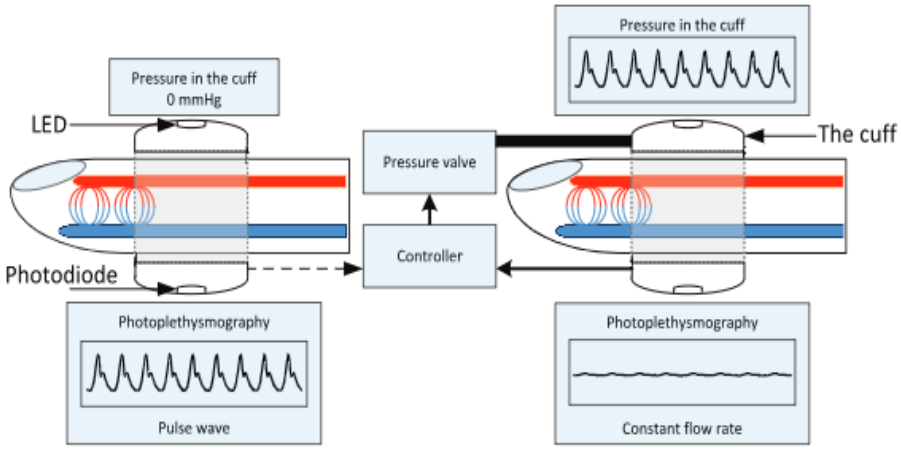


Figure 2.5: The working principle of the volume clamp method [59]

The volume clamp method is available for continuous BP monitoring. However, due to the size of the device, and the need for resting the finger from continual clamping cycles, limits its application for wearable device purposes. Wearable devices would be beneficial to the users to monitor vital signs such as BP at home over extensive periods without interruption to their daily activities [82]. For long duration BP measurements, it is, however, useful to have a BP device without such external pressure applied for the patient's comfort. The pulse arrival time method, discussed next, offers this facility.

2.4.5 Pulse Arrival Time Method

Pulse arrival time (PAT) is one promising method for cuff-less BP measurement. Generally, PAT is defined as the delay time between the R-wave peak of the Electrocardiogram (ECG) and a characteristic point of PPG in the same cardiac cycle [18]. In the literature, different characteristic points on PPG signals such as trough, middle and the peak have been studied to determine the PAT and correlated with SBP and DBP [82]. A study conducted by Choi et al. demonstrated that the SBP estimated using the delay time between the R peak of ECG on the chest and the peak of the PPG signal (PAT-peak) at the finger has a higher correlation coefficient (r = -0.71) and smaller standard deviation (SD = 3.9 mmHg) compared to other derived PAT values (PAT-trough (r = -0.09, SD = 5.5 mmHg) and PAT-middle (r = -0.32, SD = 5.3 mmHg)) [83]. Figure 2.6 shows typical ECG and PPG waveforms and the delay time between the peaks of these two signals used for PAT measurement.

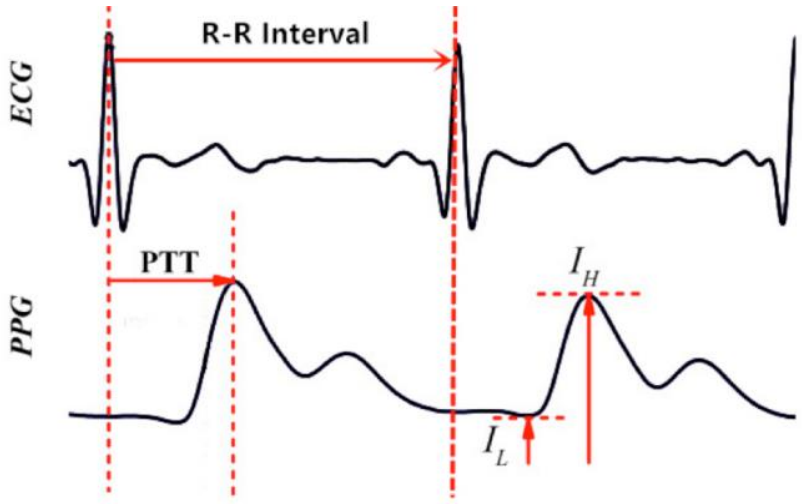


Figure 2.6: ECG and PPG waveforms for PAT measurement, I_H refers to the PPG peak, and I_L refers to PPG foot [84]

The delay time between these two signals (ECG and PPG) is shown to be correlated with BP [16], [85]. Increases in BP cause the vascular tone to increase, and hence, the arterial wall becomes stiffer, causing the PAT to shorten. Conversely, a drop in BP causes arterial wall tension and stiffness to decrease, thus increasing the PAT. This phenomenon can be explained by reference to the Moens-Korteweg equation, as shown by Equation 2.1 [86]:

$$PWV = \frac{D}{PTT} = \sqrt{\frac{gEa}{pd}} \qquad \text{Equation 2.1}$$

where PWV is pulse wave velocity, *D* is the length of the vessel, *PTT* is pulse transit time, *g* is the gravitational constant, *E* is the elastic modulus of wall tissues, *a* is the wall thickness, *p* is the density of the contained blood within the vessel and *d* is the interior diameter of the vessel. As stated in Equation 2.1, the PWV is dependent on elastic modulus, *E* and the elastic modulus increases exponentially with increasing BP as shown in Equation 2.2

$$E = E_0 e^{\gamma P} \qquad \text{Equation 2.2}$$

where E_0 is the zero-pressure modulus of the vessel wall, γ is a constant ($mmHg^{-1}$), and *P* is the BP (mmHg) within the vessel. Then, if we substitute Equation 2.2 into Equation 2.1 and rearrange we obtain Equation 2.3:

$$e^{\gamma P} = \frac{pdD^2}{gaE_0}\frac{1}{PTT^2} \qquad \text{Equation 2.3}$$

If we take the logarithm of Equation 2.3 and rearrange for P (i.e. the BP), we get:

$$P = \frac{1}{\gamma}\left(ln\frac{pdD^2}{gaE_0} - 2\ lnPTT\right) \qquad \text{Equation 2.4}$$

If the changes in *a* and *d* with respect to the change in BP are negligible, and if the change in the arterial wall tonus, E_0 is slow enough, the first term of the right-hand side can be regarded as a constant during a short period, and this can be simplified to Equation 2.5:

$$\frac{dP}{dPTT} = -\frac{2}{PTT\gamma} \qquad \text{or} \qquad \Delta P = -\frac{2}{PTT\gamma}\Delta PTT \qquad \text{Equation 2.5}$$

The change of P (ΔP) in Equation 2.5 is considered as the change of SBP or DBP [21]. Equation 2.5 shows that there is a linear relationship between pulse arrival time (PAT) and BP if the change in vessel elasticity E_0 is negligible [86]. Generally, the unknown coefficients ($\boldsymbol{\gamma}$) can be identified by individual calibration of BP with PAT. These unknown $\boldsymbol{\gamma}$ parameters change from person to person due to the subject's different physical characteristic parameters such as body weight, height and cardiac function [87]. After the coefficients are determined, the estimated BP can be calculated without recalibration as long as the elasticity of the arterial wall remains constant. It has been reported that arterial wall elasticity becomes stiffer with an increase in age, resulting in faster pulse transmission to the periphery [88]. In this research, the delay time

between the ECG R-wave peak and the peak of the PPG, labelled as PAT in Figure 2.6, were used to estimate BP.

2.5 Overview of Pulse Arrival Time (PAT) Measurement

The PAT-based method offers a number of advantages over other methods (tonometer and volume clamp) in monitoring BP continuously. First, it requires only the ECG and PPG signals and there is no danger of cessation of blood perfusion to the finger due to the occlusive cuff on finger (volume clamp method) [25]. Second, the ECG and PPG measurement device is relatively cheap and most importantly, is fully portable thus lending itself to domiciliary studies [89]. Third, the miniaturization of the ECG and PPG circuitry make the device wearable and provide convenience to the user to wear it for a long period in BP monitoring. Thus, this thesis focuses on the PAT measurement by deploying a conductive fabric electrode for ECG measurement and plastic optical fibre (POF) for PPG measurement.

In general, the PAT method involves measuring the pulse on the human body. Ultrasound Doppler, tonometer and pulse oximeter are some of the example devices available for pulse measurement. However, some of these devices are not suitable for wearable PAT measurement due to their bulky size and complexity in circuitry for signal processing. The most popular method for pulse measurement is based on PPG due to their simplicity in circuit design. The basic components required for PPG measurement are a light source and a photodetector. A light source is used to illuminate the skin tissue, and the photodetector is used to measure the light intensity associated with the changes in blood volume at the arterial site. The PPG can be classified into two configurations that are called transmittance and reflectance mode.

The transmittance mode refers to the light detector placed on the other side of the skin to the light source. Due to this arrangement, the measurement site for transmission mode is limited to a few places such as fingertips and earlobes. The light source typically used has Infra-Red wavelength due to its large penetration depth in the skin. In transmission mode, the blood absorbs the light, thus reducing the light intensity detected by the photodetector. The light intensity decreases as the blood volume increases and the translation to the PPG signal waveform is shown in Figure 2.7 [90].

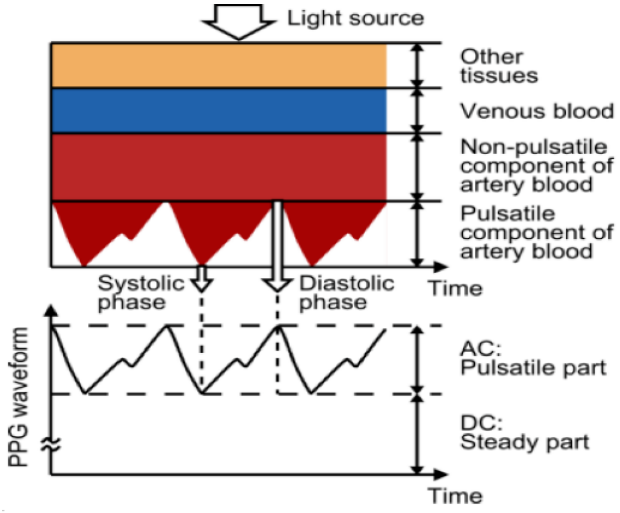


Figure 2.7: The illustration of light intensity measurement inside the tissues and the resulting PPG signal [90]

As shown in Figure 2.7, the PPG signals consist of pulsatile components (AC) and non-pulsatile components (DC). The small amplitude of the AC signal is synchronised with the heart and related to arterial pulsation. Meanwhile, the DC signals are related to light absorption in the tissues, vein and diastolic arterial blood volume. The information on the AC and DC components are useful in calculating oxygen saturation (SpO_2) [91].

Reflection mode PPG was exploited to determine the PPG at any part of the body such as at the wrist, forehead and chest. In this configuration, the photodetector and light source are both on the same side. The penetration depth of the light depends on the distance between the light source and the photodiode (detector) and the wavelength. Weak PPG signals with low amplitude and very poor signal to noise ratio are detected if the source-detector separation distance is too large [92]. Green light is most suitable for reflection mode PPG due to its short penetration depth caused by its greater absorptivity for both oxyhaemoglobin and deoxyhaemoglobin compared to infrared light [90]. This characteristic will give a clear indication of blood volume change when blood pulses through the skin and hence provides the strongest reflectance mode PPG for this wavelength.

In this thesis, three different approaches to define the PAT measurement were reviewed. The first approach is on the definition of PAT as a time difference between the Electrocardiogram (ECG) and the Photoplethysmogram (PPG). The second approach is on the definition of the PTT as a time difference between two PPG signals at different positions on the body. The third approach uses the ballistocardiography (BCG) signal as a reference signal for PAT measurement.

2.5.1 PAT Measurement: ECG to PPG

Most researchers determine the PAT by measuring the time interval between the electrocardiogram (ECG) acquired on a chest, and a photoplethysmogram (PPG) acquired at a fingertip for example [24]–[26]. These two signals are often simultaneously recorded by patient monitors in the hospital and can be accessed through the patient's database system for PAT analysis [93].

Poon et al. for example, have shown that systolic BP and diastolic BP are highly correlated with PAT [94]. The number of participants involved in this study was 85 and half of them were diagnosed with one or more chronic diseases such as hypertension, congestive heart failure and diabetes mellitus. The ECG and PPG signals were obtained from the subject's fingertips by stainless steel electrodes and a pair of the light emitting diode and a photodetector. The experiments were performed in two consecutive weeks, with three datasets being collected during each trial. The equation to estimate SBP and DBP was formulated based on the Moens-Korteweg's formula. The results showed that the standard deviation (SD) of the difference between the reference and estimated SBP is 9.8 mmHg and 5.6 mmHg for DBP. They stated that this SD (i.e. variability) was due to the fluctuation of beat to beat BP and the different mechanisms in BP detection. For example, the conventional cuff-based device measures BP at one instance while the alternative PAT technique measures pulses over a 45 second period.

He et al. also demonstrated that the PAT between the R-peak of the ECG signal and the peaks of the finger PPG signal have a high correlation with BP [93]. They obtained the ECG and PPG data from a patient's Multi-parameter Intelligent Monitoring for Intensive Care (MIMIC) database. The correlation between BP and PAT were tested using linear regression, quadratic regression and cubic regression models. Their findings showed that the cubic regression gave the highest correlation of BP with PAT compared to other models.

Real-time PAT measurement was proposed by Zhang et al. using Labview software [24]. They used a 3-lead ECG on the right and left wrists and on the left ankle to acquire the ECG signal. Optical transmittance mode was used to obtain the PPG signal on the finger. The experiment was performed on 14 healthy subjects. BP was measured by a mercury manometer immediately after performing PAT measurement.

Their result shows that the BP and PAT are almost linear with the maximum error between the calculated SBP and the measured SBP at 8.3 mmHg. They stated that the accuracy of the estimated SBP is reduced for each because they used a calibration curve from the same 14 people's data.

An Android smartphone has been exploited by Xu et al. for monitoring BP based on the PAT method [95]. Three leads of ECG electrodes are attached to the user's arms and a leg to acquire an ECG signal and a pulse sensor on the fingertip to acquire the PPG signals. The signals were sent via Bluetooth to an Android smartphone for real-time monitoring. The proposed system was able to estimate BP based on their own developed PAT- BP module.

Wearable cuff-less PAT-based systems for overnight BP monitoring was proposed by Zheng et al. [96]. They monitored BP and PAT over 24 hours using a strap-based wearable monitoring device. The device consists of textile-based ECG electrodes, an LED emitter and a photo-detector for PPG measurement. They used two straps wrapped around two arms for long-term ECG and PPG recordings. A BP monitor was wrapped on the non-dominant upper arm and set automatically to take a measurement every 30 minutes during daytime and every 45 minutes during night time. ECG and PPG signals were transferred to a mobile device via Bluetooth, and the pulse arrival time was analysed off-line using Matlab software. Their results showed that PAT estimated systolic BP most accurately during sleep time. They reported that there is a poor correlation between PAT and systolic BP during daytime due to motion artefacts on PPG signals during daily activities.

Through the literature review, the measurement of PAT based on ECG and PPG signals are a widely accepted surrogate for estimating BP. Two such commercial devices for estimating BP using the PAT are the Sotera

ViSi Mobile [97] and Somnotouch-NIBP [98]. Sotera Visi Mobile uses three lead ECG on a chest to monitor the ECG signals and the PPG signal measured on a thumb. A wrist-type monitor was used to process the signals and displayed the results such as blood oxygen level, BP, heart rate and ECG waveforms. Also, the signals can be sent wirelessly to allow doctors to monitor their patient remotely through a computer or smartphone. Figure 2.8 shows the Visi Mobile device attached to a patient's body [99].



Figure 2.8: Illustration of Sotera Visi Mobile device attached to a patient [99]

The device continuously monitors the vital signs making it suitable to be deployed for intensive care unit patients. Furthermore, the device is wearable (albeit slightly cumbersome), and with wifi technology enables the patient to move freely. Somnotouch-NIBP (SOMNOmedics GmbH, Germany) is another device that is commercially available for long term monitoring of oximetry, ECG and BP. The device monitors continuous BP based on the PAT method by acquiring the ECG signals on the chest, and PPG signals on the fingertips. The device accuracy in BP

measurement has been compared with the auscultatory method, and the results showed that the correlation coefficient r = 0.97 for SBP and r = 0.98 for DBP [98].

Most researchers used the fingertip as a measurement point to determine pulse arrival time between the ECG and PPG signals. The major drawback from this technique is the motion artefact on the PPG signal due to finger movement [100] and movement of arm position relative to the vertical body which causes an error in the PAT measurement [60]. Therefore, other researchers have used different locations on the body to acquire the PPG signal.

One of the most promising parts of the body to obtain a PPG signal using a transmission mode optical sensor is at the earlobe. The PPG signal at the earlobe gives less error in PAT measurement because there is reduced movement vulnerability, and the hydrostatic pressure is much more constant when the person moves from supine to standing [101]. Jeong et al. investigated the relationship of BP with PAT between ECG on the chest and PPG on the earlobe [60]. The ECG and PPG signals were acquired by developing suitable electronic circuitry and transmitting it wirelessly to a computer via an RF module. The initial result showed that there was a linear response between PAT and systolic BP and suggested that there was a need for individual calibration for monitoring an individual's BP continuously. However, it was reported that PPG on the ears comprised more artefacts and noise when compared with PPG at the finger [102]. This problem could be overcome with specifically designed PPG circuitry with signal processing techniques for monitoring PPG signals at the earlobe site. The transmission mode optical sensor for PPG detection shows relatively good signals compared to a reflection mode optical sensor, but, of course, it is limited to certain body parts. Alternatively, reflectance mode PPG can be placed at any measurement site such as the forehead, chest, wrist and arm [103].

Fuke et al. developed a prototype small wearable device consisting of ECG and PPG sensors for measuring PAT on the chest [104]. The sensors were placed close together (40 mm), and the PPG sensor was level with the heart to improve the accuracy of PAT measurement by eliminating the hydrostatic pressure. The findings showed that the system is able to monitor the change of blood pressure, although the pulse propagation distance is short. However, the mean error recorded by the device is still high, greater than 5 mmHg. They suggested that the sampling frequency is going to be enhanced to detect a more accurate period, and the calibration method should be simplified for daily use.

The PAT between the ECG signal on the chest and the PPG signal on the forehead was exploited by Franco et al. [105]. The PPG signal on the forehead was less affected by motion artefacts during daily activities. A Wireless Body Sensor Network (WBSN) was used as a platform to sense, process and send the signals wirelessly. A mathematical model was developed to estimate BP, and their initial results on a volunteer showed that the mean absolute error for SBP and DBP were less than 5 mmHg. Also, the developed WBSN provided free movement to the user and eliminated the discomfort produced by systems that require the installation of sensors at the fingers.

The ECG signals that are required in PAT measurement may increase the system complexity due to the additional electrodes and circuitry components [23]. Besides, electrical interference from the external device such as diathermy may disturb ECG signals, which will lead to error in PAT measurement [106]. Alternatively, the PAT measurement based on two PPGs pulses at different locations on the body were investigated by other researchers, as described in the next section.

2.5.2 PTT Measurement: PPG to PPG

PTT measurement based solely on PPG signals requires a more simple circuit compared to the technique that uses ECG measurement. Nitzan et al. showed that the PTT between finger and toe significantly decreases with the increase of systolic BP [85]. They also found that diastolic BP was not statistically significant with age. Arterial BP estimation based on pulse wave velocity between wrist and index finger were studied by McCombie et al. [107]. They used hydrostatic pressure variation (by altering the height of the wrist and hand relative to the heart) to calibrate pulse wave velocity to arterial BP. They found that the BP slightly dropped (11 mmHg) as the hand is elevated above the heart level (15 cm). Initial results suggested that the system has the potential for continuous BP measurement.

Estimating the PTT from two different measuring points such as between the sternoclavicular joint and the earlobe was studied by Jeong et al. [108]. They proposed an algorithm for estimating the BP based on PTT during body posture changes from the supine position to a sitting position. They measure 30 times (repetitions) during each body posture to get the correlation between the PAT and the SBP. After establishing a mathematical model, an experiment was performed to monitor PAT for 5 minutes for each posture of supine-sitting-supine position. BP is measured at a steady state value at each position. The findings show that they can estimate SBP in different body postures with a single equation.

Amin et al. designed an optical system to measure continuous and cuff-less BP using two PPG signals with 55 mm separation between the two transducers [23]. In this study, a different physical activity was introduced to vary the participant pulse arrival time and BP on people with different ages (16 to 52 years old). Each subject was requested to perform twenty

trials of measurements to obtain the constant coefficients with high accuracy. The result shows that the mean percentage errors (n = 15) between the cuff method and the PAT method of SBP and DBP were 6.3 ± 2.5 %, and 10.9 ± 3.9 % respectively.

PTT measurement between two PPGs pulses means that the pre-ejection period (PEP) measured in the ECG is excluded in PTT calculations. PEP is the time between the R-peak of the ECG and the opening of the aortic valve [59]. Reports show that PEP has a significant contribution to the PAT change during daily activities such as posture change and dynamic exercise [109], [110]. Findings from Proenca et al. show that there is poor correlation between PAT and SBP in healthy young subjects during a sequence of short-term physical exercise if PEP is excluded from the PAT measurements [111]. The exclusion of PEP in the PAT calculation may reduce the accuracy of BP measurement with PAT [112]. A study by Wan et al. showed that the PAT-SBP measurement between ECG (chest) and PPG (finger) have better correlation coefficient (r = -0.71) compared to PTT-SBP measured from the PPG (brachial artery) to PPG (finger) (r = 0.01) in hand elevating experiments [113].

2.5.3 PAT Measurement: BCG

Another type of pulse exploited for PAT calculation is based on ballistocardiography (BCG). BCG is a measurement of the reaction forces of the body to the cardiac ejection of blood into the aorta and is strongly correlated with the ECG signals. Generally, the BCG is measured using EMFi sensors and amplified for further processing [114]. The sensor can be located on a weighing scale [115], chair [114] or mattress pad [116] for BCG measurement. Kim et al. proposed a study

on the BCG-based PAT for cuffless BP measurement [117]. They acquired the BCG signals by standing on a weighing scale equipped with a force sensor, and the PPG was measured on the fingertips. A sustained handgrip exercise was performed for 60 seconds to vary the BP. The finding shows that the delay time between BCG and PPG signals is negatively correlated with BP with a mean correlation coefficient (*r*) of 0.62 for DBP and 0.66 for SBP.

A similar approach was applied by Martin et al. in investigating weighing scale based PAT for BP estimation [118]. The BCG signals were performed on a weighing scale and the finger PPG was acquired by a transmission-mode PPG sensor. The results show that the PAT was able to track the BP changes during interventions of mental arithmetic, cold processor test and post-exercise. However, the BCG measurement on the chair [114], weighing scale [115], and mattress pad [116] do not allow continuous and wearable monitoring.

For wearable monitoring, He et al. proposed the site behind the ear for BCG measurement using differential capacitive electrodes constructed using fabric [4]. They demonstrated that the delay time between the BCG signal (J-wave) and the chest ECG signal (R-wave) correlated to blood pressure during the Valsalva manoeuvre test. The proposed design has been upgraded by Winokur et al. [119] by introducing a portable device that acquires the ECG, BCG and PPG signals at a single area behind the ear. All the signals wirelessly transfer to the PC for data recording and analysis. They demonstrated that the delay between the R-wave of the ECG, and the principal wave of the BCG (the J-wave) have a good correlation with pre-ejection period and arterial blood pressure during the tilt table experiment.

The major drawback of the BCG signal is the signal quality. The signal can be corrupted by external interferences such as motion artefacts and

building vibrations [115]. Besides, any other movement in a human body, e.g. muscle tremor, causes disturbance to the BCG signal, which is very weak compared to the signals caused by bigger body movements [114]. Therefore, the subject should stay still and avoid any movement during the BCG measurement to minimize the disturbances.

2.5.4 PAT Measurement: Calibration Protocol

In general, a wide range of systolic and diastolic BPs are essential to generate an accurate mathematical model to estimate BP based on PAT. A variety of methods were deployed by researchers to vary BP for PAT calibration such as pedal exercise [104], treadmill jogging [120] and step climbing exercise [121]. Jeong et al. used five participants in their study to estimate BP during exercise using a portable bicycle [122]. They acquired the ECG signal on the chest, PPG signal on right index finger and BP on the left upper arm. The ECG and PPG signals were sent wirelessly to a computer and Labview software was used to monitor the signal online. The PPT was determined based on the delay time between ECG R-peak and PPG peak. The BP was recorded before, and after exercise, giving a total of 9 BP values for each participant in 3 visits. The result shows that PAT and systolic BP were highly correlated (r = -0.809), but there was a low correlation of PAT and diastolic BP (r = -0.168).

Li et al. used bicycle ergometry as a tool to perform the exercise to vary BP and hence, PAT [25]. Nine healthy subjects participated in this study. The participants were required to exercise on a bicycle for 20 minutes. The pulse arrival time between ECG signal on the chest and the PPG signal on the middle finger on the left hand were recorded continuously during the exercise. Wrist BP was used to take BP measurements every minute on the right hand. In this study, the correlation coefficients

between BP and PPG were investigated, and it was suggested that waveform morphology (area ratio of systole to diastole) could improve the performance of PPG based BP estimation.

Step climbing exercise was proposed by Teng et al. to vary BP of the participants of 15 healthy male subjects aged 24-30 years old [121]. The experimental sessions involved three periods: rest, step-climbing exercise, and recovery from exercise, each with four trials. The ECG (lead I) and PPG (on right-hand index finger) were recorded simultaneously for 18 seconds at a sampling rate of 1 kHz. BP was measured using a standard oscillometric BP at the left upper arm as a reference at the same time. All the data were recorded immediately after the exercise on each trial. They applied a continuous wavelet transform (CWT) algorithm to extract features from the PPG signal and correlated the features with BP. They found that the decay time of the PPG waveform (diastolic time) highly correlated with SBP (r = -0.81) and DBP (r = -0.69) compared to other features of PPG waveform.

In most studies, experiments conducted on volunteers in varying BP and PAT are through exercise or posture changes. Groups of patients with different health condition and ages were investigated to demonstrate the correlation between BP and PAT. Through the literature, it has been observed that most researchers determined PAT based on the delayed time of the R-wave ECG and PPG wave arriving at the fingertips. There are several points to the time stamp on the PPG waveform such as foot, peak and mid-point of the rising edge. Different algorithms have been deployed to locate the time stamp on the PPG to improve the accuracy of PAT measurement. All of the above discussed PAT/PTT research is summarised in Table 2.2.

Table 2.2: Summary of the relevant research study for PAT measurement for cuff-less BP

Measurement site	Reference Point and Method	Protocol	Measurement Result	Subjects (n)	Refs.
ECG (arm - ECG electrodes PPG (finger, reflectance PPG sensor)	PAT (R-peak of ECG to the 1st derivative of PPG) BP (Finometer) Method: PAT-PIR (PPG intensity ratio) model	Supine (5 min) to active standing (3 min). Sustained handgrip (5 min), Valsalva manoeuvre (5 min) and deep breathing (2 min)	Estimation error against finometer: SBP = 1.2 ± 5.7 mmHg DBP = 0.4 ± 7.1 mmHg,	n = 33 (19 normotensive and 14 hypertensive)	Ding et al. [16]
ECG (arm/leg - ECG electrodes) PPG (finger, PPG sensor)	PAT (R peak of ECG to the foot of PPG) BP (mercury manometer) Method: linear regression	PAT measured for 5 minutes and then measured SBP from mercury manometer	Maximum SBP error = 8.3 mmHg, minimum SBP error = 1.6 mmHg.	n = 14 (healthy volunteers)	Zhang et al. [24]
ECG (chest- ECG electrodes) PPG (finger, PPG sensor)	PAT (R-peak of ECG to the foot of PPG) – left arm BP (cuff-wrist sphygmometer) – right arm Method: linear regression	5 min rest, 20 min exercise on bicycle ergometer and 5 min rest, 1 min interval for BP measurement during the procedure	The correlation coefficient for PAT-SBP, r = -0.67 ± 0.17 and for PAT-DBP, r = -0.28 ± 0.40 (mean ± SD)	n = 9 (healthy male volunteers, age 28 ± 5 years)	Li et al. [25]
ECG (chest- ECG electrodes) PPG (finger, SpO_2 sensor)	PAT (R-peak of ECG to peak of PPG) Arterial BP (Continuous BP) Method: cubic regression	All measurement data from Patient's Database (MIMIC)	The absolute values of correlation coefficients, $\|r\| > 0.87$ for PAT versus SBP, DBP, and MBP	n = 10 (patients)	He et al. [93]
ECG (arm: textile ECG electrodes, thorax: Ag-Ag/Cl ECG electrode) PPG (arm, reflective PPG sensor)	PAT (R- peak of ECG to peak of PPG) BP (oscillometric ambulatory BP) Method: non-linear model	Measurement every 30 minutes in 24 hours	The correlation coefficient for PAT-SBP, r = -0.80 ± 0.10 (mean ± SD) RMSE = 6.2 mmHg	n = 10 (healthy subjects, age 27 ± 3 years old)	Zheng et al. [96]

ECG (chest: ECG electrode) PPG (chest, reflective PPG sensor)	PAT (R-peak of ECG to onsite time of PPG) BP (ABPM sphygmomanometer) Method: linear regression	Rest 20 minutes, ergometer exercise for 20 minutes (supine position), recovery times 20 minutes	Mean error and SD for SBP 6.9 ± 4.2 mmHg RMSE = 8.0 mmHg	n = 4 healthy volunteers (3 males, 1 female)	Fuke et al. [104]
ECG (chest: ECG electrode) PPG (forehead, reflective PPG sensor)	PAT (R-peak of ECG to mid-point of PPG) BP (oscillometric BP) Method: linear heuristic model	Two data sets were gathered, one for calibration and one for evaluation	Mean absolute error for SBP = 4.4 ± 5.5 mmHg, and for DBP = 4.2 ± 3.3 mmHg.	n = 1 healthy male	Franco et al. [105]
PPG (Wrist, reflective PPG sensor) PPG (finger, reflective PPG sensor)	PWV (onset PPG to onset PPG) – 30-second data BP (oscillometric BP) Method: blind system identification	Hydrostatic pressure by moving up and down the arm	P + 8.8 mmHg (Arterial Pressure) = 8.1 ± 0.7 m/s (PWV Mean) P = reference hydrostatic pressure	n = 1 healthy male	McCombie et al. [107]
PPG (distal finger, an optical sensor) PPG (proximal finger, an optical sensor)	PTT (peak of PPG to peak of PPG) – 30-second data BP (blood pressure manometer) Method: linear regression	Physical exercises until the submaximal heart rate was achieved, measurement after that.	The absolute values of correlation coefficients for PTT-SBP, $\|r\|$ = 0.88 ± 0.03 and for PTT-DBP, $\|r\|$ = 0.82 ± 0.05 (mean ± SD)	n = 15 healthy volunteers (10 males, 5 females, age 6 to 52 years old)	Amin et al. [23]
ECG (chest, ECG electrode)	PAT (R-peak of ECG to BCG) BP (finger cuff BP, ccNexfin) Method: linear regression	Resting (60 s), deep breathing (60 s) resting (60 s), sustained	PAT-estimated BP for SBP r = 0.66 ± 0.14 and for PAT-estimated DBP,	n = 15 healthy volunteers (10 males, 5	Kim et al. [117]

BCG (foot, weight scale, FBG sensor)		hand grip (60 s) and resting (60s), in standing position.	r = 0.62 ± 0.16 (mean ± SD)	females, age 24 ± 3 years old)	
Pulse (neck, FBG sensor) Pulse (ankle, FBG sensor)	PTT (pulse peak at neck to pulse peak at ankle) -10 second BP (electronic sphygmomanometer) Method: partial least square regression	Measurement duration about 15 s to 20 s (100 times) in the supine position.	The mean difference between BP and estimated BP in range of ± 5 mmHg.	n = 3 (healthy male)	Katsuragawa et al. [123]
PPG (finger, SpO_2 sensor) BCG (cushion seat, FBG sensor)	PAT (peak of PPG to J peak of BCG) BP (oscillometric BP) Method: linear regression	In the sitting position, signals recorded immediately after exercise.	Mean error and SD for SBP = 9 ± 5.6 mmHg, and for DBP = 1.8 ± 1.3 mmHg	n = 5 (healthy volunteers)	Zhihao Chen et al. [124]
ECG (arm, conductive textile ECG electrode) PPG (finger, reflective PPG sensor.	PAT (peak of ECG to peak of PPG) Method: linear regression	5 min rest, 5 min ride exercise bike and 5 min rest. All the measurement record continuously during the protocol.	The mean correlation coefficient for PAT-SBP, r = -0.77 and for PAT-DBP, r = -0.51	N=10 (healthy volunteers)	Chan et al. [125]
PPG (carotid artery, FBG sensor) PPG (radial artery, FBG sensor)	PTT (peak pulse pressure between two pulses) BP (Cuff BP) Method: linear regression	PTT measured for 10 min with 1 min interval for BP (sitting position)	PTT-estimated BP for SBP, r = 0.78 ± 0.01 (mean ± SD)	n = 30 healthy volunteers (18 males, 12 females, age between 24 to 29 years old)	Padma et al. [126]

2.6 Optical Fibre Sensors (OFS)

Optical fibres are widely used in fibre-optic communication, which permits digital data transmission over longer distances and at higher data rates than electronic communication [127]. They are also used to form sensors and have a wide number of applications. Optical fibres can be categorized according to the number of waveguide modes in the fibre; single-mode fibres or multi-mode fibres. Single-mode fibre allows only one mode of light to propagate but multi-mode fibre allows multiple modes to propagate through the core. A typical single-mode fibre is illustrated in Figure 2.9. It is composed of three parts; the core, the cladding, and the protective buffer coating (outer and inner coating).

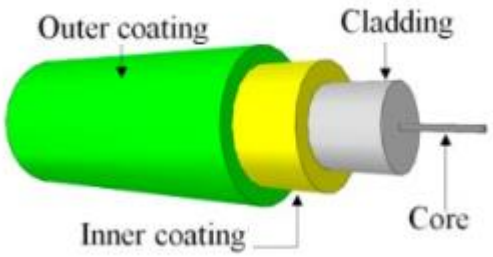


Figure 2.9: Typical cross section of optical fibre [128]

The core and cladding of fused silica fibre are made of high-purity fused silica. The typical diameter for the core is between 8 μm to 10 μm and for the cladding the diameter is approximately 125 μm [128] . The refractive index of the core (about 1.46 for silica) is slightly higher than the surrounding material or cladding, due to the presence of dopants [129]. The light rays are transmitted along the fibre core by total internal reflection at the core-cladding interface. The protective buffer coating is made up from a plastic material used to protect an optical fibre from mechanical damage and provides mechanical robustness [130].

2.6.1 OFS Measurement System

Optical fibres have favourable properties such as being lightweight, small in size, low in cost, and having low attenuation and immunity to electromagnetic interference, making them a suitable candidate for optical sensing [131]. In general, a typical optical fibre sensor (OFS) system consists of a light source, sensing element, optical receiver and data processing tools such as optical spectrum analyser and computer as shown in Figure 2.10.

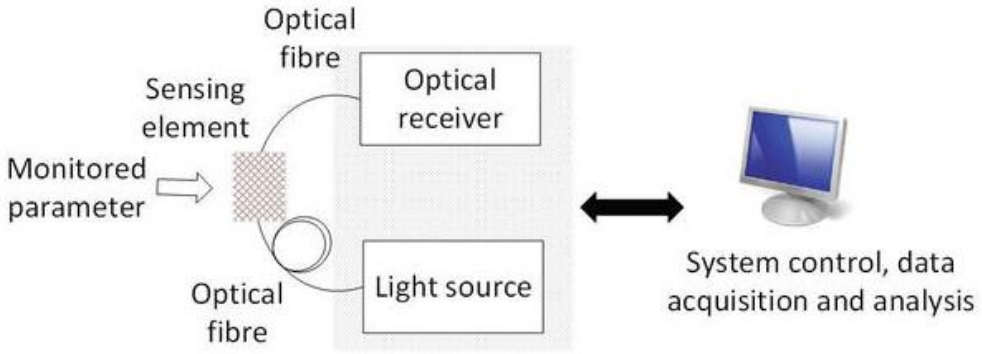


Figure 2.10. A typical setup of an OFS system [132]

The essential parts of the OFS system are the light source and the optical receiver. A laser, white light source, laser diode, and light emitting diode (LED), are the common light source uses in the OFS system. The choice of which light source to use depends on the required application. Optical receiver basically is a photodetector that is used to detect the change in the optical signal that is caused by the external interference [133]. Photodiode and phototransistor are commonly used in a low-cost OFS system to convert the optical intensity into electrical signal for further processing by the computer.

The sensing element for the OFS system can be classified as extrinsic or intrinsic. In an extrinsic sensor, the optical fibre become a medium for signal propagation between the sensor and detector. In this configuration, the fibre function as a guide to deliver light to the sensing location and the signal modulation takes place outside of the fibre. The major benefit of this configuration is the ability of the fibre to reach places which are other sensors unreachable. For intrinsic fibre sensors, the optical fibre act as a sensor by utilize a change in light propagation within itself. Thus, by detecting the modulation light inside the fibre, the external physical phenomenon or perturbation act on the fibre can be sensed and quantified.

2.6.2 OFS for BP Measurement

Optical fibre sensors are widely exploited in the monitoring of temperature, acceleration, pressure and many chemical parameters [134]. This type of sensor shows remarkable advantages compared to conventional sensors in certain applications due to their high sensitivity, small in size and no electrical power is needed at the remote location [135]. Also, fibre optics can be used as a medium to transfer and receive light, thus enabling the circuitry to be located remotely from the measurement site. Furthermore, and most significantly for this thesis, the optical fibre properties of non-toxicity and biochemical inertness make it safe to be applied on the human skin and hence opens up a wealth of wearable opportunities [136]. Through literature, fibre optic sensors are classified into three types of application such as physical sensors, chemical sensors and bio-medical sensors [129]. For pulse delay time measurement, the techniques used are limited to the fibre Bragg grating (FBG) and ballistocardiography (BCG).

In general, an FBG is a section of periodic refractive index in the core of a single-mode optical fibre created by exposing the fibre core to an intense interference pattern of UV energy. An FBG is viewed as a wavelength selective mirror, which reflects a narrow band of wavelengths back along the optical fibre while transmitting all other wavelengths [130]. The working principle of the FBG is illustrated in Figure 2.11.

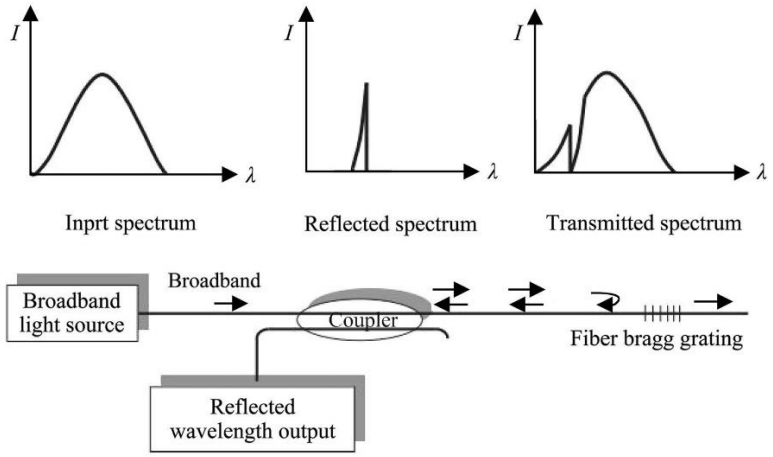


Figure 2.11: The operation of an FBG sensor [137]

As shown in Figure 2.11, a broadband light source is launched into the fibre and the reflected wavelength output shows the FBG response. Any environmental disturbance such as temperature and strain alters the period of the grating and the wavelength shift can be monitored by an FBG interrogator [126]. Generally, FBGs in the basic form can be deployed for sensing strain and temperature [138]. Pressure distribution in patients' feet during gait analysis can be monitored by incorporating the FBG sensing network into a shoe [139]. A study by Dziuda showed that the FBG embedded in a bed mattress was able to detect both respiration and heartbeat [28]. The system was also able to operate

during MRI examination, and the EM field generated by the MRI system did not disturb the sensor operation.

A FBG sensor for pulse wave measurement at the neck and ankle was proposed by Miyauchi et al. [140]. The time lag of the two waveforms' peak was computed as the pulse wave velocity (PWV). The results showed that the PWV measurement was able to estimate SBP. Meanwhile, Katsuragawa et al. exploited FBG sensors for PWV measurement between the radial artery (wrist) and the brachial artery (elbow) [123]. The PWV was calculated and correlated with the BP using the partial least squares regression (PLSR) method. The results showed that the developed system was able to estimate BP with high accuracy (the mean difference between the predicted value and the measured value within 5mmHg). Umesh et al. proposed a design of a silicone diaphragm with a hollow box for FBG attachment [126]. The sensor was attached to the carotid and the radial arterial sites for PWV measurement. They were able to demonstrate that the PWV can be monitored by the FBG technique. The findings showed that the PWV has a good correlation with SBP (the mean correlation coefficient, $r = 0.78 \pm 0.01$).

Microbending sensor technology was explored by Chen et al. for BCG measurement [124]. A multimode fibre was clamped between two microbenders to measure body vibration caused by heart beating. The sensor was inserted into a cushioned seat to perform the BCG measurement. The PPG signal was obtained on the fingertip via a SpO_2 sensor. The delay time between the BCG and PPG were calculated and correlated with SBP and DBP using linear regression analysis. The results show that the mean and standard deviation for SBP was 9 ± 5.6 mmHg and for the DBP was 1.8 ± 1.3 mmHg.

2.6.3 Overview of Plastic Optical Fibre (POF)

The first plastic optical fibre (POF) was produced by DuPont at the end of the 60s [141]. Up to now, it has been growing interest amongst researchers to explore the POF as a low-cost sensors in a variety of areas including chemical sensing, biomedicine and the measurement a range of physical parameters [142]. The most common core type for POF is polymethymethacrylate (PMMA) and the cladding material is made of fluorinated polymers. POFs with their large core sizes (diameters ranging typically from 0.25 mm to 2 mm) and high numerical apertures (0.47), make them suitable to be used as intensity-based optical fibre sensors [132]. The sensing principles used in POF are often similar to those developed in glass-based fibres, but the advantages associated with POF is on its flexibility and easy to handle makes them suitable for applications that require repeated flexing as well as for use in extremely tight areas.

In addition, the macro-bending properties make the POF suitable to be embedded into a textile. Rothmaier et al. demonstrated that a POF integrated into fabric was able to perform pulse oximetry at the forefinger tip in transmission mode [143]. A photomultiplier tube was used to detect the transmitted light, and the signals were analysed for pulse oximetry measurement. The findings suggest that the efficiency of light coupled into the fibre increases with purposefully damaged cladding or by bending the ends of the fibre by 90 degrees towards the skin. A polishing paper was used to damage the cladding, and hot air gun was used to bend the fibre ends under local heating at a temperature of 125^{o}C. Another method of coupling light through the fibre is by cutting the fibre tip at an angle of 45 degrees. Davenport et al. showed that the fibre tip cut by 45 degrees is able to reflect light laterally out through the side of the fibre [144]. This technique does not require advanced manufacturing

tools and is suitable to be deployed for transmitting or receiving light through the fibre.

In the research literature, the FBG technique was widely explored for cuffless BP measurement based on PWV. This technique is highly promising, but it currently requires a complex device to analyse the signal and is bulky in size for wearable purposes. Also, the patient location site for pulse measurement was limited because a strong pulse signal was required to trigger the FBG. The use of a plastic optic fibre (POF) in transmitting and receiving light source/signals for PPG measurements is shown to be a promising method. However, miniaturization of the electronic circuitry was essential to have a wearable fibre-based PPG measurement – one of the goals of this thesis.

2.7 Overview of Previous Cardiovascular Phantoms

In a human, the delay time between two pulses, known as the pulse transit time (PTT), is highly correlated with systolic blood pressure (SBP) [23], [108]. A physiological parameter such as heart rate and the compliance of the arteries also affects the PTT measurement [145], thus making it difficult to validate the PTT performance due to lack of control in the system. Also, the PTT has been shown to decrease with age, due to the reduction of aortic compliance which is associated with the process of hardening (“stiffening”) of the arteries [146]. Therefore, it is important to have a phantom to perform pulse delay time (PDT) simulation in a controlled environment.

In literature, a physical model of the cardiovascular system has been widely developed mainly focused on PPG pulse waveforms [147], [148] and to simulate pulse wave velocity [149], [150] leading to a PTT system. Laqua et al. constructed a phantom with two separate blood circuits to

represent fetus and mother pulses that can be controlled independently [147]. They deployed the phantom to verify algorithms for separating the weak fetal from the dominant maternal optical signal. An electronically controlled pump was proposed by Stuban et al. to generate pressure pulses in the artificial arteries made from resilient silicone tubes [148]. They investigate the strength of pulse oximeter amplitude with the artery depth, and the results from the experiment agree well with Monte Carlo simulations with an error below 24% in each case. A haemodynamic simulator was developed by Lillie et al. to study the impact of ejection time and peak pressure on PWV [149]. An adjustable rate servo motor was deployed to control ejection time and peak pressure. Their findings showed that PWV is substantially affected by ejection time (12%) and only a small shift in PWV (2%) by varying the peak pressure. A noninvasive technique for tracking the propagation of the pulse wave along the arterial wall was proposed by Apostolakis et al. using 3-D ultrasound [150]. The feasibility of this technique was validated on a silicone vessel phantom consisting of a soft and stiff segment. The magnitude of PWV was found to be higher in the stiffer segment, and the result shows a good agreement with the result obtained in a human study.

In general, a phantom system can enhance understanding of the basic principles of a physiological system such as pulse wave propagation in a blood vessel [151] and PPG characteristics in different tissue properties [152]. A pulsatile waveform was generated either by a commercial pulsatile pump [153], [154] or custom motorized pump [155]. A flexible tube was exploited by some researchers for pulse detection using ultrasound [150], [151] or by optical methods [153], [156]. A tube with different stiffness was investigated for pulse wave velocity [157]. Flexible tube is widely used in a phantom pulse system because it can be enlarged easily by small pressures [158]. The diameter of the flexible tube can change by about 8%–15% to match the changes in human

arterial diameter between the systolic and diastolic points [156]. The light intensity changes with the dilation of the tubes, thus making it possible to monitor the pulsatile signal by an optical sensor [147].

In summary, a simple and cost effective a tubular cardiovascular phantom system is required to simulate PDT in controlled environment. The system could be deployed as a validation tools for POF sensor and provide useful information on PDT measurement. In addition, the system should be able to generate a low perfusion signal to evaluate the limit of PPG sensor detection.

.

2.8 Summary of PAT Measurement

Continuous BP measurement provides highly important information on the individual's cardiovascular disease, especially during surgery and hypertensive treatment. In practice, ambulatory BP measurement (AMBP) is deployed for monitoring BP measurement in diagnosing hypertension. Unfortunately, these devices provide a measurement of systolic and diastolic at separate time intervals, thus limiting the measurement of BP variability. Also, the cuff-based AMBP may result in discomfort and inconvenience for patients wearing the device for a long period. Therefore, the cuff-less continuous BP measurement is a more desirable option as it can potentially provide deeper insight and understanding of BP variability to help identify serious cardiovascular events and allow anti-hypertensive therapy decisions.

PAT is one of the most promising methods for cuff-less continuous BP measurement. Most researchers defined PAT as the delay time between the R-wave peak of the ECG and the peak of the PPG. Most deployed ECG surface electrodes and transmission mode PPG devices to acquire ECG and PPG signals respectively. The use of ECG signals as a

reference marker means that the pre-ejection period (PEP) is included in PAT calculations. PEP changes rapidly in response to stress, emotion and physical effort and inclusion of PEP in the measurement of PAT was necessary to have an accurate PAT-based SBP estimation [112]. There was a poor correlation (r = -0.19 ± 0.45) between PAT and systolic BP in 20 healthy young subjects during a sequence of short-term physical exercise if PEP is excluded from the PAT measurements [111]. In addition, a commercial PAT device, such as Sotera ViSi Mobile or Somnotouch-NIBP was deployed with ECG and PPG signals as a marker for PAT measurement. The PAT measurements made in this thesis have, therefore been developed based upon the well-established technique of ECG and PPG signals but applied in a wearable fibre optics based setting. In order to address the limitations of the existing work in the area of wearable cuffless BP measurement, four major contributions have been made through this thesis.

The ***main contribution*** of this thesis is on the development of a wearable PAT measurement system based on ECG conductive fabrics and POFs. To date, no one has investigated the combination of POFs and textile electrodes that are well suited to smart textile applications. The use of textile is essential in wearable PAT applications because the patient needs to be monitored over extended periods in a comfortable environment. The term "wearable" refers to the feature that the device can be worn or used as a form of garment [125]. In our research group, a POF has been explored as a sensor in various applications such as humidity [159], pressure [160] and SpO_2 measurement [161]. In this project, a POF was deployed for delivering light to the tissue and collecting reflected light for PPG measurement. A green LED was deployed as a light source, and a phototransistor circuit was deployed for light detection. The PPG sensors were located on the wrist and under the foot due to the usability and accessibility of these places with a textile.

For example, the POF was attached in a long sleeve and was able to monitor PPG at the wrist; alternatively, the POF was attached to a sock being able to monitor the PPG under the foot.

Simultaneously, the ECG signal was acquired on the chest by a fabric-based ECG electrode. The delay time between the ECG and PPG signals were calculated and correlated with BP measurement. The PAT measured from a commercial sensor was used for benchmarking the PAT measured by the developed system. In the literature, the FBG technique was widely explored for PWV measurements, but as pointed out this technique required a complex device for analysing the signal. Also, the position of the sensor probe on the body for pulse measurement was limited because a strong pulse signal is required to trigger the FBG. The advantages of using a fibre as a sensor are the immunity to electromagnetic interference, and no risk of RF burns in an MRI environment. Besides, the size and bending properties of the fibre make them suitable to be embedded into fabrics for wearable sensor applications. The details of the development of the wearable PAT measurement system is presented in Chapter 3.

The ***second contribution*** of this thesis is through constructing a calibration curve of PAT and BP by using instantaneous PAT and a one-step calibration method. Beat to beat fluctuations in BP due to the interplay of different cardiovascular control systems, such as the baroreceptor reflex, the renin-angiotensin system and the changes in behavioural and emotional mechanisms [162]. The gold standard for the beat to beat BP measurement is based on an intra-arterial catheter. However this technique is usually applied for patients in serious medical conditions only [20]. Besides, this technique introduces the risk of arterial injury and skin infection to the patient and requires a complex setup procedure [163]. Thus it is not suitable for out-of-hospital hypertension monitoring [2].

In general, the intra-arterial BP and cuff-based BP are not based on the same physiological observation and measurement with different devices may not produce the same results [164]. A cuff-based system measures SBP at one cardiac cycle, and the DBP is measured at several cardiac cycles later. This problem is compounded by the PAT technique that gets a single PAT measurement (with PPG error), but usually means it is over several cardiac cycles. Hence PAT (SBP and DBP) is measured over an averaging window of say 15 seconds while the cuff is measuring SBP at one instance and then roughly 15 seconds later it measures DBP. Both methods are different, resulting in an error in the calibration process of PAT and BP. Therefore, instantaneous PAT was introduced through this research to minimize error during the calibration of PAT and BP. In these studies, the instantaneous PAT is referring to a delay time on a single pulse that was manually determined according to the value of SBP and DBP recorded from the oscillometric BP device. This method was compared with a mean of 15 beats PAT during the calibration process on volunteers. All the data were presented in the results section 5.3 (Chapter 5).

Next, the ***third contribution*** of this thesis proposed a one-step calibration method using a BP cuff oscillation waveform. The novelty of this method is because it required a single measurement of BP only using a cuff-based BP device for PAT calibration. In literature, multiple pairs of PAT and BP values were obtained during interventions that perturb BP such as bike exercise, valsalva manoeuvre, and cold pressor for constructing a calibration curve [165]. This procedure is time-consuming and not feasible in most situations [166]. In the proposed one-step calibration method, only one BP measurement using the cuff based BP device was required at the beginning of the experiment. This technique is more practical and straightforward to implement in daily practice. A study was conducted to investigate the accuracy between the one-step

calibrations and mean PAT calibration methods to estimate SBP during a tilt table experiment. The findings of this study are presented in section 5.4 (Chapter 5).

The ***fourth contribution*** of this thesis is towards the development of a tubular cardiovascular phantom system. The phantom system was developed to mimic the human blood circulatory system and to provide useful information on pulse delay time measurement. In the literature, most studies on pulse delay time measurement were carried out on human subjects. Many factors influence the pulse delay time measurements such as heart rate, arterial compliance, and age, thus making it difficult to validate this parameter on human subject.Therefore, it is important to have a phantom to perform pulse delay time simulations in a controlled environment. Through the phantom system, a simulation of pulse delay time under different conditions such as pulse pressure and pulse rate can be conducted within a controlled environment. In this thesis, a novelty of the developed phantom is a custom made chamber to simulate the delay time between two pulses with pulse pressure amplitude. The pressure at the outlet of the chamber increases with the increase of water level, thus increasing the amplitude of pulse pressure. It is expected that the delay time decreases with an increase in pulse pressure as theoretically suggested by Moens-Korteweg equation (Equation 2.1). The water level inside the chamber was controlled manually by opening and closing a stopcock located at the top of the chamber. A highly flexible tube was exploited to mimic the human blood vessel for pulse measurements. Through this system, a low perfusion signal can be generated to evaluate the limit of PPG sensor detection and its performance under these conditions. In conclusion, the innovation of the phantom system is a simpler and cost-effective design compared to others in the literature. The details of the design and the findings from the phantom simulation are presented in Chapter 4.

Chapter 3 Design and Development of Wearable PAT Device

3.1 Introduction

This chapter describes the process involved in designing and developing a wearable pulse arrival time (PAT) device for cuff-less blood pressure measurement. The PAT is determined based on the delay time between the R-peak of Electrocardiogram (ECG) signals and the peak of Photoplethysmogram (PPG) signals. In general, this development is divided into two parts; hardware and software. The hardware part is involved in designing electronic circuitry for PPG measurement and the software part involved in analysing the data using Matlab software. The system block diagram of wearable PAT device is shown in Figure 3.1:

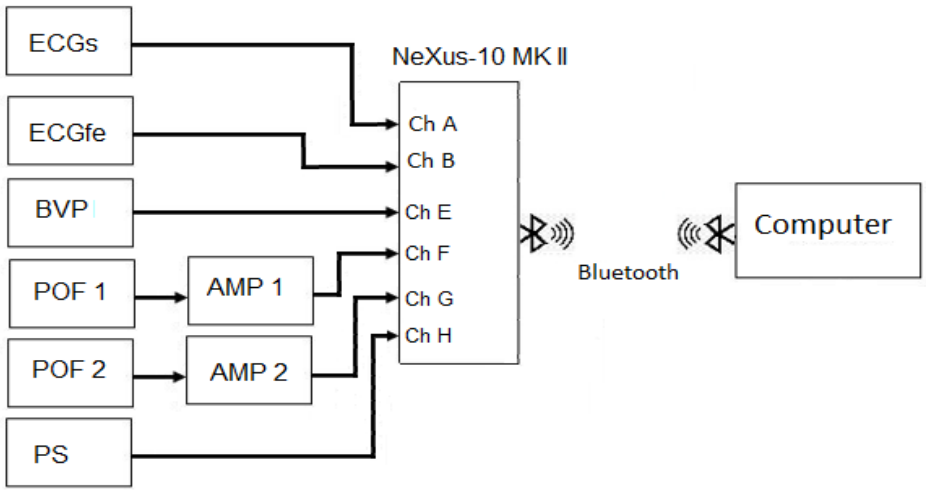


Figure 3.1: System block diagram of wearable PAT device

In Figure 3.1, ECGs represents ECG surface electrode, ECGfe represents ECG conductive fabrics electrode, BVP refers to blood volume pulse sensor, POF 1 refers to plastic optical fibre 1, POF 2 refers to plastic optical fibre 2, AMP 1 is an operational amplifier 1, AMP 2 is an operational amplifier 2 and PS refers to a pressure sensor for BP cuff oscillation measurement. All the signals were acquired by the data acquisition device, NeXus-10 Mark II. This device is a general purpose signal acquisition system for obtaining high-quality physiological measurements simultaneously.

As shown in Figure 3.1, six analogue inputs are connected to the NeXus device, through the input namely Ch A, Ch B, Ch E. Ch F, Ch G and Ch H with the Ch represent the Channel. ECGs connected to Ch A and ECGfe connected to Ch B for ECG measurement on the chest. BVP connected to Ch E for PPG measurement on the index finger (right arm). POF 1 and POF 2 were deployed for PPG measurement on the wrist and under the foot, respectively. These signals were amplified by AMP 1 and AMP 2 and then transferred to NeXus device by Ch F and Ch G respectively. The output from the PS for BP cuff oscillation measurement connected to Ch H. All these signals are converted to digital signals via 24 bits analogue to digital converter (ADC) built-in inside the Nexus device. The device synchronised all the signals and transferred to a Microsoft computer via Bluetooth. In the computer, BioTrace+ software is deployed for display and recording the signals. The PAT is computed and correlated with BP using Matlab software.

3.2 Development of POF for PPG Measurement

A POF probe was developed to measure PPG at the wrist and under the foot simultaneously. Four plastic optical fibres (DB-500(MY), Asahi Kasei) were used; two fibres for the transmitter and another two fibres for the receiver. The diameter of the fibre is 500 ± 23 um, and the core material is made of poly-methyl-methacrylate (PMMA). Figure 3.2 shows the design of POF probe for the PPG measurement.

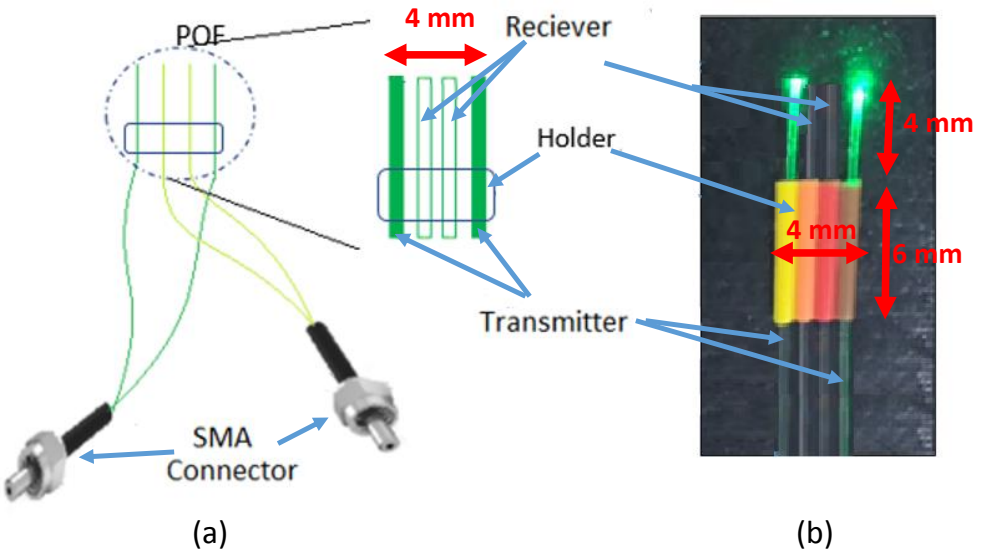


Figure 3.2: (a) Illustration of POF probe with SMA connector (b) Photograph of POF PPG probe

As shown in Figure 3.2 (b), the POFs were held together by a holder made from a flat ribbon cable. The pitch of the cable was 1 mm, and the internal cable diameter was 0.5 mm. The outer fibres (far left and far right) act as transmitters which transfer green light to the skin. The green light has been used as a light source because it has much greater absorptivity by blood vessel, resulting in a better signal-to-noise ratio compared to

red and infrared light for reflectance mode PPG measurement [90]. The two fibres in between the transmitters were the receivers, which received the reflected light from the skin. The distance between transmitters was 4 mm, with the gap between each fibre 1 mm. The subminiature assembly (SMA) connectors were used to couple the transmitter fibres to the light source and couple the receiver fibre to the phototransistor.

The POF PPG probe was placed in a flat position on the skin for the PPG measurement, as shown in Figure 3.3 (a). The tip of the fibres was cut to 45 degrees to transmit the light to the skin and to receive the reflected light. The tip angle (45 degrees) reflects the light laterally out or in through the side of the fibre, as shown in Figure 3.3 (b).

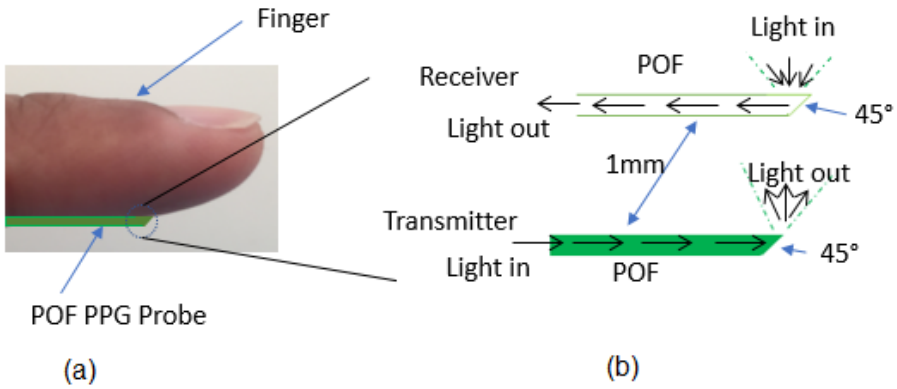


Figure 3.3: (a) The position of POF PPG probe under the finger, (b) The illustration of the light out at the 45-degree tip of the transmitter and the receiver fibre

The tip of the fibre was cut to 45 degrees using a sharp knife. A 45-degree triangle ruler was used to guide the cutting process. After that, the tip was polished using the polishing machine (DAP-5, Struers) as shown in Figure 3.4.

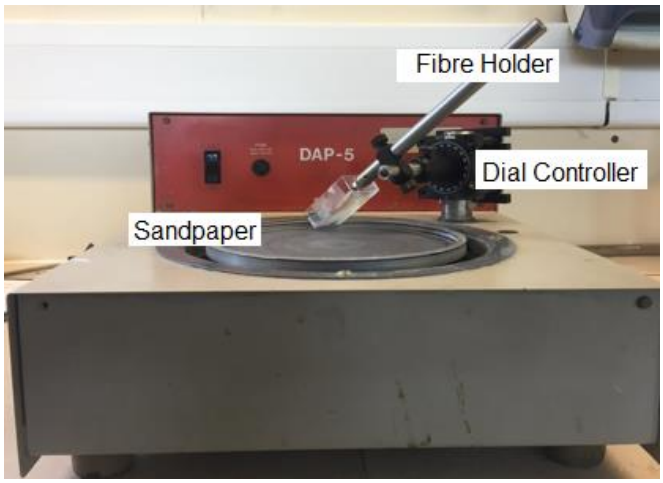


Figure 3.4: Polishing machine

The following steps operate the polishing machine to polish the tip of the fibre:

1. Setup the experiment, as shown in Figure 3.4.
2. Stick the fibre to the fibre holder using tape. The fibre tips should face towards the sandpaper (Grit 500).
3. Set the dial controller to 100 scale point (45 degrees).
4. Place a few drops of water on top of the sandpaper.
5. Switch ON the polish machine.
6. Gently press the holder towards the sandpaper and wait for 1 minute.
7. Switch OFF the machine and clean the tip of the fibre with water.

The polished fibre is ready to be used after this process.

3.2.1 Light Source: Green LEDs

A high powered green LED (LT W5SN-KYLY-25-0, Osram) was used as a light source for the reflection mode PPG measurement. In superficial tissue, light with wavelengths between 500 nm to 600 nm such as blue or green exhibits the largest modulation depth with pulsatile blood absorption, thus give a clear indication of blood volume change [167]. It has been suggested that the penetration depth of green light inside the skin at the wrist is deep enough to sense blood pulsations and is less influenced by the DC component of tissues [168]. The peak emission wavelength was 528nm, and the dimensions of the LED are 7.2mm x 6.2mm x 2.0mm. Table 3.1 shows the LED's electrical characteristic at T=25°C.

Table 3.1: Electrical characteristic of green LED

Characteristic Name	**Value**
Peak emission wavelength	528 nm
Forward current	100 mA (min) 700 mA (max)
Operating temperature	-40 °C to +125 °C
Forward voltage@ 700 mA	3.55 V
Luminous intensity	38.6 mcd

Thermal adhesive tape (Akasa, AK-TT12-80) was used to mount the LED with the heat sink. The purpose of the heat sink was to dissipate the heat emitted from the LEDs and to stabilize the LEDs' currents [169]. Figure 3.5 shows the attachment of the LED and the heat sink.

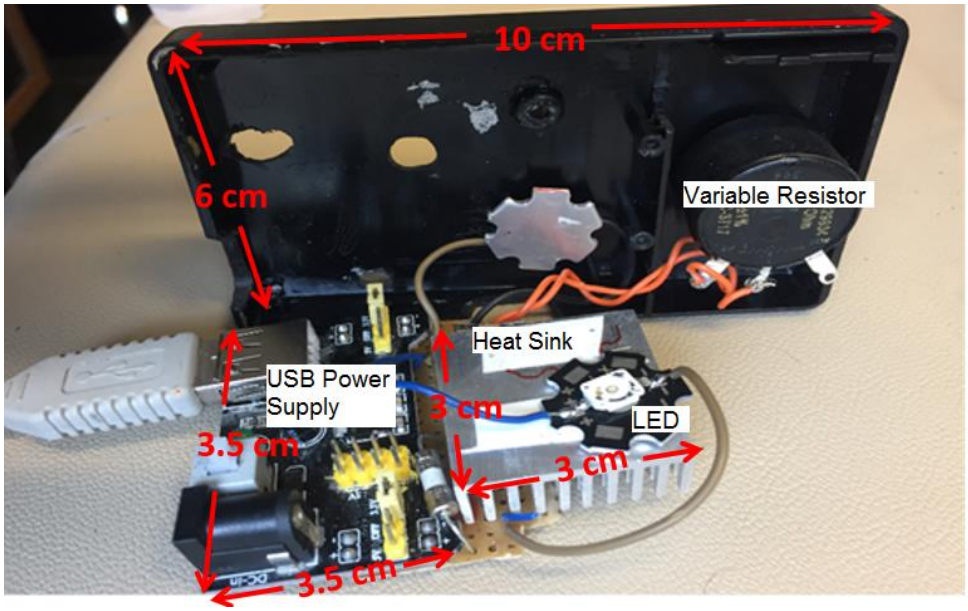


Figure 3.5: LED attached to the heat sink. The size of the main components is stated in the figure

The LED was driven by the circuit shown in Figure 3.6. The circuit consists of 5V supply voltage, a metal film fixed resistor 10Ω, ± 5% and 50Ω, ± 10% variable resistor (RS PRO, 1 Watt). The variable resistor was used to control the current, and the fixed resistor in series that limit the current if the variable resistor was turned to zero ohms.

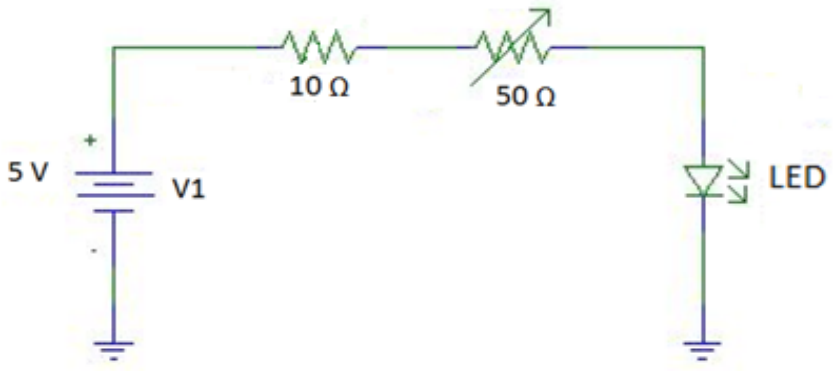


Figure 3.6: LED driver circuit

The variable resistance was varied between 0 Ω to 50 Ω to drive current between 98 mA to 500 mA (± 10%) to the LED. There is a mark on the variable resistor to make sure the resistance was varied within the range. When the potentiometer is accidentally set to zero ohms, then the fixed resistor limited the current to prevent the LED from burn out.

3.2.2 Photodetector Module

In this setup, the POF was deployed as a medium to transfer and receive light from the skin for PPG detection. The optical fibre are connected to the light source and photodetector via SMA fibre optic connectors (Amphenol Socapex). A photodetector module (TEMT-6000, Sparkfun) was used as an optical detector to measure the light coming from the skin delivered using optical fibre positioned 1 mm away from the light emitting fibre connected to the LED. The distance between the transmitting and the receiving light was set by the distance between the POF (Figure 3.1). The detection module consists of phototransistor (TEMT – 6000) and 10 kΩ surface mount resistor as shown in Figure 3.7. The supply voltage (VCC) for the module was 5V. The electrical characteristic of the phototransistor is shown in Table 3.2.

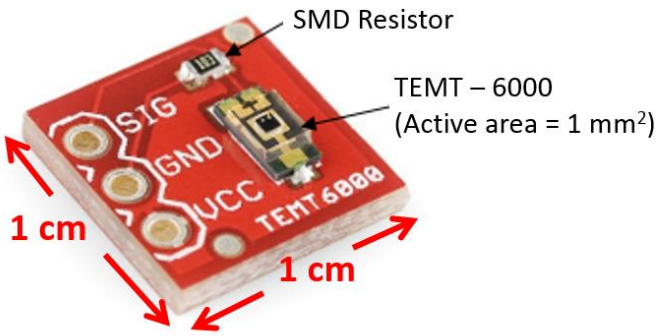


Figure 3.7: Phototransistor module for PPG measurement

Table 3.2: Electrical characteristic of phototransistor (TEMT 6000)

Characteristic Name	**Value**
The wavelength of Peak Sensitivity	570 nm
The range of spectral bandwidth	360 nm to 970 nm
Active area	1 mm^2
Power dissipation	100 mW
Collector-emitter voltage	6.0 V
Collector current	20 mA
Collector dark current	3 nA
Collector Light Current	10 uA (Ev = 20 lx) 50uA (Ev = 50 lx)
Operating temperature range	-40°C t o 100°C

The phototransistor (TEMT6000) was deployed to detect the photons passing out of the skin surface, and it was measured in illuminance (lx) unit. The wavelength for the peak sensitivity was 570 nm (green light). The sensor output was current, where the current increases with the increase in illuminance. The current was converted to a voltage by applying series resistors to the sensor output. This design is simple and

less complex compared to the current to voltage converter circuit in photodiode, thus the phototransistor is preferred for this project.

Generally, common collector or common emitter configuration was deployed to convert the current to voltage. The common emitter generates an output that moves from high voltage (5 V) state to low voltage state when the light is detected at the base. Meanwhile, the common collector generates an output that moves from the low state to high state when the light is detected at the base region. Figure 3.8 shows the schematic diagram for a common collector phototransistor circuit.

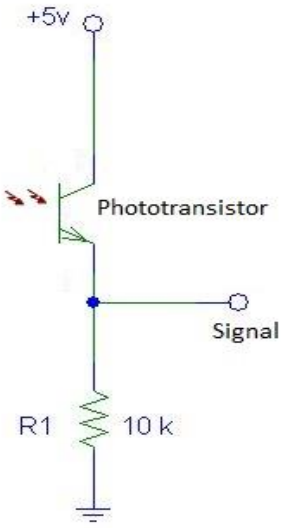


Figure 3.8: Schematic of common collector phototransistor circuit

The supply voltage for the phototransistor module was 5V. The phototransistor acts as an NPN transistor with the detection wavelength spectrum ranging from 360 nm – 970 nm. The base current (I_b) increased with the increase of light detected by the phototransistor, thus increasing the current that flows from collector to emitter (I_c). A 10kΩ resistance, R1 is connected in series with the signal output to convert the current to

voltage. According to Ohm's law, the voltage output, V_{out} increased with the increase in emitter current, I_e as stated in Equation 3.1

$$V_{out} = I_e R \qquad \text{Equation 3.1}$$

The output voltage V_{out} will be zero when there is no light, and then the voltage starts to increase as the level of light increases. This voltage output is transferred to the PPG amplifier circuit for further processing.

3.2.3 PPG Amplifier Circuit

In this project, the PPG amplifier circuit is designed according to the Pulse Sensor (SEN-11574) schematic diagram. The pulse sensor (SEN-11574) is a plug-and-play device and used for heartbeat detection [170]. The schematic for the PPG amplifier is shown in Figure 3.9. The amplifier filters and amplifies the photodetector output before being fed into the Nexus device. The first stage of the circuit was an RC low pass filter with a cut-off frequency of 3.8 Hz (R = 10 kΩ and C = 4.7 µF). A nominal PPG signal has frequencies lower than 4 Hz [171]. The bandwidth for the filter circuit is 3.8 Hz, so it can measure the pulse rate up to 3.8*60 = 228 bpm [172].

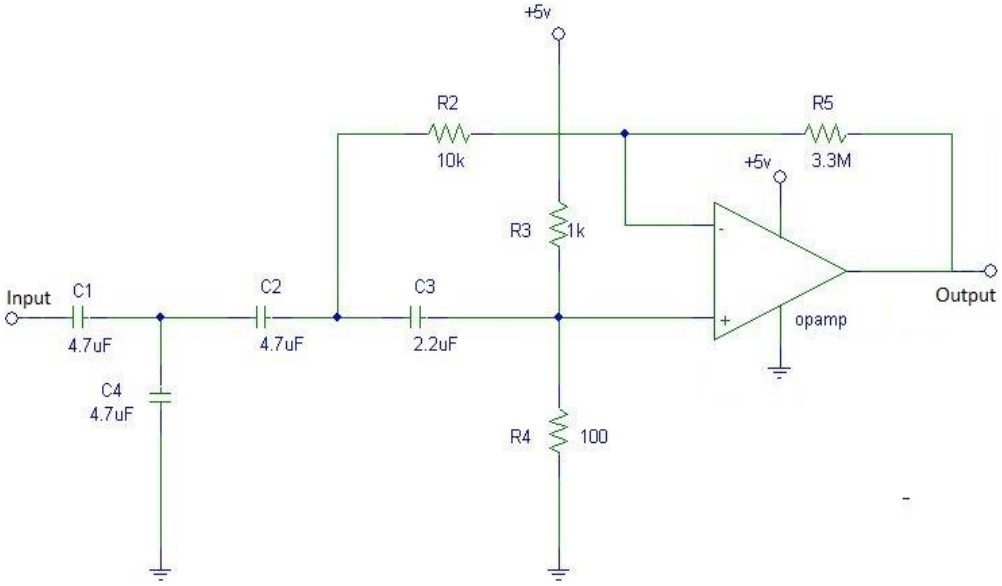


Figure 3.9: Schematic of PPG amplifier

The filter will remove the frequency above the cut-off frequency and smooth the signals for pulse detection. Operational Amplifier (Texas Instruments, LM358) was used to amplify the signal with the gain of 330 before it was converted to digital signals by the Nexus ADC device. Figure 3.10 shows the completed PPG circuit used on the project board.

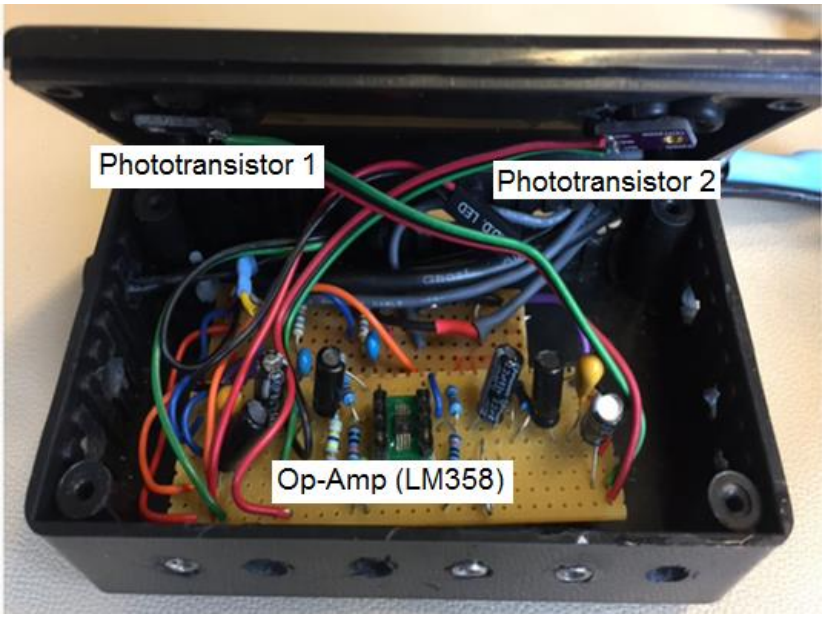


Figure 3.10: PPG amplifier circuit with soldering components on the project board. The casing size is 6 cm x 10 cm (length x width)

3.3 ECG Measurement

The ECG measurement was performed using two different types of electrodes, the surface electrode (ECGs) and conductive fabric electrode (ECGfe) as showed in Figure 3.11 (a). Both electrodes were placed on the right chest (negative electrode) and at the lower left rib (positive electrode). A differential recording was measured simultaneously using lead II of Einthoven's triangle which measures the signal between a negative electrode and a positive electrode [6]. Lead II is the most commonly used for electrode placement, as the QRS axis normally aligns with these leads [165]. Figure 3.11 (b) shows a typical view of lead II ECG waveform [173]. Basically, an ECG signal is a series of a P-wave, QRS complex, and a T-wave which represents the electrical activity of the four chambers of the heart. The P-wave indicates atrial depolarization,

the Q, R, and S-waves are usually considered as the QRS-complex, which stipulates ventricular depolarization and atrial repolarization and T-wave is caused by ventral repolarisation [173].

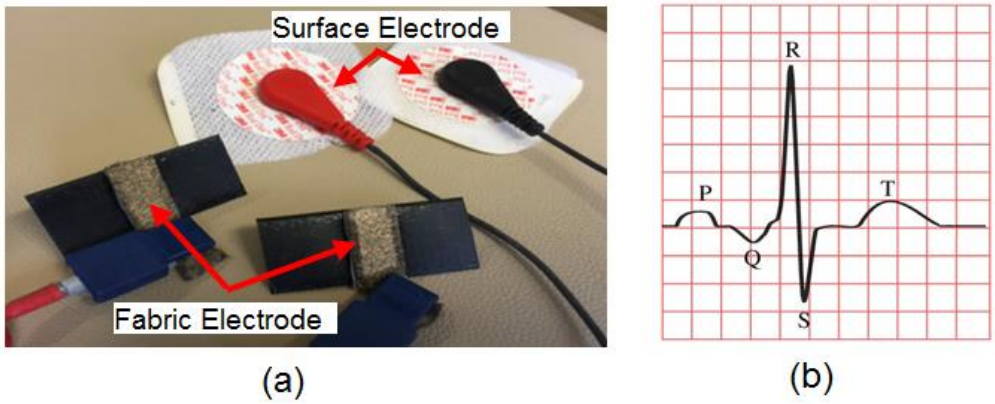


Figure 3.11: (a) The surface electrode and fabric electrode for ECG measurement, (b) Wave of typical lead II ECG signal [173]

In this research, the performance of the conductive fabric ECG electrode was evaluated and compared with the commercial ECG electrode (surface electrode). The purpose of using conductive fabric electrodes was to assess the feasibility of embedding them into a shirt for wearable textile-based ECG monitoring applications. The advantage of the fabric-based ECG electrodes are that they are free from electrode gel and there is more flexibility for the users to do their activity during the ECG measurement [174]. Before the experiment, the conductive fabric electrodes were moistened with tap water to reduce the skin-electrode impedance for biopotential measurement [175]. A chest strap was used to secure the conductive electrodes onto the chest to have good contact between the electrode and the skin. Practically, the chest strap is not convenient for the user to wear for a long time, but this technique has been deployed throughout the experiment.

3.4 BP Measurement

Blood pressure was measured on the upper left arm using a non-invasive blood pressure monitor (P2, OSTAR Meditech Corp.). The device is an automated sphygmomanometer that operates based on the oscillometric method for BP measurements [176]. The BP readings (systolic and diastolic) were displayed on an LCD screen with the pulse rate values. Figure 3.12 shows the BP monitor and the specification is listed in Table 3.3. In this research, the BP and the PAT were measured simultaneously, and the correlation between PAT and BP were investigated on volunteers during pedal bike exercises and tilt table experiments.



Figure 3.12: BP monitor (Ostar P2)

Table 3.3: Ostar BP monitor specification

Specifications	
Weight (Includes cuff and bags)	438 g
Dimension	200*140*70 mm
Pressure:	30~280 mmHg
Pulse:	40~200/seconds
Cuff (in the box)	24~32 cm

3.4.1 Evaluated Ostar BP Monitor using NIBP Analyser

The performance of the Ostar BP monitor was validated using a BP Analyser (CuffLink, Fluke) supplied by the Nottingham Queens Medical Centre, Clinical Engineering Department. In general, the analyser produced an oscillogram waveform that simulates systolic BP (SBP) and Diastolic BP (DBP) at fractions 50% and 67% of the mean BP (MBP) value [66]. The analyser is used in a clinical environment for ensuring the calibration of ward-based BP monitors during routine maintenance calibration [177]. The NIBP simulator output is very stable, thus the device was able to assess the measurement repeatability and reproducibility [66]. In this work, the performance of the Ostar BP monitor was assessed by the Cufflink analyser, and the measurement setup is shown in Figure 3.13.

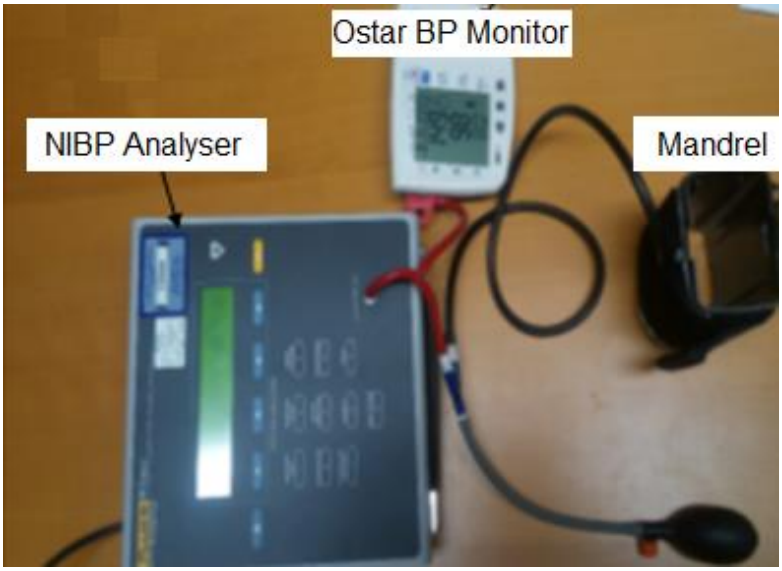


Figure 3.13: Measurement setup for NIBP analyser and BP monitor

The Ostar BP monitor was evaluated according to the following procedure:

1. First, wrap the mandrel with the BP cuff and insert the cuff adapter into the pressurized line as shown in Figure 3.13.
2. Set the analyser with desired BP values (Systolic/Diastolic)
3. Press the start button on the analyser
4. Record the measurement on the Ostar BP monitor screen.
5. Repeat the pressure measurement five times for each set of values.

All the recorded data are summarized in Table 3.4. The measurement of pressure ranged from low (80/50 mmHg) to high (200/150 mmHg) and followed the protocol proposed by Balestrieri et al. [66].

Table 3.4: Validation result on Ostar BP monitor

CuffLink SBP /DBP (mmHg)	**Ostar Mean SBP/DBP (mmHg)**	**Standard Deviation SBP/DBP (mmHg)**	**Mean Error SBP/DBP (%)**
80/50	81.4/52.0	0.6/2.0	1.8/4.0
100/65	102.0/68.0	0.7/0.7	2.0/4.6
120/80	122.4/84.4	0.9 /0.6	2.0/5.5
150/100	149.8/98.4	2.2/1.5	0.1/1.6
200/150	199.8/147.4	1.6/1.6	0.1/1.7

In Table 3.4, Cufflink SBP and Cufflink DBP refer to the BP setting value at the cufflink analyser. Five measurements were taken on the Ostar BP monitor for each setting. The mean value was determined, as shown by the Ostar Mean SBP and Ostar Mean DBP. The standard deviation and the mean error were calculated based on the measurement data. The results show that the maximum mean error was 2% for the SBP at 100

mmHg (row three, column four) and 120 mmHg (row four, column four). Meanwhile, the maximum mean error for DBP was 5.5% at 80 mmHg (row four, column four). Overall, the result showed that the Ostar BP device can provide consistent BP readings according to the simulating oscillations waveform provided by the CuffLink BP analyser.

3.4.2 Ostar BP Waveform Measurement using Pressure Sensor

In this research, the cuff pressure was measured along with ECG and PPG signals and synchronised by the Nexus device. The pressure inside the BP cuff was monitored by the Pressure sensor (MPX4250DP). A Y-tube connector was used to link the BP monitor with the BP cuff and the pressure sensor as shown in Figure 3.14.

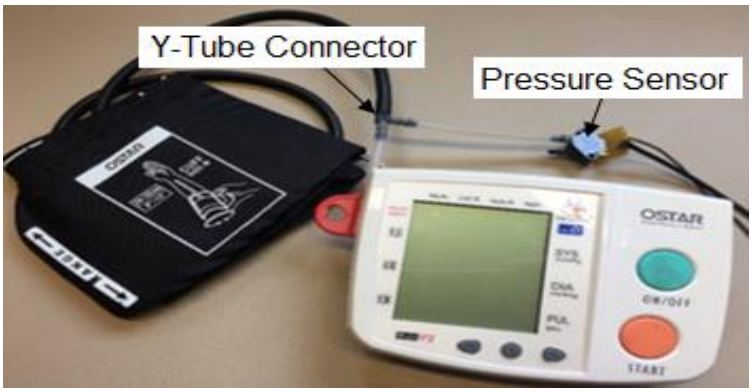


Figure 3.14: Ostar BP monitor with a pressure sensor

The pressure sensor measures the pressure inside the cuff and gives the output as voltage. The voltage was converted to the corresponding values in mmHg according to the equation provided in the pressure sensor (MPX 4250) datasheet as shown by Equation 3.2.

$$Vout = 0.0025P + 0.2 \quad \text{Equation 3.2}$$

where *Vout* is the voltage in volts and *P* is the pressure in mmHg unit. The cuff pressure waveform was usedas an indicator for mean and instantaneous PAT measurement. The PAT values were correlated with the BP reading from the Ostar BP device, and the relationship between PAT and BP was investigated on each volunteer during pedal exercise and a tilt table experiment. Moreover, the oscillation of the BP cuff pressure was used in a for one-step calibration technique to estimate the SBP.

3.5 Nexus-10 Mark II Data Acquisition Device

In this research, NeXus device (NeXus-10 Mark II, Mindmedia) was used for data acquisition to convert the analogue signal into digital and send it to the computer for further processing. The device has a built-in amplifier with very low input noise, very high input impedance and very high common mode rejection ratio. The device is battery-operated and can store data on an SDHC memory card. The real-time data can be transmitted to the computer via Bluetooth or USB connection. All the data measurement can be processed and recorded through application

software (BioTrace+) installed on the computer. Figure 3.15 shows the Nexus device with the connection input.

The size of the device (body only) is 120 mm X 140mm X 45 mm (length x width x height) and the weight is 500 gram (including battery pack).

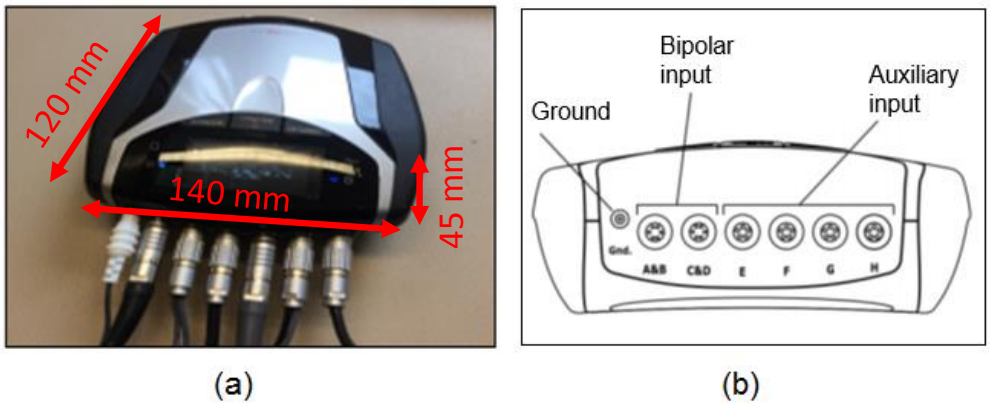


Figure 3.15: a) Nexus device (NeXus 10 Mark-II) b) Front channel view with input channels as per show in Figure 3.1

In general, the Nexus device has ten input channels for physiological measurement. It has 24-bit A-D converters per channel with data acquisition sampling rates up to 2048 samples per second. The first four channels (A&B, C&D) are bipolar channels that can be used for acquiring electrophysiological signals such as electroencephalogram (EEG), electrocardiogram (ECG), and electromyography (EMG). These channels have a built-in amplifier with a gain of 20. Thus an external active amplifier was not required for each electrophysiological measurement. The ground (reference) electrode is required to be connected with the patient, and its location depends on the application. This electrode was needed to keep the patient's potential and Nexus'

potential at about the same level to reduce the noise level. The specification for the bipolar channels is shown in Table 3.5.

Table 3.5: Bipolar channel specification

Item	**Values**
Typical noise level	≤ 0.8 μV rms (@ 256 SPS)
Gain	20
Input signal difference	< 0.1 V
Input common mode range	-2V to +2V
Input impedance	> 10^{12} Ω
CMRR	100 dB
Accuracy	± 2%
Connector	LEMO 6 pin

The second four channels (E, F, G and H) were called auxiliary input channels that can be used for respiration, blood volume pulse, skin temperature, and skin potential measurements. These channels include an instrumentation amplifier with a gain of 1. The output from the amplifier goes to the ADCs without any filtering. The remaining two channels were SpO_2 oximetry and the event synchronization channel which were located at the back of the device. The specification for the auxiliary channels is shown in Table 3.6.

Table 3.6: Auxiliary channel specification

Item	**Values**
Gain	1
Input signal difference	-2V to +2V
Input common mode range	-2V to +2V
Input impedance	> 10^{10} Ω
CMRR	100 dB
Accuracy	± 2%
Output voltage	+5 V, -5 V, max. 5 mA per channel
Connector	LEMO 6 pin

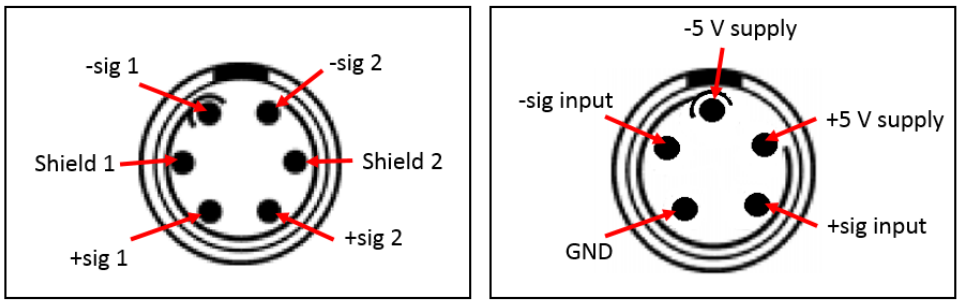
This device provides a platform for the researcher to simultaneously record various physiological signals for stress measurement [178]-[179], and measurement of muscle tension for obsessive-compulsive disorder (OCD) prediction [180]. In this research, The Nexus device was used to measure ECG, PPG and the pressure inside the BP cuff. Channel A was used for ECG measurement using surface electrodes, and Channel B was used for ECG measurement using conductive fabric electrodes. The ECG was measured according to lead II configuration. The positive and negative electrodes were connected to the Nexus device via NX1-EXG2- snap cable and the ground electrode connected to the Nexus device via NX-EXG-Ref1- snap cable. Figure 3.16 shows the cable used for the ECG measurement.



(a) (b)

Figure 3.16: ECG Measurement Cable (a) NX1-EXG2-snap cable (b) NX-EXG-Ref1-snap cable

As shown in Figure 3.16 (a), the Red snap cable represents a positive sign, and the Black snap cable represents a negative sign for ECG measurement. The red and black snaps marked with '1' will record data for Channel A, and the snap marked with '2' will record Channel B. The ground cable (NX-EXG-Ref1-Snap, Figure 3.16 (b)) is connected to the input marked 'Gnd' on the Nexus device. Meanwhile, a 5-pin Lemo connector (FGG.0B.305.CLAD52Z) was used for channel E, F, G and H. Figure 3.17 (a) and Figure 3.17 (b) shows the connector diagrams for 6-pins and 5-pins respectively.



(a) (b)

Figure 3.17: Lemo connector (a) 6-pins, (b) 5-pins

The signal from the phototransistor at the wrist and under the foot was amplified through the PPG amplifier circuits and connected to Channel E and Channel F respectively via 5-pins Lemo connectors. The phototransistor output connected to the +sig input pin and the ground connected to the -sig input and GND pin. The +5V supply pin was used as the power supply for the PPG amplifier circuit.

The PPG at the finger was measured by the Nexus BVP blood volume sensor (NX-BVP1A). This signal was monitored by Channel G and used to benchmark PPG measurement. The sensor used a finger clip is to secure the infra-red light source and photodetector for transmission mode PPG measurement. Principally, the infra-red light is transmitted through the tissues, then the light absorbed by the haemoglobin of the red blood cells and reflected by other tissues before reaching the photodetector that located opposite to the light source [90]. The amount of light detected by the photodetector is proportional to the relative volume of blood present in the tissue and this correspond to changes in the heart rate and blood flow. This sensor is sensitive to the hand movement and motion artefact; therefore the volunteers needed to stay still during the measurement.

Channel H was used to monitor pressure inside the BP cuff via differential pressure sensor (MPX4250). The output from the sensor connected to the Nexus device via a Lemo 5-pins connector. The +sig input pin was connected to the sensor output, and the -sig input and GND pin were connected to the sensor ground pin. At the top of the Lemo connector, there is a red dot to guide user attached the connector to the Nexus device. The connector attached to the Nexus device by pointing the red dot at the connector to the red dot at the Nexus device. The Nexus device can be connected to a computer via USB connection or Bluetooth. In this thesis, Bluetooth pairing was used to connect the device to a computer. The Bluetooth dongle was connected to the computer and the data

transferred wirelessly. BioTrace+ software was used to display and record the data from the six channel inputs in real-time for further processing. First, in the software environment, the *object* from the *object Toolbar* is placed on the grid screen. The object will graphically show the output of the sensor and is set according to the input channel requirements. The sample rates for each channel were set at 256 samples/seconds. The input signals for each channel and the specification for the signal range are shown in Table 3.7. The output signal will saturate at 0 volts if the input signal is over the signal range.

Table 3.7: List of input channels

Channel	**Measurement**	**Signal Range**
A	ECG (Fabrics electrode)	-100 mV to +100 mV
B	ECG (Surface electrode)	-100 mV to +100 mV
E	PPG at the wrist (Amplifier)	-2 V to +2V
F	PPG under foot (Amplifier)	-2 V to +2V
G	PPG at finger (BVP Sensor, Nexus)	-2 V to +2V
H	Cuff Pressure	-2 V to +2V

All the signals are displayed on the software (BioTrace+) screen in real time. The session overview and the real-time mode can be toggled by clicking button *session overview/real-time mode* on the software screen. The signals were recorded by clicking the *save* button. All the recorded signals were selected to be exported and saved to MATLAB format (.mat) for subsequent processing.

3.6 MATLAB Software for Signal Analysis

MATLAB software (R 2014b) was used to develop the programme for ECG and PPG peak detection and to determine the delay time between two signals. The algorithm used for peak detection is summarized in the flow chart as shown in Figure 3.18.

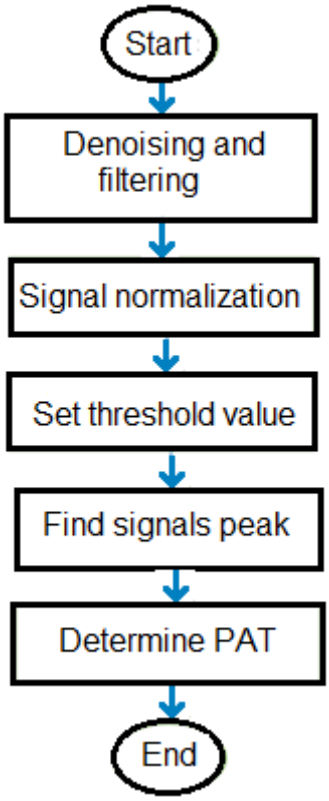


Figure 3.18: Flow Chart of the algorithm to detect signal peaks and determine PAT

3.6.1 Denoising and Filtering of ECG and PPG Signals

Firstly, the ECG and PPG signal recorded by the BioTrace+ software were imported to the Matlab environment. These signals are prone to noise such as from 50Hz power line interference and motion artefacts [181]. Generally, high frequency noise can be filtered out using a low pass filter, but cancellation of movement noise is hard to achieve [171]. The noise in ECG and PPG measurement distorts the signals shapes, and such distortion of the signals results in wrong diagnoses in peak detection. However, the quality of these signals can be improved by applying a denoising technique using a digital filter [182]. In this thesis, a linear phase FIR (Finite Impulse Response) filter is implemented using Matlab software to remove unwanted noise in PPG and ECG signals. The Matlab code used to filter the PPG signals is described below.

```
% Design lowpass filter using FIR for PPG signal
% convert Hz to rad/s = xhz*2/256
     lpFilt =
designfilt('lowpassfir','PassbandFrequency',0.03125, ...
         'StopbandFrequency',0.125,'PassbandRipple',0.5, ...
         'StopbandAttenuation',65,'DesignMethod','equiripple');
     Pcuffac= filtfilt(d1,PPGfwa);
 plot(timea,PPGfwa);
hold on
plot(timea,Pcuffac);
```

The ‘d1’ state in the above Matlab code refers to the FIR lowpass filter specification. Typically, the range of PPG signals is between 0.5 Hz to 4 Hz [183]. Therefore, the cut-off frequency of the filter is set to 4 Hz to remove the high frequency noise on the PPG signals. For the ECG signals, a bandpass FIR filter with pass band of 0.5 Hz to 40 Hz is implemented to attenuate noise contained in the signals [184]. A lower

cut-off frequency for the bandpass filter is set to 0.5 Hz corresponding to the lowest heart rate of 30 bpm and to remove the baseline wandering. The u pper band cut-off frequency is set to 40 Hz to remove unwanted high frequency noise and to suppress the power-line (50 Hz) interference. The Matlab code for this filter is similar to that applied to the PPG signal except for different choice of the cut-off frequencies. Figure 3.19 shows PPG and ECG signals after filtering.

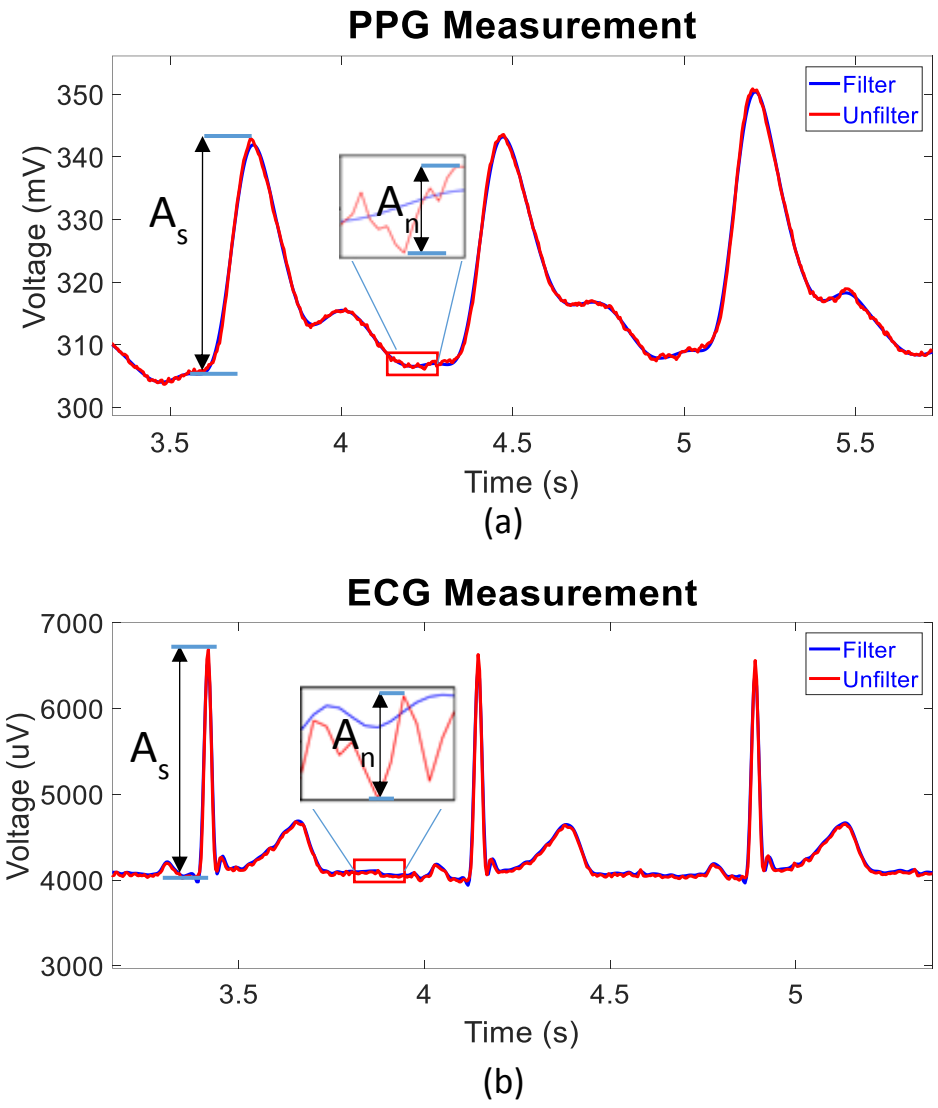


Figure 3.19: (a) Filtered and unfiltered (a) PPG signals (b) ECG signals

The results show that the filtered and unfiltered signal overlap each other, and there is no phase delay added to the filtered signals. As shown in the zoom section (A_n - noise), the filtered signal has a lower amplitude fluctuation at high frequency compared to unfiltered signals. The signal-to-noise ratio (SNR) is calculated to determine the signal strength relative to background noise:

$$SNR = 20\ log_{10} \frac{A_s}{A_n} \qquad \text{Equation 3.3}$$

where A_s is the peak to peak amplitude of the QRS-wave for ECG and the PPG and A_n is the noise defined by the peak to peak amplitude around the isoelectric region of ECG measurement [185] (Figure 3.19). The SNR of about 31.5 dB is obtained for unfiltered PPG signals and the SNR of 33.8 dB for unfiltered ECG signals. The SNR slightly improved after the filtering process with the SNR calculated for the PPG about 40.4 dB and the SNR for the ECG about 41.3 dB. These results indicate that the filtering process successfully removes some noise in the PPG and ECG signals and show better signal quality compared to unfiltered signals. Next, the amplitudes of these signals are normalized for graphical comparison and for peak signal detection.

3.6.2 Signal Normalization

The amplitude of filtered ECG and PPG signals are in different scales, therefore normalization is required. Matlab software is used to re-scale the amplitude of these signals from 0 to 1 using min-max normalization method [186]. In this method, the minimum value of the sample data is transformed into a 0, the maximum value is transformed into a 1, and every other value is transformed into a decimal between 0 and 1. The Matlab code to perform the normalization is stated as follows:

```
% Normalization of PPG signal
% applied min-max normalization method
time11=time1(mi:ma);
PPGwafn=PPGwafn_11;
maxVp=max(PPGwafn);
minVp=min(PPGwafn);
dp=maxVp-minVp;
PPGwafn_1=(PPGwafn-minVp)/dp;
figure
plot(time11,PPGwafn_1);
```

Figure 3.20 shows the ECG and PPG signals before and after applying the signal normalization.

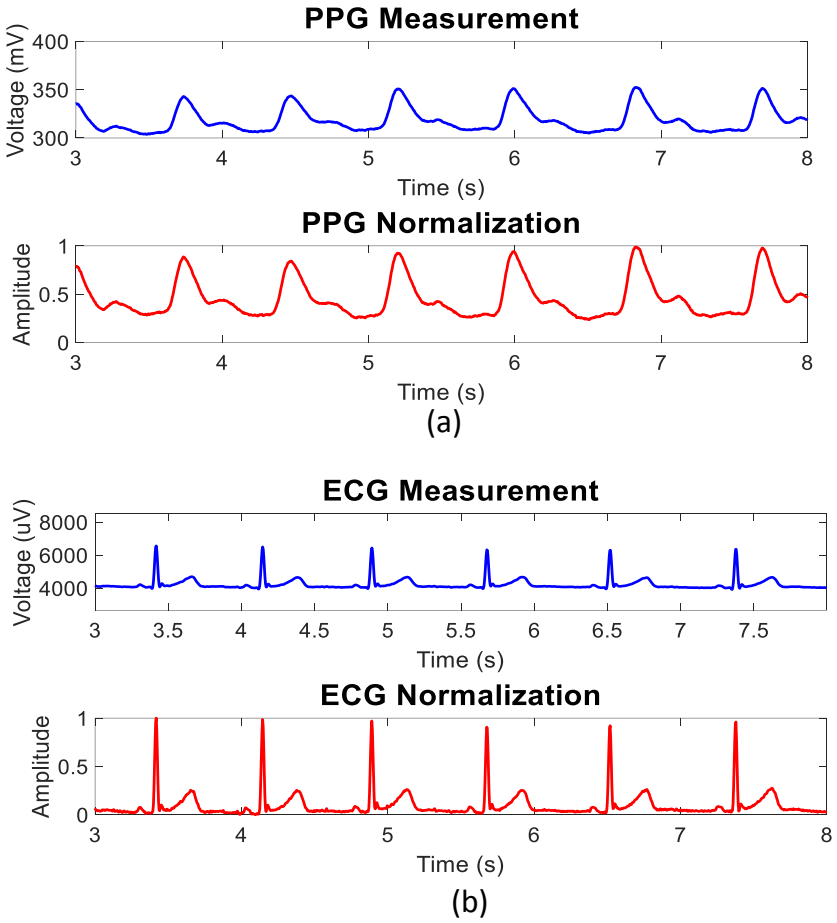


Figure 3.20: Normalization process (a) PPG signals (b) ECG signals

As shown in Figure 3.20, a linear transformation is performed on the original data and mapped within the interval values of 0 and 1. After the normalization process, the peak of the R-wave ECG and the peak of PPG signals were determined and the delay time between these two signal were calculated for PAT measurement.

3.6.3 Thresholding and Peak Detection Algorithm

Next, thresholding and peak detection algorithms were applied to the normalisation signals. The algorithm for peak detection was based on *findpeaks* function in the Matlab Signal Processing toolbox. The *findpeaks* determines the maximum point based on a data sample that was larger than its two neighbouring samples. If the peak was flat, the function returned only the point with the lowest index. A threshold level was set to make sure the maximum point detected referred to the peak of PPG and ECG signals. The algorithm to perform the thresholding and peak detection is stated as follows:

```
% PPG Peak detection algorithm based on findpeaks function
% Thresholding is set for more accurate peak detection
[pksPw,locsPw] =
findpeaks(PPGwafn_1,timea,'MinPeakDistance',0.4);
m4=1;
PPGwpeaks=[];
for i4=1:length(pksPw)
    if(pksPw(i4) > 0.5)
        PPGwpeaks(m4)=pksPw(i4);
        nlocsPw(m4)=locsPw(i4);
        m4=m4+1;
    end
end
```

The “findpeaks” function is used to detect the peaks in the signals and an additional input parameters “MinPeakDistance” is used to reduce the possibility of mistaken peaks by specifying a number of separation samples. Thresholding (Th) is used to limit the peaks detection by eliminated peaks that below the threshold value. The Th value for PPG

is set to 0.6 and for the ECG, the Th value is set to 0.5. Figure 3.21 shows the ECG and PPG signals after being passed through the thresholding and peak detection functions.

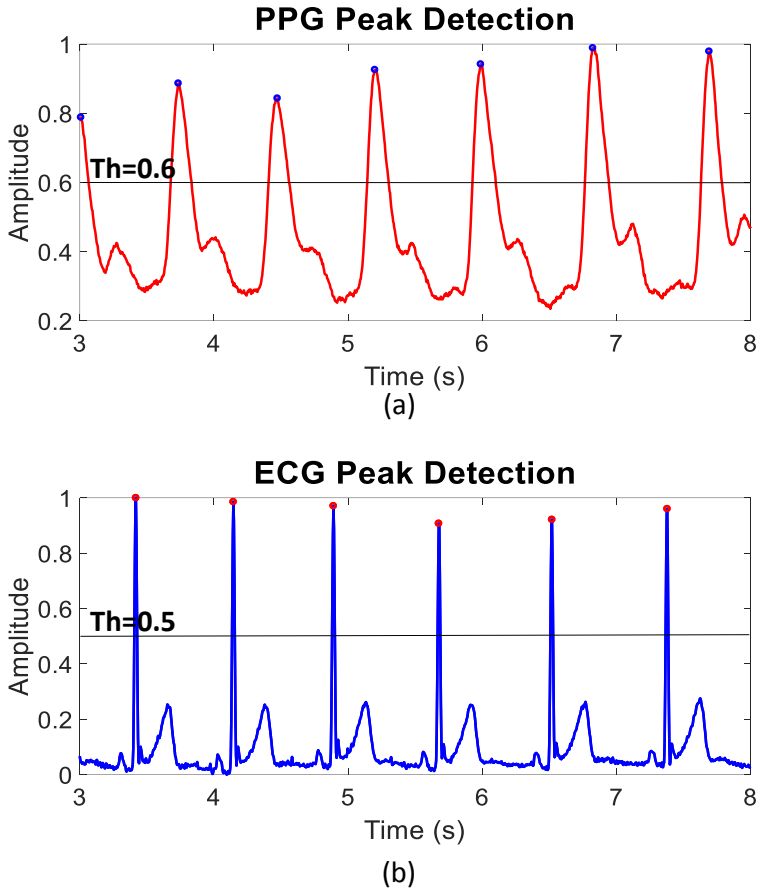


Figure 3.21: Thresholding and peak detection (a) PPG signals (b) ECG signals

As showed in Figure 3.21, the Matlab algorithm is able to detect the peaks of PPG and ECG signals and mark it with the blue and the red circles respectively. The peaks location for each signals were saved for further use in the PAT calculation.

3.6.4 PAT Calculation

The PPG and ECG signals were synchronized by the Nexus data acquisition device. The “pairs” between them were determine with the ECG is considered as a “reference” signal. The PAT is determined by subtracting the peak location of PPG with the peak location of the R-wave ECG in the same cardiac cycle. The Matlab code to determine the PAT as showed below and the graphical representation of the PAT definition is showed in Figure 3.22:

```
%Calculate PAT
%Check which signal is first before do subtraction
n11=2;
PAT=[];% PAT for ECGnexus-PPGnexus
for k=2:length(A1)-1
    if A2(k)<A3(k)
        PTT(k)=A3(k)-A2(k);
        PTT=PTT';
    else
     n11=n11+1;
    PAT1(n11)=A3(n11)-A2(k);
     PAT=PAT1';
        end
end
```

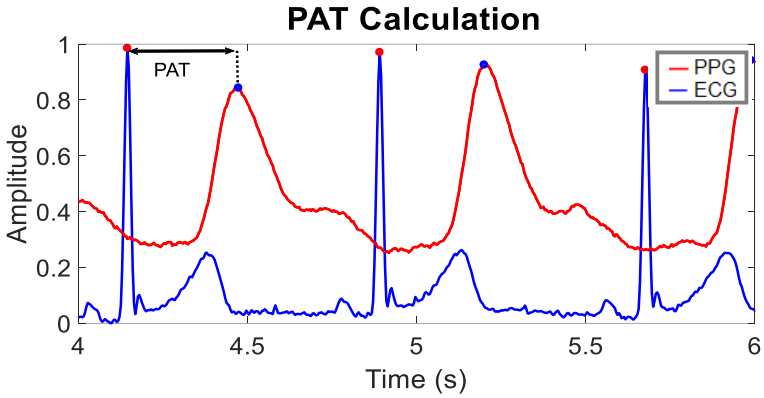


Figure 3.22: A graphical representative of PAT (the delay time is calculated from the peak of R-wave ECG signal to the peak of PPG signal in one cardiac cycle)

A manual check on these data was performed to ensure the peak is correctly located on each ECG and PPG signals. Some of the peaks were not properly detected especially on a corrupted signal due to motion artefact will be replaced by the interpolation data [187]. A linear interpolation method was applied to determine the missing peak by finding a mean between the peak values before and after the missing data. Next, a mean value of 15 “pair” of pulses are taken to represent a PAT corresponding to a BP reading. The PAT and BP values were stored in computer in excel format (.xls) for PAT calculation. The overall Matlab code is supplied in Appendix B2.

3.7 PAT Measurement System

The overall system for PAT measurement is shown in Figure 3.23. The system consists of a BP monitor, Nexus-10 MKII device, ECG fabric electrodes, ECG surface electrode, Light source box (green LED), power bank (5 V supply voltage), photodetector box (phototransistor and PPG amplifier circuit), POF probe and Nexus PPG finger probe.

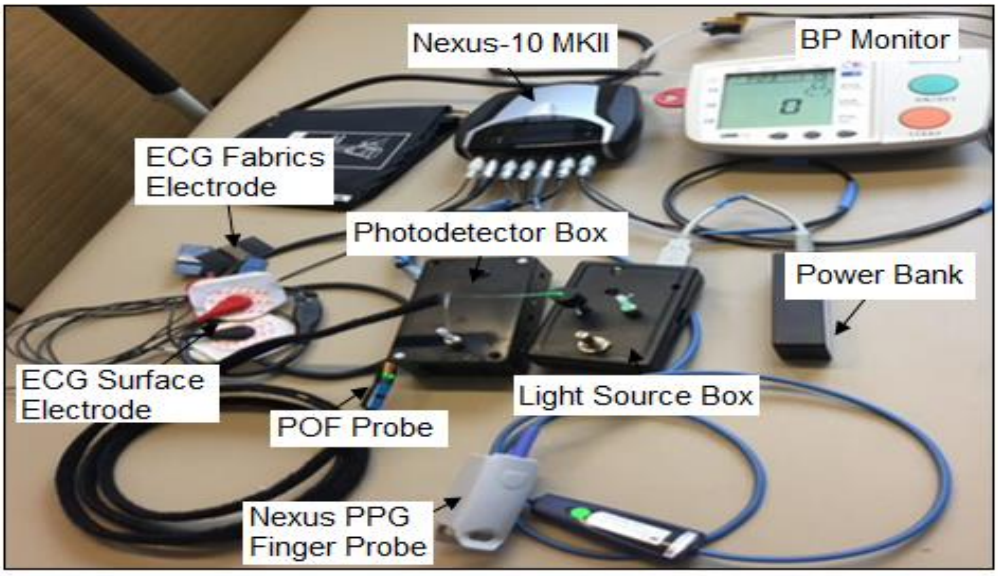


Figure 3.23: PAT measurement system

The PAT measurement system is used for pulse delay measurement in chapter 4. Next, the performance of this system is evaluated in a volunteer study involving bike exercise and tilt table experiment. The details of this experiment are described in Chapter 5.

3.8 Summary

This chapter provides information on the measurement setup for developing a wearable PAT measurement system. The first section described the development of a POF for PPG measurement. The details of the POF probe preparation were discussed, and the schematic diagram for the PPG circuit was presented. For the ECG measurement, surface type ECG electrodes and conductive fabric electrodes were used along with the Nexus device. The BP measurement was performed using an Ostar BP monitor. The performance of the BP monitor was validated using a Cufflink BP analyser, and the results showed that the Ostar BP monitor performance is consistent with the BP setting at the analyser. The pressure inside the cuff was measured by the external pressure sensor. The information from the pressure sensor was used to synchronize measurements between the BP and PAT for calibration purpose. All the signals from the sensors were connected to the Nexus device via Lemo connectors and the signals were displayed and stored on a specific channel by using BioTrace+ software. Matlab software was used to determine the peak of the PPG and ECG signals using the *findpeaks* function. The PAT was calculated based on the delayed time between the two signals. The last section of this chapter presented the overall system for PAT measurement and the performance of the system will be demonstrated in the Chapter 4 and Chapter 5.

Chapter 4 Development of Tubular Cardiovascular Pulse Delay Time Phantom System

4.1 Introduction

In this chapter, a tubular cardiovascular phantom system was developed to mimic the human blood circulatory system and to provide useful information on pulse delay time (PDT) measurement. The system was designed based on the Windkessel model representing arterial compliance [147]. The designed and fabricated model simulates the arterial compliance in a human system by controlling the amount of air and pressure inside a custom made chamber. A highly flexible tube was exploited to mimic the human blood vessel for pulse measurements using the previously described POF system. The flexible tube expanded with the corresponding volume change, thus increasing the light absorption and reducing the amount of reflected light detected by the photodiode [158]. In this experiment, the PDT measured by the two POF sensors were compared with the PDT measured by the two in-line pressure sensor for validation purposes. The PDT between the two optical detectors is to simulate the pulse transit time (PTT) for PPG to PPG measurement on human body. The details of the designed a tubular phantom system and the results of the findings from the experimental testing are presented in this chapter and demonstrate trends consistent with a human model.

4.2 The Design of a Tubular Cardiovascular Phantom System

Figure 4.1 illustrates a schematic of the designed tubular cardiovascular phantom system. The system consists of a diaphragm water pump (MO-PUMP-R385, China), two in-line pressure sensors (PS1 and PS2, PendoTECH, PREPS-N-025), two Plastic Optical Fibres (POF 1 and POF 2), a one-way valve and a rotary valve (RV, FCH-M-PP-LC, Bio-Tech). The pump circulates water from reservoir 2 to reservoir 1 and then back to reservoir 2. The operation of the pump is controlled by the relay (BB-RELAY-5V-02, China) and microcontroller (Arduino Mega 250) circuit. The pulse waveform is detected by the pressure sensors (PS1 and PS2) and the optical sensors (POF 1 and POF 2). The POFs are located under flexible tubes (FT, T4X0.5ST40, Polymax, UK). In this system, two delay time are determined based on the pulse detected by the two in-line pressure sensors (PS) and the plastic optical fibres (POF), respectively. The first PDT is between PS1 and PS2, and the second PDT is between POF1 and POF2. The flexible tube expands as the pulse wave travels through it. Clear water is used in this experiment to ensure the reflected light from the expanding upper wall tube can be detected by the receiving fibre.

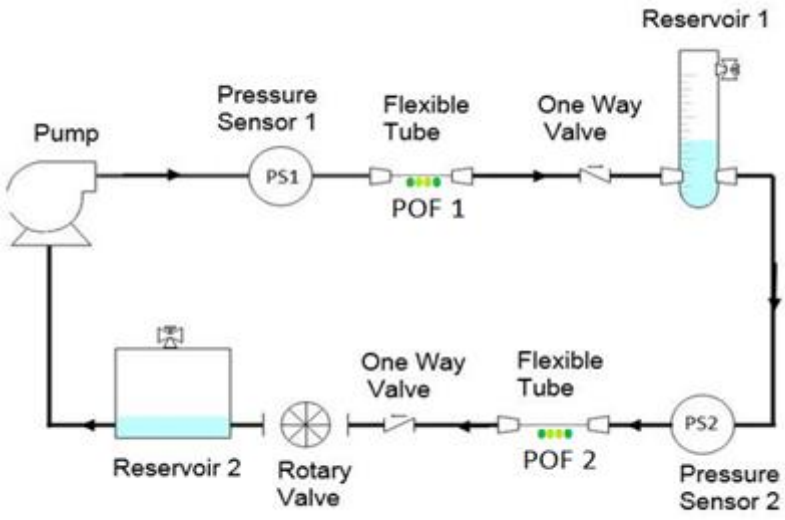


Figure 4.1: Schematic of the designed pulse delay time tubular cardiovascular phantom system

4.2.1 Water Pump

A diaphragm water pump is the heart of the system and works to circulate water around the phantom (Figure 4.1). The working voltage for the pump was in the range of 6 to 12 Volts with a maximum flow rate of 1.6 L/min. The pulse wave was generated by switching the pump ON and OFF via the relay circuit. A microcontroller was programmed in C++ language to trigger the relay for pulse wave modulation. The connection between the pump and the trigger circuit is shown in Figure 4.2.

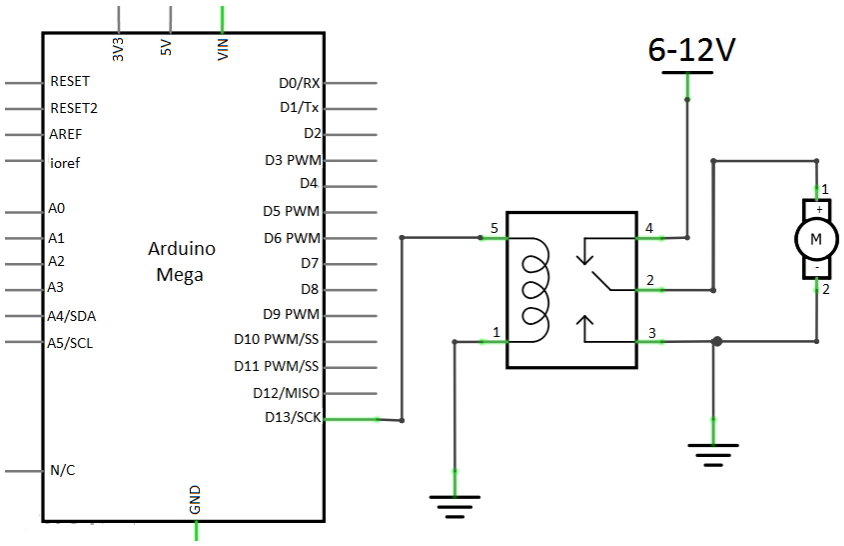


Figure 4.2: The pump and the trigger control circuit

A DC power supply (Tenma, 72-10505) and the pump were connected to the relay in a Normally Open (NO) configuration. The pump is connected to the power supply when the relay is activated and the power disconnects when the relay is inactive. The water is pushed out and flows through the system as the pump is operated.

4.2.2 PendoTECH pressure sensor

Two inline pressure sensors labelled PS1 and PS2 in Figure 4.1 were used to measure water pressure inside the tube. Figure 4.3 shows the pressure sensor with internal sensor illustration.

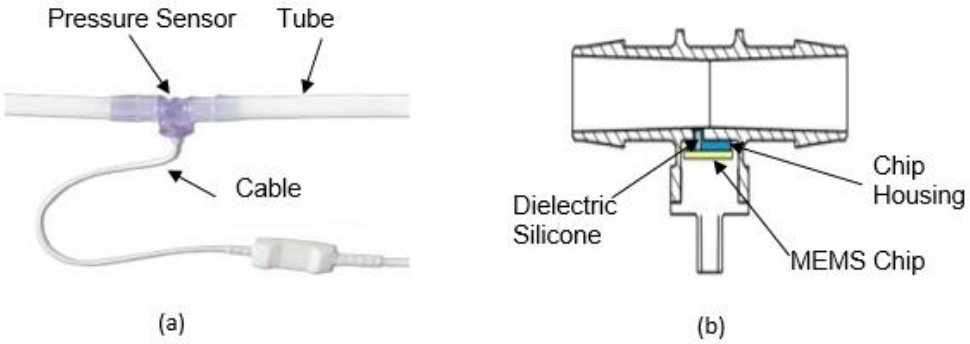


Figure 4.3: PendoTECH pressure sensor (PREPS-N-025); (a) Sensor attachment to the tube (b) Internal sensor illustration

In Figure 4.3 (a), a silicone tube (T4X1ST60, Polymax, UK) with an external diameter of 4 mm was connected to the pressure sensor. An electrical cable is attached to the electrical contact of the microelectromechanical system (MEMS) of the pressure sensor (MEMS-HAP^{TM}) chip and silicone layer and transfers the MEMS output signals to the external circuit. As shown in Figure 4.3 (b), a special material called “dielectric silicone” is used to isolate the fluid path from the electronics part and conveys pressure. A MEMS chip which includes a piezoresistive sensing element was embedded on the silicone substrate. The sensor is attached to the body of the polycarbonate tube via the chip housing. The water pressure applied to the sensing element in a Wheatstone bridge circuit induced an output voltage proportional to pressure [188]. The sensor generated an output of 0.2584mV/psi per volt excitation. The output voltage increases with an increase in excitation voltage. The detailed specifications of the sensor are shown in Table 4.1.

Table 4.1: Pressure sensor (PendoTECH, PREPS-N-025) specifications

Details	**Specifications**
Accuracy	+/- 2% of reading in the range of 0 to 6 psi; +/- 3% of reading in the range of 6 to 30 psi; +/- 5% of reading in the range of 30 to 60 psi
Pressure range	-7 to 75 psi
Operating temperature	2° C to 50° C
Storage temperature	-25° C to 65° C
Excitation voltage	2.5 to 10 volts DC
Connector	4 pin connector; signal +/- and excitation +/-
Sensor Output	0.2584 mV/psi/volt excitation
Wetted Materials	Polysulfone
Process Connection	1/4" Hose Barb

Figure 4.4 shows the pressure sensor connection between the pressure sensor and the difference amplifier circuit. The amount of pressure acting upon the sensor results in a change in resistance ± ∆R and it is proportional to the voltage across R1 and R2. The output voltage of the sensor was 0.2584 mV/psi per 5 Volt excitation voltage. The excitation voltage was set to 5 V as recommended by the manufacturer in the datasheet. The output voltage from the sensor was then amplified by a difference amplifier circuit using a single power supply AD820 operational amplifier (see Figure 4.4). The single op amp difference amplifier is a simple technique and well-suited for use with a Wheatstone bridge sensor.

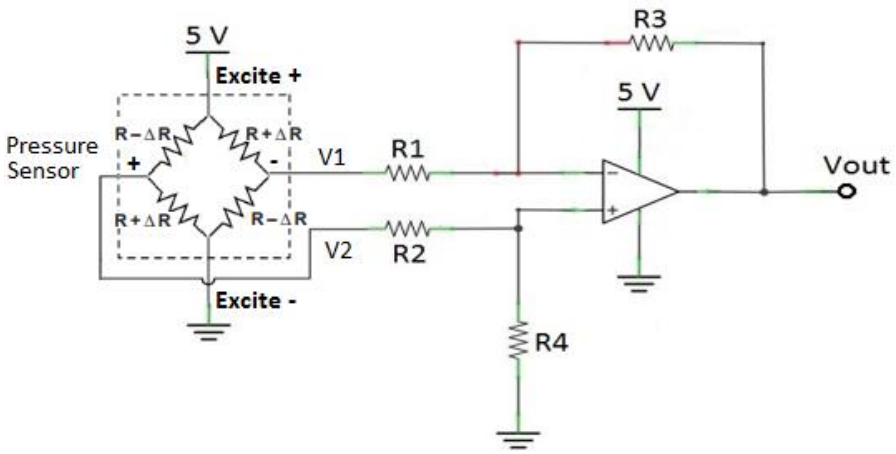


Figure 4.4: Pressure sensor and difference amplifier circuit

In Figure 4.4, the resistance R1= R2 = 470Ω ± 5% and the resistance for R3 = R4 = 470kΩ ± 5%. The gain and the voltage output (V_{out}) for the amplifier is calculated according to Equation 4.1 [189].

$$Vout = \frac{R3}{R1}(V2 - V1) \qquad \text{Equation 4.1}$$

Based on Equation 4.1, the difference voltage between two nodes (V1 and V2) was amplified by the gain of 1000. A calibration procedure was carried out to convert the output voltage into units of mmHg. Figure 4.5 shows the calibration setup.

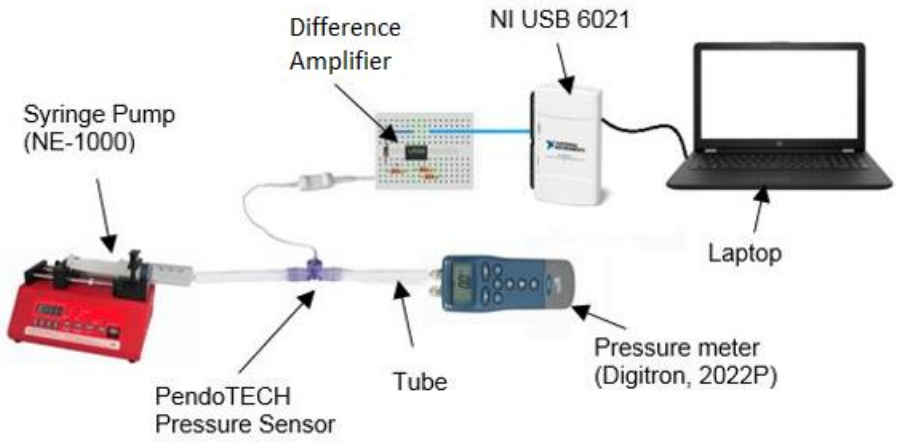


Figure 4.5: Calibration setup for PendoTech pressure sensor

In Figure 4.5, the PendoTech pressure sensor was placed in the middle of the piping between the syringe pump and a commercial pressure meter (Digitron 2022P). The flow rate for the syringe pump was set to 25ml/min and the volume was set to 2ml. The start button was pressed and held for 10 seconds (manually) to start the operation. The air flow from the syringe was transferred to the pressure sensor and then to the pressure meter via the silicone tube having an internal diameter (ID) = 4mm. The voltage output from the PendoTech pressure sensor is amplified by the difference amplifier and then transferred to a computer via a data acquisition card (National Instruments USB 6021). Simultaneously, the air pressure in the piping was monitored by the pressure meter (Digitron, 2022P). The measurements were recorded by Labview software, and a graph of voltage (V) versus pressure (mmHg) was plotted as shown in Figure 4.6.

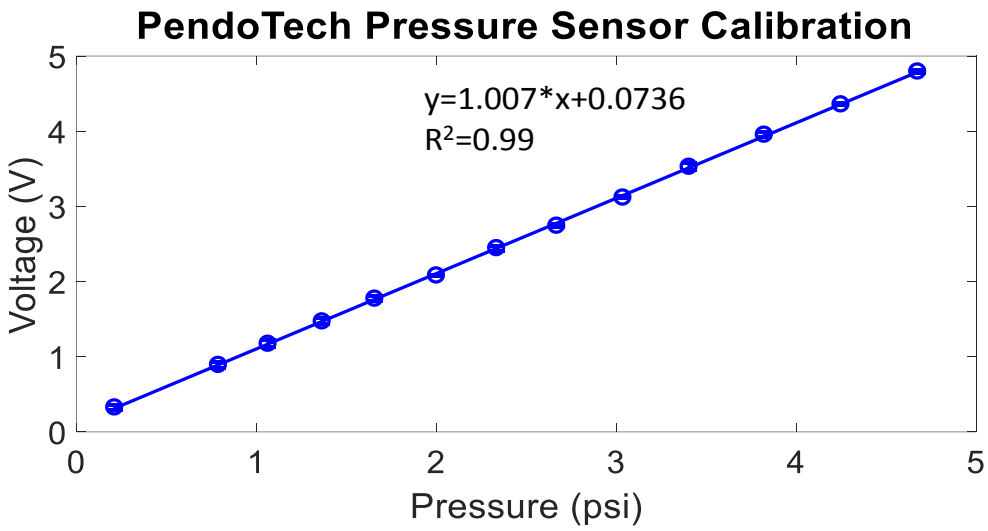


Figure 4.6: The response of PendoTech pressure sensor. Note that the error bars are smaller than the size of the symbols

As shown in Figure 4.6, the Y-axis represents the voltage (V) detected by the pressure sensor, and the X-axis represents the pressure monitored by the pressure meter in psi units. The measurement was repeated twice, and the repeatability of the result was very high with standard deviation near to zero (Figure 4.6). The best linear fit was applied to the data points and the equation was generated as shown by Equation 4.2.

$$y = 1.007 * x + 0.0736 \qquad \text{Equation 4.2}$$

where *y* is the voltage in volts and *x* is the pressure in psi units. This equation was used to convert voltage to pressure in psi units. The psi unit is then converted to mmHg by multiplying the *x* value (psi) with 51.71 mmHg [190]. The pulse generated by the relay circuit (see Fig 4.2)

triggered the pump to switch ‘ON’ and ‘OFF’. The pump switches ‘ON’ when it is connected to the supply voltage and switches ‘OFF’ when disconnected from the power. The relay module was active low, thus the pump switched ‘ON’ when the relay was activated. The timing specification is shown in Table 4.2. Figure 4.7 shows the response of pulse pressure according to duty cycle.

Table 4.2: The pulse timing specification

Duty Cycle (%DC)	Timing Specifications		
	Positive Pulse Width (t_high) (ms)	**Negative Pulse Width (t_low) (ms)**	**Total Pulse Duration, T (ms)**
90	900	100	1000
80	800	200	1000
60	600	400	1000

A duty cycle is commonly expressed as a percentage of a pulse width (positive pulse) over the total pulse duration [191]:

$$\%DC = \frac{t_high}{t_{_high} + t_low} \qquad \text{Equation 4.3}$$

where *%DC* is a duty cycle percentage, *t_high* is positive pulse width, and the t_low is negative pulse width

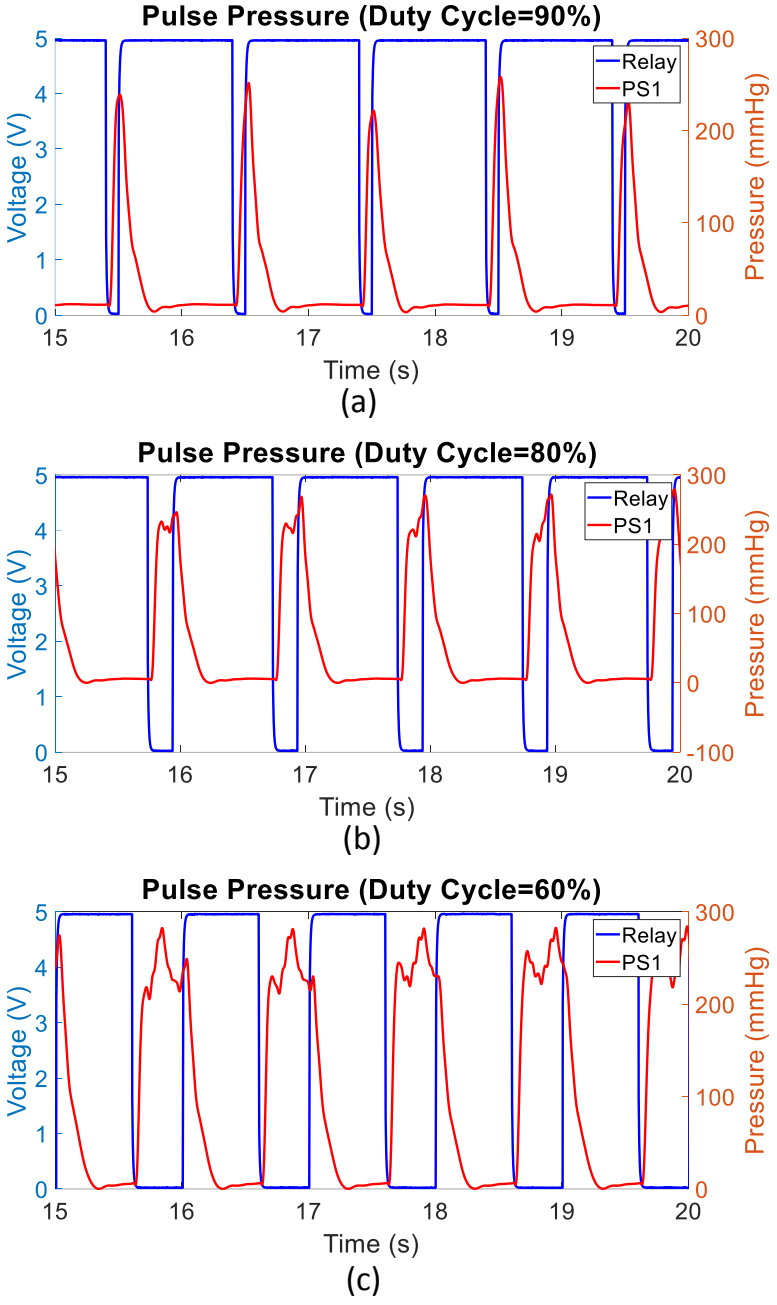


Figure 4.7: The response of pulse pressure measured by the pressure sensor 1 (PS1) according to the setting (a) The duty cycle = 90%, (b) The duty cycle = 80% and (c) The duty cycle = 60%

A microcontroller generated a pulse waveform (blue trace) that triggers the relay circuit and operates the diaphragm pump. The pulse waveform is represented by voltage, where 5 V is for high pulse and 0 V is for low pulse (Y-axis, left scale). A volume of water pushed by the pump and circulated inside the tubing is detected by the pressure sensor 1 (PS1) as shown by the red trace in mmHg unit (Y-scale, right scale)

As shown in Figure 4.7, the effect of the relay signal (blue trace) triggering the pulse pressure (red trace) is observed at the pressure sensor 1 (PS1). The relay output in voltage varies from 0 to 5 Volts, and the PS1 scale is in mmHg and varies from 0 to 200 mmHg. The power supply and the pump were connected to the relay with Normally Open (NO) contact, thus the pump operated (ON) when it receives an active low signal from the microcontroller (Figure 4.7). From the result, one can see that the shape of the pulse pressure follows the pattern of liquid flow. For example, the pulse pressure increases sharply and fluctuates as the water flows through the tube. The pressure then gradually decreases as the water stops flowing. The pulse pressure waveform at 90% of the duty cycle is compared to PPG signals as showed in Figure 4.8.

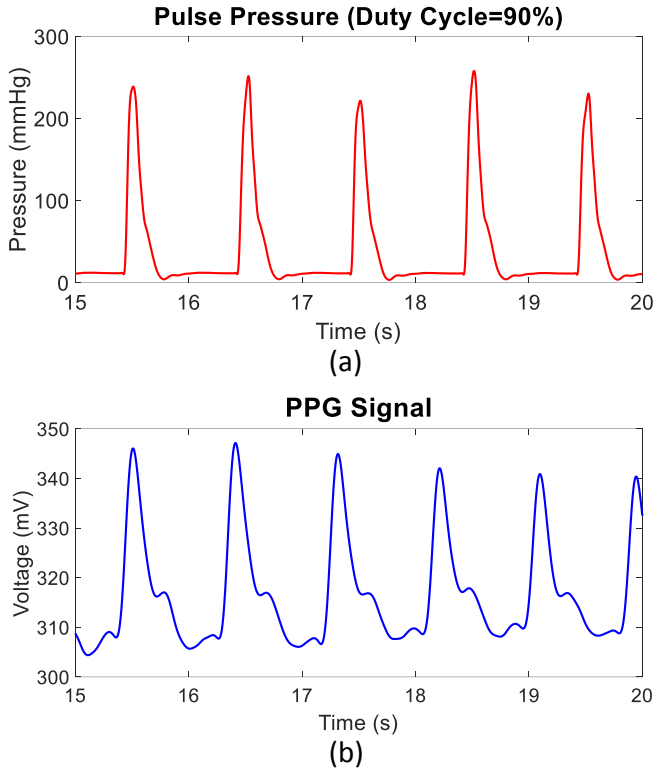


Figure 4.8: (a) Pulse pressure signal when the duty cycle is set to 90%,(b) A typical PPG signal measured at the wrist

As can be seen, the shape of pulse pressure is similar to the PPG shape (sharp peak with a broad base) when the duty cycle is set to 90%. The peak of the pulse pressure detected by the PS1 becomes more fluctuating and wider when the duty cycle decreases from 90% to 60%. As a result, the duty cycle was set to 90% to generate the required pulse pressure throughout these tests. In order to control the relay, a microcontroller (Arduino Mega 2560) was programmed to control the relay circuit (Figure 4.2) and was programmed in C++ language. The code is supplied in Appendix B1.

4.2.3 Reservoir 1

Reservoir 1 was made from a modified syringe as shown in Figure 4.9 (a) and the illustration diagram of reservoir 1 is shown in Figure 4.9 (b). The function of reservoir 1 was to implement the Windkessel model in order to represent the human circulatory system [192] but also to buffer the pulse pressure from PS1 to PS2. According to the Windkessel analogy, the elastic arteries (aorta) can be represented by a chamber filled with water and a pocket of air [192]. In this experiment, reservoir 1 represents the vessel dimensions and the air within the chamber represents the vessel elasticity, or a 'Windkessel' compliance. As it is pumped, the water compresses the air, which in turn pushes the water out of the chamber.

In addition, the pressure at the outlet of reservoir 1 increases with the increase of water level, thus increasing the amplitude of pulse pressure. Low arterial compliance was simulated by decreasing the amount of air and pressure inside the chamber. The pulse pressure is increased when compliance is reduced. Theoretically, the compliance is referred to the elasticity and extensibility of the structure, and is determined by dividing the change in volume with the change in pressure [193]. In the human body, the wall of the compliant aorta expands to accommodate the increase in blood volume. The compliance decreases with stiffening of the arterial wall, thus increasing the BP [194].

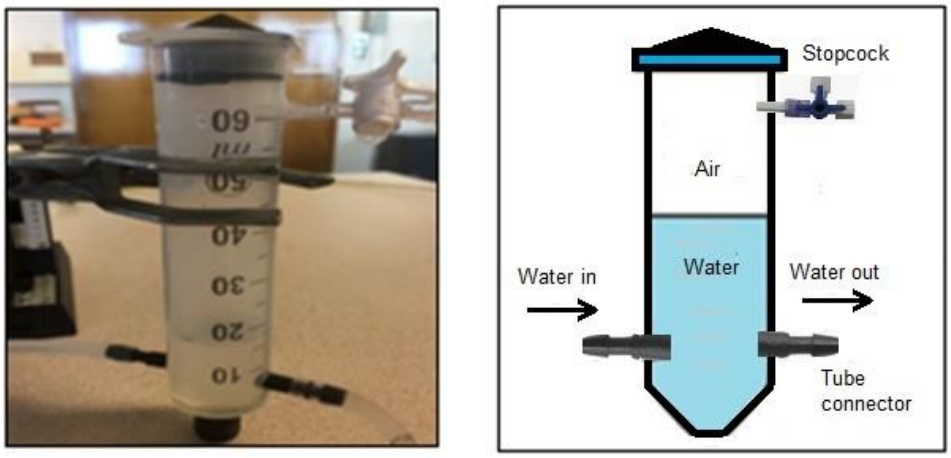


Figure 4.9: (a) The design of reservoir 1, (b) Illustration diagram of reservoir 1

The water level inside reservoir 1 was controlled manually by opening and closing the stopcock. As shown in Figure 4.9 (b), a 3-way stopcock (B. Braun Medical Inc.) was located at the top of the reservoir and acted like a valve that connects ambient air to the reservoir. The water level increases when the stopcock is open due to the low pressure created inside the reservoir. When the stopcock is in the closed position (closing the air path to the reservoir) both the pressure and water level are maintained inside the reservoir. A pulse wave flows from the silicone tube through the reservoir via a tube connector (ID = 4 mm) and then out the other side.

4.2.4 One Way Valve

A one-way valve was placed between the pressure sensor PS1 and the reservoir 1. This valve is used to allow the water to flow through it in only one direction. Figure 4.10 (a) and Figure 4.10 (b) shows the one-way valve and its internal schematic diagram, respectively.

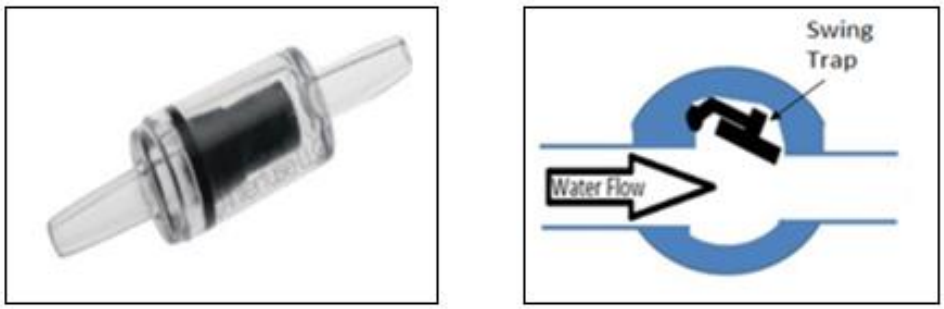


Figure 4.10: (a) One-way valve (b) Schematic illustration of the internal structure of one-way valve. The valve size is 53 mm x 15 mm (length x width), and the valve is compatible with a tube of 4 mm inner diameter

As shown in Figure 4.10 (b), there is a swing trap (shaded black) that covers the flow pathway internally. The swing is open when the water pushes forward, but it will close when there is either no flow of water through it from left to right or the water flow direction reverses. The closed condition will prevent water from flowing back to both the pressure sensor and the pump (Figure 4.1). The second one way-wave is located at the end of tube (just before the rotary valve in Figure 4.1) to produce a high resistance point. The resistance value affects the decay time of the pulse wave whilst mimicking the moment of reaching the diastole phase.

4.2.5 Flexible Silicone Tube

In the phantom system, the brachial artery was modelled by the silicon tube with a diameter of 4 mm (T4X0.5ST40, Polymax, UK). A typical range for brachial artery diameter is from 2.9 mm to 5.6 mm [195]. The wall thickness of the silicone tube is 0.4 mm, give the tube flexibility to inflate and deflate in representing the movement of a pulsatile waveform. An experiment was carried out to determine the expansion of the flexible tube under static pressure. Figure 4.11 shows the experimental setup for the measurement.

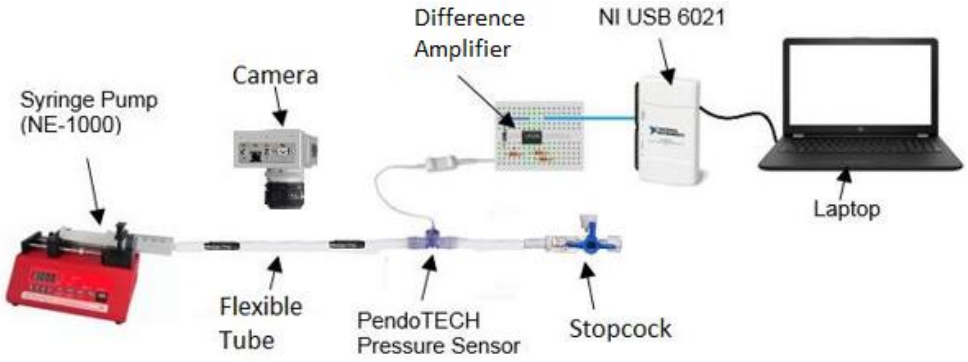


Figure 4.11: Experiment Setup for tube flexibility measurement

As shown in Figure 4.11, the flexible tube was connected to the harder silicone tube via a 4 mm tube pipe connector. The syringe pump was used to push water into the flexible tube. The pressure inside the tube was measured with a pressure sensor (PendoTECH, PREPS-N-025). The stopcock was used to hold the water inside the tube and to maintain the basal pressure. The expansion of the tube due to the increase of static pressure was monitored by an Optronis CL600x2 camera. Table 4.3 shows the important features of the camera.

Table 4.3. The high-speed camera Optronis CL600x2 specification

Resolution (max.)	1280 x 1024 pixel
The frame rate for max. resolution	500 fps
Image Sensor	Progressive scan CMOS
Exposure time	≥ 1μs
Pixel Size	14 μm x14 μm
Dimensions	56 mm x 56 mm x 44 mm

The camera was located above the flexible tube positioned a distance of 5 cm away. An Xcelera-CL PX4 frame grabber was used to acquire the image and transfer the image to a computer. The focal lens for the camera was adjusted until a sharp image appeared on the computer screen. An image of the flexible tube, holding a certain amount of pressure was captured during the measurement. Post processing was carried out on the acquired image to determine the new outer diameter of the tubing with the applied pressure. Figure 4.12 shows the initial condition of the flexible tube before being pressurized.

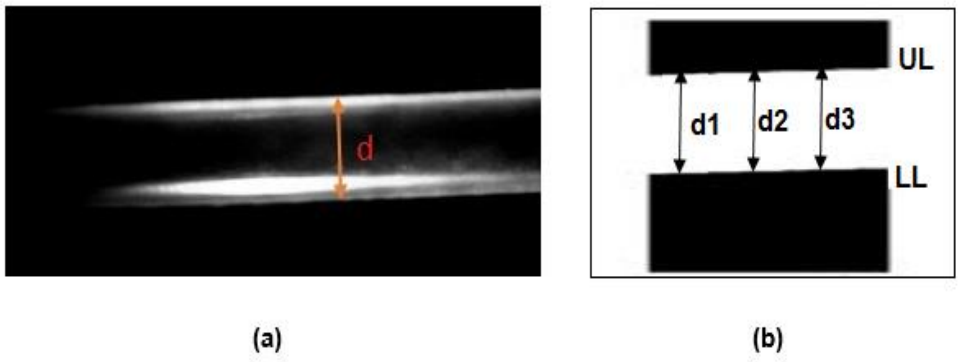


Figure 4.12: Image of a flexible tube filled with water (a) Initial tube condition (b) Region of interest for tube expansion calculation between the upper line (UL) and lower line (LL). d1, d2 d3 are the distances between UL and LL at specific positions to calculate tube's diameter

The software environment, Matlab (R 2014b), was used to analyse the acquired images. First, the image was converted to a binary image (black '0' and white '1'). Then, a specific region on the image was selected, and the internal area of the tube was replaced by white colour, as shown in Figure 4.12(b). The distance between two boundaries (upper and lower line) was calculated according to the total number of white pixels '1' in a specific row (d1, d2 and d3). The mean of the total number of pixels at positions d1, d2 and d3 were calculated and converted to millimetres (mm) by assuming a linear relationship between the number of pixels and distance. A technique using a high-speed camera for tube wall displacement measurement has been demonstrated by Lillie et al. [149] and the result shows that the tube expansion and the static pressure are linearly related. Figure 4.13 shows the results of tube diameter expansions under varying water pressure for two different wall thicknesses (WT) of 0.4 mm and 1 mm.

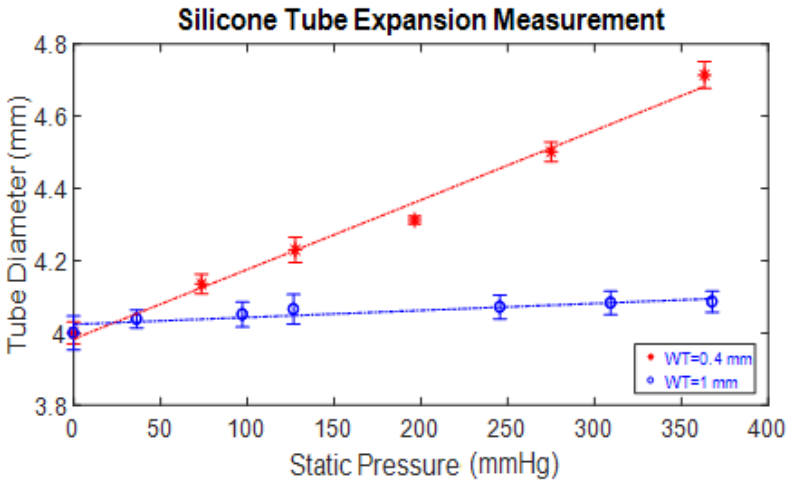


Figure 4.13: Flexible tube expansion measurement with static water pressure for two different wall thicknesses (WT). The error bar represents the standard deviation at three different tube positions while converting the mean number of pixels to the distance

The Y-axis represents the tube expansion in mm, and the X-axis represents the static water pressure measured in mmHg. One can see that the flexible tube with WT of 0.4 mm expanded greater than the tube with a WT of 1 mm. For example, the tube with a 0.4 mm WT expanded up to 4.56 mm (14 %) from its initial state (4 mm) with an applied pressure of 300 mmHg. However, the tube with WT of 1 mm expanded only to 4.08 mm (2 %) from its initial state (4 mm) with the same applied pressure. To put this into context, in the literature (Stubán et al. [156]), it has been noted that a human arterial diameter between diastolic and systolic points can change by about 8 % to 15 %. Therefore, in this study, a highly flexible tube with a wall thickness (WT) of 0.4 mm was deployed to model an artery for pulse wave measurement using optical sensors.

4.2.6 Resistance (Rotary valve)

A rotary valve (FCH-M-PP-LC, Bio-Tech) was placed at the end of the PAT tubular phantom system (Figure 4.1) to produce a high resistance point. According to the two-element Windkessel model, the exponential decay time depends on the product of peripheral resistance, R, and total arterial compliance, Co (the RCo time) [196]. Based on this, the decay time will, of course, be longer with higher resistance. The rotary valve is shown in both photographic form and schematic cross section in Figure 4.14 (a) and Figure 4.14 (b) respectively.

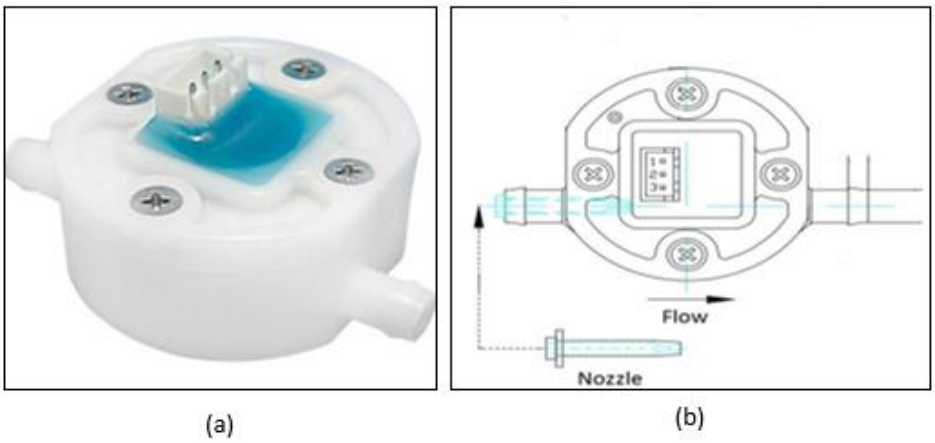


Figure 4.14: (a) Rotary valve deployed in Figure 4.1; (b) Illustration of the internal structure of the rotary valve. The dimension of the rotary valve is 54.4 mm x 26.5 mm x 36.3 mm (length x width x height) and the diameter of the port connection (both side) is 6 mm. The diameter for the nozzle is 1 mm

The diameter of the rotary valve (RV) port connector was 6 mm while the diameter for the nozzle was 1 mm (inside the RV). The water travels towards the nozzle and becomes slower due to the sudden decrease in cross-sectional area. The water resistance increases with a decrease in the area, which affects the decay time of the pulse wave whilst mimicking the diastolic moment. The water then passes through the rotor, causing it to turn with an angular velocity that is proportional to the fluid velocity. A Hall-Effect sensor detects the rotation of the rotor and converts this to an electrical pulse signal (i.e. a frequency). The signal frequency generated from the Hall sensor is proportional to the flow rate and can be monitored through an oscilloscope, for example.

4.2.7 Reservoir 2

The last stage of the phantom system is reservoir 2. Reservoir 2 is made of a Perspex acrylic panel (3 mm thick) of size 10 cm length x 10 cm width x 10 cm height. The pump pulls water from reservoir 2 which is discharged into the tubular phantom system. An inflation bulb was connected to the top of reservoir 2 in order to pressurize the system. The complete set-up is illustrated in Figure 4.15.

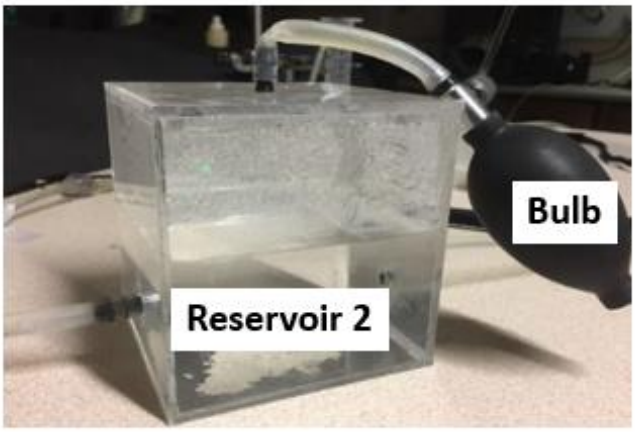


***Figure 4.15**: Reservoir 2 with inflation bulb connected at the top. The size of reservoir 2 is 10 x 10 x 10 cm (length x width x height)*

4.3 Pulse Delay Time Phantom System – Experimental Setup

The complete PDT phantom system was successfully developed and constructed as shown in Figure 4.16. The total length of the harder silicone tube (ID = 4 mm, wall thickness = 1 mm) was 170 cm. The distance between PS1 and PS2 was set to 45 cm. The pulse wave was

generated by switching the pump ON and OFF via the relay circuit (5V10A2 Channel Relay Module). A microcontroller (Arduino Mega 250) was programmed to trigger the relay module for pulse wave modulation. The Phantom system was used to validate the performance of the plastic optical fibre (POF) sensors to sense the PDT between two pulses.

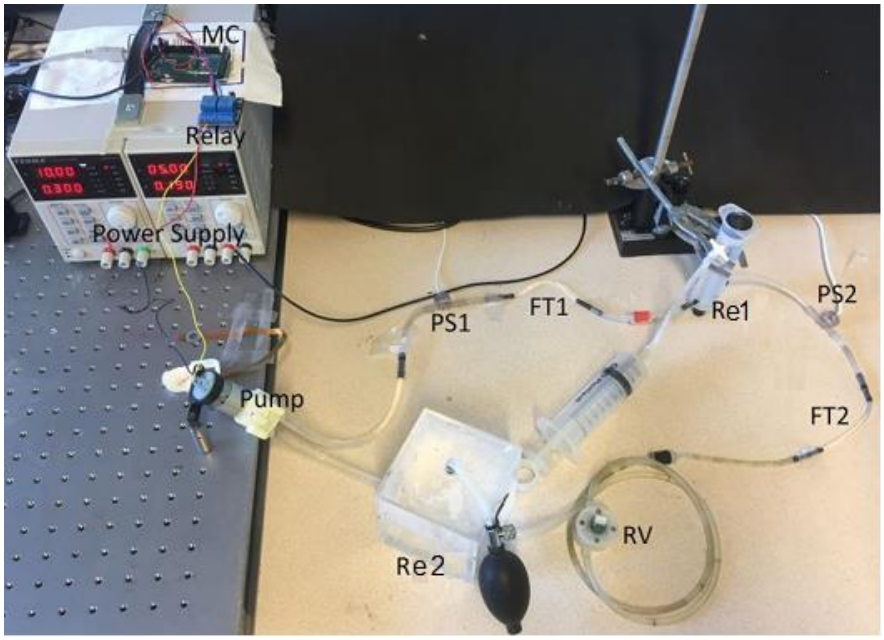


Figure 4.16: Photograph of the tubular cardiovascular pulse delay time phantom system. PS1 and PS2 are the pressure sensor 1 and pressure sensor 2, FT1 and FT2 are the flexible tube 1 and flexible tube 2, Re1 and Re2 are reservoir 1 and reservoir 2, MC is a microcontroller and RV is a rotary valve

In this setup, two reflectance mode POF sensors were located under the flexible tubes FT1 and FT2 (ID = 4mm, wall thickness = 0.4 mm). The distance between the two sensors was 45 cm to match the separation between PS1 and PS2. Figure 4.17 shows the position of one of the POF probes under one of the flexible tubes.

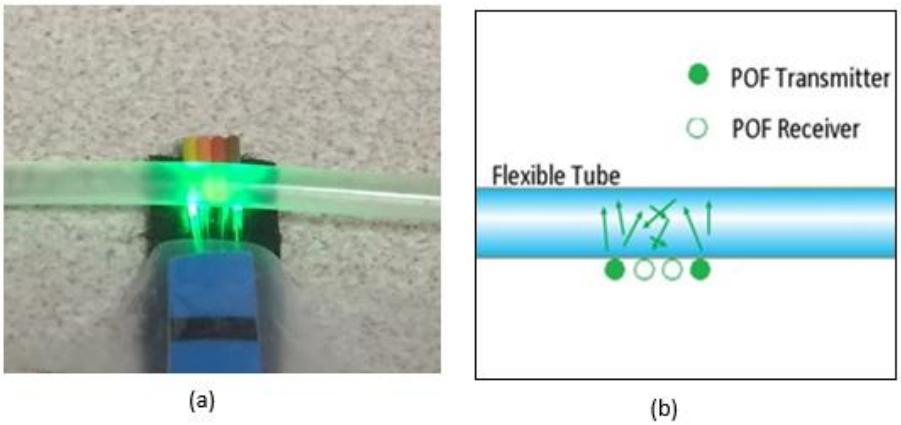


Figure 4.17: (a) The position of POF probe for optical pulse measurement, (b) Illustration of the POF under the flexible tube. The two fibres in between the transmitters were the receivers, with the gap between each fibre was 1 mm

Micropore tape was used to secure the flexible tube on top of the POF to prevent the structure from moving and creating motion artefacts. A black cloth was also deployed to cover the measurement area (i.e. the POF probe region) to prevent external ambient light sources from influencing the measurement. The increase in pulse pressure produces an increase in the volume of water. This, in turn, causes an expansion of the flexible tube. The stretching of the flexible tube due to the pulse waveform that travels along the tube was detected by the POF sensors. The green LED light from the transmitted fibre illuminated the tube and the reflected light from the upper wall of the flexible tube was detected by the receiving fibre. The light intensity decreases as the tube expands due to the increase in the distance (and hence volume) between the receiver point and the reflection point. The receiver fibre sends the captured reflected light to a phototransistor where the light intensity is then converted to a voltage by multiplying the collector current with the resistance of the load resistor (10 kΩ). The collector current increases with the increase of base-emitter current due to the increase of photocurrent when the light

strikes the phototransistor. It is noted that the signal detected by the POF is not due to a change in absorption as no dye was used, but it is due to a change in the reflectivity of the light from the back wall of the tube. Figure 4.18 shows the block diagram for the pulse measurement using the pressure sensor and the POF probe.

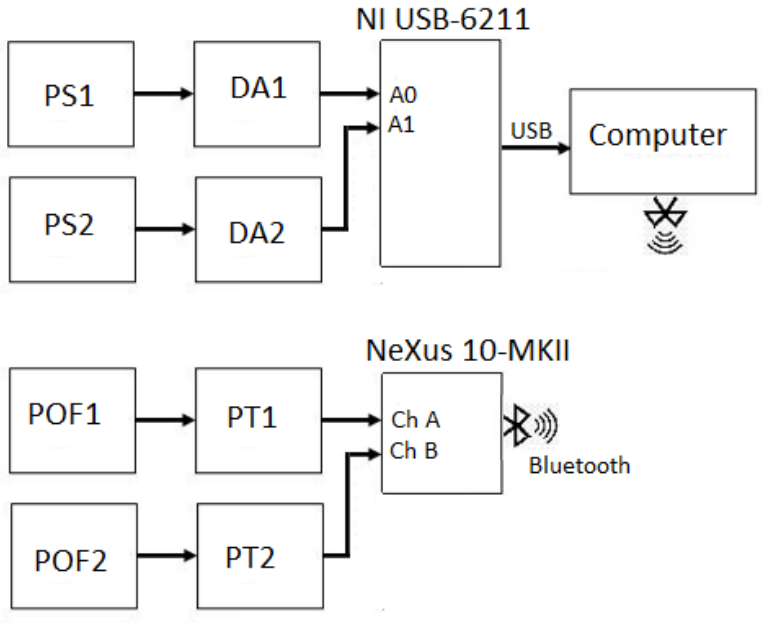


Figure 4.18: Block diagram of pulse measurement on a tubular cardiovascular phantom system

As shown in Figure 4.18, PS1 and PS2 are the pressure sensor 1 and pressure sensor 2, DA1 and DA2 are difference amplifier 1 and difference amplifier 2, A0 and A1 are analogue input 0 and analogue input 1 for NI USB-6211 data acquisition card, POF1 and POF2 are the plastic optical fibre 1 and plastic optical fibre 2, PT1 and PT2 are phototransistor 1 and phototransistor 2, Ch A and Ch B are channel A and channel B of the NeXus 10-MKII.

The output from the PS1 and PS2 were amplified using DA1 and DA2, respectively. The output from DA1 is connected to channel A0, and the output from DA2 is connected to channel A1 at the National Instruments (NI-USB 6211) Data Acquisition (DAQ) card. The NI USB 6211 has eight analogue inputs (A0 to A7) with 16 bits ADC resolution. The signal is then transferred to a computer via a USB cable. Labview software was programmed to display and record the signals from the pressure sensors with a sampling frequency of 1000 Hz. The code for the Labview programed is supplied in Appendix B3. Simultaneously, the signals from the POF1 and POF2 were converted to voltage via PT1 and PT2 respectively. Both signals were connected to Channel A and Channel B of the NeXus 10-MKII device.

The analogue signals are then converted to digital signals through a 24 bit ADC built inside the device and then sent to a computer via Bluetooth. BioTrace+ software was deployed to display and record the signals measured by the POF probes with a sampling frequency of 256 Hz. The stored data from the PS and POF probes were analyzed offline and manually aligned using Matlab for the PDT measurement. The PDT measurement for the PS were calculated based on the time between PS1 and PS2 and for the POF, the PDT were calculated based on the PDT between POF1 and POF2.

4.4 Result and Discussion

4.4.1 Pulse Delay Time with Pump Voltage

The first experiment was conducted to investigate the effect of diaphragm pump voltage to the amplitude of pulse pressure and the PDT. The aim is to determine an appropriate pump voltage to produce a pulse waveform that can stretch the flexible tube and be detected by the POF sensors. The pump supply voltage (Tenma, 72-10505) was varied from 6 Volt to 12 Volt. The pulse rate was set at 60 pulses/minute, and the water level inside reservoir one was set at 25 ml. A syringe is used to insert a volume of water into the reservoir 1 at the beginning of the experiment. Initially, the amount of 25 ml of water in reservoir 1 is to generate a robust pulsatile waveform for expanding the flexible tube, hence the POF sensor be able to sense the signals. The pulse wave that travels inside the tube was measured by the pressure sensors (PS1 and PS2) and POF probes (POF1 and POF2). Figure 4.19 shows the pulse waveform with the pump voltage set to 6 volts.

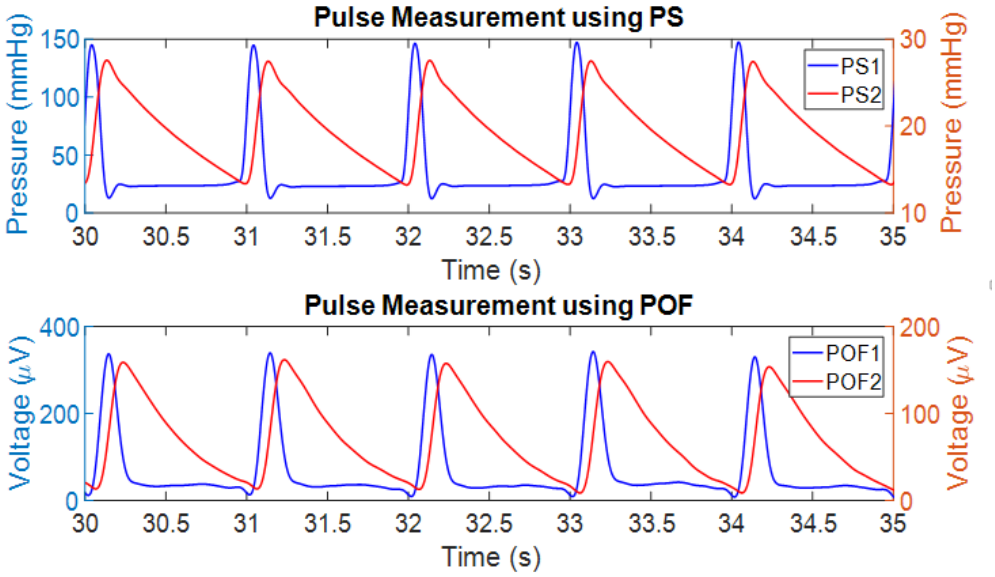


Figure 4.19: ***Typical pressure sensor signals (PS1 and PS2 top trace) and resulting plastic optical fibre sensors (POF1 and POF2 lower trace) when the diaphragm pump power supply was set at 6V, the pulse rate was set at 60 pulses/minute and the water level inside reservoir 1 was set at 25 ml***

As shown in Figure 4.19, upper trace, the Y-axis represents water pressure detected by the pressure sensor (PS) measured in mmHg. The expansion of the flexible tube due to the water flow was detected by the plastic optical fibre (POF) and is measured in microvolts. The complete experiment was conducted by varying the pump supply voltage from 6 V to 12 V with a step increase of 1 V. The signals were recorded for 1 minute at each voltage level. The output signals from the phototransistor were inverted by the Matlab software for peak detection. The delay time between two pulses detected by pressure sensors (PS1 and PS2) and the Plastic Optical Fibre (POF1 and POF2) were determined, and the results are illustrated in Figure 4.20. The PDT were plotted based on mean ± SD of 15 pulses at each voltage level.

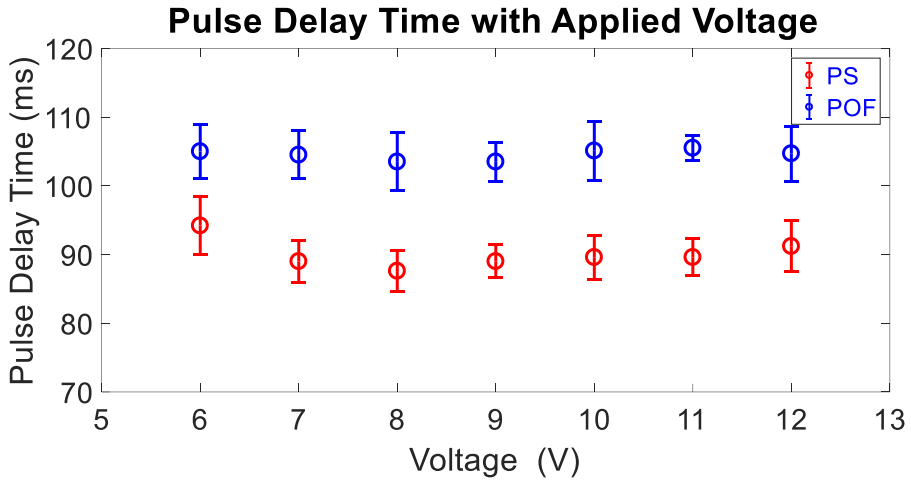


Figure 4.20: Pulse delay time measurement (mean ± SD of 15 pulses) between PS1 and PS2 as well as POF1 to POF2 for varying pump supplied voltage from 6 V to 12 V. The pulse rate was set at 60 pulses/minute and the water level inside reservoir one was set at 25 ml

The result in Figure 4.20 indicates that the PDT recorded by either the PS or POF was relatively constant as the pump voltage increases. The result indicates that the voltage applied to the pump only marginally affects (~5 %) the PDT. The variation in delay time between PS and POF is approximately 10 ms (see Figure 4.20). The variation may be due to the different stiffness of the tube at the measurement site, where the PS is located at the rigid tube (wall thickness = 1 mm) and the POF is located at the highly flexible tube (wall thickness = 0.4 mm). According to Korteweg-Moens equation, an increase in arterial stiffness leading to an increase in elastic modulus, E, thus decreasing the PTT [197]. A study by Tardy et al. demonstrated that the PTT recorded in a compliant tube much slower than a rigid tube [157]. The characteristics of the pulse waveform detected by the PS1 and PS2 are summarised in Table 4.4.

Table 4.4: The pulse waveform data obtained using pressure sensors PS1 and PS2 in the tubular phantom

Supplied Voltage (V)	**Mean Pulse Pressure PS1 (mmHg) n = 15**	**Mean Pulse Pressure PS2 (mmHg) n = 15**	**Mean Pulse Delay Time PS2-PS1 (ms) n = 15**	**Standard Deviation of the PTT (PS1-PS2) (ms) n = 15**
6	114	12	94.2	4.2
7	152	16	89.0	3.0
8	155	16	87.6	3.0
9	186	18	89.0	2.4
10	191	18	89.6	3.2
11	194	19	89.6	2.7
12	194	19	91.2	3.7

As shown in Table 4.4, the mean pulse pressure measured by PS1 increased by 60 % as the supply voltage increased from 6 V to 9 V. At this point, the mean pulse pressure remains approximately constant (~1.5 %) as the voltage increases to 12 V. A similar pattern was observed at PS2, as the mean pulse pressure increases by 50 % as the supply voltage increased from 6 V to 9 V and the mean pulse pressure remains approximately constant (~5 %) as the voltage increased to 12 V. The results showed that the pulse pressure increases with the increase of pump voltage in a nonlinear relationship. The mean of PDT recorded by PS is 90 ± 2 ms as the pump's voltage increased from 6 V to 12 V. The results indicate that the PDT is not significantly affected by the pump voltage, especially in the voltage range 9 V to12 V. For the next following experiment, the PDT with an increase of pulse rate, diastolic basal pressure, and pulse pressure is investigated.

4.4.2 Pulse Delay Time Measurement with Pulse Rate

The second experiment conducted was to measure the PDT with an increase of pulse rate from 60 pulses/minute to 160 pulses/minute. The pump's pulse rate experiment is to mimic the heart rate variability in a human model. This range of pulse rates covered the PTT variability over an acceptably wide range of heart rate as per Murakami et al. [198]. The pulse rate was controlled by programming the microcontroller with the mark/space settings, as shown in Table 4.5. The experiment was conducted with the pump supply voltage set at 10 V and the initial water level in reservoir 1 set at 25 ml.

Table 4.5: Pulse rate setting parameters

Pulse Rate (Pulse/Min)	T_high (ms) "mark"	T_low (ms) "space"	Total Duration, T (ms)	Pulse Frequency (Hz)
60	900	100	1000	1.0
80	650	100	750	1.3
100	500	100	600	1.7
120	400	100	500	2.0
140	330	100	430	2.3
160	270	100	370	2.7

As shown in Table 4.5, the pulse rate increases with the increase of pulse frequency. This is dictated by the high and low settings of the pump and trigger relay timing circuit (Figure 4.2). Figure 4.21 shows the pulse rate at 160 pulses/minute measured by both PS sensors and POF sensors. The result demonstrates that the PS and POF are able to respond to the pulse wave generated by the pump at frequency up to 160 pulses/min. The peak of the pulses was located, and the delay time between two pulses (PS1 to PS2 and POF1 to POF2) were calculated using Matlab

software (see Appendix B2). Figure 4.22 shows the plotted of pulse delay time measurement (mean ± SD of 15 pulses) at a specific pulse rate (pulse/minute).

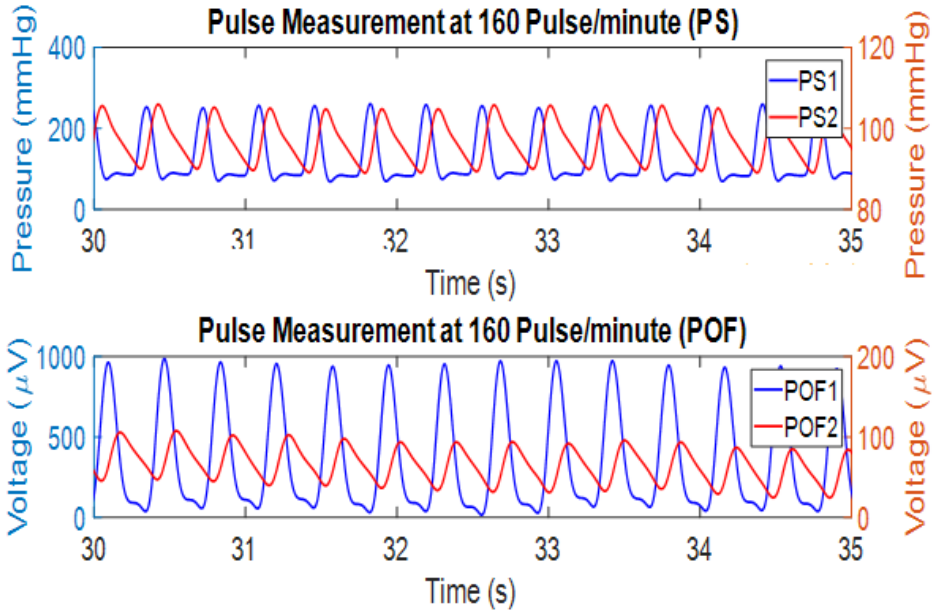


Figure 4.21: Pulse waveform measured by both PS (upper trace) and POF (lower trace) when the pump power supply was set at 10 V and the pulse rate was set at 160 pulses/minute

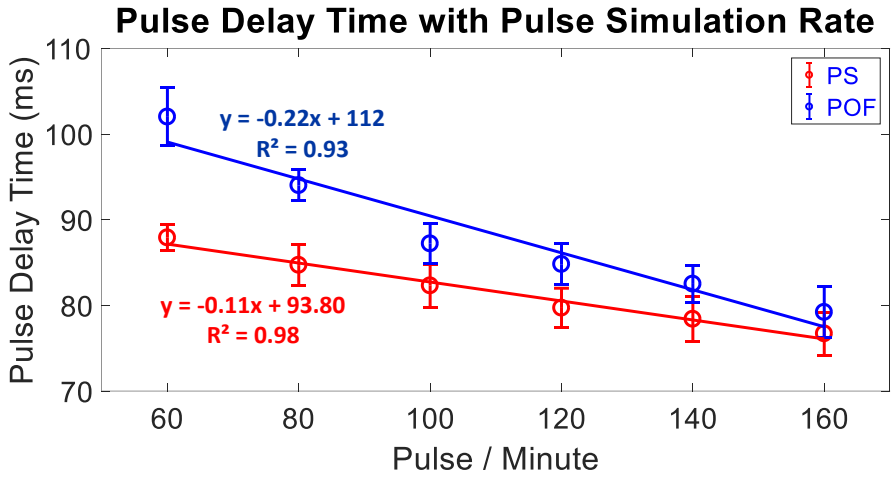


Figure 4.22: The pulse delay time (mean ± SD of 15 pulses) with increasing pulse rate with the pump power supply set at 10 V

As shown in Figure 4.22, the pulse delay time measured by both sensors (PS and POF) decreases with increases in pulse rate. Based on the graph slope, it was observed that the POFs have different sensitivity responses, especially at high pulse rate (above 100 pulses/minute). The flexible tube becomes stiffer at a higher pulse rate due to the increase in basal pressure that may result in a less sensitive PDT measurement. It was observed that the PS2 reading for systolic pressure increased from 74 mmHg to 101 mmHg and the diastolic basal pressure increased from 54 mmHg to 85 mmHg as the pulse rate increased from 100 pulses/min to 160 pulses/min. The results showed that the amplitude of pulse pressure decreased as the pulse rate increased due to an increase in pressure inside the tubing. Meanwhile, the sensitivity for the PS measurement was almost constant over the entire range of pulse rate.

The tube material may affect the sensitivity of the response recorded by both sensors. The pressure sensor was placed inside Polysulfone material and connected to the silicone tube with a wall thickness of 1 mm. Meanwhile, the POF sensor was placed at the silicone tube with wall

thickness of 0.4 mm. This condition showed that the tube connected to the PS was stiffer than the tube at the POF. Therefore, the gradient for PS consistently decreased with the increase of pulse rate. Meanwhile, the flexible tube becomes stiffer at a higher pulse rate due to the increase in diastolic basal pressure, thus showing less sensitivity. Besides, the different mechanism of detection may lead to a different sensitivity response for both sensors. For example, the POF responded to mechanical change (tube expansion) in pulse detection while the PS responded to the water pressure inside the tube. The pulse pressure reduced as the pulse rate increased, resulting in less tube expansion at the higher pulse rate that will affect the pulse detection by using the optical method. The response, however, from both sensors (PS and POF) were similar to the response observed in a human. For example, in a human study, the PTT was strongly negatively correlated with heart rate, i.e. the PTT linearly decreases with an increase in heart rate [198]. As the heart rate increases, the cardiac output, which is related to the amount of blood pumped by the heart per minute also increased, resulting in increased BP. The BP reported in the literature increased linearly with heart rate [11].

4.4.3 Pulse Delay Time Measurement with Diastolic Basal Pressure

The third experiment was on the measurement of the PDT with the increase in diastolic basal pressure. This experiment was conducted in order to have better understanding on the relationship between the delay time and basal pressure. This is important because the basal pressure inside the system fluctuates and is not controlled especially in experiment involved increases in pump's pulse rate (section 4.4.2). An inflatable bulb

was used to control the basal pressure at PS2. The PS2 basal pressure was increased by pumping air into reservoir 2, and the pressure decreased when the air was released through the valve (see section 4.2.7).

Initially, the water level at reservoir 1 was set to 25 ml and the pump's supply voltage is set to 10 V. The pulse rate was set to 60 pulses/ min. At this stage, the basal diastolic pressure at PS2 was recorded at 37 mmHg. Next, the inflatable bulb was manually pumped to increase the PS2 basal pressure until to the desired pressure, and then the PDTs were recorded for one minute. This procedure is repeated at different basal diastolic pressures, and the results were recorded in Table 4.6.

Table 4.6: Pulse delay time measurement with increased of PS2 basal pressure

Basal Diastolic Pressure at PS2 (mmHg)	**Mean Pulse Pressure PS1 (mmHg) n = 15**	**Mean Pulse Pressure PS2 (mmHg) n = 15**	**Mean Pulse Delay Time PS2-PS1 (ms) n = 15**	**Standard Deviation of PS1-PS2 delay time (ms) n = 15**
37	186	20	87	3
72	184	21	86	3
98	172	22	86	2
121	168	22	85	2
145	163	22	84	2
167	150	23	84	2

As shown in Table 4.6, the mean pulse pressure measured at PS1 decreased by 19% with an increase in PS2 basal pressure from 37 mmHg to 167 mmHg as a result of the pressure resistance increasing. As the PS2 basal pressure increased, the water level inside reservoir 1

increased from 25 ml to 28 ml (4%), resulting in an increase of pulse pressure at PS2 (15%). The PDT measured between PS1 and PS2 decreases by 3 with an increase of 351 % in the PS2 basal pressure. Figure 4.23 shows the pulse waveforms with different PS2 basal pressure measured. The minimum pressure at PS2 was used to indicate the “basal pressure” for the PDT measurement. Figure 4.24 shows the pulse delay time measurement (mean ± SD of 15 pulses) at specific basal pressure measured by using the PS and the POF sensors.

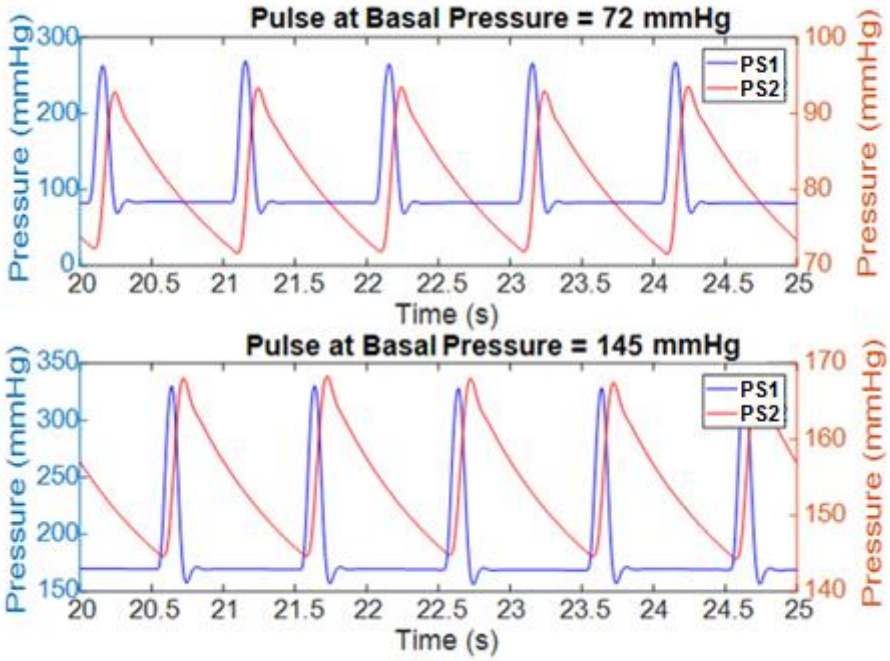


Figure 4.23: Pulse measurement with two different PS2 basal pressures with the pump power supply set at 10 V and the pulse rate was set at 60 pulse/min

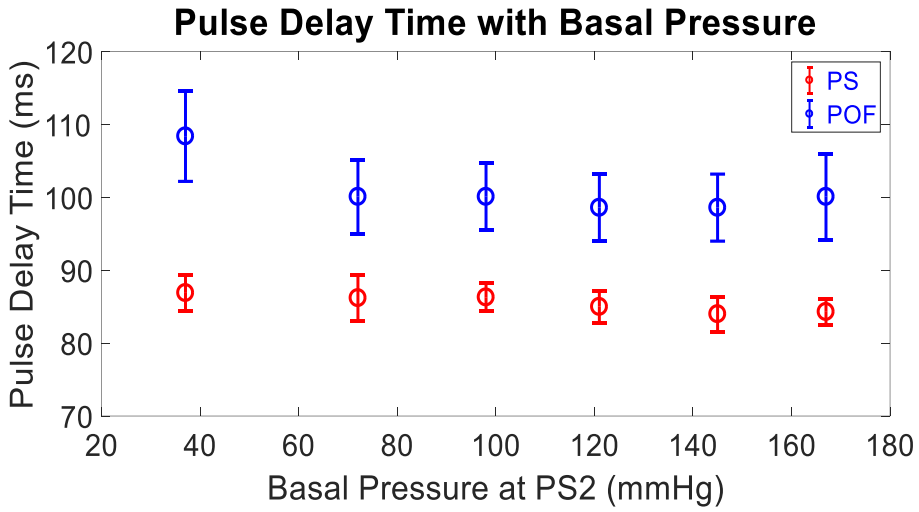


Figure 4.24: The pulse delay time (mean ± SD of 15 pulses) with the PS2 basal pressure. The pump power supply set at 10 V and the pulse rate was set at 60 pulse/min

The results (Figure 4.24) showed that the PDT fluctuated at 85 ± 1 ms for PS and 101 ± 4 ms for POF as the basal pressure increased from 37 mmHg to 167 mmHg. The findings suggest that the PDT was not significantly influenced by the increase in basal diastolic pressure.

4.4.4 Pulse Delay Time Measurement with Pulse Pressure

The fourth experiment was the measurement of the PDT with pulse pressure by increasing the water level inside reservoir 1. This experiment was conducted to simulate the effect of pulse pressure to the PDT and match to a human model. According to the Windkessel model, the large arteries in the human circulatory system can be represented by a chamber filled with water and a pocket of air [192]. The pump pushes the

water into reservoir 1 and compresses the air inside it, resulting in the water being pushed out from the chamber. The pressure to push out the water increases as the water level inside reservoir one increases. In this experiment, the water level inside reservoir 1 varied from 25 ml to 65 ml by controlling the stopcock (Figure 4.8). The experiment was conducted by setting the pulse rate to 60 pulses /min and the pump's supply voltage to 10 volts. The pulse wave that travelled inside the tube was measured by the pressure sensors (PS1 and PS2) and POF probes (POF1 and POF2). Figure 4.25 shows the pulse waveform recorded by the PS and POF when the water level inside reservoir 1 is set to 60 ml.

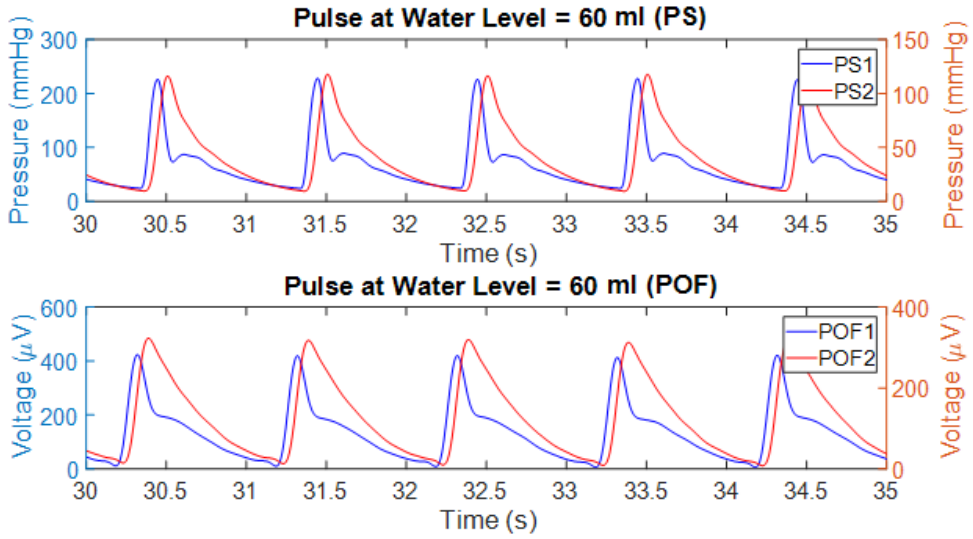


Figure 4.25: Typical pressure sensor signals (PS1 and PS2 top trace) and resulting plastic optical fibre sensors (POF1 and POF2 lower trace) when the pump power supply was set at 10 V, pulse rate set at 60 pulse/min and water level at reservoir 1 set to 60 ml

Figure 4.25 and Figure 4.19 were compared, and the results showed that the amplitude of pulse pressure measured by the PS2 and POF2 increases with the increase of water level inside reservoir 1. The result of the pulse amplitude measurement detected by the PS sensors as a function of water level in reservoir 1 is shown in Table 4.7.

Table 4.7: Pulse amplitude measurement by PS by varying reservoir 1 water level

Water Level at Reservoir 1 (ml)	**Mean Pulse Pressure PS1 (mmHg) n = 15**	**Mean Pulse Pressure PS2 (mmHg) n = 15**	**Mean Pulse Delay Time PS2-PS1 (ms)**	**Standard Deviation of PS1-PS2 delay time (ms) n=15**
25	180	22	87	3
35	183	31	85	2
45	179	39	82	2
55	182	57	77	2
60	192	80	71	2
65	201	106	63	1

This result illustrates that the pulse pressure measured at PS2 increases by 382% with an increase of 160% of the water level. The PDT measured by the PS sensors reduced as the pulse pressure (PS2) increased. A similar result was observed on the POF measurement, as shown in Figure 4.26.

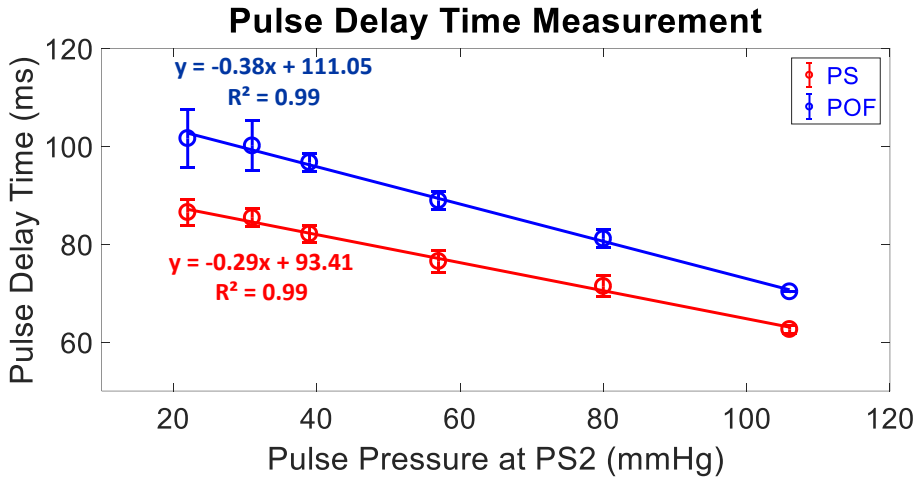


Figure 4.26: Pulse delay time measurement on PS and POF (mean ± SD of 15 pulses) with an increase of pulse pressure at PS2 with the power supply set at 10 V and pulse rate set at 60 pulse/min

The result demonstrates that the PDT recorded by both sensors decreased with the increase of pulse pressure. The sensitivity response for both PS and POF were calculated based on the slope of the graph, and the result showed that the sensitivity was -0.29 ms/mmHg and -0.39 ms/mmHg, respectively. The results indicate that the POF was more sensitive in pulse detection and gave a better response compared to the PS. In the literature, pulse wave velocity (PWV) was reported to increase with the peak pressure and the mean flow velocity [149]. The PWV was strongly affected by the tube elasticity with the velocity higher on the stiff tube compared to the soft tubes [150]. In a typical blood circulatory system, the arterial compliance reduced due to a loss of vessel wall elasticity resulting in an increased pulse wave velocity [48]. Aging is one of the factors in human arterial compliance loss that increases the blood pressure [47]. With aging, the arterial wall loses its compliance and becomes much stiffer, thus the arteries lose their ability to distend in response to increased pressure. Other factors that may affect arterial

compliance are diet, concurrent disease and life style [199]. According to the Bramwell–Hill equation, PAT varies with the arterial compliance [200] Since arterial compliance decreases as blood pressure (BP) increases, thus PAT is inversely correlated with BP (i.e. the PAT decreases with the increase of SBP [22], [201]).

In addition, the phantom can be used to vary the pulse amplitude and is able to simulate low perfusion signals as obtained in the neonate and those with peripheral flow problems such as atherosclerosis and blood clots. As shown in Table 4.5, the pulse amplitude increased with the increase in pulse pressure theoretically suggesting that the amplitude of the PPG increases with an increase in BP in the human circulatory system. However, the peak of the inverted PPG has been found to be an unreliable indicator of SBP due to the peak distortion by the reflection of pressure waves from the terminal arteries [20]. Overall, the pulse delay time phantom system is therefore able to simulate the arterial compliance condition and these results on the phantom study showed a similar pattern to the human model.

4.5 Conclusion

The tubular cardiovascular pulse delay time phantom system was successfully developed and tested on the wearable POF sensors. In-line pressure sensors were used as a benchmark for the PDT measurement. The performance of the POF on pulse wave detection were tested in four different configurations. The first configuration was by varying the voltage pump level. The results showed that the pulse amplitude and the delay time measured by the PS and POF were almost constant especially in the voltage range 9-12 V. The second configuration was to investigate

the effect of pulse rate on the PDT. The pulse rate increased with the increase of triggered pulse frequency at the pump. A microcontroller was programmed to control the pulse frequency. The results showed that the PDT decreased with the increase in pulse rate. Similar responses have been observed in a human system with the PTT decreasing as the heart rate increased [198]. In the third configuration, the effect of PS2 diastolic basal pressure to the PDT was investigated. The basal pressure was measured concerning PS2 and showed an increase from 37 mmHg to 167 mmHg by pumping air to the reservoir 2. As the basal pressure increased, the PDT recorded by PS and POF fluctuated at 85 ± 1 ms, and 100 ± 4 ms respectively. The results suggested that the PDT is not significantly influenced by the PS2 basal pressure. The fourth and final configuration was by varying the pulse amplitude by controlling the amount of water inside the reservoir 1. The PDT between two pulses was calculated, and a negative correlation with pulse pressure was observed. These findings agreed with the finding observed by other researchers in human studies, where PAT was reported as inversely related to systolic blood pressure (SBP) [22], [199]. Overall, the phantom system was successfully developed and the performance of the POF sensors were successfully evaluated for PDT measurement. Significantly, the phantom system designed was able to generate low perfusion signals, which are essential to validate the sensor performance on PPG measurement devices for cases such as in pathophysiology of the newborn, and other low perfusion cases.

Chapter 5 Verification and Validation of the Cuffless Blood Pressure Monitoring System

5.1 Introduction

In this Chapter, the performance of the proposed wearable cuffless blood pressure monitoring system has been evaluated on volunteers. A non-invasive cuffed blood pressure monitor (OSTAR, P2) was used as a blood pressure reference measurement. The experimental setup and procedure for pulse arrival time (PAT) and BP measurements is discussed in detail. The first experiment was performed on a group of healthy volunteers to establish a relationship between PAT and BP through a pedal exercise. An investigation of the accuracy in determining BP was carried out based on instantaneous PAT and mean PAT (15 pulses). A second experiment was performed using a tilt table to vary the BP. Through this experiment, the one-step calibration method was proposed to estimate SBP, and the results were compared with a calibration curve obtained through the pedal exercise (first experiment). The one-step calibration method required only one BP measurement using a reference method (cuff) at the beginning of the experiment. The findings on the experiments and brief conclusions are presented at the end of this chapter.

5.2 Experimental Setup

Experiments to measure the physiological measurement were conducted in the Optics and Photonics Research Group Laboratory (Room 1002) in the Tower Building, Nottingham University. The experiment has been approved by the Faculty of Engineering Ethical Review Committee. Each volunteer was asked to read through the Participant Information Sheet (see **Appendix A**) and complete the participant consent form before the start of the experiment. A briefing was conducted on the procedure and safety precautions during the experiment. The device used for acquiring signals from the volunteer's body was battery operated to reduce electrocution risk from the mains supply. Four hours before the study, the volunteer was asked to avoid drinks that contained caffeine or taking a heavy lunch to prevent a large variability in blood pressure. The experiments, taking a maximum of 90 minutes of volunteer's time, were divided into two sections - pedal exercise and tilt table. The steps conducted before the experimental procedure were as follows:

1. Volunteer agrees to participate by signing a consent form.
2. A volunteer is asked to sit and relax on the exercise bike.
3. POFs were attached to the volunteer's right foot and wrist for reflective mode PPG measurement. The Blood Volume Pulse (BVP) Sensor (NX-BVP1A) was connected to the right index finger for transmission mode PPG measurement. Conductive fabric (Ag-Nylon, MedTex180, VTT/Shieldex Trading, USA) and adhesive surface ECG electrodes (Ag/AgCl, AMBU Blue Sensor, Medisave, UK) were connected on the chest for the ECG measurement. A BP monitor (OSTAR, P2) was connected to the volunteer's left arm. Figure 5.1 shows all the sensors connections on the volunteer's body.

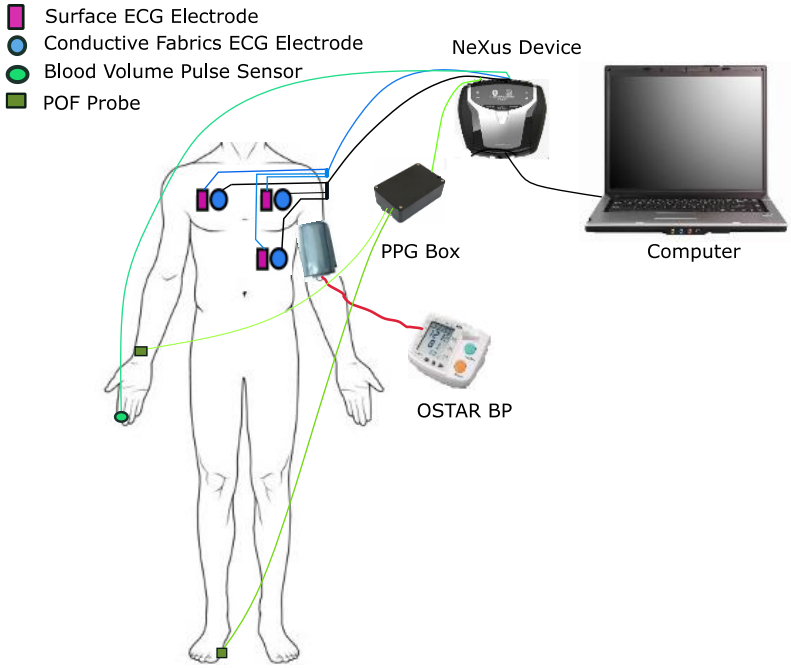


Figure 5.1: Sensor placement on the volunteer. ECG surface electrodes and ECG fabric electrodes on the chest, POF on the wrist (right arm) and underfoot (right leg), Blood Volume Pulse sensor on the index finger (right arm) and Ostar BP on the left arm

5.2.1 Sensors Positions

The ECG signals were measured on the chest according to the lead II measurement because the QRS axis normally aligns with these leads [165]. Lead II can be achieved by measuring the potential difference between the right chest (negative electrode), and the lower left rib (positive electrode), in the same way as the Einthoven triangle (right arm position in the negative electrode and left leg position in the positive electrode) [200]. The surface electrode and the fabric electrode were placed side by side, as shown in Figure 5.1. The chest strap was used

on top of the fabric electrode to secure it to the body and to ensure there is good contact between the electrode and skin for ECG measurement. The PPG was measured at three locations; index finger (right arm), wrist (right arm) and under the foot (right leg). The PPG on the index finger was measured using a Blood Volume Pulse (BVP) sensor (Nexus, NX-BVP1A) based on transmission mode. Reflection mode POF was used to measure the PPG on the wrist and under the foot. Figure 5.2 (a-c) shows the position of PPG sensors that are attached to the finger, wrist and under foot, respectively.

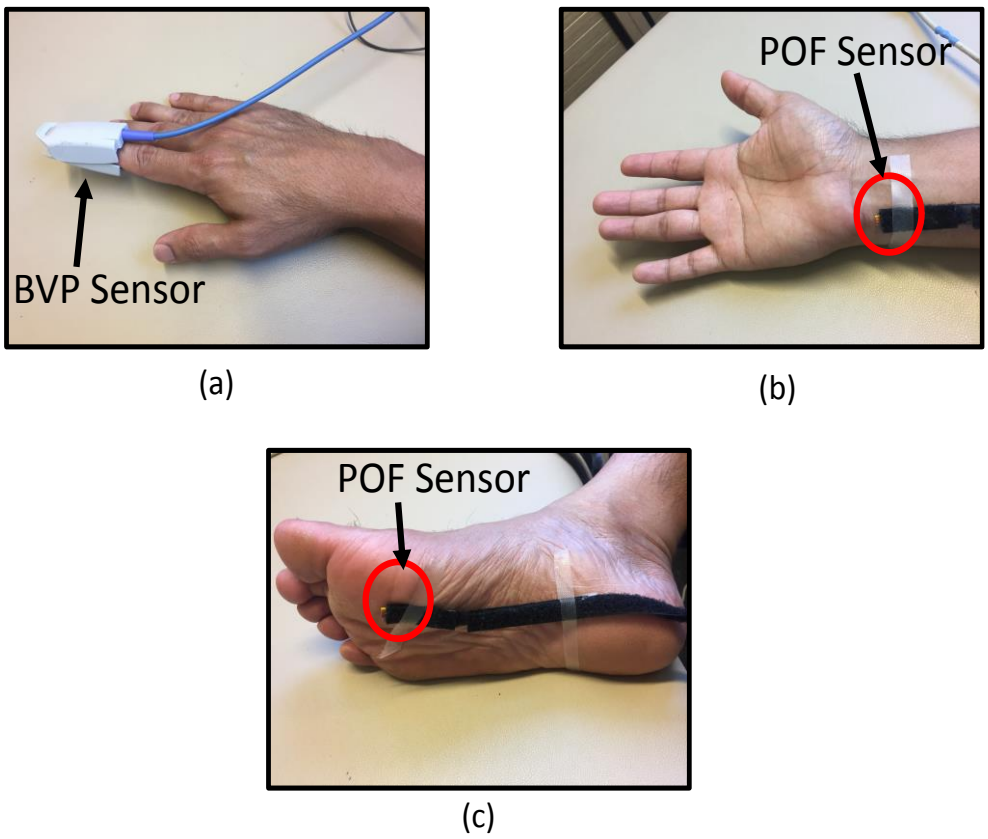


Figure 5.2: The position of PPG sensors; (a) at the index finger (Blood Volume Pulse (BVP) sensor, NX-BVP1A, (b) at the wrist (POF), and (c) under the foot (POF)

The POFs were attached to the skin surface by using medical tape (3M Transpore). The tape was used to prevent the sensors from becoming detached from the skin during the experiment. A liner sock was used to channel the POF from the foot to the PAT measurement system. The volunteers wore their shoes for pedalling the exercise bike. Blood pressure was measured by a standard oscillometric BP device (Ostar, P2) at the left upper arm to monitor BP during the experiment. As shown in Figure 5.1, the PPG probe is not on the same arm as the BP device to avoid PPG signal distortion caused by the occlusion phase of the cuff [121]. The method proposed for the placement of the sensor for PAT and BP evaluation is based on work by Jernsted and Newcomer [201]. The experiment was started when all the sensors were connected and the volunteers ready.

5.2.2 Measurement on Volunteers

Initially, 15 volunteers were employed, but only 13 volunteer's data were utilised for further analysis. The other two volunteer's data has been excluded because of illegible or missing response of some PPG signals under the foot and the BP measurement device repeatedly reporting an error during the experiment. The missing PPG signals may be influenced by the pressure exerted on the skin during the pedal exercise experiment. An irregular heart rate during or after the exercise may produce errors in the BP measurement. All volunteers are healthy and the age ranges from 17 to 42 years. This research is limited to male participants because it involves male researchers attaching electrodes to the chest of volunteers. The details of the volunteer physical information are shown in Table 5.1.

Table 5.1: Volunteers physical information

Volunteer Code	Age (years)	Gender	Height (cm)	Weight (Kg)	BMI (kg/m^2)
1001	42	Male	180	65	20.0
1020	30	Male	168	68	24.1
1300	31	Male	172	75	25.4
4010	37	Male	165	60	22.0
5001	28	Male	168	68	24.1
1580	30	Male	168	58	20.5
1205	27	Male	166	65	23.6
4163	28	Male	171	55	18.8
1325	30	Male	169	65	22.8
2615	33	Male	167	60	21.5
5843	33	Male	168	64	22.7
3598	17	Male	151	55	24.1
6485	19	Male	152	58	25.1

All the volunteers stated that they were healthy, with no cardiovascular disease and physical abnormality. A 4-digit volunteer code was used to identify each volunteer. The information on age, gender, height (centimetre, cm) and weight (kilogram, Kg) were provided by the volunteer in written form. BMI is the body mass index calculated as the body mass (weight in Kg) divided by the square of the body height in meter (m). The BMI is used to estimate body type or categorize person into a specific category. A BMI below 18.5 is considered underweight, a BMI between 18.5 and 24.9 is considered normal, a BMI between 25.0 and 29.9 is considered overweight, and a BMI over 30 is considered

obese. As shown in Table 5.1, 84.6% of the volunteers fall in the normal category, and 15.4% are considered overweight. All the volunteers were fit and able to perform the task required.

5.3 First Experiment: Pedal Exercise

The first experiment was performed to determine a calibration curve of PAT and BP and then estimated the BP based on the calibration curve obtained. In general, the cuff based BP device takes systolic BP (SBP) at one moment and then diastolic BP (DBP) at another. In another words, there is a considerable delay between ECG at SBP and ECG at DBP of at least 15 ECG beats. The variation of 15 beats BP measured by Finapres BP was 6 mmHg for SBP and 3 mmHg for DBP [202]. Hence this variation results in a variation in PAT over several ECGs. Then using several PATs as opposed to the instantaneous PAT at the SBP moment could potentially result in a wide spreading of the PAT error. Therefore, this work will compare the instantaneous PAT and mean PAT with BP measurement to establish the calibration curve of PAT-BP on each volunteer.

In this experiment, the PAT and the BP of volunteers were monitored before, during and after pedal exercise. It is expected that BP will increase as the heart rate increases during the exercise. The volunteer was required to cycle on an Exercise Bike (Domyos VM740) as shown in Figure 5.3 (a) with the work rate level for the exercise was set according to Figure 5.3 (b). The volunteers were asked to stay in the same position during BP and PAT measurement, as shown in Figure 5.3 (c).



(a)



(b)



(c)

Figure 5.3: Experimental setup for pedal exercise (a) Exercise bike, Domyos VM740, (b) Setting programmed for the exercise work rate level and (c) Volunteer position on an exercise bike for PAT and BP measurement.

The detailed procedure for pedal exercise experiment was as follows:

1. First, the volunteer was asked to relax in a sitting position on the bike for 6 minutes (rest phase). During this stage, the PAT was recorded continuously, and the BP was recorded once every 2 minutes.
2. Next, the volunteer was asked to perform pedal exercise according to the setting work rate level, as shown in Figure 5.4 (pedal exercise phase). The exercise was stopped at position A, B, and C (Figure 5.4) for BP measurement.
3. After completing the task, the volunteer was asked to stay still on the bike for 6 minutes (recovery phase), and the BP was recorded once every 2 minutes. The time required for each volunteer to finish the experiment is approximately 32 minutes.
4. The ECG and PPG were recorded continuously at 256 samples/second during the experiment, which therefore allowed continuous calculation of PAT. Simultaneously, a total of 9 BP measurements were recorded using cuff-based BP monitor (OSTAR BP) during the experiment.

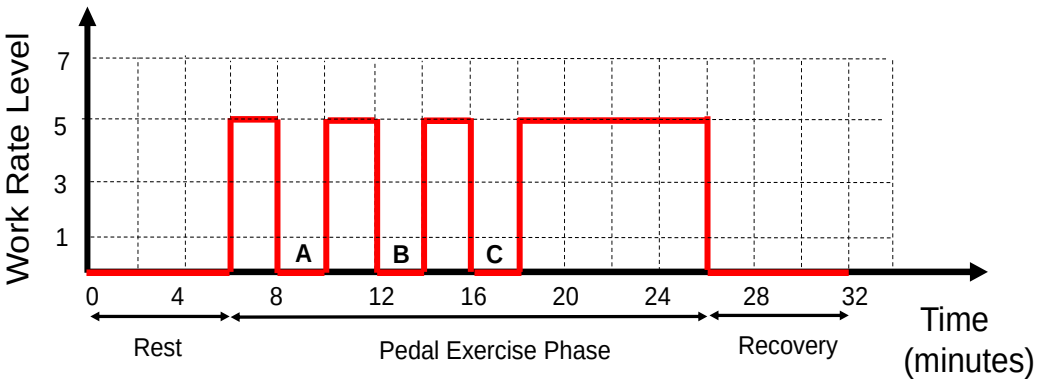


Figure 5.4: Test protocol for the pedal exercise using exercise bike (Domyos VM740)

All the signals were acquired by the data acquisition device (NeXus-10 Mark II, Mindmedia) through the input Ch A, Ch B, Ch E. Ch F, Ch G and Ch H with the Ch represent the Channel. Ch A and Ch B are the bipolar channels for ECG measurement using conductive fabric electrodes and surface electrode, respectively. The PPG on the fingertip was monitored using Ch E using Blood Volume Pulse (BVP) sensor.

The POF was deployed for the PPG measurement on the wrist (Ch F) and the PPG measurement under the foot (Ch G). In this experiment, six BP readings were taken during the rest section (before and post-exercise), and three BP readings were taken during the exercise section. This leads to nine BP measurements during the whole experiment. A method for recording the PAT and BP before, during and after exercise has been implemented by other researchers to assess the relation between PAT and BP [22], [203]. Ch H is used to monitor the pressure inside the BP cuff using a pressure sensor (MPX 4250). The oscillation of the BP cuff waveform is used to synchronise between the BP and the PAT reading. A Y-tube connection was deployed to connect the pressure sensor, BP cuff and Ostar BP Monitor, as shown in Figure 5.5.

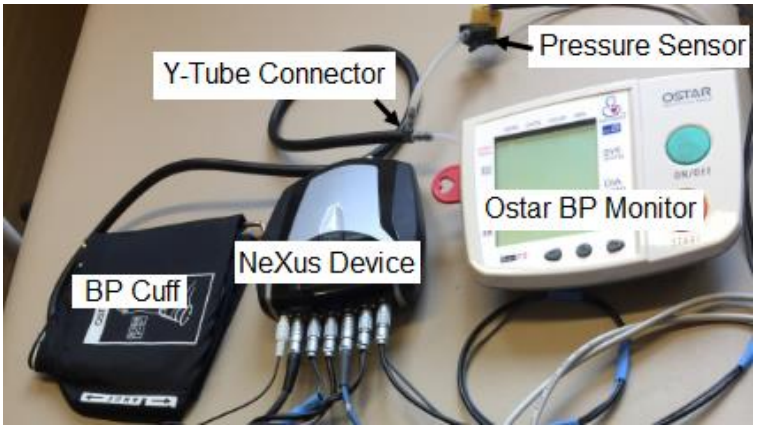


Figure 5.5: A measurement setup to measure the pressure inside the BP cuff

The output from the pressure sensor (MPX 4250) is a voltage which is sent to the NeXus device simultaneously with ECG and PPG signals. The signals were then sent wirelessly via Bluetooth to a computer as graphically displayed by the BioTrace+ software (Mind Media B.V. Netherlands), and Matlab software was used for analyzing the signals. The blood pressure waveform was used as an indicator for mean and instantaneous PAT measurement. In addition, the oscillation pulse wave that was extracted from the deflation cuff was used for one-step calibration method for estimating SBP based on PAT measurement.

5.3.1 Blood Pressure Cuff Waveform: Mean and Instantaneous PAT

In general, a mean PAT is determined based on the mean of several ECG to PPG pulse delays whilst instantaneous PAT refers to a single ECG to PPG pulse delay. A review by Van Velzen et al. reported that the averaging periods in determining PAT ranged from 8 seconds to 6 minutes, with an averaging period of 1 minute being the most common [204]. Poon et al. showed that beat-to-beat PAT and SBP were highly correlated within a short period number of beats [205]. They reported that the correlation coefficient (r) decreased from -0.73 to -0.63 when the number of beats increased from 15 to 360 beats. The PAT value obtained from long averaging periods may be affected by unsuitable pulse waves due to movement and associated noise [22]. In this experiment, the PAT measurements were calculated based on a mean of 15 seconds during the cuff deflation (dash circle) as shown in Figure 5.6.

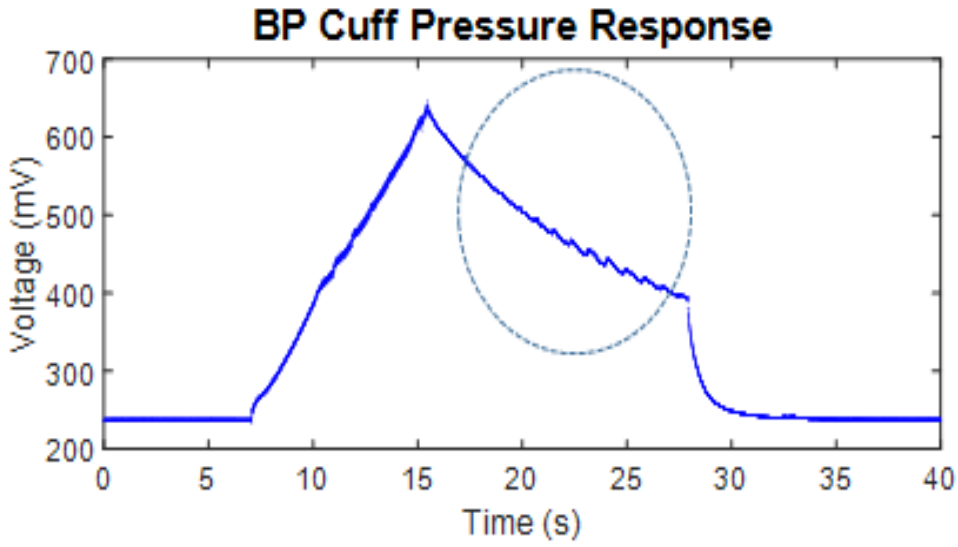


Figure 5.6: BP cuff pressure waveform for volunteer 1 (Volunteer code: 1001)

Fundamentally, the oscillometric BP device measures BP by detecting the maximal oscillation in the BP cuff caused by blood flow and uses an empirical ratio to determine SBP and DBP [206]. The BP in the PAT method was determined continuously based on the delay time between the peak of ECG R-wave and the peak of the PPG pulse. A measuring difference in both methods is present, thus it is difficult to measure the BP and PAT at exactly the same time point without proper synchronization [96]. In this work, a synchronization between a single pulse wave PAT and BP measurement was achieved by measuring the pressure inside the BP cuff simultaneously whilst measuring the ECG and PPG signals. All the signals were synchronised with the NeXus device and the signals were transmitted to a computer via Bluetooth. Matlab software was programmed to plot the signals on the same axis, as shown in Figure 5.7.

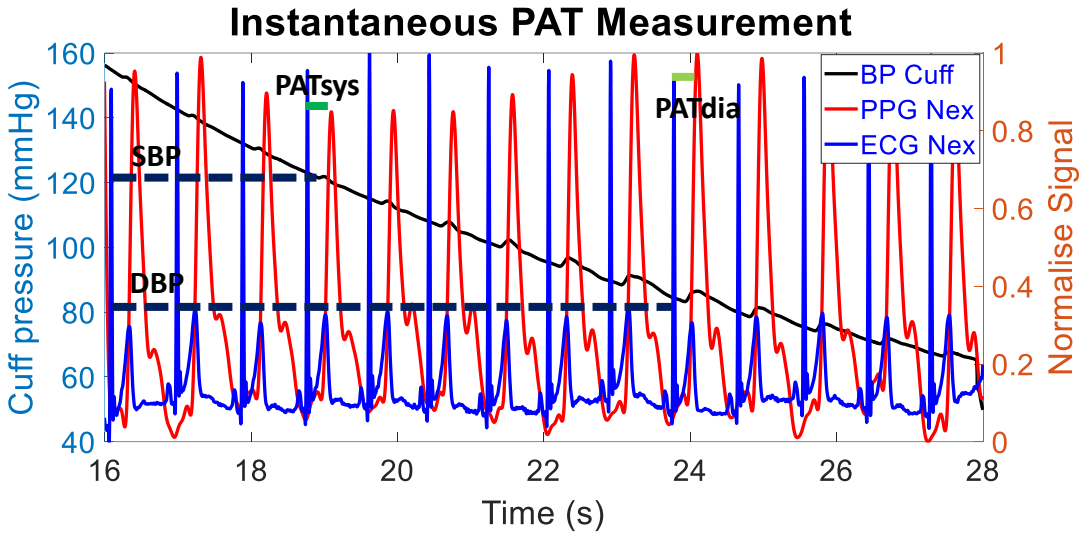


Figure 5.7: Instantaneous PAT measurement for SBP (PATsys) and DBP (PATdia). The black trace represents the deflation of the BP curve (BP Cuff), the blue trace represents the ECG measured using surface electrode (ECG Nex) and the red trace represents the PPG on the fingertip measured by the BVP sensor (PPG Nex)

A single pulse that represents instantaneous PAT was manually selected according to the moment where the SBP and DBP were being recorded by the oscillometric BP device. As shown in Figure 5.7 for example, the SBP measured by the Ostar BP device is 120 mmHg (as shown by the device's monitor), and this value was marked manually on the cuff oscillation curve. An ECG pulse wave that occurred at that point was identified, and the delay time between the ECG and PPG was computed, resulting in an instantaneous PATsys measurement (Figure 5.7). The same procedure was applied to identify instantaneous PAT for DBP (80 mmHg) as indicated by PATdia (Figure 5.7). In this thesis, the accuracy in estimating BP based on mean and instantaneous PAT were investigated.

5.3.2 PAT Measurement for Calibration Curve

In this study, PAT is defined by the time difference between the R-wave peak of the Electrocardiogram (ECG) and the peak of the Photoplethysmogram (PPG). PAT is grouped into three (3) categories which depends on the spatial position of the PPG signal measured; finger, wrist and underfoot as showed in Figure 5.8

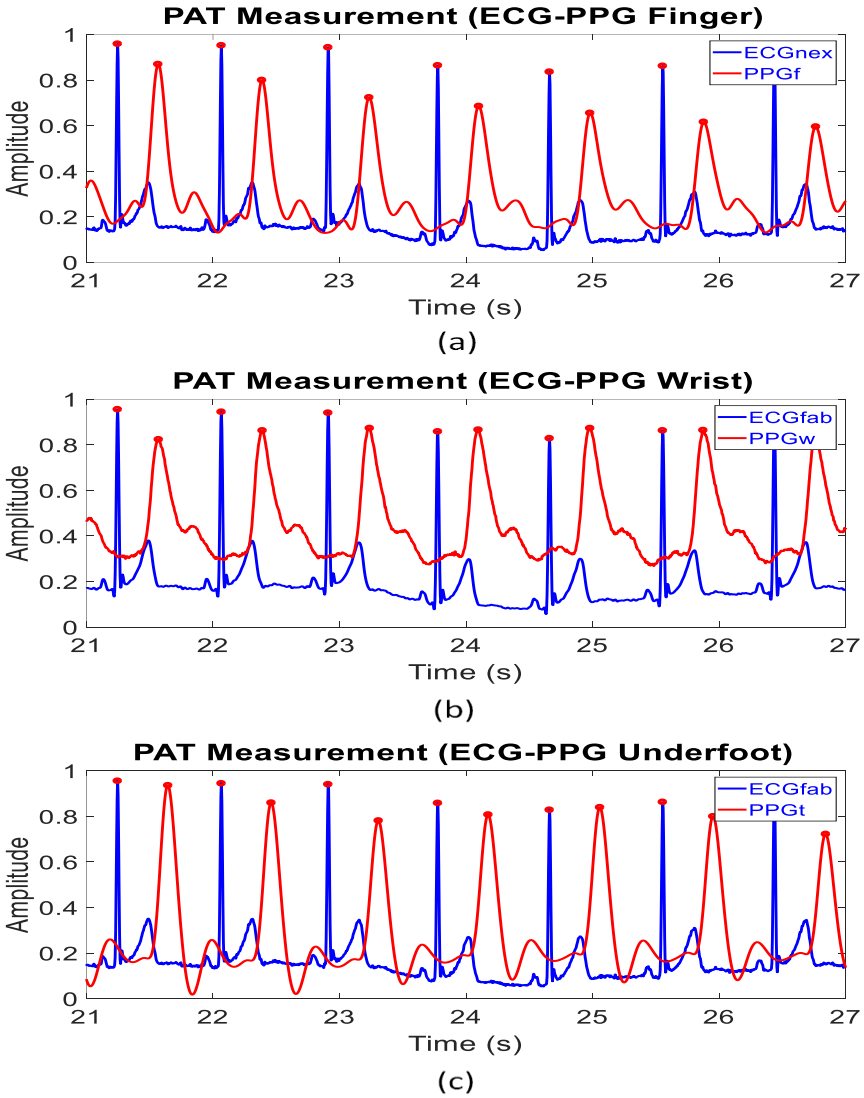


Figure 5.8: PAT measurement according to the spatial position of the PPG signal measured; (a) at the finger, (b) at the wrist and (c) under the foot

As shown in Figure 5.8, ECGnex (a) refers to ECG measured by the surface electrode and ECGfab (b and c) refers to the ECG measured by the conductive fabrics electrode. For the PPG measurement, PPGf (a) refers to PPG measured by blood volume pulse sensor on the right finger and the PPGw (b) and the PPGt (c) refers to the PPG measured by the plastic optical fibre sensor on the right wrist and under the right foot, respectively. The Nexus device (NeXus 10 Mark II) acquired the signal simultaneously and then displayed them through BioTrace+ software.

Next, the ECG and PPG signals were analyse offline using Matlab software. In Matlab, a linear phase FIR (Finite Impulse Response) filter is implemented to remove the unwanted noise generated in PPG and ECG signals. Then, these signals were aligned within the same scale by normalization method within the interval values between 0 and 1. Subsequently, thresholding and peak detection algorithm (*findpeak*) were applied to the normalisation of the signals. The details of the signal processing for peak detection is described in Chapter 3. The peaks of the ECG and PPG are marked by a red circle (Figure 5.8). The delay times between ECG and PPG were determined and correlated to the BP measurement. The results are presented in the next section.

5.3.3 The result on Pedal Exercise: Mean PAT

The study has been conducted on 13 volunteers to determine PAT and BP before, during and after pedal exercise. All the measurements were recorded simultaneously using a Nexus device. The results for PAT with systolic blood pressure (SBP) and PAT with diastolic blood pressure (DBP) on volunteer 1 (Vol1, volunteer code: 1001) were plotted as shown in Figure 5.9, the y-axis for both figures represents PAT in units of

seconds (s), and the x-axis represents BP in a unit of mmHg. The red trace represents the delay time between ECG to PPG at the finger (PATf), the blue trace represents the delay time between ECG to PPG on the wrist (PATw), and the black trace represents the delay time between ECG to PPG underfoot (PATt).

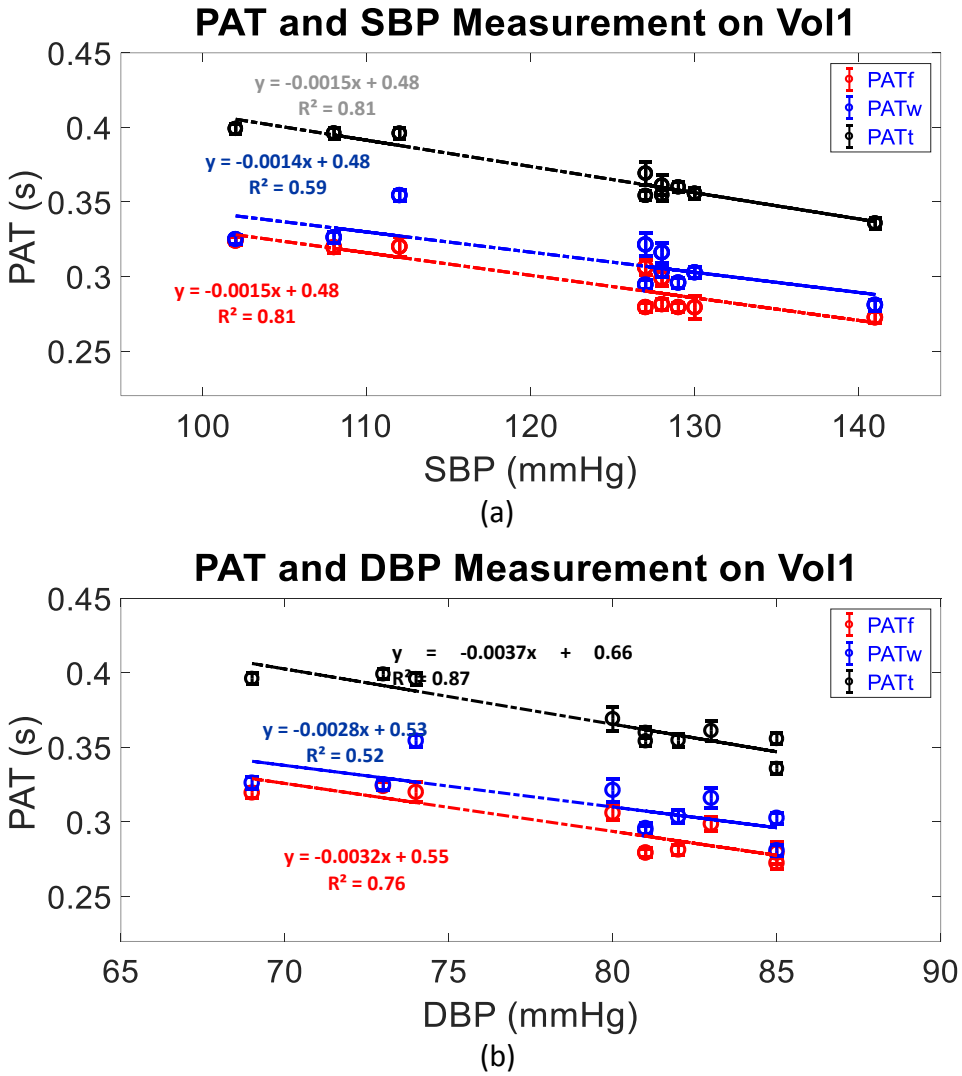


Figure 5.9: The relationship between (a) PAT and SBP (b) PAT and DBP measurement. The PPGs signals were measured at a finger (red trace), wrist (blue trace) and underfoot (black trace) on volunteer 1 (volunteer code: 1001). The PATs data is plotted based on the mean ± SD of 15 pulses of PPG signals

Figure 5.9 showed the PAT data plotted based on the mean of 15 pulses, and the error bar is indicating the standard deviation of the mean for each data. The mean PAT was calculated during the deflation of the BP cuff during BP measurement (Figure 5.6 – the circled region). The typical time required to deflate the BP cuff was 15 seconds and the time required will be longer than this if there is a large difference between SBP and DBP. In general, there will be 15 pulses over 15-second duration for a heart rate of 60 bpm. A linear regression model was used to fit the data in Figure 5.9. The results show that the PATf, PATw and PATt decreased with the increase of BP.

As shown in Figure 5.9, the delay time recorded at the finger (PATf) is less than the delay time recorded on the wrist (PATw). A statistical software SPSS 23.0 (IBM SPSS Statistics, IBM Corporation, Armonk, New York) was deployed to analyze a statistical difference between the mean of PATf and the mean of PATw. The Shapiro-Wilk test was performed to test data distribution, and the results show that all the data normally distributed ($p > 0.05$). The results of the student t-test showed that the mean value of PATf and PATw were statistically different with the p-value equal to 0.000136 ($p < 0.05$).

Theoretically, the PATf should be longer than PATw due to the distance of the finger further away from the heart. This contradictory result obtained may be due to the different electronic response in PPG detection. The PPG at the fingertip was measured by the transmission mode using a commercial sensor from the Nexus device. The sensor was clipped to the finger and uses IR light source to transmit the light through the skin. The photodetector receives the light and converts the light intensity into the current. The amount of current is converted to the voltage by the conditioning circuit inside the Nexus device box and the result is displayed through the software.

In contrast, the PPG detection on the wrist is based on reflection mode using fibre optics. The green LED used to illuminate the light to the skin and the reflection of the light detected by the phototransistor. The light intensity is converted to the current, and the signals amplified and filtered with a RC low pass filter (cut-off frequency 3.8 Hz), before it is sent to the Nexus device for recording. The difference in terms of the electronic components and filter design may generate a difference in PAT measurement, although the finger and the wrist are very close in distance.

Meanwhile, the delay time between the ECG and the PPG on the arm is less than the delay time between ECG to the PPG on the leg mainly due to the much shorter distance of arm to the heart. A student t-test performed by the SPSS software showed that there is a statistical difference between the mean of PATf and the mean of PATt ($p < 0.05$). As shown in Figure 5.9, the mean time difference between PATf and PATt was approximately 50 ms. From the literature, PTT of two PPG signals between finger and toe is reported around 100ms with the subjects in the supine position [207]. The delay time would be expected to increase with the subject in supine position due to the effect of hydrostatic pressure [113]. In pedal exercise, the leg position was below the heart level (sitting position), resulting in the delay time between ECG to PPG under the foot being faster than in supine position.

5.3.4 Mean and Instantaneous PAT

Instantaneous PAT was determined according to the method proposed in section 5.3.1. In this method, the instantaneous PAT will have one value that represents SBP and one PAT value that represents DBP. In contrast, in the mean PAT method, the SBP and DBP will share a group of PAT values over 15 seconds, producing a mean PAT. In the literature, the PAT was determined based on a mean at a certain number of heartbeats or a certain period but none of them deployed a single pulse wave for PAT calculation [204]. In this work, a mean of 15 beats was deployed, and the accuracy of this method was compared with a single pulse wave PAT or instantaneous PAT. Figure 5.11 shows the instantaneous and mean PAT with BP at three different sites of PPG measurement; finger, wrist and underfoot on volunteer 1 (volunteer code: 1001). All the data were plotted based on a mean ± SD of 15 pulses that corresponds to SBP and DBP recorded by the BP monitor.

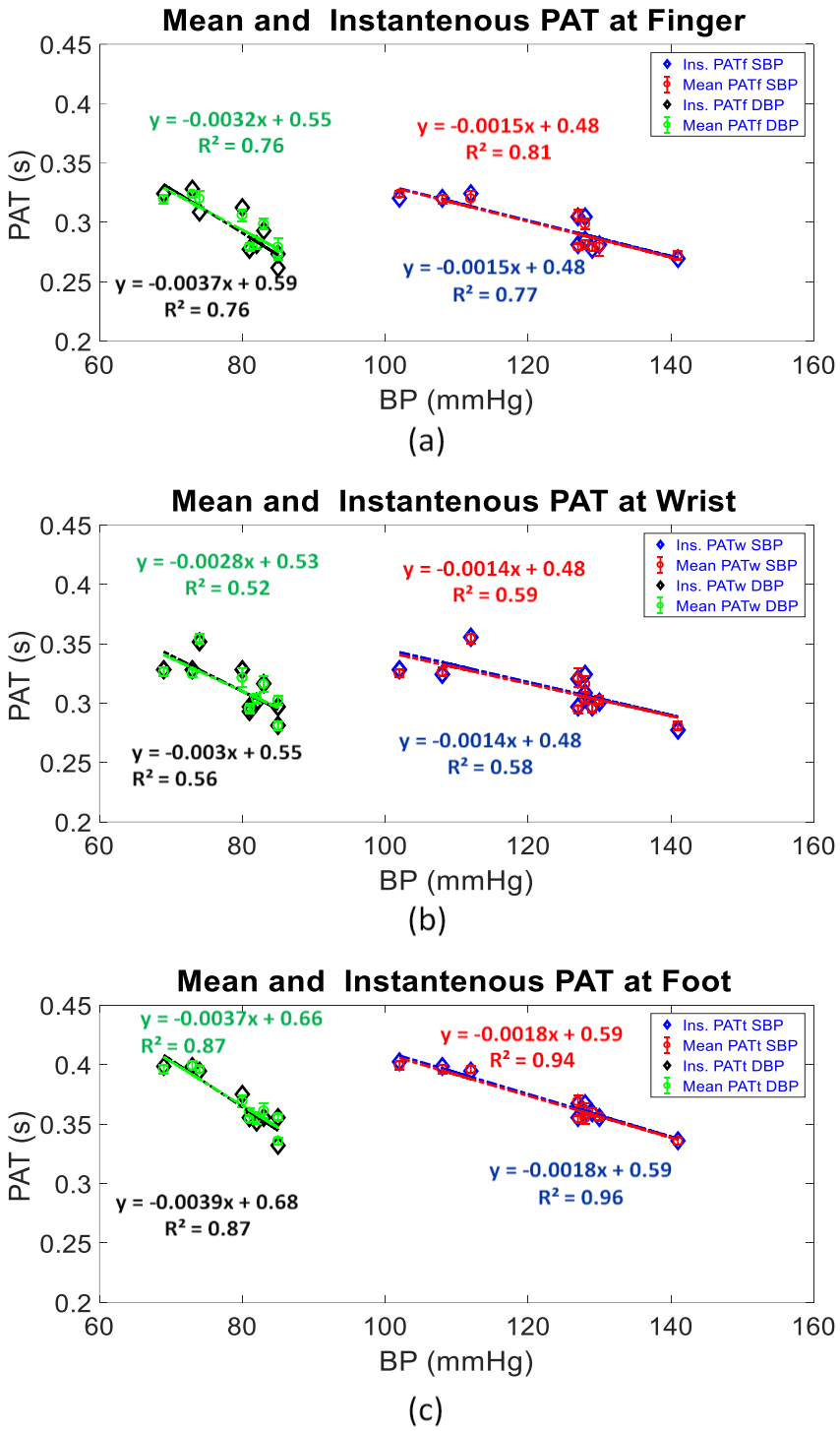


Figure 5.10: Mean PAT and instantaneous (Ins.) PAT measured at ifferent spatial positions (a) PATf (finger), (b) PATw (wrist), and (c) PATt (underfoot)

By referring to the linear equation and the R-squared valued (as shown in Figure 5.11), there appears to be not much difference in the regression line between instantaneous PAT and mean PAT versus BP. SPSS software was used to perform statistical analysis on the mean and instantaneous PAT. There were six pairs compared; mean PATf SBP and Ins. PATf SBP, mean PATf DBP and Ins PATf DBP, mean PATw SBP and Ins. PATw SBP, mean PATw DBP and Ins. PATw DBP, mean PATt SBP and Ins. PATt SBP, mean PATt DBP and Ins. PATt DBP. All the data were normally distributed according to the Shapiro-Wilk test ($p > 0.05$). A student t-test was performed to determine the statistical difference between the mean and instantaneous PAT. The results showed that there is no statistically significant difference between the mean and instantaneous PAT for all the data pairs ($p > 0.05$).

A linear regression model was applied to mean/instantaneous PAT-BP data and the Pearson correlation coefficient, *r* was determined on each volunteer. In general, the Pearson correlation coefficient, r provides a measure of the strength of linear association between two variables [208]. It provides information on how close the points lie to the straight line on the scatter plot. A correlation coefficient of +1 indicates that the two variables are perfectly related in a positive (linear) manner, a correlation coefficient of -1 indicates that two variables are perfectly related in a negative (linear) manner and a correlation coefficient of zero indicates that there is no linear relationship between the two variables being studied [209]. The *r* values were calculated according to Equation 5.1 [210]:

$$r = \frac{\sum_{i=1}^{n}(x-\bar{x})(y-\bar{y})}{\sqrt{\sum_{i=1}^{n}(x-\bar{x})^2}\sqrt{\sum_{i=1}^{n}(y-\bar{y})^2}} \qquad \text{Equation 5.1}$$

where x is BP, $\bar{x}$ is the mean of BP, y is PAT and $\bar{y}$ is the mean of PAT. The results were tabulated in Table 5.2 for SBP and Table 5.3 for DBP. In this table, the absolute value of correlation coefficient, |r| is used to show the relationship strength between PAT and SBP/DBP. The greater the value of |r|, the stronger the linear relationship between PAT and SBP/DBP.

Table 5.2: Absolute correlation coefficient (|r|) of mean and instantaneous PAT for (a) SBP and (b) DBP. The |r| values less than 0.5 are written in red colour and the number is highlighted with a yellow colour if |r| for the instantaneous PAT is greater than |r| for the mean PAT

Volunteer Code	Mean PATf-SBP (|r|)	Ins. PATf-SBP (|r|)	Mean PATw-SBP (|r|)	Ins. PATw-SBP (|r|)	Mean PATt-SBP (|r|)	Ins. PATt-SBP (|r|)
1001	0.90	0.88	0.77	0.76	0.97	0.98
1020	0.88	0.93	0.90	0.86	0.92	0.93
1300	0.81	0.83	0.61	0.62	0.64	0.76
4010	0.72	0.76	0.51	0.63	0.27	0.76
5001	0.95	0.94	0.85	0.71	0.83	0.80
1580	0.81	0.60	0.34	0.29	0.04	0.13
1205	0.83	0.75	0.44	0.37	0.61	0.54
4163	0.87	0.87	0.74	0.67	0.34	0.09
1325	0.79	0.67	0.52	0.88	0.62	0.55
2615	0.68	0.76	0.31	0.51	0.69	0.78
5843	0.75	0.74	0.71	0.59	0.52	0.63
3598	0.72	0.76	0.30	0.77	0.69	0.47
6485	0.64	0.69	0.96	0.63	0.88	0.64

Table 5.3: Absolute correlation coefficient (|r|) of mean and instantaneous PAT for DBP. The |r| < 0.5 is labelled red whilst yellow indicates instantaneous PAT "|r|" is more correlated than the mean PAT

Volunteer Code	Mean PATf-DBP (|r|)	Ins. PATf-DBP (|r|)	Mean PATw-DBP (|r|)	Ins. PATw-DBP (|r|)	Mean PATt-DBP (|r|)	Ins. PATt-DBP (|r|)
1001	0.87	0.87	0.72	0.75	0.93	0.93
1020	0.59	0.71	0.55	0.65	0.55	0.61
1300	0.70	0.71	0.49	0.51	0.69	0.46
4010	0.21	0.27	0.36	0.35	0.26	0.15
5001	0.22	0.26	0.48	0.46	0.32	0.02
1580	0.05	0.17	0.15	0.23	0.04	0.05
1205	0.56	0.48	0.09	0.06	0.70	0.39
4163	0.34	0.45	0.68	0.61	0.42	0.01
1325	0.07	0.28	0.20	0.11	0.01	0.13
2615	0.27	0.27	0.01	0.58	0.08	0.29
5843	0.26	0.32	0.28	0.35	0.66	0.41
3598	0.07	0.66	0.88	0.72	0.74	0.51
6485	0.65	0.67	0.86	0.64	0.59	0.71

The interpretation of |r| values by Mukaka et al. stated that |r| from 0.0 to 0.3 is a negligible correlation, |r| from 0.3 to 0.5 showed low correlation, |r| from 0.5 to 0.7 showed moderate correlation, |r| from 0.7 to 0.9 showed a high correlation, and |r| from 0.9 to 1.0 showed very high correlation [210]. As shown in Table 5.2 and Table 5.3, the |r| values <

0.5 are labelled red and the |*r*| value > 0.5 is written in black. In general, the results in Table 5.2 shows that the PAT has a good correlation with SBP, especially for PATf (mean and instantaneous PAT), with 100% of volunteers achieving |*r*| > 0.5. The results show that a weak correlation between PAT and DBP, with the majority of volunteers achieving a |*r*| value < 0.5 for all categories, PATf, PATw and PATt (mean and instantaneous PAT). The |*r*| values between mean and instantaneous PAT were compared within their categories (PATf, PPTw and PATt) for SBP and DBP. The data has been highlighted in yellow if the instantaneous PAT |*r*| value is more correlated than the mean PAT (Table 5.2 and Table 5.3). As shown in Table 5.2, the mean and instantaneous PATf shared a similar |*r*| value for most volunteers. For PATw, there are a few cases that show that the |*r*| value for instantaneous PAT is much higher than mean PAT, for example, see Table 5.2, volunteer code 3598, row 13, and column 5. A similar case was observed in PATt categories as shown by volunteer code 4010 (Table 5.2, row 5, column 7) with the |*r*| value for instantaneous PAT being higher than the mean PAT by 0.49.

Statistical analysis using the two proportion Z-test was performed to compare the proportions of data distribution (numbers written in black (|*r*| > 0.5) over the total numbers in cells) in Table 5.2 (SBP) and Table 5.3 (DBP). The |*r*| values less than 0.5 (weak correlation) are written in red colour (Table 5.2 and Table 5.3). The null hypothesis (H_0) for this test is that the proportions in SBP and DBP are the same and the alternate hypothesis (H_1) is that the proportions are not the same. The data for the Z-test is summarized in Table 5.4.

Table 5.4: The numbers of data Irl > 0.5 and Irl < 0.5 in PAT-SBP and PAT-DBP for proportions Z-test

Category	**Number of Irl > 0.5**	**Number of Irl < 0.5**	**Total number of samples (n)**	**Proportions for Irl > 0.5**
SBP	66	12	78	0.85
DBP	34	44	78	0.44
Total	100	56	156	

The results in Table 5.4 showed that, 85 % of SBP have a good correlation with PAT (Irl > 0.5), compared to 44 % recorded by DBP. Next, the Z-score and the p-value is calculated with the alpha level is set to 0.05 using two-tailed Z-test. From the Z-test analysis, the value of the Z-score is -3.8629 and the p value is 0.00012 ($p < 0.05$) suggested that the null hypothesis (H_0) was rejected and there is a statistically significant difference between the proportions of data distribution (Irl > 0.5), in SBP and DBP.

Next, a Shapiro-Wilk test was performed to test the normality of the data distribution. The result from this test showed that $p > 0.05$ for each data on all categories PATf, PATw and PATt (mean and instantaneous PAT) indicated that the data were normally distributed. Therefore, the student t-test was performed to check the statistically significant difference between the mean and instantaneous PAT-BP in 6 pairs; mean PATf-SBP with Ins. PATf-SBP, mean PATw-SBP with Ins. PATw-SBP, mean PATt-SBP with Ins. PATt-SBP, mean PATf-DBP with Ins. PATf-DBP, mean PATw-DBP with Ins. PATw-DBP and mean PATt-DBP with Ins. PATt-DBP. The results showed that the p-value greater than 0.05 ($p > 0.05$), for all pairs except for mean PATf-DBP with Ins. PATf-DBP. The p-value > 0.05 suggested that the null hypothesis (H_0) was accepted and

statistically showed that there is no difference in the I*r*I value between mean and instantaneous PAT-BP. The p-value for mean PATf-DBP with Ins. PATf-DBP is less than 0.05 ($p = 0.039, < 0.05$), indicated that the null hypothesis (H_0) was rejected and that there is a statistically significant different between mean PATf and instantaneous PATf with DBP. This can be clearly seen in Table 5.3, which shows that the I*r*I values for instantaneous PATf are higher than mean PATf in most volunteers.

The variation in BP over several beats gets in the way of a mean value calculation of PAT when compared to an instantaneous PAT resulting a different in I*r*I value obtained in some volunteers. In general, a single outlier that appeared on the PAT-BP plotted line may dramatically alter the correlation coefficient, *r*, and reduce the accuracy of the equation in estimating BP [209]. In the next section, a calibration curve for each volunteer was generated using the best linear fit equation on the data of mean PAT-SBP and instantaneous PAT-SBP during the pedal exercise experiment.

5.3.5 PAT-SBP Calibration Curve Based on Pedal Exercise

To allow the stand-alone PAT device to estimate BP, a calibration curve has to be determined for each volunteer. In general, a first step for constructing a calibration curve is measure PAT and BP simultaneously from a subject during interventions that perturb BP [165]. Next, multiple pairs of PAT and BP data are plotted, and a linear regression line generated that fits the data gathered. In this work, a calibration curve on each volunteer was obtained through pedal exercise by measuring PAT

at finger and wrist simultaneously with oscillometric BP. The PAT measured between ECG and PPG at the finger were deployed by standard sensors (ECG surface electrode and blood volume sensor) from the NeXus device. Simultaneously, PAT at the wrist was measured by conductive fabric electrodes for the ECG measurement on the chest and POF for the PPG measurement. Figure 5.12 shows the mean PAT calibration curve at the finger (PATf) and at the wrist (PATw) on volunteer 1 (Vol1, volunteer code: 1001).

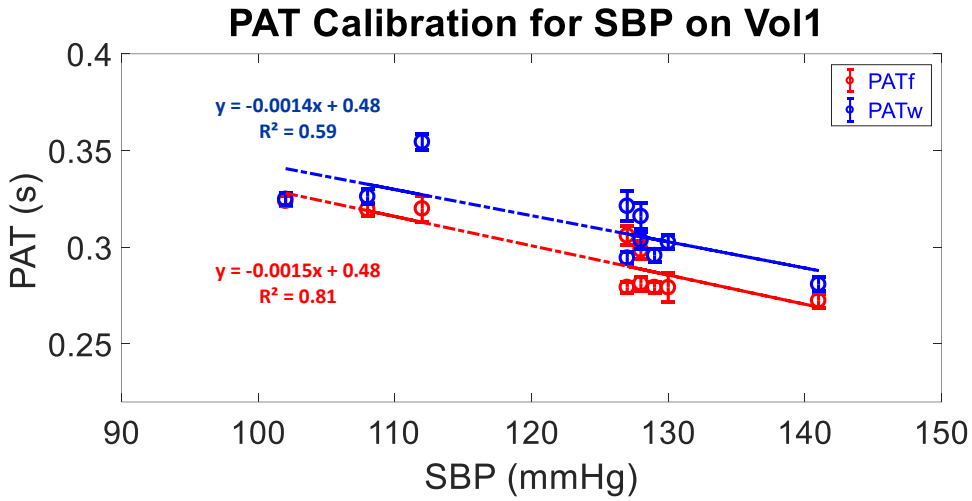


Figure 5.11: Exercise calibration curve at the finger (PATf-SBP) and at the wrist (PATw-SBP). The PATf (red marker) and PATw (blue marker) is plotted based on mean ± SD of 15 pulses

As shown in Figure 5.12, the y-axis represents the PAT (ECG to PPG) in units of seconds (s), and the x-axis represents SBP in mmHg. A linear regression line was drawn according to a linear equation, $Y = mX + c$; with m representing the graph slope and c represents the point where the line crosses the y-axis. The R-squared value for PATf-SBP ($R^2 = 0.81$) is higher than PATw-SBP ($R^2 = 0.59$) indicated that the strong relationship between PAT-SBP at the finger compared to the wrist. Table

5.5 shows the calibration equations for the mean PAT-SBP and Table 5.6 shows the calibration equations on instantaneous PAT-SBP on each volunteer.

Table 5.5: Calibration equation on each volunteer based on mean PAT with SBP. Y represents the PAT and X represents blood pressure in mmHg

Volunteer Code	**Calibration equation for mean PAT-SBP (finger)**	**Calibration equation for mean PAT-SBP (wrist)**
1001	$Y = -0.001512X + 0.48$	$Y = -0.001352X + 0.48$
1020	$Y = -0.001155X + 0.43$	$Y = -0.001569X + 0.49$
1300	$Y = -0.001801X + 0.52$	$Y = -0.00263X + 0.64$
4010	$Y = -0.002621X + 0.58$	$Y = -0.003438X + 0.68$
5001	$Y = -0.001709X + 0.51$	$Y = -0.00202X + 0.56$
1580	$Y = -0.001511X + 0.46$	$Y = -0.001777X + 0.53$
1205	$Y = -0.0008339X + 0.40$	$Y = -0.0007729X + 0.41$
4163	$Y = -0.002225X + 0.54$	$Y = -0.003139X + 0.66$
1325	$Y = -0.00212X + 0.55$	$Y = -0.001061X + 0.37$
2615	$Y = -0.001581X + 0.48$	$Y = -0.001333X + 0.48$
5843	$Y = -0.001416X + 0.45$	$Y = -0.002796X + 0.65$
3598	$Y = -0.001617X + 0.44$	$Y = -0.0007571X + 0.39$
6485	$Y = -0.00137X + 0.42$	$Y = -0.002829X + 0.67$

Table 5.6: Calibration equation on each volunteer based on instantaneous (Ins.) PAT with SBP. Y represents the PAT and X represents blood pressure in mmHg

Volunteer Code	Calibration equation for Ins. PAT-SBP (finger)	Calibration equation for Ins. PAT-SBP (wrist)
1001	$Y = -0.0015X + 0.48$	$Y = -0.0014X + 0.48$
1020	$Y = -0.0013X + 0.46$	$Y = -0.0015X + 0.48$
1300	$Y = -0.0019X + 0.53$	$Y = -0.0026X + 0.64$
4010	$Y = -0.0025X + 0.56$	$Y = -0.0041X + 0.74$
5001	$Y = -0.0017X + 0.51$	$Y = -0.0019X + 0.54$
1580	$Y = -0.0012X + 0.44$	$Y = -0.0015X + 0.49$
1205	$Y = -0.0009X + 0.42$	$Y = -0.0008X + 0.42$
4163	$Y = -0.0023X + 0.54$	$Y = -0.0032X + 0.65$
1325	$Y = -0.0015X + 0.41$	$Y = -0.003X + 0.65$
2615	$Y = -0.0031X + 0.64$	$Y = -0.0028X + 0.64$
5843	$Y = -0.0017X + 0.49$	$Y = -0.0018X + 0.54$
3598	$Y = -0.0028X + 0.36$	$Y = -0.0026X + 0.59$
6485	$Y = -0.0017X + 0.48$	$Y = -0.0018X + 0.53$

Figure 5.12 shows plot of boxplots of the gradient (m) and Y-intercept for calibration equation (mean and instantaneous PAT) for all volunteers at finger and wrist. The horizontal lines (red lines) show the median or the middle (50%) of the data. The upper and lower edges of the boxes (blue boxes) indicate the 75th and 25th percentiles, respectively. The 5-95% range of the data is indicated by the ends of the vertical lines (black lines).

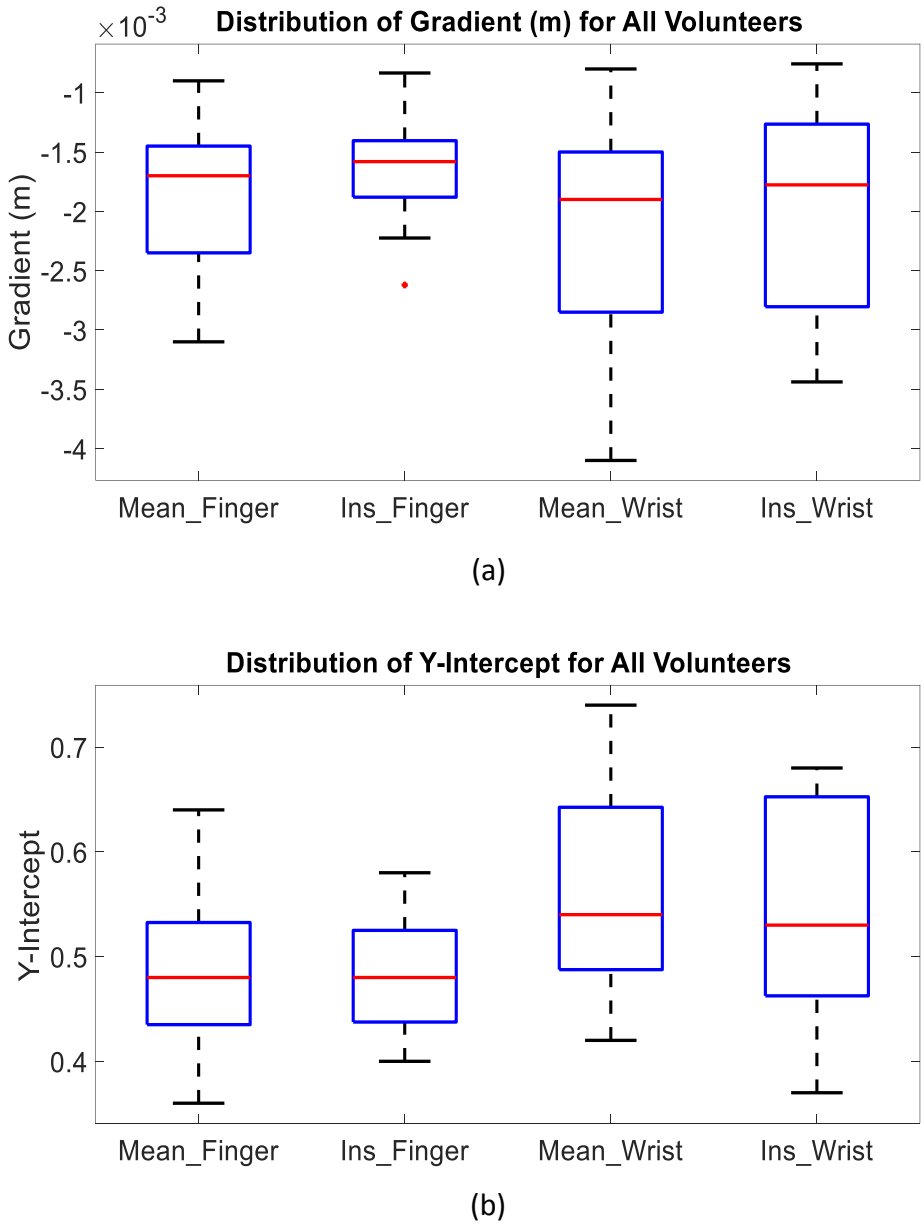
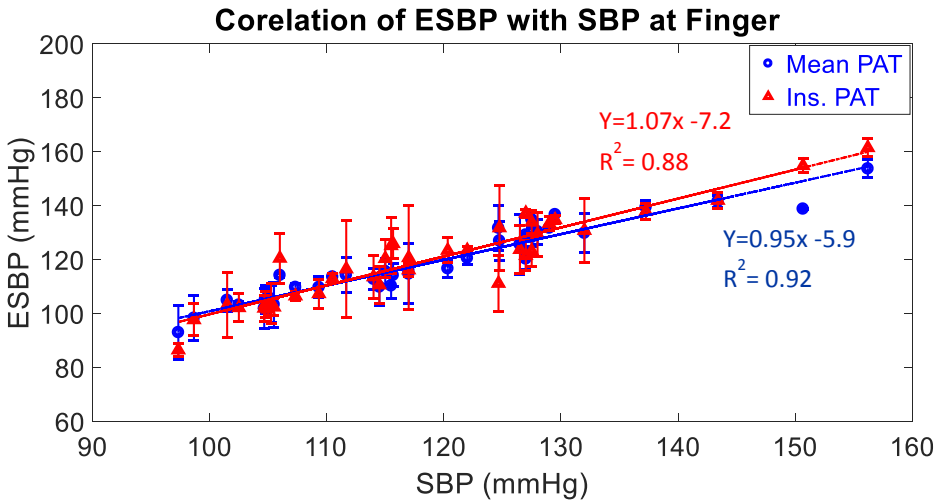


Figure 5.12: The distribution of (a) gradient (m) and (b) Y-intercept for calibration equation in Table 5.5 and Table 5.6. Mean Finger and Mean_Wrist represents the calibration equation for mean PAT-SBP at finger and wrist respectively. Ins_Finger and Ins_Wrist represents the calibration equation for instantaneous PAT-SBP at finger and wrist respectively

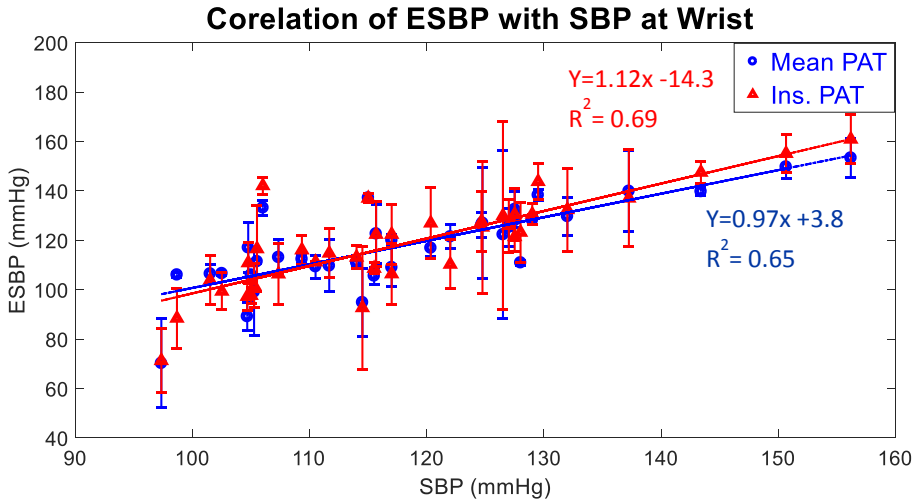
The results in Figure 5.12 (a) shows that the median (red lines) of the slope (m) for the Mean_Finger is -0.0017 and for the Ins_Finger is -0.0019. The median of the m value for the Mean_Wrist and the Ins_Wrist is -0.0016 and -0.0018 respectively. In Figure 5.12 (b) the median for both condition (Mean_Finger and the Ins_Finger) is 0.48. For Mean_Wrist and Ins_Wrist, the Y-intercept value is 0.53 and 0.54 respectively. A Student's t-test was applied to check the statistically significant difference of the graph slope (m) and Y-intercept between these pairs: Mean_Finger with Ins_Finger and Mean_Wrist with Ins_Wrist. The results showed that all pairs giving $p > 0.05$, regarded as statistically insignificant changes of the calibration equation using mean or instantaneous PAT in each volunteer.

5.3.1 Comparison Between instantaneous and mean PAT calibration equation on estimated SBP

The equations in Table 5.5 and Table 5.6 were obtained by fitting a linear regression model to instantaneous and mean PAT-SBP measurements. An estimated BP for each volunteer is calculated according to the calibration equation, and the results are plotted in Figure 5.13. The plotted data is based on the mean ± SD of three repeats measurement of SBP and PAT at each phase (rest, pedal exercise and recovery) during the pedal bike experiment (see Figure 5.4).



(a)



(b)

Figure 5.13: The estimated systolic blood pressure (ESBP) based on mean PAT (blue marker) and instantaneous PAT (red marker) (a) at the finger and (b) at the wrist. The R-squared value for ESBP-SBP at finger is higher than R-squared ESBP-SBP at wrist indicated that the strong relationship between ESBP-SBP at the finger compared to the wrist

The regression coefficient *r* and the root mean square error (RMSE) in Figure 5.13 were analysed, and the results shown in Table 5.7. The RMSE helps to provide a complete picture of the error distribution on the fitting line of mean and instantaneous PAT at finger and wrist [211].

Table 5.7: Correlation coefficient, r and RMSE for mean and instantaneous PAT at finger and wrist

Calibration Type	**Correlation coefficient *(r)***	**Root mean square error (RMSE) (mmHg)**
Mean PATf-SBP	0.96	4
Ins. PATf-SBP	0.94	6
Mean. PATw-SBP	0.81	10
Ins. PATw-SBP	0.83	11

The results in Table 5.7 show that there was a strong correlation between ESBP and SBP at the finger with $r = 0.96$, for mean PAT and $r = 0.94$ for the instantaneous PAT method. Meanwhile, there is a relatively good correlation between ESBP and SBP at the wrist with $r = 0.81$ and $r = 0.83$ for mean PAT and instantaneous PAT respectively. The RMSE between the ESBP and reference SBP at finger is 4mmHg (mean PAT) and 6mmHg (instantaneous PAT). The RMSE recorded at the wrist using the mean PAT is 10mmHg, and the RMSE using instantaneous PAT is 11mmHg. In the literature, the correlation coefficient *r* for PAT-SBP relationship varies from 0.73 to 0.99, and for the RMSE, this varies from 1.7 mmHg to 15.4 mmHg [165]. The information suggests that the

findings from the experiment in this thesis are “on a par” with the results obtained by other researchers.

Statistical software (SPSS 23.0) was deployed to analyse the data distribution and to compare statistically the difference between mean PAT and instantaneous PAT in estimating SBP. The results from the Shapiro-Wilk test showed that one of the datasets (Ave.PATw) was non-normally distributed with the p-value recorded equal to 0.027 ($p < 0.05$). Therefore, the Wilcoxon signed rank test was deployed in the statistical analysis when the two samples cannot be assumed to be normally distributed [212]. The results from the Wilcoxon signed rank test showed that the p-value less than 0.05 ($p < 0.05$) for all pairs (meanPATf with Ins. PATf, and meanPATw with Ins. PATw), indicating that there was no significant difference between two samples (mean and instantaneous PAT) in estimating SBP. However, the mean PAT method gives a marginally better correlation on PAT-SBP compared to the instantaneous PAT method as shown in a Bland-Altman plot (Figure 5.14)

As shown in Figure 5.14 (a), the limits of agreement (± 2 SD) were ± 8 mmHg for mean PAT and ± 11 mmHg for instantaneous PAT for the calibration method at the finger. A wide variation of ESBP were observed by using the calibration method at the wrist (Figure 5.14 (b)), where the limits of agreement (± 2 SD) were ± 19.5 mmHg for mean PAT and ± 21.5 mmHg for instantaneous PAT.

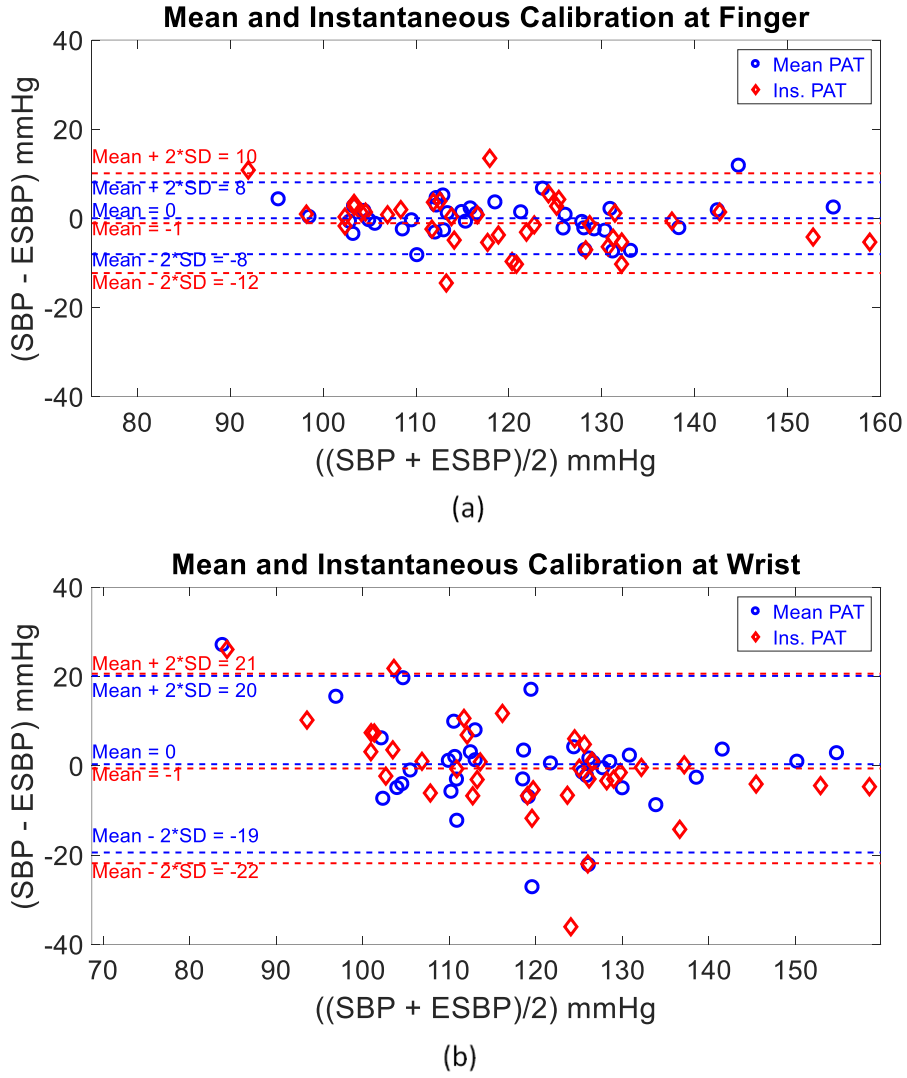


Figure 5.14: The Bland-Altman plot for ESBP using calibration equation (a) at the finger and (b) at the wrist

In summary, a mean PAT method showed advantages over the instantaneous method by mitigating the effects of measurement and physiologic (e.g., respiratory) artefacts as well as erroneous beat detections [165]. Therefore, the calibration equation based on the mean PAT was used to estimate SBP in the next tilt table experiments.

5.4 Second Experiment: Tilt Table

The second experiment involved a tilt table to vary the BP by moving the body in controlled safe way from a supine to standing position and then back to a supine position. This method, as will be seen, showed significant changes in SBP and DBP due to postural changes as reported in the literature [213]. The same group of volunteers involved in this study are as shown in Table 5.1. Two volunteers in Table 5.1 (volunteer code 1325 and 3598) withdrew from this experiment due to a technical recording problem, resulting only eleven volunteers that participated in this experiment. The experiment was approved by the Faculty of Engineering Ethical Review Committee, and the ethics application form is supplied in **Appendix A**.

The volunteer was briefed about the procedure and safety precautions before experimenting. All the sensors were attached to the volunteers, as shown in Figure 5.1. The ECG surface electrode (ECGs) and the ECG fabric based electrode (ECGfe) were placed side by side on volunteer's chest based on the lead II Einthoven triangle measurement [200]. The PPG was measured at three locations; index finger (right arm), wrist (right arm) and under the foot (right leg). A protocol for the tilt table experiment, adapted from Arza et al. [213], was as follows:

1. First, the volunteer was asked to rest horizontally on the tilt table for 6 minutes.
2. Then, the tilt table was tilted up from 0 degrees to 70 degree (where 0 is horizontal supine position). The volunteer was in this position for 6 minutes.
3. After that, the table was tilted down to the initial position (0 degrees), and the volunteer stayed in this position for a further 6 minutes.

In this experiment, the PAT was recorded continuously at 256 samples/second, and the BP was recorded every two minutes at each position (step number 1 to step number 3).

Figure 5.15 (a) shows the volunteer in a supine position and Figure 5.15 (b) shows an illustration of how the tilt table moved from the supine position to the tilt-up position. BioTrace+ software (Mind Media B.V. Netherlands) was used to record all the data, and Matlab software was deployed for subsequent analysis.

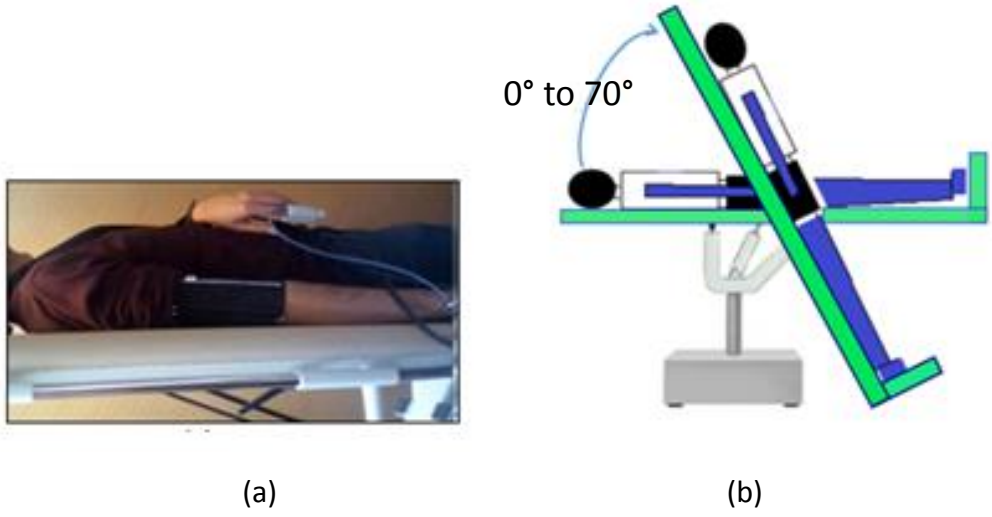


Figure 5.15: Experiment setup for tilt table (a) Volunteer on the tilt table in the supine position (0°), (b) Illustration of a volunteer on tilt table moving from supine position to tilt-up position (0° to 70°)

Approximately 30 minutes were required to complete the tilt table experiment (include setup and settling down) for each volunteer. The ECG and PPG were continuously recorded at 256 samples/second during the experiment. Simultaneously, BP was recorded manually every two minutes. The BP cuff oscillation was monitored by the external

pressure meter (MPX 4250AD) for one-step calibration purposes as presented in the next section.

5.4.1 One-Step Calibration Based on BP Cuff Oscillation Waveform

In the academic literature, most of the individual calibration curves were obtained by performing physical exercise [22], [214], [215]. Through exercise, multiple pairs of PAT and BP were recorded, and a mathematical model was established to relate PAT and BP on each volunteer. This method required a protocol and a reference method in BP measurement. Thus the measurement of absolute BP using PAT is time-consuming and not feasible in most clinical situations [19]. Therefore, in this work, we proposed a one-step calibration of the PAT-BP relationship, which required only one measurement of BP using an oscillometric BP device.

During the BP measurement, the Ostar BP monitor inflates the BP cuff to a certain pressure (above systolic pressure) and then the pressure slowly released at a typical bleed rate of 3mmHg/second [41]. During the deflation, the cuff sensed the small oscillations indicating the pulsations that are caused by the arterial pressure [65]. At the same time, the external pressure sensor (MPX 4250AD) recorded the oscillation signal and sent the signal to the computer via the NeXus device. A high pass filter with a cut off frequency 0.2 Hz was deployed to extract the oscillometric pulses from the cuff deflation curve. The ECG signals and the cuff oscillation signal were aligned, as shown in Figure 5.16.

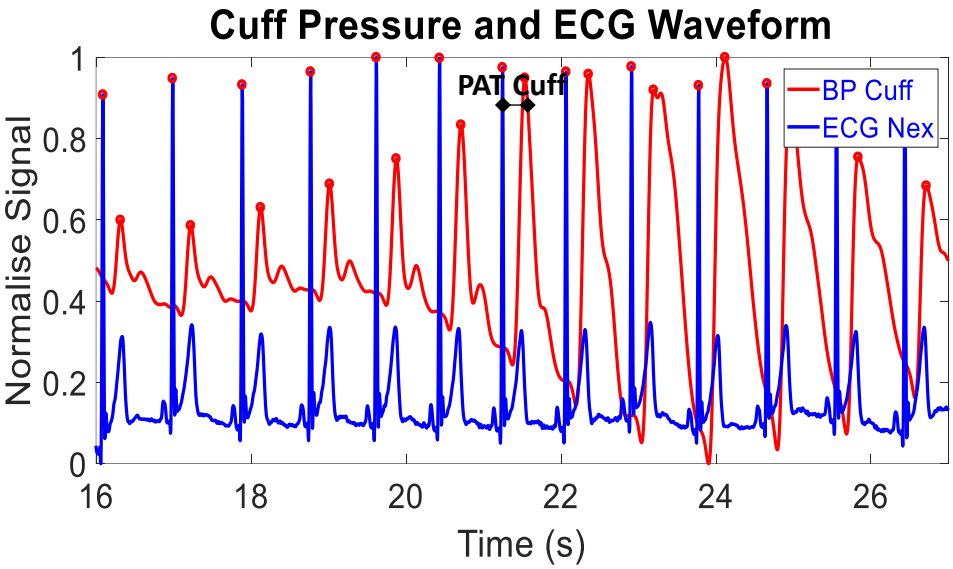


Figure 5.16: PATcuff measurement on volunteer 1 (Vol1, volunteer code: 1001). The ECG signals are represented in red (ECG Nex) and the BP cuff oscillation during deflation are represented in blue (BP Cuff)

The delay time between the peak cuff oscillation waveform and the R peak of ECG waveform was identified and denoted as PATcuff. The PATcuff signal was then plotted against the deflation cuff pressure for each volunteers at the beginning of the experiment. Figure 5.17 shows the plotted of PATcuff and BP cuff pressure on three volunteers, named as Volunteer 1 (Vol1), Volunteer 2 (Vol 2) and Volunteer 3 (Vol3).

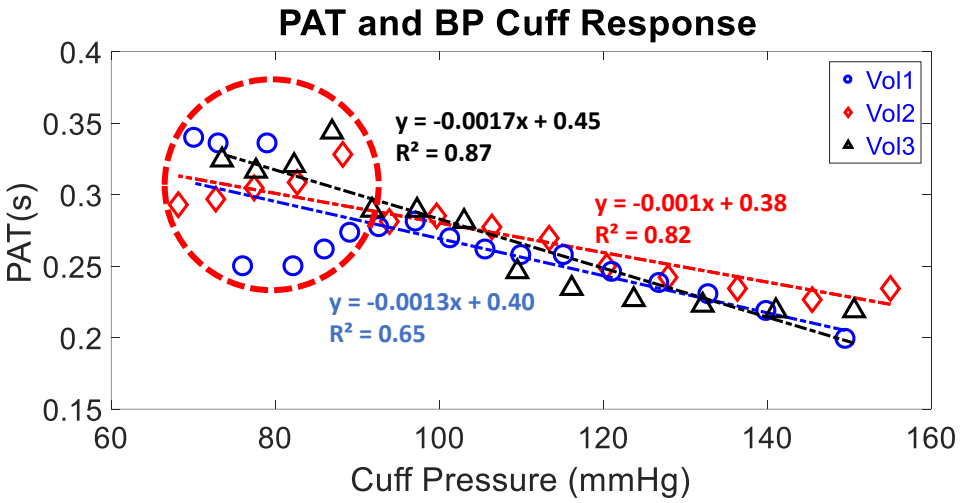


Figure 5.17: PAT and BP cuff pressure response on three volunteers (Vol1, Vol2 and Vol3)

As shown in Figure 5.17, the PATcuff decreases with cuff pressure applied over the brachial artery during the BP cuff deflation. However, at low cuff pressure values (dotted red line circle), PATcuff fluctuations were observed for all volunteers. During the cuff deflation, the radius of the brachial artery on the upper arm relatively increases as the cuff pressure decreases from systolic blood pressure (SBP) to diastolic blood pressure (DBP), thus increasing the PAT [216]. After the DBP point, the brachial artery wall no longer collapses by the BP cuff allowing the blood flow becomes normal again without turbulence and thus produces no further changes in the PATcuff. A linear equation that represented a calibration curve was obtained by fitting the data with a regression line on all volunteers. Based on the regression line a one-step PAT calibration method is proposed as showed in Figure 5.18.

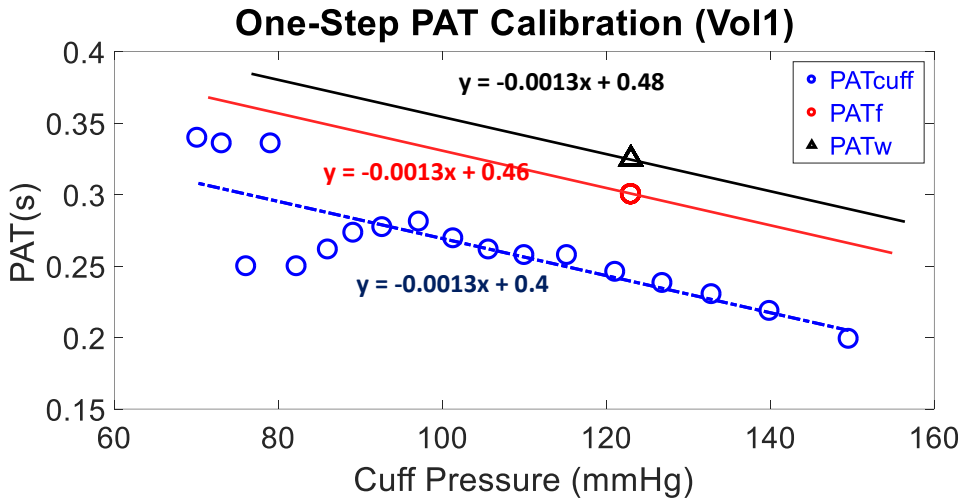


Figure 5.18: A calibration curve on volunteer 1 (Vol1) based on PATcuff–cuff pressure relation (blue trace). One-step calibration curve for PATf (red trace) and PATw (black trace) obtained by shifting the PATcuff regression line (blue trace) to the PATf position (red marker) and to the PATw position (black marker) respectively

Based on the PATcuff regression line, the gradient of the calibration curve is determined and shifted this baseline to a new position based on the PAT obtained from the finger and the wrist (Figure 5.18). The shifting procedure is related to the arterial wave propagation modelled by the Moens-Korteweg equation (Equation 2.1) [22]. In this model, it was assumed that the blood vessel is regarded as a thin-walled linear elastic tube and the PWV is directly proportional to the square root of the Young elasticity modulus (E). The propagation speed of pulse waves is about 5 ms^{-1} at the ascending aorta, and this value increases toward peripheral arteries [35]. The pulse wave that travels along the brachial artery to the radial artery is considered as a regional PWV [217], therefore the baseline plotted (PATcuff) is shifted to the other different position due to the difference in distance relative to the heart.

In this experiment, the calibration curve for PTTcuff–cuff pressure obtained by a single oscillometric BP measurement. For example, in Figure 5.18, a BP measurement on V1 showed a result of the SBP = 123 mmHg, PATf = 0.3003 and PATw = 0.325. One-step calibration curve at the finger was generated by shifting the PATcuff regression line (blue trace) to the PATf position (red marker). Meanwhile, one-step calibration curve at the wrist obtained by shifting the PATcuff regression line (blue trace) to the PATw position (black marker). The blue regression line (Figure 5.17) is represented by the linear equation as stated in Equation 5.2:

$$ycuff = -0.0013xcuff + Ccuff \qquad \text{Equation 5.2}$$

with *ycuff* is PAT (s), *xcuff* is cuff pressure, and *Ccuff* is equal to 0.399 (PAT- intercept on the y-axis). For one-step calibration at the finger, the calibration curve (Equation 5.2) was shifted along the y-axis to the position of the red marker (SBP, PATf). Therefore, the new y-axis interception for the curve was calculated by substituting Equation 5.2 of *ycuff* with PATf value (PATf = 0.3003 seconds) and *xcuff* with SBP value (SBP = 123 mmHg). The y-axis interception denoted as *CPATf* was calculated as follows:

$$ycuff = ycuff + 0.0013(xcuff)$$

$$ycuff = PTTf = 0.30\ s$$

$$cuff = SBP = 123\ mmHg$$

$$Ccuff = Cpttf$$

$$Cpttf = 0.3003 + 0.0013(123) = 0.46\ s$$

$$y1 = -0.0013x1 + 0.46 \qquad \text{Equation 5.3}$$

with *y1* is PATf (s) and *x1* is SBP (mmHg). A similar approach was deployed to determine one-step calibration curve at the wrist. The new y-axis interception denoted as CPATw was calculated based on the PATw = 0.325 s and SBP = 123 mmHg as follows:

$$Cpttw = 0.325 + 0.0013(123)$$

$$Cpttf = 0.48\ s$$

$$y2 = -0.0013x1 + 0.48 \qquad \text{Equation 5.4}$$

with *y2* is a PATw and x1 is a SBP. Equation 5.3 and Equation 5.4 are the equations for one-step calibration for PATf-SBP and PATw-SBP, respectively (for volunteer 1 (Vol1)). This method was deployed to the eleven volunteers in determining the one-step calibration equation, and the results are shown in Table 5.8.

Table 5.8: One-step calibration equation for all volunteers based on PATf-SBP and PATw-SBP with y1 is PATf, y2 is PATw and x1 is SBP

Volunteer Code	One-step calibration equation for PATf- SBP (Finger)	One-step calibration equation for PATw- SBP (Wrist)
1001	$y1 = -0.0013x1 + 0.46$	$y2 = -0.0013x1 + 0.48$
1020	$y1 = -0.0012x1 + 0.43$	$y2 = -0.0012x1 + 0.45$
1300	$y1 = -0.0011x1 + 0.42$	$y2 = -0.0011x1 + 0.43$
4010	$y1 = -0.0016x1 + 0.46$	$y2 = -0.0016x1 + 0.50$
5001	$y1 = -0.0009x1 + 0.39$	$y2 = -0.0009x1 + 0.40$
1580	$y1 = -0.0018x1 + 0.49$	$y2 = -0.0018x1 + 0.54$
1205	$y1 = -0.0015x1 + 0.47$	$y2 = -0.0015x1 + 0.49$
4163	$y1 = -0.0007x1 + 0.37$	$y2 = -0.0007x1 + 0.41$
1325	$y1 = -0.0017x1 + 0.50$	$y2 = -0.0017x1 + 0.57$
2615	$y1 = -0.001x1 + 0.39$	$y2 = -0.001x1 + 0.41$
5843	$y1 = -0.0005x1 + 0.34$	$y2 = -0.0005x1 + 0.37$
3598	$y1 = -0.0013x1 + 0.46$	$y2 = -0.0013x1 + 0.48$
6485	$y1 = -0.0012x1 + 0.43$	$y2 = -0.0012x1 + 0.453$

Based on the equation in Table 5.8, an estimated SBP were calculated according to PATf/PATw data obtained during the tilt table experiment. The accuracy of estimated SBP is compared with a calibration equation based on physical exercise (Table 5.4), and the results are presented in the next section.

5.4.2 PAT Measurement on Tilt Table

Traditionally, a tilt table test is deployed to diagnose patients with orthostatic hypotension (OH). Common symptoms for OH patients include dizziness, light headedness, blurred vision, weakness, fatigue, nausea, palpitations, and headache [218]. A patient that suffers from OH

shows a decrease in SBP by 20 mmHg or a DBP decrease by 10 mmHg within 3 minutes of an upright tilt [78]. A healthy patient that goes through this test shows a decrease in SBP of only 5 mmHg to 10 mmHg, with a corresponding increase in DBP of 5 mmHg to10 mmHg, and an increase in pulse rate of 10 bpm to 25 bpm during the upright tilt [218].

In the experiment carried out in this thesis, the tilt table test was held in the supine position for 6 minutes, then in the tilt-up position for 6 minutes and then returned to the supine position (tilt-down) for 6 minutes in the same manner as described in section 5.4. The delay time between the ECG to PPG on the finger (PATf), ECG to PPG on the wrist (PATw) and ECG to PPG under foot (PATt) were recorded simultaneously with the BP on the left arm. All the PPG sensors were located on the right arm (finger and wrist) and under the right foot. The right arm was placed near to the heart level to maintain the arm position level with the heart during the tilt moving from supine to standing position. The PAT of eleven volunteers were monitored on the tilt table, and the result was plotted on boxplot, as shown in Figure 5.19. The PAT was calculated based on a mean of 15 pulses at each position.

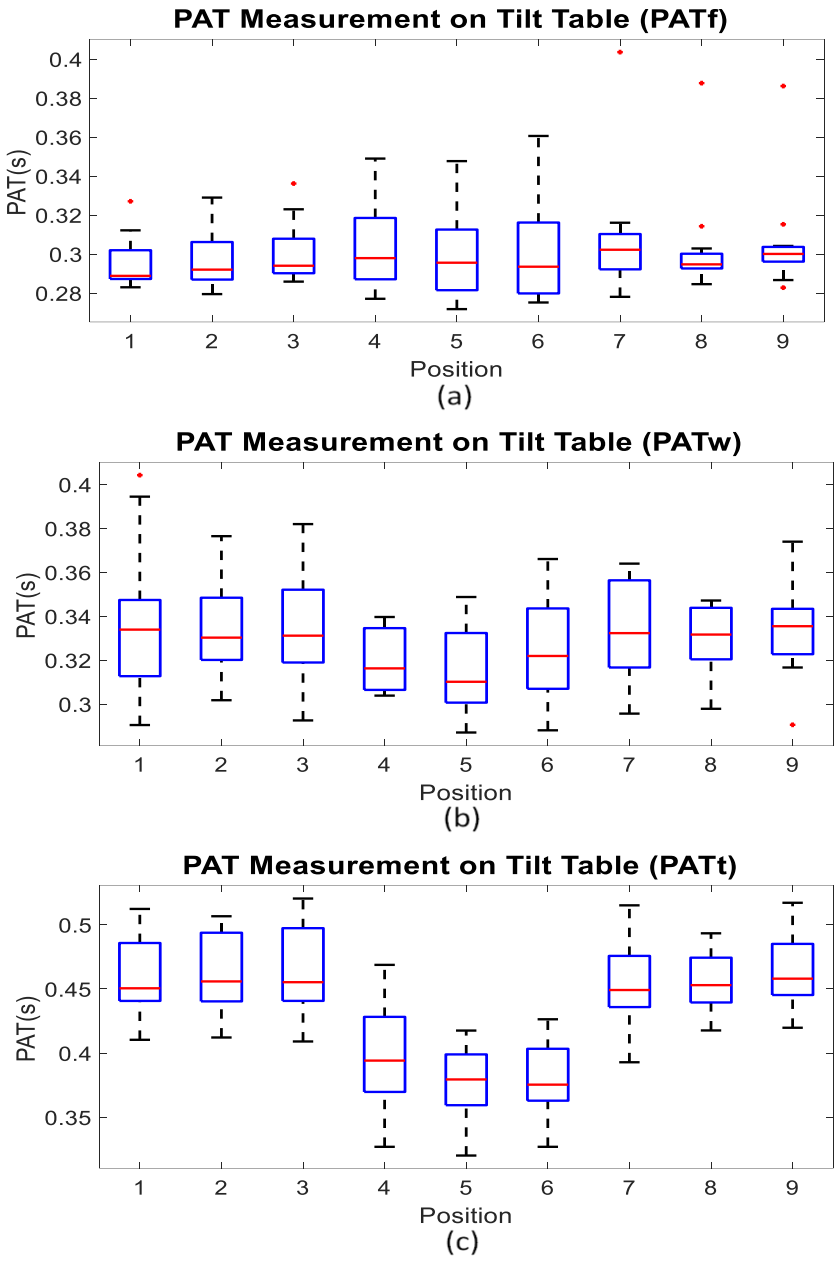


Figure 5.19: PAT measurement during the tilt table experiment on eleven volunteers. The y-axis on the left side refers to PAT measurement, and the x-axis refers to the tilt table position with the number 1,2, and 3 refers to supine position, 4,5 and 6 refers to tilt-up position (70° degree) and 7,8, and 9 refers to tilt-down (supine) position. (a) The PATf refers to the delay time between ECG to PPG at the finger, (b) The PATw refers to the delay time between ECG to PPG on the wrist, and (c) The PATt refers to the delay time between ECG to PPG underfoot

The mean of PAT and BP at the supine (position 1, 2, and 3) and the tilt up (position 4, 5 and 6) were calculated and compared statistically using statistical software SPSS 23.0 (IBM SPSS Statistics, IBM Corporation, Armonk, New York). The Kolmogorov-Smirnov test was performed to test data distribution, and the results show that all the data are normally distributed ($p > 0.05$). The results of the student t-test showed that the mean values of PATf and PATw were not statistically different between two conditions (supine and tilt up) with the p values equal to 0.311 for the PATf ($p > 0.05$), and the p-value equal to 0.108 for the PATw ($p > 0.05$). However, there is a statistically significant difference recorded for the PATt between supine and tilt up a position with $p < 0.001$. The mean value of PATt recorded at the supine position is 0.45 seconds, and this mean value dropped to 0.38 seconds when the tilt table moves to the tilt-up position.

This finding is in contrast with the results published by Allen et al. [219] which stated that there were no differences in beat-to-beat pulse arrival time (to foot of pulse, PATf) at toe during changes from baseline (subject supine) to tilt up position (head-up to 70°). Similar to the tilt-table experiment, a change in position from horizontal to vertical (supine to standing) led to a decrease in the PAT at the toe were reported by other researchers [220], [221].

In this experiment, it can be clearly seen in Figure 5.19 (c), the PATt sharply drops during the tilt table moving from the supine position to the tilt-up position. The change in PATt is due to the posture change when the foot is below to the heart level as the tilt table moves from supine to tilt up. In the tilt-up position, the blood flow increases toward to the leg due to the changes of hydrostatic pressure induced by gravity, resulting in the PAT values dropping at the lower leg [221], [222]. All the PATs return to the baseline (initial condition) when the tilt table moves from the

tilt-up to the tilt-down condition (position 7, 8 and 9 in Figure 5.19). For the BP measurement, the boxplot for the BP recorded at the different tilt table position for all volunteers is shown in Figure 5.20.

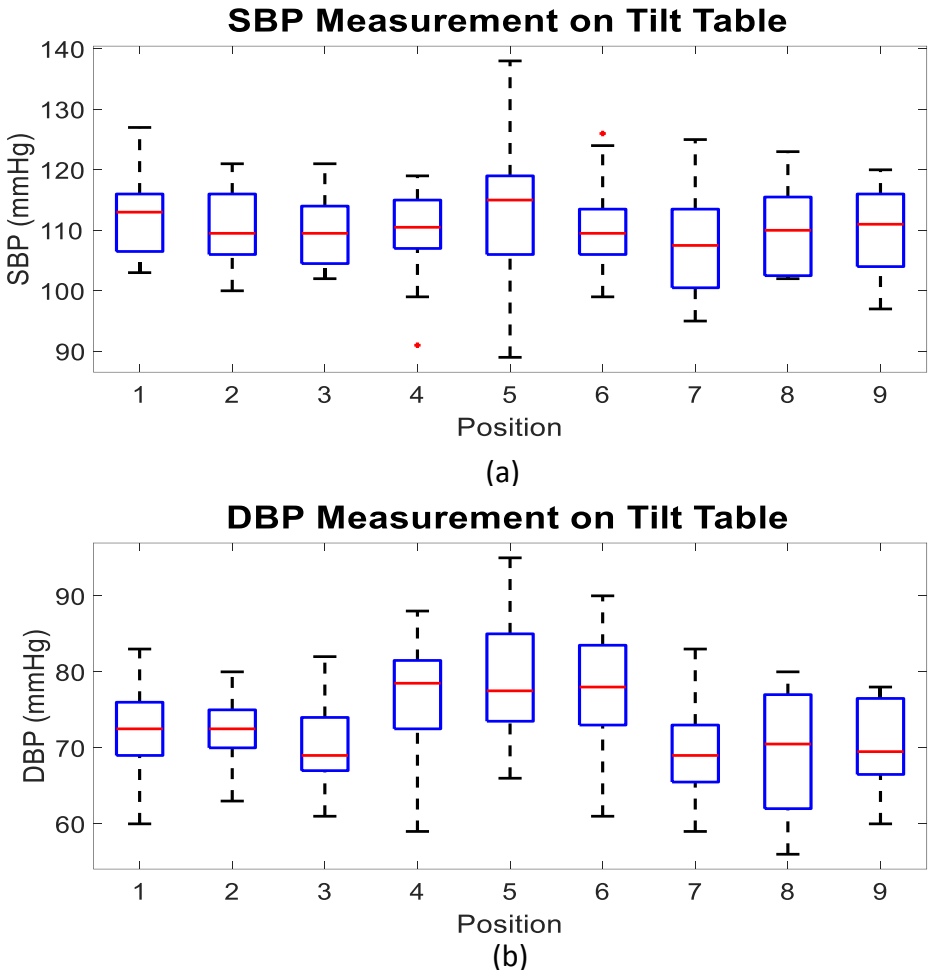


Figure 5.20: (a) The SBP measurement and (b) The DBP measurement recorded on eleven volunteers according to the tilt table position; 1,2, and 3 refers to supine position, 4,5 and 6 refers to tilt-up position (70° degree) and 7,8, and 9 refers to tilt-down (supine) position

As shown in Figure 5.20 (a), there is not much difference between the mean SBP at the supine (position 1, 2 and 3) and the mean SBP at the tilt up (position 4, 5, and 6). Meanwhile, the DBP at tilt-up position is slightly higher than in supine position, as shown in Figure 5.20 (b). Statistical analysis by the SPSS 23.0 software showed that there is no significant difference in mean systolic BP between the supine and standing positions with the p-value recorded as 0.963, ($p > 0.05$). Meanwhile, there is a statistically significant difference in mean diastolic BP between the supine and the standing positions with the p-value given as 0.01 ($p < 0.05$). The relation between PAT and SBP were investigated in the next section.

5.4.3 Comparison between Exercise and BP Cuff Calibration on ESBP (Tilt Table)

The accuracy of using a calibration curve to estimate SBP during the tilt table experiment was investigated for all volunteers. Two methods were deployed to generate the calibration curve. The first method is based on pedal exercise, and the second method used BP cuff oscillation waveforms (one-step calibration). The calibration equation for each volunteer is shown in Table 5.4 for pedal exercise and Table 5.7 for one-step calibration. An estimated systolic BP (ESBP) was calculated based on the PAT measurement at the finger and wrist during the tilt table experiment.

Comparison between the two calibration methods in estimating SBP was plotted against systolic blood pressure (SBP) as shown in Figure 5.21 (a) for PPG measured at the finger, and Figure 5.21 (b) for PPG measured at the wrist. All the data were plotted based on the mean ± SD of the set

of three repeats measurement of SBP and PAT at supine, tilt-up and tilt-down position. The regression coefficient *r* and the root mean square error (RMSE) to both methods were analysed, and the results are shown in Table 5.9.

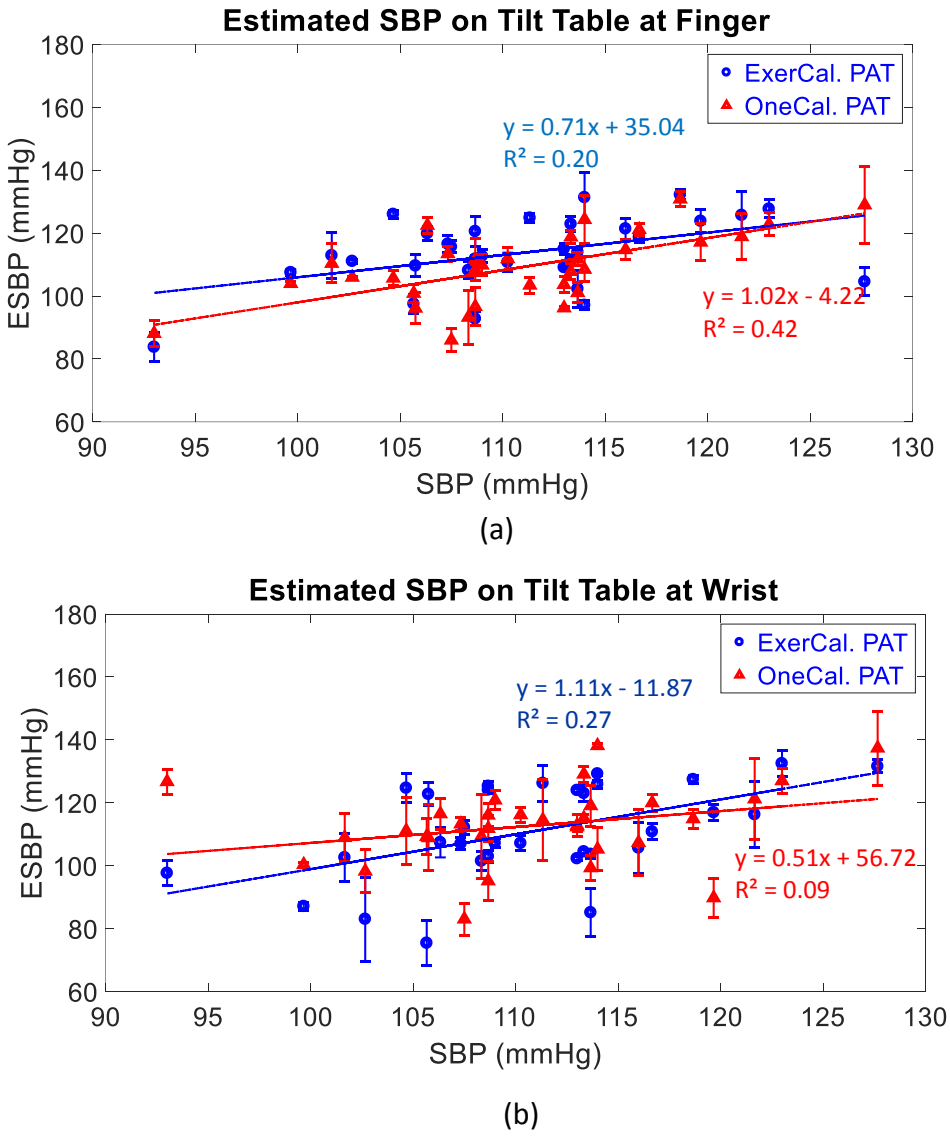


Figure 5.21: The correlation of ESBP with SBP during the tilt table experiment based on PAT measurement (a) at the finger (PATf) and (b) at the wrist (PATw). The ESBP calculated based on exercise calibration equation (ExerCal. PAT, blue marker) and one-step calibration equation (OneCal. PAT, red marker)

Table 5.9: Coefficient correlation, r and RMSE for ESBP-SBP relationship

Calibration Type	**Correlation coefficient ESBP with SBP *(r)***	**Root mean square error (RMSE) ESBP with SBP (mmHg)**
Pedal Exercise (Finger)	0.45	10
One-step Calibration (Finger)	0.65	9
Pedal Exercise (Wrist)	0.52	13
One-step Calibration (Wrist)	0.29	12

The results in Table 5.9 show that one-step calibration method at the finger shows a good correlation between ESBP and BP measurement with the correlation coefficient, *r* equal to 0.65, and RMSE 9 mmHg. The one-step calibration method at the wrist shows a weak correlation with *r* equal to 0.29 and the RMSE equal to 12 mmHg. The calibration equation based on pedal exercise shows a weak correlation to the SBP with the *r*-value at 0.45 at the finger and r equal to 0.52 at the wrist. The RMSE recorded using this method is 10 mmHg and 13mmHg at the finger and wrist, respectively.

Mean absolute error (MAE) in estimating systolic BP for both methods was calculated, and the results at the finger show that MAE is 7 ± 7 mmHg for one-step calibration method and 9 ± 7 mmHg for pedal exercise calibration method. Meanwhile, the MAE at the wrist shows slightly higher than the result obtained at the finger with the MAE recorded by the one-step calibration method is 10 ± 9 mmHg, and the MAE recorded by the pedal exercise is 11 ± 8 mmHg. According to the American Association for the Advancement of Medical Instrumentation (AAMI) standard, blood pressure estimation, for both SBP and DBP,

must have an absolute value of mean error less than 5 mmHg and the error standard deviation less than 8 mmHg [83]. Unfortunately, the findings on the MAE did not meet the AAMI requirement. However, the single-cuff measurement calibration method shows better performance than the pedal exercise calibration method on both positions (finger and wrist).

A statistical software (SPSS 23.0) was deployed to analyse the data distribution and to compare statistically the difference between one-step calibration and pedal exercise calibration method in estimating SBP at the finger and the wrist. The results from the Shapiro-Wilk test showed that one of the data sets (ExerCal PATw) in Figure 5.21 was non-normally distributed with the p-value recorded less than 0.05 ($p < 0.05$). The results from the Wilcoxon signed rank test showed that all the data sets in Figure 5.21 have the p-value greater than 0.05 ($p > 0.05$), indicating that there was no significant difference between two samples (one-step calibration and pedal exercise calibration) in estimating SBP at the finger and at the wrist. Bland-Altman plots were performed to assess the overall agreement between SBP measured by Ostar BP monitor and the calculated BP (ESBP) by using the pedal exercise and one-step calibration method. Figure 5.22 (a) shows the Bland-Altman for PAT measured at the finger and Figure 5.22 (b) shows the Bland-Altman for PAT measured at the wrist (PATw). All the data were analysed based on a mean of the set of three repeats measurement of SBP and PAT at supine, tilt-up and tilt-down position. The ESBP calculated based on exercise calibration equation (ExerCal. PAT, blue marker) and one-step calibration equation (OneCal. PAT, red marker).

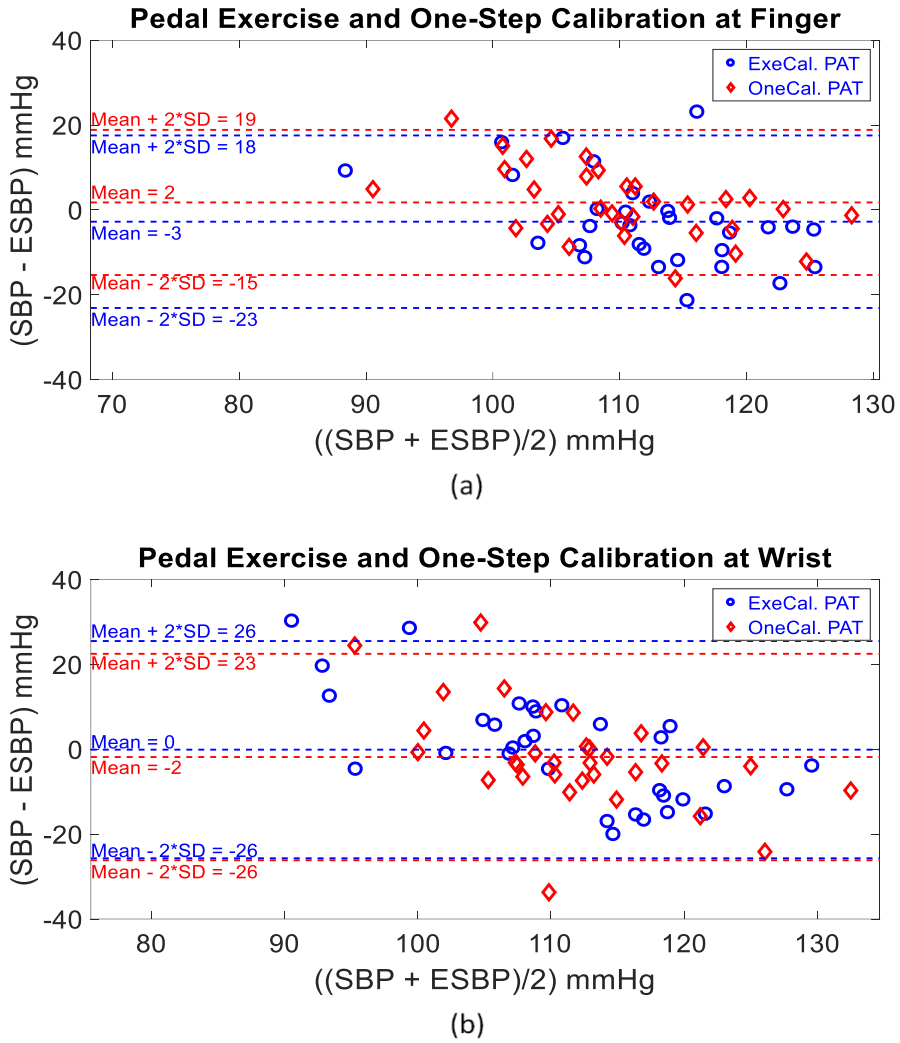


Figure 5.22: Bland-Altman plot for ESBP and SBP with PAT measurement (a) at the finger and (b) at the wrist. The ESBP calculated based on pedal exercise calibration equation (ExerCal. PAT, blue marker) and one-step calibration equation (OneCal. PAT, red marker)

The range of mean differences (limits of agreement) was set to 2 standard deviations (SD), approximately 95% limits of agreement [22]. The result in Figure 5.22 (a) shows that the limits of agreement are ± 21 mmHg by the pedal exercise calibration method and ± 17 mmHg by the one-step calibration method when estimating SBP with the finger as a

reference point. The data in Figure 5.22 (b) shows the limit of agreement was about ± 26 mmHg for pedal exercise calibration method and ± 24.5 mmHg for one-step calibration method when the PAT measurement was performed at the wrist. Overall, the one-step calibration method shows marginally better performance than the pedal exercise calibration method in estimating SBP at the finger and wrist.

In the literature, a one-point calibration method was proposed by Gesche et al. [166]. In this method, only one BP measurement is required using a reference method (cuff) at the beginning of the patient's investigation. They deployed an empirical PWV-BP function obtained from a group of 13 volunteers as a general function in one-step calibration. Their findings show that the SBP calculated from the pulse arrival time using a one-point calibration correlates significantly with the SBP measured by the cuff method and agreement limits (2SD) from the Bland–Altman plot were ± 20mmHg. In the present study, the one-step calibration method was proposed based on an individual BP calibration cuff. The result obtained by this method showed that the agreement limit (2SD) reached values up to 17 mmHg at the finger and up to 25 mmHg at the wrist. Additionally the result of the one-step calibration method shows better performance than the result obtained by the pedal exercise calibration method in estimating SBP during the tilt-table experiment. Advantageously, this method apparently need one measurement of BP using a cuff-based reference, make a calibration of PAT-SBP become simple and straightforward.

5.5 Summary

This chapter aimed to investigate the performance of a wearable PAT measurement system on healthy volunteers. The POF was successfully developed and was able to measure PPG signals on the wrist and under the foot. ECG conductive fabric electrodes performed well for acquiring the ECG R-wave signals on the chest. The delay time between the peak of the ECG and the peak of the PPG was calculated and denoted as PAT. The commercial sensor from the Nexus device was used as a benchmark sensor to validate the performance of the developed sensors in this thesis. Three locations were chosen for the PPGs detection for PAT measurement. The first location was at the finger denoted as PATf, the second location was at the wrist denoted as PATw, and the third location was under the foot, denoted as PATt. A commercial PPG sensor from the NeXus (Blood volume pulse sensor) was used to measure the PPG at the finger, and POF (developed sensor) were used to measure PPG at the wrist and under the foot.

A commercial non-invasive blood pressure monitor, Ostar P2 was used to monitor the blood pressure during the experiment. A Y-tube connector was attached to the BP cuff, and a pressure sensor (MP4250) was deployed to monitor the cuff pressure externally. The delay time between the peak of the ECG and the peak of the cuff oscillation during cuff deflation was calculated and denoted as PATcuff. In this study, the BP cuff waveform was deployed for the instantaneous PAT measurement, and the PATcuff was deployed for one-step calibration for estimating SBP. A study has been conducted on eleven volunteers to investigate the relationship between BP and PAT through pedal exercise and the results obtained were used to estimate SBP on a tilt table experiment. The results on the pedal exercise show that there was a strong correlation between PAT and SBP and a weak correlation between PAT

and DBP. In this study, PATf shows an improved correlation with SBP compared to PATw and PPt. An absolute correlation coefficient, I*r*I based on the mean and instantaneous PAT with BP were investigated during the pedal exercise. A statistical analysis of results showed that there is no difference on the I*r*I value mean between mean and instantaneous PAT-BP for all five pairs (Mean.PATf SBP with Ins.PATf SBP, Mean.PATw SBP with Ins.PATw SBP, Mean.PATw DBP with Ins.PATw DBP, Mean.PATt SBP with Ins.PATt SBP, and Mean.PATt DBP with Ins.PATt DBP). Only one pair, Mean.PATf DBP and Ins.PATf DBP shows a statistically significant difference between mean PATf and instantaneous PATf with DBP.

A comparison has been made between two calibration methods for estimating SBP during the tilt table experiment. The first method was based on pedal exercise calibration method (mean PAT) and second calibration method is based on BP cuff calibration (one-step calibration). Both methods were deployed to estimate SBP based on PAT measurement at the finger (PATf) and the wrist (PATw). The results show that the one-step calibration method gives a marginally better correlation coefficient, *r* and smaller root mean square error (RMSE) on estimated systolic BP compared to the pedal exercise calibration method at the finger and at the wrist. On top of that, the main purpose of this study was to benchmark the performance of the developed POF system with a commercial sensor. The PAT measured using POF, and conductive fabric performed very well, and the results show similar patterns as observed by the commercial sensor. A major disadvantage is that the POF is based on reflectance mode, and the measurement point is on the wrist, which may limit the signal quality compared to a standard sensor measuring PPG at the fingertip using transmission mode.

Chapter 6 Conclusion and Future Work

6.1 Conclusion

The previous five chapters cover the state of the art in pulse arrival time (PAT) measurement, development of a phantom cardiovascular system and design and development of optical fibre sensors for PAT monitoring. In practice, the hypertensive patient is required to monitor their blood pressure every 15 to 30 minutes over 24 hours using a cuff-based ambulatory blood pressure monitor (ABPM). Some patients may feel discomfort, be distracted and be inconvenienced to have their blood pressure measured by a cuff based BP instrument. Furthermore, the cuff-based blood pressure measurement device gives intermittent BP readings with no information on beat to beat BP. Therefore, in this research, a cuff-less continuous BP measurement was proposed based on PAT techniques.

A comprehensive literature review is presented in Chapter 2, providing relevant background about the physiological heart system, BP measurement as well as PAT techniques. Through the information gathering and knowledge obtained from the literature review, the principles of BP and PAT measurement are further understood. The fundamental and state of art of PAT techniques were reviewed, and the research gap in this field was identified and highlighted. Wearable technologies have gained popularity in commercial sectors and clinical practice, and this supports exploring the innovative idea of combining

POF and fabric based ECG electrodes for textile wearable PAT measurement. Another research gap that has been identified is on the calibration method between PAT and cuff-based BP monitor. Fundamentally, both methods are different. With PAT, the BP is measured continuously whilst the cuff based BP system determines the BP intermittently. These issues led to an investigation on the correlation of instantaneous PAT and mean PAT with BP measurement. In order to generate a practical and straightforward individual calibration curve for BP estimation, a single cuff measurement calibration method was proposed. Lastly, a cardiovascular phantom system was proposed to provide PAT simulations under different conditions within a controlled environment.

In Chapter 3, the development of a wearable PAT measurement system was described. Through this chapter, details of the design and development of electronic circuitry for plastic optical fibre (POF) sensors for PPG measurement were presented. The miniaturization of the optical sensor system is one of the contributions of this thesis. The flexibility of POF make it suitable to be embedded into textiles and potentially for wearable sensors application. To realize wearable textile based PAT measurement, the ECG signal was acquired using conductive fabric electrodes. The combination of POFs and ECG textile electrodes were investigated for PAT measurement on volunteers, and the findings of this combination method are the first reported to date. The commercial sensor from Nexus device (ECG surface electrode and Blood Volume Pulse (BVP) sensor) was deployed as a benchmark to validate the performance of developed sensors (ECG conductive fabric electrodes and POFs). All the sensor signals were transferred to the Nexus-10 MK II device in order for the signals to be synchronized. The signals were then transferred wirelessly to the computer through a Bluetooth connection. BioTrace+ software was programmed to display and record

the data in a computer, and subsequent analysis on PAT was performed by Matlab software. It has been demonstrated that the PPG signals and the ECG signals were able to be monitored by both the POF and conductive fabric electrodes, respectively. The findings have been successfully validated by comparison with the commercial sensor, and this showed that the proposed system could be deployed for wearable PAT measurement.

Chapter 4 described the development of a tubular cardiovascular pulse delay time phantom system. This system was proposed to perform pulse delay time simulation in a controlled environment to validate the PAT measurement system. A novelty of the developed phantom is that the technique was deployed on a custom made chamber to simulate the delay time between two pulses with pulse pressure amplitude. The innovation of the phantom system means that the design is simpler and more cost-effective compared to others in the literature. A diaphragm pump is the heart of the system and circulates fluid (water) around the phantom via a silicone tube. An electronically controlled module was developed to control pump operation for pulse generation. Plastic optical fibre (POF) sensors were used to measure the pulse signal on the flexible tube, and the results were compared with an in-line pressure sensor. In this experiment, the delay time between two pulses was calculated offline using Matlab software and correlated with pulse pressure. The result demonstrates that the pulse delay time recorded by both sensors decreased with the increase of pulse rate and pulse pressure. These phantom results showed a similar pattern to the human model, thus indicating that the system can simulate pulse delay time for sensor validation purposes.

Chapter 5 focused on the verification and validation of the cuffless blood pressure monitoring system on volunteers during pedal exercise and tilt table experiments. In this study, the time delay between the R-wave peak

of the Electrocardiogram (ECG) and the peak of the Photoplethysmogram (PPG) was measured and denoted as PAT. The PAT is grouped into three categories which depends on the position of the PPG signal measured; finger (PPTf), wrist (PATw) and under the foot (PATt). An oscillometric cuff-based blood pressure instrument (Ostar, P2) was used as a BP reference during the experiment. The ECG and the PPG signals were synchronized using a Nexus-10 MK II data acquisition device along with Matlab software for subsequent analysis for PAT measurements. The first experiment involved performing a pedal exercise to establish a calibration curve of PAT and BP on each volunteer. In the literature, the PAT was determined based on a mean at a certain number of heartbeats or a certain period but none of them deployed a single pulse wave for PAT calculation. Hence one of the contributions of this work is on a comparison of the instantaneous PAT and the mean PAT with BP measurement. A linear regression model was applied to mean/instantaneous PAT-BP data and the absolute correlation coefficient, *|r|* was determined on each volunteer. The student t-test was performed to test the statistical significance of mean and instantaneous data using IBM SPSS Statistic 23.0 software. The findings show that there is no significant difference between mean and instantaneous PATf with SBP ($p > 0.05$), but there is a significant difference between mean and instantaneous PATf with DBP ($p = 0.039$, <0.05). It was noted that the standard deviation of mean PAT was small, thus there is not much difference in the regression line of PAT and BP plotted.

The best linear fit equation generated by the PAT-SBP plot was used to estimate BP of each volunteer. Based on the equation, the estimated BP can be determined by deploying the PAT values only. Practically, multiple pairs of PAT and BP were recorded, and a mathematical model was established to relate PAT and BP on each volunteer. This method is time-consuming and not feasible in most clinical situations. Therefore, in this

work, one-step calibration was proposed to obtain the relationship between PAT and BP. This method only required one measurement of BP using an oscillometric BP device. The one-step calibration method and pedal exercise calibration method were evaluated to assess the relationship between PAT and SBP during tilt table experiment. Statistical software (SPSS 23.0) was deployed to analyse the data distribution and to compare statistically the difference between one-step calibration and pedal exercise calibration method in estimated SBP at the finger and the wrist. The results from the Wilcoxon signed rank test showed that the p-value was greater than 0.05 ($p > 0.05$) for all data sets, indicating that there was no significant difference between the two methods (one-step calibration and pedal exercise calibration) in estimating SBP at the finger and at the wrist. Although, the one-step calibration method gives a marginally better correlation coefficient, r and smaller root mean square error (RMSE) on estimated systolic BP (r = 0.65, RMSE = 9 mmHg) at finger compared to the pedal exercise calibration method (r = 0.45, RMSE = 10 mmHg). Result from Bland-Altman plot showed that the limit of agreement (2SD) between estimated SBP and SBP were 21 mmHg at finger and 26 mmHg at wrist by deployed pedal exercise calibration method. In comparison, one-step calibration method show marginally better performance with the limit of agreement was 17 mmHg at finger and 24.5 mmHg at wrist. Advantageously, the one-step calibration method only needs one measurement of BP using a cuff-based reference, and the technique is feasible in most situations.

In conclusion, through this thesis four significant contributions have been made to the literature:

1. The development of a wearable PAT measurement based on ECG conductive fabrics and POFs;

2. The innovation of a simple and cost-effective tubular cardiovascular phantom system for PTT simulation
3. Constructing a calibration curve of PAT and BP by using mean and instantaneous PAT.
4. Proposed a one-step calibration method using a BP cuff oscillation waveform for individual PAT-SBP calibration.

On top of that, this work has showed that the POF can be integrated into electronic circuitry for PPG measurement and further analysis using Matlab software able to realize the correlation of PAT and BP measurement. All the contributions were achieved by fulfilling the aim of this research, which was to monitor the pulse arrival time using optical fibre sensors.

6.2 Future Work

For future work, there are a few areas where the performance of the developed system could be improved. The first area is on the reflectance mode PPG, which deployed plastic optical fibres (POF) as a sensor. In this research, the diameter size of the POF is 500µm. At this size, it was a significant challenge to couple LED light into the fibre. Furthermore, the reflected light that is transferred to the phototransistor is also limited by the fibre diameter. Therefore, the design of the POF sensor should be optimised for PPG detection. The optimization can be achieved in several ways. The easiest way is by using a bundle of POFs to transmit and receive the light for the PPG measurement. The amount of DC light that enters the skin increases with an increase in the number of transmitting fibres. This DC light passes through the skin and is absorbed and scattered. A small portion is detected by the receiver fibre positioned approximately 1 mm away from the transmitting fibre. The amount of

received light increases with the increase in the total number of fibres, which will increase the signal to noise ratio of PPG signals.

Also the distance between the transmitting and receiving fibres could be varied to optimise the intensity of reflected light detected by the fibre. Another way to increase the amount of returned light to the fibre is by applying a plastic microlens structure placed on the tip of the fibre. This structure will capture a large area of light and focuses it to a point for the fibre. This technique may increase the light intensity at the collected fibre, thus increasing the amount of light transferred to the photodiode circuit for PPG detection. It is well known that PPG signals are very sensitive to interference from ambient light and motion artefacts [90]. In the reflection mode POFs, motion artefacts may distort the PPGs signal due to a varying and inefficient coupling of light from the tissue to the optical fibre during relative movement of the fibres and the tissue. To reduce this problem, a special casing to position the POF sensor should be designed (i.e. finger probe) to secure the interface between POF and the skin. Another type of artefact is caused by ambient light that, either directly or by transmission through the POF, couples with the PPG detector, resulting in distortion of the PPG signals. Therefore, the POF should be covered with black tape and the optical detection circuit placed in a sealed box to reduce the interference effect from ambient light.

Another area with the opportunity for improvement is in signal processing of the PAT measurement. The PAT was measured based on the peak of the R-wave ECG signal and the peak of the PPG signal. The peak detection can be improved by applying more advanced signal processing methods such as wavelet transform [223]. Multiresolution analysis deployed in the wavelet-based peak detection makes it more accurate and robust than threshold or curve-fitting-based peak detection methods. The trough and middle point of the PPG waveform can also be used as a marker for PAT calculation. A study on a correlation of the BP with the

delay time between the ECG signals to the different characteristic point on PPG signals such as peak, trough and middle point should be carried out in future. Also, interpolation can be applied to increase the original sample rate of PPG signals to a higher rate. High sampling rates allow more accurate capture of the peak values of the PPG signals and lead to more accurate PAT measurement. Moreover, a noisy PPG signal can lead to measurement inaccuracies and even wrong diagnosis. Therefore, denoising technique is important to reduce the noise and improve the quality of the signal. One of the denoising methods is by implementing an artificial neural network (ANN) to recover the corrupted PPG. In this technique, a set of significant features of good quality PPG signals is set to be a reference input for ANN to rectify morphology of corrupted PPG. In addition, input from a multi-channel PPG or other sensor such as accelerometer can be used as a reference signals for noise cancellation.

The present study used the PAT measurement based on the delay time between the ECG signal and PPG signal and correlated these with the SBP. Further investigation on the correlation of PAT and DBP should be carried out. For a next step, PTT methods could be performed for cuff-less BP measurement and its performance compared with the PAT method. Besides, higher correlation may be obtained using multivariate analysis by including physiological characteristics such as heart rate, height, weight and age into the mathematical model of PAT-BP. All these physiological parameters can serve as important predictors for cuffless BP measurement. Further validation of the proposed one-step calibration method to estimate BP is required on different settings of the experiment, such as treadmill exercise, hand gripping, and Valsalva manoeuvre.

In addition, the total number of a volunteers involved in this study should be increased and tested on a different gender to give a better picture of the performance of the developed device in monitoring BP. Also, the protocol for the pedal bike exercise should be reviewed to improve the

variation of a volunteer's BP. The volunteers should perform the pedal exercise aiming for a target heart rate before stopping for the BP readings. After the exercise, the volunteers should be sitting on a chair with the arm rested on a table during the BP measurement to minimize error in the BP readings. The calibration process of the PAT-BP trace was made using as the cuff-based oscillometric BP device. The PAT and oscillometric BP however are two different techniques for determining BP, which may produce an error during the calibration process. Therefore the calibration process of PAT-BP should be referred to the continuous BP measurement device such as Finometer and Tonometry to minimize the error.

For further work, the POF and conductive fabric ECG electrodes should be integrated into a garment for a smart textile application. Both sensors could be knitted or woven into the garment to enhance the comfort for the wearer. The miniaturization of the electronic circuit for processing the signals are essential, and the circuitry can be placed in a small box attached to the subject's body for ambulatory monitoring. In addition, an internet of things (IoT) based remote system could be developed to send the BP measurement to an online platform. This method could help a patient with hypertension so as to automatically send BP reading to the doctor or healthcare provider supported by Artificial Intelligence. This will help clinicians identify patients that require intervention.

Lastly, the tubular cardiovascular pulse delay time phantom system can be improved by deploying a commercially available cardiac replication pump such as SuperPump Pulsatile Pump (Vivtro Labs, Victoria, BC, Canada) and Pulsatile Blood Pump (Harvard Apparatus Co.). These pumps are able to simulate the pumping action of the heart and will provide more controlled parameters such as stroke volume, cardiac output and flow rate during the PTT simulation. The tube connector should be replaced with a proper connector and sealed with super glue

to make sure there is no air leakage during high tube pressurization. In the present study, the flexible tube is not surrounded by a scattering medium or any artificial skin layer. The POF sensor was attached directly to the tube, and this may distort the light measurement due to the undesired vibrations of the tubes. One of the solutions to overcome this problem is to place the tube inside a skin phantom that has properties of the scattering coefficient μ_s, and absorption coefficient μ_a, similar to real tissues. Further, artificial blood could be deployed in the phantom system to enhance light absorption and to mimic the real conditions within human skin. With these improvements, the phantom system will more accurately simulate PTT measurements mimicking more closely the human body.

References

[1] B. V. Mittal and A. K. Singh, “Hypertension in the developing world: challenges and opportunities,” *Am. J. Kidney Dis.*, vol. 55, no. 3, pp. 590–598, 2010.

[2] Z. Taha, L. Shirley, M. Azraai, and M. Razman, “A review on non-invasive hypertension monitoring system by using photoplethysmography method,” *Movement, Heal. Exerc.*, vol. 6, no. 1, pp. 47–57, 2017.

[3] W. H. Day, A global brief on Hypertension: A global brief on Hyper tension Silent killer, global public health crisis. 2013.

[4] D. Da He, E. S. Winokur, T. Heldt, and C. G. Sodini, “The ear as a location for wearable vital signs monitoring,” in *2010 Annual International Conference of the IEEE Engineering in Medicine and Biology Society, EMBC’10*, 2010, pp. 6389–6392.

[5] E. Grossman, “Ambulatory blood pressure monitoring in the diagnosis and management of hypertension.,” *Diabetes Care*, vol. 36, no. 2, pp. 307–311, Aug. 2013.

[6] M. C. van der Wel, I. E. Buunk, C. van Weel, T. A. B. M. Thien, and J. C. Bakx, “A novel approach to office blood pressure measurement: 30-minute office blood pressure vs daytime ambulatory blood pressure.,” *Ann. Fam. Med.*, vol. 9, no. 2, pp. 128–35, 2011.

[7] I. Z. Ben-Dov, L. Ben-Arie, J. Mekler, and M. Bursztyn, “Normal ambulatory blood pressure: A clinical-practice-based analysis of recent American Heart Association recommendations,” *Am. J. Med.*, vol. 119, no. 1, pp. 13–18, Jan. 2006.

[8] A. Almas, F. T. Sultan, and K. Kazmi, “Increased level of morning surge in blood pressure in normotensives: ACross-Sectional Study from Pakistan.,” *J. Coll. Physicians Surg. Pak.*, vol. 26, no. 10, pp. 818–821, Oct. 2016.

[9] C.-E. Chiang *et al.*, “2015 Guidelines of the Taiwan Society of Cardiology and the Taiwan Hypertension Society for the management of hypertension,” *J. Chinese Med. Assoc.*, vol. 78, no. 1, pp. 1–47, Jan. 2015.

[10] A. Vlahandonis, S. N. Biggs, G. M. Nixon, M. J. Davey, L. M. Walter, and R. S. C. Horne, “Pulse transit time as a surrogate measure of changes in systolic arterial pressure in children during sleep,” *J. Sleep Res.*, vol. 23, no. 4, pp. 406–413, 2014.

[11] R. Wang, Wenyan Jia, Zhi-Hong Mao, R. J. Sclabassi, and Mingui Sun, “Cuff-free blood pressure estimation using pulse transit time and heart rate,” *12th Int. Conf. Signal Process.*, pp. 115–118, 2014.

[12] E. Chung, G. Chen, B. Alexander, and M. Cannesson, “Non-invasive continuous blood pressure monitoring: a review of current applications.,” *Front. Med.*, vol. 7, no. 1, pp. 91–101, 2013.

[13] S. Ye, G. Kim, and D. Jung, “Estimation of systolic and diastolic pressure using the pulse transit time,” *World Acad. Sci. …*, vol. 4, no. 7, pp. 726–731, 2010.

[14] T. Tu, P. C. Chao, and Y. Lee, “A new non-invasive cuff-less blood pressure sensor,” in *Sensors*, 2013, no. 1, pp. 3–6.

[15] D. Buxi, J.-M. Redouté, and M. R. Yuce, “A survey on signals and systems in ambulatory blood pressure monitoring using pulse transit time,” *Physiol. Meas.*, vol. 36, no. 3, pp. R1–R26, 2015.

[16] X. Ding, B. P. Yan, Y.-T. Zhang, J. Liu, N. Zhao, and H. K. Tsang, “Pulse transit time based continuous cuffless blood pressure estimation: a new extension and a comprehensive evaluation,” *Sci. Rep.*, vol. 7, no. 1, pp. 11554–11565, 2017.

[17] R.-C. Peng, W.-R. Yan, N.-L. Zhang, W.-H. Lin, X.-L. Zhou, and Y.-T. Zhang, “Cuffless and continuous blood pressure estimation from the heart sound signals,” *Sensors*, vol. 15, no. 9, pp. 23653–23666, 2015.

[18] J. Allen, “Quantifying the delays between multi-site photoplethysmography pulse and electrocardiogram r-r interval changes under slow-paced breathing,” *Front. Physiol.*, vol. 10, no. SEP, pp. 1190–1196, Sep. 2019.

[19] a. Hennig and a. Patzak, “Continuous blood pressure measurement using pulse transit time,” *Somnologie - Schlafforsch. und Schlafmedizin*, vol. 17, no. 2, pp. 104–110, 2013.

[20] M. Sharma *et al.*, “Cuff-Less and continuous blood pressure monitoring: a methodological review,” *Technologies*, vol. 5, no. 2, pp. 1–21, 2017.

[21] Y. Chen, C. Wen, G. Tao, M. Bi, and G. Li, “Continuous and noninvasive blood pressure measurement: A novel modeling methodology of the relationship between blood pressure and pulse wave velocity,” *Ann. Biomed. Eng.*, vol. 37, no. 11, pp. 2222–2233, 2009.

[22] T. Wibmer *et al.*, “Pulse transit time and blood pressure during cardiopulmonary exercise tests.,” *Physiol. Res.*, vol. 63, no. 3, pp. 287–296, 2014.

[23] M. Amin, Y. Heravi, and M. A. Khalilzadeh, “Designing and

constructing an optical system to measure continuous and cuffless blood pressure using two pulse signals," *Iran. J. Med. Phys.*, vol. 10, no. 4, pp. 215–223, 2014.

[24] J. M. Zhang, P. F. Wei, and Y. Li, "A LabVIEW based measure system for pulse wave transit time," in *5th Int. Conference on Information Technology and Applications in Biomedicine.*, 2008, pp. 477–480.

[25] Y. Li, Z. Wang, L. Zhang, X. Yang, and J. Song, "Characters available in photoplethysmogram for blood pressure estimation: Beyond the pulse transit time," *Australas. Phys. Eng. Sci. Med.*, vol. 37, no. 2, pp. 367–376, 2014.

[26] L. Terminelli *et al.*, "Photoplethysmography and electrocardiography for real time evaluation of pulse transit time," in *Fotonica AEIT Italian Conference on Photonics Technologies*, 2014, pp. 2–5.

[27] M. Kachuee, M. M. Kiani, H. Mohammadzade, and M. Shabany, "Cuff-Less high-accuracy calibration-free blood pressure estimation using pulse transit time," in *International Symposium on Circuits and Systems*, 2015, no. 2, pp. 1006–1009.

[28] L. Dziuda, J. Lewandowski, F. Skibniewski, and G. Nowicki, "Fibre-optic sensor for respiration and heart rate monitoring in the mri environment," in *Procedia Engineering*, 2012, vol. 47, pp. 1291–1294.

[29] L. Vojtech, R. Bortel, M. Neruda, and M. Kozak, "Wearable textile electrodes for ECG measurement," *Adv. Electr. Electron. Eng.*, vol. 11, no. 5, pp. 410–414, 2013.

[30] J. Taelman, T. Adriaensen, C. van der Horst, T. Linz, and A.

Spaepen, “Textile integrated contactless emg sensing for stress analysis,” in *Annual International Conference of the IEEE Engineering in Medicine and Biology Society*, 2007, vol. 2007, pp. 3966–3969.

[31] J. Meyer, P. Lukowicz, and G. Troster, “Textile pressure sensor for muscle activity and motion detection,” in *2006 10th IEEE International Symposium on Wearable Computers*, 2006, pp. 69–72.

[32] M. Sibinski, M. Jakubowska, and M. Sloma, “Flexible temperature sensors on fibers,” *Sensors*, vol. 10, no. 9, pp. 7934–7946, Aug. 2010.

[33] M. Krehel, M. Wolf, L. F. Boesel, R. M. Rossi, G.-L. Bona, and L. J. Scherer, “Development of a luminous textile for reflective pulse oximetry measurements,” *Biomed. Opt. Express*, vol. 5, no. 8, p. 2537, 2014.

[34] F. Shaffer, R. McCraty, and C. L. Zerr, “A healthy heart is not a metronome: an integrative review of the heart’s anatomy and heart rate variability,” *Front. Psychol.*, vol. 5, pp. 1–19, 2014.

[35] J. Alastruey, K. H. Parker, and S. J. Sherwin, “Arterial pulse wave haemodynamics,” in *11th International Conference on Pressure Surges*, 2012, pp. 401–443.

[36] M. H. Azizi, T. Nayernouri, and F. Azizi, “A brief history of the discovery of the circulation of blood in the human body,” *Arch. Iran. Med.*, vol. 11, no. 3, pp. 345–350, 2008.

[37] J. Tu, K. Inthavong, and K. K. L. Wong, “Computational hemodynamics - theory, modelling and applications,” in *Biological and Medical Physics, Biomedical Engineering*, 2015, pp. 21–42.

[38] H. Ali and L. Mossa, “Engineering modeling of human cardiovascular system,” *1 st Reg. Conf. Eng. Sci. NUCEJ Spat. ISSUE*, vol. 1111, no. 22, pp. 307–314, 2008.

[39] S. S. Dey, N., Das, P., Biswas, S., Das, A., & Chaudhuri, “Lifting wavelet transformation based blind watermarking technique of photoplethysmographic signals in wireless telecardiology,” in *In 2012 World Congress on Information and Communication Technologies*, 2012, pp. 230–235.

[40] E. Meaney, F. Alva, R. Moguel, A. Meaney, J. Alva, and R. Webel, “Formula and nomogram for the sphygmomanometric calculation of the mean arterial pressure [1],” *Heart*, vol. 84, no. 1, p. 64, 2000.

[41] C. F. Babbs, “Oscillometric measurement of systolic and diastolic blood pressures validated in a physiologic mathematical model,” *Biomed. Eng. Online*, vol. 11, no. 1, p. 56, 2012.

[42] E. Z. Malik, B. Abdulhadi, K. N. Mezue, E. V. Lerma, and J. Rangaswami, “Clinical hypertension: Blood pressure variability,” *Disease-a-Month*, vol. 64, no. 1, pp. 5–13, 2018.

[43] J. Olbers, A. Gille, P. Ljungman, M. Rosenqvist, J. Östergren, and N. Witt, “High beat-to-beat blood pressure variability in atrial fibrillation compared to sinus rhythm,” *Blood Press.*, vol. 27, no. 5, pp. 249–255, 2018.

[44] G. Mancia, “Short- and long-term blood pressure variability: Present and future,” *Hypertension*, vol. 60 (2), pp. 512–517, 2012.

[45] W. Xu, Yang and Ping, Peng and Wang, Dong and Zhang, “Continuous non-invasive arterial pressure shows high accuracy in comparison to invasive intra-arterial blood pressure measurement,” *J. Healthc. Eng.*, vol. 2018, pp. 1–10, 2018.

[46] G. Mancia *et al.*, “Daily life blood pressure changes are steeper in hypertensive than in normotensive subjects,” *Hypertension*, vol. 42, no. 3, pp. 277–282, 2003.

[47] E. Pinto, “Blood pressure and ageing,” *Postgrad. Med. J.*, vol. 83, no. 976, pp. 109–114, 2007.

[48] J.-Q. Engle, K. M.; Mei, T-S.; Wasa, M.; Yu, “Aging,arterial stiffness and hypertension,” *Acc. Chem. Res.*, vol. 45, no. 6, pp. 788–802, 2008.

[49] H. P. Cotrim *et al.*, “Nonalcoholic fatty liver disease in Brazil: clinical and histological profile,” *Ann. Hepatol.*, vol. 10, no. 1, pp. 33–37, 2011.

[50] L. B. K. Hill, J. J. Sollers, and J. F. Thayer, “Evaluation of a simple estimation method for the derivation of cardiac output from arterial blood pressure and heart rate,” *Biomed. Sci. Instrum.*, vol. 48, pp. 165–70, 2012.

[51] T. Minh and N. Minh, “Changes in blood pressure classification, blood pressure goals and pharmacological treatment of essential hypertension in medical guidelines from 2003 to 2013,” *IJC Metab. Endocr.*, vol. 2, pp. 1–10, 2014.

[52] A. Sahoo, P. Manimegalai, and K. Thanushkodi, “Wavelet based pulse rate and blood pressure estimation system from ECG and PPG signals,” *2011 Int. Conf. Comput. Commun. Electr. Technol.*, pp. 285–289, 2011.

[53] J. Kijonka and M. Penhaker, “Electronic invasive blood pressure simulator device for patient monitor testing,” *Elektron. ir Elektrotechnika*, vol. 122, no. 6, pp. 49–54, 2012.

[54] J. W. Dunne, “Invasive monitoring in the intensive care unit,” *Crit. Care*, vol. 24, no. 5, pp. 430–435, 2013.

[55] K. Lim, D. Abbott, M. Elgendi, R. Ward, G. Martínez, and N. Howard, “Can photoplethysmography replace arterial blood pressure in the assessment of blood pressure?,” *J. Clin. Med.*, vol. 7, no. 10, p. 316, Sep. 2018.

[56] M. Z. Ali and Y. Radeep, “Design of electronic sensor for blood pressure monitoring system based on zigbee module system,” *Int. J. Sci. Eng. Technol. Res.*, vol. 03, no. 50, pp. 10200–10208, 2014.

[57] A. S. Meidert and B. Saugel, “Techniques for non-invasive monitoring of arterial blood pressure,” *Front. Med.*, vol. 4, p. 231, 2018.

[58] Y. Yoon, J. H. Cho, and G. Yoon, “Non-constrained blood pressure monitoring using ECG and PPG for personal healthcare,” *J. Med. Syst.*, vol. 33, pp. 261–266, 2009.

[59] L. Peter, N. Noury, and M. Cerny, “A review of methods for non-invasive and continuous blood pressure monitoring: Pulse transit time method is promising?,” *Irbm*, vol. 35, no. 5, pp. 271–282, 2014.

[60] G.-Y. Jeong, K.-H. Yu, and N.-G. Kim, “Continuous blood pressure monitoring using pulse wave transit time,” in *International Conference on Control, Automation and Systems*, 2005, pp. 2–5.

[61] G. Beevers, G. Y. H. Lip, and E. O’brien, “Blood pressure measurement: Part I—Sphygmomanometry: Factors common to all techniques,” *BMJ Br. Med. J.*, vol. 322, no. 7292, pp. 981–985, 2001.

[62] F. Pan, P. He, C. Liu, T. Li, A. Murray, and D. Zheng, “Variation of

the korotkoff stethoscope sounds during blood pressure measurement: Analysis using a convolutional neural network," *IEEE J. Biomed. Heal. Informatics*, vol. 21, no. 6, pp. 1593–1598, 2017.

[63] G. Ogedegbe and T. Pickering, "Principles and techniques of blood pressure measurement," *Cardiol Clin.*, vol. 28, no. 4, pp. 571–586, 2010.

[64] R. Danielsen, "Blood pressure measurement," in *Essential Clinical Procedures*, 2007, pp. 33–46.

[65] M. Forouzanfar, H. R. Dajani, S. Member, and V. Z. Groza, "Oscillometric blood pressure estimation : past , present , and future," *IEEE Rev. Biomed. Eng.*, vol. 8, pp. 44–63, 2015.

[66] E. Balestrieri and S. Rapuano, "Instruments and methods for calibration of oscillometric blood pressure measurement devices," *IEEE Trans. Instrum. Meas.*, vol. 59, no. 9, pp. 2391–2404, 2010.

[67] Y. Wang *et al.*, "Improving auscultatory blood pressure measurement with electronic and computer technology: The visual auscultation method," *Am. J. Hypertens.*, vol. 22, no. 6, pp. 624–629, 2009.

[68] D. K. Park, H. S. Oh, J. H. Kang, I. Y. Kim, Y. J. Chee, and J. S. Lee, "Novel method of automatic auscultation for blood pressure measurement using pulses in cuff pressure and korotkoff sound," in *Computers in Cardiology*, 2008, pp. 181–184.

[69] C. H. Kuo, C. J. Wu, H. C. Chou, G. T. Chen, and Y. C. Kuo, "Development of a blood pressure measurement instrument with active cuff pressure control schemes," *J. Healthc. Eng.*, vol. 2017, pp. 1–15, 2017.

[70] W. Yuqi, X. Haiyan, L. Yinhua, and Y. Mengsun, “Application of the visual auscultatory blood pressure measuring system,” *2009 9th Int. Conf. Electron. Meas. Instruments*, pp. 3–325, 2009.

[71] E. O’Brien, “Replacing the mercury sphygmomanometer : Requires clinicians to demand better automated devices,” *BMJ Br. Med. J.*, vol. 320, no. 7238, pp. 815–816, 2000.

[72] M. G. Myers, “Office blood pressure 21st century,” *J. Clin. Hypertens.*, vol. 20, no. 7, pp. 1104–1107, 2018.

[73] J. Liu *et al.*, “Patient-specific oscillometric blood pressure measurement,” *IEEE Trans. Biomed. Eng.*, vol. 63, no. 6, pp. 1220–1228, 2016.

[74] J. Liu, H. M. Cheng, C. H. Chen, S. H. Sung, J. O. Hahn, and R. Mukkamala, “Patient-specific oscillometric blood pressure measurement: validation for accuracy and repeatability,” *IEEE J. Transl. Eng. Heal. Med.*, vol. 5, no. November 2016, pp. 1–10, 2017.

[75] P. K. Lim *et al.*, “Improved Measurement of blood pressure by extraction of characteristic features from the cuff oscillometric waveform,” *Sensors*, vol. 15, no. 6, pp. 14142–14161, 2015.

[76] J. Benes, “Continuous non-invasive arterial pressure assessment during surgery to improve outcome,” *Front. Med.*, vol. 4, no. November, pp. 1–8, 2017.

[77] C. Ilies *et al.*, “Detection of hypotension during caesarean section with continuous non-invasive arterial pressure device or intermittent oscillometric arterial pressure measurement,” *Br. J. Anaesth.*, vol. 109, no. 3, pp. 413–419, 2012.

[78] B. M. T. Deegan, M. O'Connor, D. Lyons, and G. OLaighin, "A new blood pressure and heart rate signal analysis technique to assess Orthostatic Hypotension and its subtypes.," *Conf. Proc. IEEE Eng. Med. Biol. Soc.*, vol. 2007, pp. 935–8, 2007.

[79] P. Salvi, A. Grillo, and G. Parati, "Noninvasive estimation of central blood pressure and analysis of pulse waves by applanation tonometry," *Hypertens. Res.*, vol. 38, no. 10, pp. 1–3, 2015.

[80] K. Shioya and T. Dohi, "Blood pressure measurement device based on the arterial tonometry method with micro triaxial force sensor," in *The 17th International Conference on Solid-State Sensors, Actuators and Microsystems*, 2013, no. June, pp. 2389–2392.

[81] Wang, Shouping, et al. "Digital control method of volume clamp method." I*nternational Conference on Mechatronics, Electronic, Industrial and Control Engineering (MEIC-15).* Atlantis Press, 2015, pp. 691–694.

[82] V. Ho *et al.*, "Cuff-Less and continuous blood pressure monitoring: a methodological review," *Technologies*, vol. 5, no. 2, p. 21, 2017.

[83] Y. Choi, Q. Zhang, and S. Ko, "Noninvasive cuffless blood pressure estimation using pulse transit time and Hilbert-Huang transform," *Comput. Electr. Eng.*, vol. 39, no. 1, pp. 103–111, 2013.

[84] Y. Chen, S. Shi, Y. Liu, S. Huang, and T. Ma, "Cuffless blood-pressure estimation method using a heart-rate variability- derived parameter Cuffless blood-pressure estimation method using a heart-rate variability-derived parameter," *Physiol. Meas.*, vol. 39, no. 9, pp. 095002–095013, 2018.

[85] M. Nitzan, B. Khanokh, and Y. Slovik, "The difference in pulse

transit time to the toe and finger measured by photoplethysmography," *Physiol. Meas.*, vol. 23, no. 1, pp. 85–93, Feb. 2002.

[86] B. M. McCarthy, B. O'Flynn, and A. Mathewson, "An investigation of pulse transit time as a non-invasive blood pressure measurement method," *J. Phys. Conf. Ser.*, vol. 307, no. 1, pp. 012060–012066, 2011.

[87] J. H. Shin, K. M. Lee, and K. S. Park, "Non-constrained monitoring of systolic blood pressure on a weighing scale.," *Physiol. Meas.*, vol. 30, no. 7, pp. 679–93, 2009.

[88] J. Allen and A. Murray, "Age-related changes in peripheral pulse timing characteristics at the ears, fingers and toes," *J. Hum. Hypertens.*, vol. 16, no. 10, pp. 711–717, Oct. 2002.

[89] R. Shriram, A. Wakankar, N. Daimiwal, and D. Ramdasi, "Continuous cuffless blood pressure monitoring based on PTT," *ICBBT 2010 - 2010 Int. Conf. Bioinforma. Biomed. Technol.*, pp. 51–55, 2010.

[90] T. Tamura, Y. Maeda, M. Sekine, and M. Yoshida, "Wearable photoplethysmographic sensors—past and present," *Electronics*, vol. 3, no. 2, pp. 282–302, 2014.

[91] B. Sangeeta and S. Laxmi, "A real time analysis of ppg signal for measurement of spo2 and pulse rate," *Int. J. Comput. Appl.*, vol. 36, no. 11, pp. 45–50, 2011.

[92] T. Y. Abay and A. Panayiotis, "Optimal spacing between transmitting and receiving optical fibres in reflectance pulse oximetry Optimal spacing between transmitting and receiving optical fibres in reflectance pulse oximetry," *J. Phys. Conf. Ser.*, vol.

85, no. 1, pp. 1–8, 2007.

[93] X. He, R. A. Goubran, I. Fellow, X. P. Liu, and I. Senior, “Evaluation of the correlation between blood pressure and pulse transit time,” in *International Symposium on Medical Measurements and Applications (MeMeA)*, 2013, pp. 17–20.

[94] C. C. Y. Poon and Y. T. Zhang, “Cuff-less and noninvasive measurements of arterial blood pressure by pulse transit time.,” in *International Conference of the Annual International Conference of the Engineering in Medicine and Biology Society*, 2005, pp. 5877–5880.

[95] L. Xu, X. Guo, F. Yang, S. Yin, X. Zhang, and M. Q. H. Meng, “Implementation of cuff-less continuous blood pressure measurement system based on Android,” in *International Conference on Information and Automation*, 2012, pp. 552–556.

[96] Y. L. Zheng, B. P. Yan, Y. T. Zhang, and C. C. Y. Poon, “An armband wearable device for overnight and cuff-less blood pressure measurement,” *IEEE Trans. Biomed. Eng.*, vol. 61, no. 7, pp. 2179–2186, 2014.

[97] N. E. Wineinger *et al.*, “Cardiovascular and nervous system changes during meditation,” *Front. Hum. Neurosci.*, vol. 9, p. 145, Mar. 2015.

[98] G. Bilo, C. Zorzi, J. E. Ochoa Munera, C. Torlasco, V. Giuli, and G. Parati, “Validation of the Somnotouch-NIBP noninvasive continuous blood pressure monitor according to the European Society of Hypertension International Protocol revision 2010,” *Blood Press. Monit.*, vol. 20, no. 5, pp. 291–294, 2015.

[99] M. Weenk *et al.*, “Continuous monitoring of vital signs using

wearable devices on the general ward: pilot study.," *JMIR mHealth uHealth*, vol. 5, no. 7, pp. 91–100, Jul. 2017.

[100] J. Y. a Foo, S. J. Wilson, G. R. Williams, M. Harris, and D. M. Cooper, "Motion artefact reduction of the photoplethysmographic signal in pulse transit time measurement.," *Australas. Phys. Eng. Sci. Med.*, vol. 27, no. 4, pp. 165–173, 2004.

[101] D. G. Guo *et al.*, "A long-term wearable vital signs monitoring system using BSN," in *11th EUROMICRO Conference on Digital System Design Architectures, Methods and Tools*, 2008, pp. 825–830.

[102] D. Špulák, R. Čmejla, and V. Fabián, "Experiments with blood pressure monitoring using ECG and PPG," in *Proceedings of the Conference Technical Computing Bratislava*, 2010, pp. 1–5.

[103] D. Jarchi, D. Salvi, L. Tarassenko, and D. A. Clifton, "Validation of instantaneous respiratory rate using reflectance ppg from different body positions," *Sensors (Basel).*, vol. 18, no. 11, pp. 3705–3723, Oct. 2018.

[104] S. Fuke, T. Suzuki, K. Nakayama, H. Tanaka, and S. Minami, "Blood pressure estimation from pulse wave velocity measured on the chest," in *International Conference of the IEEE Engineering in Medicine and Biology Society (EMBC)*, 2013, pp. 6107--6110.

[105] J. Franco, J. Aedo, and F. Rivera, "Continuous, non-invasive and cuff-free blood pressure monitoring system," in *Andean Region International Conference (ANDESCON)*, 2012, pp. 31–34.

[106] M. Moni, J. Rajda, and U. Lakshmanadoss, "Artefactual spikes in electrocardiography : a worthwhile introspection," vol. 54, no. 2, pp. 1–4, 2013.

[107] D. B. McCombie, A. T. Reisner, and H. H. Asada, “Adaptive blood pressure estimation from wearable PPG sensors using peripheral artery pulse wave velocity measurements and multi-channel blind identification of local arterial dynamics,” in *International Conference of the IEEE Engineering in Medicine and Biology Society*, 2006, pp. 3521–3524.

[108] H. Jeong *et al.*, “A study on estimating blood pressure during body pos tur al change based on pulse transit time,” in *Health Innovations and Point-of-Care Technologies Conference*, 2014, pp. 153–156.

[109] J. Muehlsteff, X. A. Aubert, and G. Morren, “Continuous cuff-less blood pressure monitoring based on the pulse arrival time approach: The impact of posture,” in *2008 30th Annual International Conference of the IEEE Engineering in Medicine and Biology Society*, 2009, pp. 1691–1694.

[110] J. Muehlsteff, X. L. Aubert, and M. Schuett, “Cuffless estimation of systolic blood pressure for short effort bicycle tests: The prominent role of the pre-ejection period,” in *Annual International Conference of the IEEE Engineering in Medicine and Biology - Proceedings*, 2006, pp. 5088–5092.

[111] J. Proenca, J. Muehlsteff, X. Aubert, and P. Carvalho, “Is pulse transit time a good indicator of blood pressure changes during short physical exercise in a young population?,” in *Annual International Conference of the IEEE Engineering in Medicine and Biology Society, EMBC’10*, 2010, pp. 598–601.

[112] M. Wong and Y. T. Zhang, “The effects of pre-ejection period on the blood pressure estimation using pulse transit time,” *2008 5th Int. Summer Sch. Symp. Med. Devices Biosens.*, pp. 254–255,

2008.

[113] W. Suhaimizan, W. Zaki, R. Correia, S. Korposh, R. Barrie, and S. P. Morgan, “Cuff-less continuous blood pressure monitoring system using pulse transit time techniques,” *Int. J. Integr. Eng.*, vol. 8, no. 1, pp. 51–57, 2016.

[114] T. Koivistoinen, S. Junnila, A. Värri, and T. Kööbi, “A new method for measuring the ballistocardiogram using EMFi sensors in a normal chair.,” in *International Conference of the IEEE Engineering in Medicine and Biology Society.*, 2004, pp. 2026–2029.

[115] O. T. Inan, M. Etemadi, R. M. Wiard, L. Giovangrandi, and G. T. A. Kovacs, “Robust ballistocardiogram acquisition for home monitoring,” *Physiol. Meas.*, vol. 30, no. 2, pp. 169–185, 2009.

[116] D. C. Mack, J. T. Patrie, P. M. Suratt, R. A. Felder, and M. Alwan, “Development and preliminary validation of heart rate and breathing rate detection using a passive, ballistocardiography-based sleep monitoring system,” *IEEE Trans. Inf. Technol. Biomed.*, vol. 13, no. 1, pp. 111–120, 2009.

[117] C.-S. Kim, A. Carek, R. Mukkamala, O. Inan, and J.-O. Hahn, “Ballistocardiogram as proximal timing reference for pulse transit time measurement: potential for cuffless blood pressure monitoring,” *IEEE Trans. Biomed. Eng.*, vol. 62, no. 11, pp. 2657–2664, 2015.

[118] H. Ashouri *et al.*, “Weighing scale-based pulse transit time is a superior marker of blood pressure than conventional pulse arrival time,” *Sci. Rep.*, vol. 6, no. 1, p. 39273, Dec. 2016.

[119] E. S. Winokur, S. Member, D. Da He, G. Charles, and a H. B. Bcg, “A wearable vital signs monitor at the ear for continuous heart rate

and pulse transit time measurements," in *International Conference of the IEEE EMBS*, 2012, pp. 2724–2727.

[120] Y. Zheng, B. Leung, S. Sy, Y. Zhang, and C. C. Y. Poon, "A clip-free eyeglasses-based wearable monitoring device for measuring photoplethysmograhic signals," in *International Conference of the IEEE Engineering in Medicine and Biology Society, EMBS*, 2012, pp. 5022–5025.

[121] X. F. Teng and Y. T. Zhang, "Continuous and noninvasive estimation of arterial blood pressure using a photoplethysmographic approach," in *International Conference of the IEEE Engineering in Medicine and Biology Society*, 2003, pp. 3153–3156.

[122] In Cheol Jeong and J. Finkelstein, "Potential value of electrocardiogram and photoplethysmogram for non-invasive blood pressure estimation during exercise," in *International Conference of the IEEE Engineering in Medicine and Biology Society*, 2013, pp. 2304–2307.

[123] Y. Katsuragawa, "Non-invasive blood pressure measurement by pulse wave analysis using FBG sensor," in *IEEE International Instrumentation and Measurement Technology Conference*, 2015, pp. 1–5.

[124] Zhihao Chen, Xiufeng Yang, Ju Teng Teo, and Soon Huat Ng, "Noninvasive monitoring of blood pressure using optical ballistocardiography and photoplethysmograph approaches," in *35th Annual International Conference of the IEEE Engineering in Medicine and Biology Society (EMBC)*, 2013, pp. 2425–2428.

[125] C. H. Chan and Y. T. Zhang, "Continuous and long-term arterial

blood pressure monitoring by using h-shirt," in *5th Int. Conference on Information Technology and Applications in Biomedicine, ITAB 2008 in conjunction with 2nd Int. Symposium and Summer School on Biomedical and Health Engineering.*, 2008, pp. 267–269.

[126] S. Padma, A. Kalegowda, S. Umesh, S. Ambastha, and S. Asokan, "Pulse transit time differential measurement by fiber Bragg grating pulse recorder," *J. Biomed. Opt.*, vol. 20, no. 5, p. 057005, 2015.

[127] K. Varsha, HS and Upadhyay, Gaurav and Shashikala, "Design and implementation of an optical transceiver card for intra-satellite communication," *GSJ*, vol. 6, no. 7, pp. 836–845, 2018.

[128] Y. Bao, Y. Huang, M. S. Hoehler, and G. Chen, "Review of fiber optic sensors for structural fire engineering," *Sensors (Switzerland)*, vol. 19, no. 4. MDPI AG, p. 87, 02-Feb-2019.

[129] H. Fidanboylu, KA and Efendioglu, "Fiber optic sensors and their applications," in *5th International Advanced Technologies Symposium (IATS'09)*, 2009, pp. 1–3.

[130] R. Correia, S. James, S. W. Lee, S. P. Morgan, and S. Korposh, "Biomedical application of optical fibre sensors," *Journal of Optics (United Kingdom)*, vol. 20, no. 7. IOP Publishing, pp. 1–25, 2018.

[131] X. Lu, P. J. Thomas, and J. O. Hellevang, "A review of methods for fibre-optic distributed chemical sensing," *Sensors (Switzerland)*, vol. 19, no. 13. MDPI AG, p. 2876, 28-Jun-2019.

[132] Y. S. Ong, I. Grout, E. Lewis, and W. Mohammed, "Plastic optical fibre sensor system design using the field programmable gate array," in *Selected Topics on Optical Fiber Technologies and Applications*, InTech, 2018, pp. 125–151.

[133] H. Kadhum Hisham, “Optical fiber sensing technology: basics, classifications and applications,” *Am. J. Remote Sens.*, vol. 6, no. 1, pp. 1–5, Feb. 2018.

[134] K. T. V Grattan and T. Sun, “Fiber optic sensor technology: An overview,” *Sensors Actuators, A Phys.*, vol. 82, no. 1, pp. 40–61, 2000.

[135] B. Zheng, “Research on fiber optic sensor based on fuzzy control theory,” *J. Networks*, vol. 8, no. 8, pp. 1882–1889, 2013.

[136] D. Lau *et al.*, “Intensity-modulated microbend fiber optic sensor for respiratory monitoring and gating during MRI,” *IEEE Trans. Biomed. Eng.*, vol. 60, no. 9, pp. 2655–2662, 2013.

[137] H. Gong, M. S. Kizil, Z. Chen, M. Amanzadeh, B. Yang, and S. M. Aminossadati, “Advances in fibre optic based geotechnical monitoring systems for underground excavations,” *Int. J. Min. Sci. Technol.*, vol. 29, no. 2, pp. 229–238, Mar. 2019.

[138] S. Umesh and S. Asokan, “A brief overview of the recent bio-medical applications of fiber bragg grating sensors,” *J. Indian Inst. Sci.*, vol. 94, no. 3, pp. 319–328, 2014.

[139] D. Vilarinho *et al.*, “Foot plantar pressure monitoring with cytop bragg gratings sensing system,” in *International Joint Conference on Biomedical Engineering Systems and Technologies*, 2018, vol. 1, no. Biostec, pp. 25–29.

[140] Y. Miyauchi, S. Koyama, and H. Ishizawa, “Basic experiment of blood-pressure measurement which uses FBG sensors,” in *IEEE Instrumentation and Measurement Technology Conference*, 2013, pp. 1767–1770.

[141] L. Bilro, N. Alberto, J. L. Pinto, and R. Nogueira, “Optical sensors based on plastic fibers,” *Sensors (Switzerland)*, vol. 12, no. 9. pp. 12184–12207, 2012.

[142] K. S. C. Kuang, S. T. Quek, C. G. Koh, W. J. Cantwell, and P. J. Scully, “Plastic optical fibre sensors for structural health monitoring: A review of recent progress,” *J. Sensors*, vol. 2009, pp. 1–13, 2009.

[143] M. Rothmaier, B. Selm, S. Spichtig, D. Haensse, and M. Wolf, “Photonic textiles for pulse oximetry.,” *Opt. Express*, vol. 16, no. 17, pp. 12973–12986, 2008.

[144] J. J. Davenport, M. Hickey, J. P. Phillips, and P. A. Kyriacou, “Method for producing angled optical fiber tips in the laboratory,” *Opt. Eng.*, vol. 55, no. 2, pp. 1–6, 2016.

[145] M. J. Drinnan, J. Allen, and A. Murray, “Relation between heart rate and pulse transit time during paced respiration,” *Physiol. Meas.*, vol. 22, no. 3, pp. 425–432, Aug. 2001.

[146] J. Allen, “Photoplethysmography and its application in clinical physiological measurement.,” *Physiol. Meas.*, vol. 28, no. 3, pp. 1–39, 2007.

[147] D. Laqua, S. Pollnow, J. Fischer, S. Ley, and P. Husar, “A phantom with pulsating artificial vessels for non-invasive fetal pulse oximetry,” in *2014 36th Annual International Conference of the IEEE Engineering in Medicine and Biology Society, EMBC 2014*, 2014, vol. 2014, pp. 5631–5634.

[148] N. Stuban, M. Niwayama, and H. Santha, “Phantom with pulsatile arteries to investigate the influence of blood vessel depth on pulse oximeter signal strength,” *Sensors*, vol. 12, no. 1, pp. 895–904, 2012.

[149] J. S. Lillie *et al.*, “Pulse wave velocity prediction and compliance assessment in elastic arterial segments,” *Cardiovasc. Eng. Technol.*, vol. 6, no. 1, pp. 49–58, 2015.

[150] I. Z. Apostolakis, P. Nauleau, C. Papadacci, M. D. McGarry, and E. E. Konofagou, “Feasibility and validation of 4-D pulse wave imaging in phantoms and in vivo,” *IEEE Trans. Ultrason. Ferroelectr. Freq. Control*, vol. 64, no. 9, pp. 1305–1317, 2017.

[151] Z. Wang, Y. Yang, L. J. Yuan, J. Liu, Y. Y. Duan, and T. S. Cao, “Noninvasive method for measuring local pulse wave velocity by dual pulse wave doppler: In vitro and in vivo studies,” *PLoS One*, vol. 10, no. 3, pp. 1–13, 2015.

[152] T. J. Akl, M. A. Wilson, M. N. Ericson, and G. L. Coté, “Quantifying tissue mechanical properties using photoplethysmography,” *Biomed. Opt. Express*, vol. 5, no. 7, p. 2362, 2014.

[153] H. Njoum *et al.*, “Photoplethysmography for an independent measure of pulsatile pressure under controlled flow conditions,” *Physiol. Meas.*, vol. 38, no. 2, pp. 87–100, 2017.

[154] K. Rhode, G. Ennew, T. Lambrou, D. Hawkes, and A. Seifalian, “The measurement of blood flow from dynamic digital x-ray images using a weighted optical flow algorithm: validation in a moving-vessel flow phantom,” in *Conference Proceedings - Medical Image Understanding and Analysis*, 2001, pp. 4–7.

[155] M.-H. Jun, Y. J. Jeon, J.-H. Cho, and Y.-M. Kim, “Pulse wave response characteristics for thickness and hardness of the cover layer in pulse sensors to measure radial artery pulse,” *Biomed. Eng. Online*, vol. 17, no. 1, p. 118, 2018.

[156] N. Stubán and M. Niwayama, “Adjustable fetal phantom for pulse

oximetry," *Rev. Sci. Instrum.*, vol. 80, no. 5, pp. 78–82, 2009.

[157] Y. Tardy *et al.*, "Latex vessels with customized compliance for use in arterial flow models," *Physio. Meas.*, vol. 20, pp. 277–286, 1999.

[158] D. Laqua, S. Ley, P. Husar, and I. Methods, "Development of a phantom to modulate the maternal and fetal pulse curve for pulse oximetry measurements development of a phantom to modulate the maternal and fetal pulse curve for pulse oximetry measurements," no. June 2014, pp. 1–5, 2012.

[159] D. Gomez, S. P. Morgan, B. R. Hayes-Gill, R. G. Correia, and S. Korposh, "Polymeric optical fibre sensor coated by SiO_2 nanoparticles for humidity sensing in the skin microenvironment," *Sensors Actuators, B Chem.*, vol. 254, pp. 887–895, Jan. 2018.

[160] R. Correia *et al.*, "Highly sensitive contact pressure measurements using FBG patch in endotracheal tube cuff," in *6th European Workshop on Optical Fibre Sensors*, 2016, p. 99161F.

[161] C. Liu, R. Correia, H. K. Ballaji, S. Korposh, B. R. Hayes-Gill, and S. P. Morgan, "Optical fibre-based pulse oximetry sensor with contact force detection," *Sensors (Basel).*, vol. 18, no. 11, p. 3632, Oct. 2018.

[162] V. M. Chadachan, M. T. Ye, J. C. Tay, K. Subramaniam, and S. Setia, "Understanding short-term blood-pressure-variability phenotypes: From concept to clinical practice," *International Journal of General Medicine*, vol. 11. Dovepress, pp. 241–254, 2018.

[163] P. Fung, G. Dumont, C. Ries, C. Mott, and M. Ansermino, "Continuous noninvasive blood pressure measurement by pulse transit time.," *Conf. Proc. IEEE Eng. Med. Biol. Soc.*, vol. 1, no. 4,

pp. 738–741, 2004.

[164] S. Ribezzo, E. Spina, S. Di Bartolomeo, and G. Sanson, “Noninvasive techniques for blood pressure measurement are not a reliable alternative to direct measurement : A randomized crossover trial in ICU,” *Sci. World J.*, vol. 2014, pp. 1–9, 2014.

[165] R. Mukkamala *et al.*, “Toward ubiquitous blood pressure monitoring via pulse transit time: Theory and practice,” *IEEE Trans. Biomed. Eng.*, vol. 62, no. 8, pp. 1879–1901, 2015.

[166] H. Gesche, D. Grosskurth, G. Küchler, and A. Patzak, “Continuous blood pressure measurement by using the pulse transit time: Comparison to a cuff-based method,” *Eur. J. Appl. Physiol.*, vol. 112, no. 1, pp. 309–315, 2012.

[167] Y. Maeda, M. Sekine, and T. Tamura, “The advantages of wearable green reflected photoplethysmography,” *J. Med. Syst.*, vol. 35, no. 5, pp. 829–834, 2011.

[168] V. Vizbara, “Comparison of green, blue and infrared light in wrist and forehead photoplethysmography,” *17th Int. Conf. Biomed. Eng. 2013*, vol. 17, no. 1, pp. 78–81, 2013.

[169] Y. Tang *et al.*, “Thermal management of high-power LEDs based on integrated heat sink with vapor chamber,” *Energy Convers. Manag.*, vol. 151, no. June, pp. 1–10, 2017.

[170] K. Aziz, S. Tarapiah, S. H. Ismail, and S. Atalla, “Smart real-time healthcare monitoring and tracking system using GSM/GPS technologies,” *2016 3rd MEC Int. Conf. Big Data Smart City, ICBDSC 2016*, pp. 357–363, 2016.

[171] D. Ban and S. Kwon, “Movement noise cancellation in PPG

signals,” *2016 IEEE Int. Conf. Consum. Electron. ICCE 2016*, no. January 2016, pp. 47–48, 2016.

[172] A. K. Mallick, Bandana and Patro, “Heart rate monitoring system using finger tip through arduino,” *Int. J. Sci. Eng. Technol. Res.*, vol. 5, no. 1, pp. 84–89, 2016.

[173] M. Mondéjar-Guerra, V., Novo, J., Rouco, J., Penedo, M.G. and Ortega, “Heartbeat classification fusing temporal and morphological information of ECGs via ensemble of classifiers,” *Biomed. Signal Process. Control*, vol. 47, pp. 41–48, 2019.

[174] B. Taji, S. Shirmohammadi, V. Groza, and I. Batkin, “Impact of skin – electrode interface on electrocardiogram measurements using conductive textile electrodes,” *IEEE Transactions on Instrumentation and Measurement,* vol. 63, no. 6, pp. 1–11, 2013.

[175] M. M. Puurtinen, S. M. Komulainen, P. K. Kauppinen, J. A. V. Malmivuo, and J. A. K. Hyttinen, “Measurement of noise and impedance of dry and wet textile electrodes, and textile electrodes with hydrogel,” in *Annual International Conference of the IEEE Engineering in Medicine and Biology - Proceedings*, 2006, pp. 6012–6015.

[176] T.-Y. Chang, C.-S. Liu, K.-H. Huang, R.-Y. Chen, J.-S. Lai, and B.-Y. Bao, “High-frequency hearing loss, occupational noise exposure and hypertension: a cross-sectional study in male workers.,” *Environ. Health*, vol. 10, no. 1, p. 35, 2011.

[177] A. Wongkamhang, N. Thongpance, M. Sangworasil, K. Roongprasert, and T. Matsuura, “Development of the low - Cost blood pressure simulator,” in *BMEiCON 2014 - 7th Biomedical Engineering International Conference*, 2015, pp. 1–4.

[178] H. A. Aysan, “The effects of archery as a sports branch on coping with stress,” *Stud. Ethno-Medicine*, vol. 10, no. 1, pp. 39–43, 2016.

[179] A. A. Vladimirov and Y. I. Andriyashek, “Neurophysiological markers of stress within a recovery period after acute complications of cardiovascular diseases,” *Neurophysiology*, vol. 46, no. 3, pp. 225–232, 2014.

[180] Z. Zhang, M. Wang, X. Miao, Y. Li, G. Hitchman, and Z. Yuan, “Individuals with high obsessive-compulsive tendencies or undermined confidence rely more on external proxies to access their internal states,” *J. Behav. Ther. Exp. Psychiatry*, vol. 54, pp. 263–269, 2017.

[181] B. D. Joshi, Prakruti J and Patkar, Vivek P and Pawar, Akshay B and Patil, Prasad B and Bagal, UR and Mokal, “ECG denoising using matlab,” *Int. J. Sci. Eng. Res.*, vol. 4, no. 5, pp. 1401–1405, 2013.

[182] Y. Liang, M. Elgendi, Z. Chen, and R. Ward, “Analysis: An optimal filter for short photoplethysmogram signals,” *Sci. Data*, vol. 5, no. 1, pp. 1–12, May 2018.

[183] B. Lin, M. Atef, and G. Wang, “14.85 μW analog front-end for photoplethysmography acquisition with 142-dbΩ gain and 64.2-pArms noise,” *Sensors (Switzerland)*, vol. 19, no. 3, p. 512, Jan. 2019.

[184] F. Buendía-Fuentes *et al.*, “High-Bandpass Filters in Electrocardiography: Source of Error in the Interpretation of the ST Segment,” *ISRN Cardiol.*, vol. 2012, pp. 1–10, 2012.

[185] H. Li *et al.*, “Baseline optimization of SQUID gradiometer for magnetocardiography,” *Chinese Phys. B*, vol. 24, no. 2, 2015.

[186] G. N. Rao Salanke S, M. V Vijaya Kumar, and A. Samraj, “Performance Evaluation of PPG based multimodal biometric system using modified min-max normalization,” *Int. J. Appl. Eng. Res.*, vol. 13, no. 13, pp. 11279–11284, 2018.

[187] A. Choi and H. Shin, “Quantitative analysis of the effect of an ectopic beat on the heart rate variability in the resting condition,” *Front. Physiol.*, vol. 9, no. JUL, Jul. 2018.

[188] L. R. Bink and J. Furey, “Using in-line disposable pressure sensors to evaluate depth filter performance,” *BioProcess Int*, vol. 8, no. 2, pp. 44–48, 2010.

[189] B. Harsono, J. Liman, A. Kurniawan, J. Iskandar, E. Rohaeti, and Irzaman, “Ba0.5Sr0.5TiO3 based photodiode application as light sensor for automatic lighting control switch,” in *The 1st International Conference on Science, Technology and Interdisciplinary Research 2015*, 2005, pp. 388–391.

[190] A. Krol, M. Szarko, A. Vala, and J. De Andres, “Pressure monitoring of intraneural an perineural injections into the median, radial, and ulnar nerves; lessons from a cadaveric study.,” *Anesthesiology and pain medicine,* vol. 5, no. 3, pp. 0–7, 2015.

[191] E. Intensity *et al.*, “Efficacy of pulsed 405-nm light-emitting diodes for antimicrobial photodynamic inactivation: Effects of intensity, frequency, and duty cycle,” *Photomed. Laser Surg.*, vol. 35, no. 3, pp. 150–156, 2017.

[192] M. Silva Vieira, T. Hussain, and C. Alberto Figueroa, “Patient-specific image-based computational modeling in congenital heart disease: A clinician perspective,” *J. Cardiol. Ther.*, vol. 2, no. 6, pp. 436–448, 2015.

[193] S. Magder, “Volume and its relationship to cardiac output and venous return,” *Crit. Care*, vol. 20, no. 1, pp. 1–11, 2016.

[194] D. Zheng, J. Allen, and a. Murray, “Effect of external cuff pressure on arterial compliance,” *Comput. Cardiol. 2005*, pp. 315–318, 2005.

[195] V. E. Claydon, J. P. Moore, E. R. Greene, O. Appenzeller, and R. Hainsworth, “Evaluation of forearm vascular resistance during orthostatic stress: Velocity is proportional to flow and size doesn’t matter,” *PLoS One*, vol. 14, no. 11, p. e0224872, Nov. 2019.

[196] N. Westerhof, J. W. Lankhaar, and B. E. Westerhof, “The arterial windkessel,” *Med. Biol. Eng. Comput.*, vol. 47, no. 2, pp. 131–141, 2009.

[197] P. R. Painter, “The velocity of the arterial pulse wave: A viscous-fluid shock wave in an elastic tube,” *Theor. Biol. Med. Model.*, vol. 5, pp. 1–6, 2008.

[198] K. Murakami and M. Yoshioka, “Pulse transit time variability on a range of heart rates between resting and elevated states,” *Proc. - 2015 IEEE Int. Conf. Syst. Man, Cybern. SMC 2015*, pp. 1579–1582, 2016.

[199] J. Fiala *et al.*, “An implantable optical blood pressure sensor based on pulse transit time,” *Biomed. Microdevices*, vol. 15, no. 1, pp. 73–81, 2013.

[200] P. D. Arini, S. Liberczuk, J. G. Mendieta, M. Santa Mariá, and G. C. Bertrán, “Electrocardiogram delineation in a wistar rat experimental model,” *Comput. Math. Methods Med.*, vol. 2018, pp. 1–10, 2018.

[201] G. C. Jernstedt and J. P. Newcomer, “Blood pressure and pulse

wave velocity measurement for operant conditioning of autonomic responding," *Behav. Res. Methods Instrum.*, vol. 6, no. 4, pp. 393–397, 1974.

[202] F. Miao *et al.*, "A novel continuous blood pressure estimation approach based on data mining techniques," *IEEE J. Biomed. Heal. Informatics*, vol. 21, no. 6, pp. 1730–1740, 2017.

[203] S. Sun, R. Bezemer, X. Long, J. Muehlsteff, and R. M. Aarts, "Systolic blood pressure estimation using PPG and ECG during physical exercise," *Physiol. Meas.*, vol. 37, no. 12, pp. 2154–2169, 2016.

[204] M. H. N. van Velzen, A. J. Loeve, S. P. Niehof, and E. G. Mik, "Increasing accuracy of pulse transit time measurements by automated elimination of distorted photoplethysmography waves," *Med. Biol. Eng. Comput.*, vol. 55, no. 11, pp. 1989–2000, Nov. 2017.

[205] C. C. Y. Poon, Y.-T. Z. Y.-T. Zhang, G. Wong, and W. S. P. W. S. Poon, "The beat-to-beat relationship between pulse transit time and systolic blood pressure," *2008 Int. Conf. Inf. Technol. Appl. Biomed.*, no. 1, pp. 342–343, 2008.

[206] B. G. Celler, A. Argha, P. N. Le, and E. Ambikairajah, "Novel methods of testing and calibration of oscillometric blood pressure monitors," *PLoS One*, vol. 13, no. 8, 2018.

[207] J. Allen and A. Murray, "Age-related changes in peripheral pulse timing characteristics at the ears, fingers and toes," *J. Hum. Hypertens.*, vol. 16, no. 10, pp. 711–717, 2002.

[208] P. Sedgwick, "Pearson's correlation coefficient.," *BMJ Br. Med. J.*, vol. 345, p. 4483, 2012.

[209] N. J. Gogtay and U. M. Thatte, “Principles of correlation analysis,” *J. Assoc. Physicians India*, vol. 65, pp. 78–81, 2017.

[210] M. M. Mukaka, “Statistics corner: A guide to appropriate use of correlation coefficient in medical research.,” *Malawi Med. J.*, vol. 24, no. 3, pp. 69–71, Sep. 2012.

[211] T. Chai and R. R. Draxler, “Root mean square error (RMSE) or mean absolute error (MAE)?,” *Geosci. Model Dev. Discuss.*, vol. 7, no. 1, pp. 1525–1534, 2014.

[212] A. Imam and M. Abanyam, “On consistency and limitation of paired t-test , sign and wilcoxon sign rank test,” IOSR Journal of Mathematics, vol. 10, no. 1, pp. 1–6, 2014.

[213] A. Arza, J. Lázaro, and E. Gil, “Pulse transit time and pulse width as potential measure for estimating beat-to-beat systolic and diastolic blood pressure,” *Comput. Cardiol. (2010).*, vol. 40, pp. 887–890, 2013.

[214] M. A. Younessi Heravi, M. A. Khalilzadeh, and S. Joharinia, “Continuous and cuffless blood pressure monitoring based on ECG and SpO_2 signals by using Microsoft Visual C sharp.,” *J. Biomed. Phys. Eng.*, vol. 4, no. 1, pp. 27–32, Mar. 2014.

[215] M. Y.-M. Wong, C. C.-Y. Poon, and Y.-T. Zhang, “An evaluation of the cuffless blood pressure estimation based on pulse transit time technique: a half year study on normotensive subjects.,” *Cardiovasc. Eng.*, vol. 9, no. 1, pp. 32–38, 2009.

[216] Y. S. Yan and Y. T. Zhang, “A model-based calibration method for noninvasive and cuffless measurement of arterial blood pressure,” *IEEE 2006 Biomed. Circuits Syst. Conf. Healthc. Technol. BioCAS 2006*, pp. 234–236, 2006.

[217] T. Pereira, C. Correia, and J. Cardoso, “Novel methods for pulse wave velocity measurement,” *J. Med. Biol. Eng.*, vol. 35, no. 5, pp. 555–565, 2015.

[218] J. B. Lanier, M. B. Mote, and E. C. Clay, “Evaluation and management of orthostatic hypotension,” *Am. Fam. Physician*, vol. 84, no. 5, pp. 527–536, 2011.

[219] J. Allen, A. Murray, C. Di Maria, and J. L. Newton, “Chronic fatigue syndrome and impaired peripheral pulse characteristics on orthostasisa new potential diagnostic biomarker,” *Physiol. Meas.*, vol. 33, no. 2, pp. 231–241, 2012.

[220] J. Y. A. Foo, S. J. Wilson, G. Williams, M. A. Harris, and D. Cooper, “Pulse transit time as a derived noninvasive mean to monitor arterial distensibility changes in children,” *J. Hum. Hypertens.*, vol. 19, no. 9, pp. 723–729, Sep. 2005.

[221] Y. Obata *et al.*, “Noninvasive assessment of the effect of position and exercise on pulse arrival to peripheral vascular beds in healthy volunteers,” *Front. Physiol.*, vol. 8, no. FEB, p. 47, Feb. 2017.

[222] M. Berthelot, G.-Z. Yang, and B. Lo, “Preliminary Study for Hemodynamic Monitoring using a Wearable Device Network,” in *IEEE 14th International Conference on Wearable and Implantable Body Sensor Networks (BSN)*, 2017, pp. 115–118.

[223] A. Sahoo and G. Rath, “Real time estimation of various physiological parameters by analysis of PPG signal,” *Int. J. Comput. Appl.*, vol. 57, no. 15, pp. 11–15, 2012.

Appendix A

2016-17 academic year only

The University of Nottingham

Faculty of Engineering
Process for approval of research study involving human participants

Introduction
This document describes the process to be followed when planning and obtaining approval for studies involving human participants within the Faculty of Engineering. This process is based on one previously run within the School/Dept M3. The process is administered by the Faculty Research Ethics Committee, and managed by the Chair of the Ethics Committee, Dr. Gary Burnett, and Faculty Research Ethics Officer, Dr. Sarah Sharples. All queries regarding the process should be initially sent to the Faculty Ethics Administrator, Jo Deeley.

What is Ethics Approval?

When conducting any study or observation or collecting data about individuals, it is essential that full consideration is given to ethical issues and that steps are taken to ensure participant well-being throughout the study.

Participants involved in research studies have a right to:
- Know the goals of the study and who is funding the work
- Make an informed decision about whether or not they wish to participate
- Leave the study at any time if they do not wish to continue
- Know what will happen to them during the study and how long it will take
- Know if they may experience any discomfort
- Know what will happen to the findings
- Privacy of personal information
- Be treated courteously

The University of Nottingham and Faculty of Engineering have an ethics procedure that requires all staff and students to submit an application for ethical approval before conducting any research study involving human participants. Members of the Ethics Committee read through study proposals to check that the researcher has demonstrated that they have given full consideration to ethical issues and that they have provided participants with appropriate and sufficient information.

Who needs Ethics Approval?

ANY member of staff or registered student of the University of Nottingham involved in conducting any study or observation or collecting data about individuals **MUST** adhere to the University Code of Research Conduct and Research Ethics. Those affiliated with the Faculty of Engineering **MUST ALSO** comply with the Faculty ethical approval process before commencing their study.

Ethics application procedure

The attached document outlines the ethics approval process within the Faculty of Engineering. For all applications required to undergo formal review, applications must be submitted to the **Ethics Administrator**, Faculty of Engineering Research Office, Coates Building. The application will then be reviewed by the ethics committee. We aim to return a decision to applicants within two weeks but the procedure may be delayed if the ethics committee require further information. It is the applicant's responsibility to make sure that applications are submitted in good time.

THE STUDY MAY **NOT** START UNTIL ETHICAL APPROVAL HAS BEEN AWARDED

2016-17 academic year only

Information you should give to ALL participants

The following list describes the information that should be given to all participants. Normally this should be given in a participant information sheet at the beginning of the study, and participants should be required to confirm that they have understood the nature of the study, and that they are happy to participate.
The following information should be included:

- Details of who will be conducting the study.
- Details about who is sponsoring the study and what the terms of the sponsorship are (i.e. who will 'own' the data and how the data will be used).
- Details about the nature, purpose and duration of the study. (Participants whose first language is NOT English may need further explanation of what is involved as their understanding of some of the terminology may be limited).
- What kinds of procedures will be used and what participant will be asked to do.
- Details about any hazards, inconveniences and risks associated with the study.
- What procedures will be followed if a participant is injured. (only needed if risk of injury has been identified)
- What benefits (payments, expenses etc) are attached to the study.
- What they need to do in order to receive the payments described above.
- What procedures will be employed to maintain confidentiality and anonymity (e.g. removing personal details from data/reports, keeping data in locked files)
- What will happen to the data (how it will be used, how it will be stored, in what form it will be disseminated and if it is likely to be used for further analysis).
- How you will use photographs or video records (data analysis, illustration purposes, displayed to sponsors/ non-public academic audiences, printed in public domain documents etc).
- Details about who to contact if questions or problems arise.
- ALL participants must be told that any involvement in the study is voluntary and they are free to withdraw at any time. You should also explain any consequences for the participant of withdrawing from the study and indicate what will be done with the participant's data if they withdraw.

Appendix A

2016-17 academic year only

Faculty of Engineering
Application for approval of research study involving human participants

ALL applicants must provide the following information
The applicant must be the person who will conduct the investigations; each application must be made by one applicant:

- usually the student in the case of taught or research courses,
- usually the researcher (the member of university research or academic staff) who will conduct the study in the case of funded research projects,
- usually the principal investigator in the case of applications for ethics approval in advance of submission of a research proposal

If the applicant is an Undergraduate or Postgraduatetaught or research student please complete the information below. The application must be approved by a Supervisor.

Name of student:	Wan Suhaimizan Wan Zaki	Student No:	4229653
Course of study:	PhD in Electrical and Electronic Engineering	Email address:	eexwswa@nottingham.ac.uk
Supervisor:	Prof. Steve Morgan		

If the applicant is a member of university research or academic staff, please complete the information below: For research staff, the application must be approved by the Principal Investigator

Name:		PrincipalInvestigator (Budget Holder)	
Email address:		PI Signature:	

Title of investigation: Cuff-Less Blood Pressure Measurement Using Pulse Transit Time Techniques

Planned date for study to begin 15 May 2017 Duration of Study 5 Months

Please state whether this application is:

■ New ☐ Revised ☐ A renewal ☐ For a continuation study

Selection of review process

Please indicate whether the application is required to go forward to the ethics committee for formal review, or, in the case of projects completed by ***taught undergraduate and postgraduate students only***, whether the application can be approved by the supervisor under the expedited review process*.

■ Formal review, application will be submitted to ethics committee

☐ Expedited review, application is approved by supervisor*
* This option can only be selected if the Supervisor is a member of the Faculty Ethics committee

Approval by supervisor: expedited review

I approve the application as supervisor of this project, under the expedited review procedure.

Name of supervisor..... Signature..... Date.....

Office use only

Date form received: **Date decision returned to applicant:**
Passed to reviewers: 1. Name..... Date.....
(formal review only) 2. Name..... Date.....

2016-17 academic year only
Ethical Issues Checklist

The purpose of this Checklist is to facilitate the review process and to identify any ethical issues that may concern the Committee. It is meant to be an aid to both the researcher and the Committee. Listed below are areas which require some justification and attention on your part in specifying your study protocol. Please answer each question honestly, giving full details where required. Answering "YES" to any of the questions will not necessarily lead to a negative response to your application but it will draw issues to your attention and give the reviewers the opportunity to ensure appropriate steps are being taken. In expedited review, supervisors should ensure that for any questions where the answer "YES" has been given, appropriate measures have been taken to maintain ethical compliance.

Applicant's full name.. Wan Suhaimizan Wan Zaki

You must complete ALL of this section before submitting your application

1 Who is the population to be studied?

Healthy volunteers. Primarily members of the research team (academic staff, researchers, PhD students) in the Optics and Photonics Group.

2 Please give details of how the participants will be identified, approached and recruited. (Include any relationship between the investigator and participants e.g. instructor-student).

Participants will be identified by giving a number and recruited from the members of research team in Optics and Photonics Group.

3 Will the population studied include any vulnerable members of the public? **YES** ☐ **NO** ■
Note: for the purpose of ethics approval this includes participants who are under 18, people who are disabled or in poor health, and also those who are non-English speakers and may not be able to understand the consent forms. (If YES, please give further details)

4 Will it be possible to associate specific information in your records with specific participants on the basis of name, position or other identifying information contained in your records? **YES** ☐ **NO** ■

5 What steps have you taken to ensure confidentiality of personal information and anonymity of data both during the study and in the release of its findings?

Data/images will be published anonymously and data is locked by a password-protected computer.

Only members of the research group will have access to the data.

6 Describe what data will be stored, where, for what period of time, the measures that will be put in place to ensure security of the data, who will have access to the data, and the method and timing of disposal of the data.

Paper records should be stored in a locked filing cabinet. Digital data should be stored only on a password-protected computer and/or on a secure server. In accordance with the Data Protection Act, the data needs to be kept securely for seven years following publication kept securely for seven years following publication of results. After this time, electronic files will be deleted and any hard copies will be destroyed.

At the end of a student project, students are responsible for ensuring that all data from the study is passed on to their academic supervisor/s. The supervisors/s will then have responsibility for the storage of that data.

2016-17 academic year only

The data that will be recorded are the Photopleythsmogram (PPG) signal , the Electrocardiogram (ECG) signal and Blood Pressure recorded by OSTAR Blood Presure Monitor. All the paper records will be stored in a locked filing cabinet and the digital data will be stored on a password-protected computer. All the data will be kept securely for a period of seven years following any publication. Access will be to members of the research team via password protected computers.

		YES	NO
7	Will persons participating in the study be subjected to physical or psychological discomfort, pain or aversive stimuli which is more than expected from everyday life? (If YES, please give further details) In tilt table test, the participant may feel a little bit dizzy when their body moved from supine to tilt up condition but shouldn't be uncomfortable. In cold immersion test, the hand will be cooled but this should not cause discomfort or pain. At any time the participant may withdraw from participation in this experiment if they feel uncomfortable.	■	☐
8	Will participants engage in strenuous or unaccustomed physical activity? (If YES, please give further details)	☐	■
9	Will the investigation use procedures designed to induce participants to act contrary to their wishes? (If YES, please give further details)	☐	■
10	Will the investigation use procedures designed to induce embarrassment, humiliation, lowered self esteem, guilt, conflict, anger, discouragement or other emotional reactions? (If YES, please give further details)	☐	■
11	Will participants be induced to disclose information of an intimate or otherwise sensitive nature? (If YES, please give further details)	☐	■
12	Will participants be deceived or actively misled in any manner? (If YES, please give further details)	☐	■
13	Will information be withheld from participants that they might reasonably expect to receive? (If YES, please give further details)	☐	■
14	Will the research involve potentially sensitive topics? (If YES, please give further details)	☐	■

2016-17 academic year only

15 Will data be collected which requires potentially invasive procedures (eg attaching electrodes to the skin) and/or other health-related information to be identified (eg heart rate). If yes please give details **YES** ■ **NO** □

In this experiments, Electrocardiogram (ECG) signals will be acquired using textile based conductive electrodes and commercial ECG surface electrode. Both types of electrodes will be placed at 3 positions on the on the chest. For the Photopleythsmography (PPG) measurements, the Pulse Sensor (commercial sensor) and a sensor that uses Plastic Optical Fibers (POF) to deliver and receive light will be used. The PPG sensors will be allocated at two different sites on body (upper arm and wrist).

If you require space for additional information, please add it here and identify the question to which it refers:

Checklist of information to include with your application:
Please tick the boxes below to confirm that you have included the following information with your submission. Failure to include the required information may result in your ethics application and approval for start of your research to be delayed.

■ A brief description of the study design:
- number and type of participants
- number and duration of activities participants will be involved in
- equipment and procedures to be applied
- information about how participants will be recruited
- whether participants will be paid (state how this will be done)
- plans to ensure participant confidentiality and anonymity
- plans for storage and handling of data
- information about what will happen to the data after the study
- information about how any data and images may be used
- state whether it will be possible to identify any individuals.

■ Copies of any information sheets to be given to participants (include recruitment information (e.g. adverts, posters, letters, etc)

■ A copy of the participant consent form

■ Copies of data collection sheets, questionnaires, etc

I confirm that all of the above is included in the application:

As the applicant I confirm that I have read and understand the Ethical requirements for my study and have read and complied with the University of Nottingham Code of Research Conduct and Research Ethics.

Signature of applicant ..... Date 04.05.2017

As supervisor, I confirm that I have checked the details of this application.

Signature of supervisor ..... Date 04.05.2017

NB The signature of the supervisor on this part of the application DOES NOT indicate supervisor approval for expedited review. If supervisor approval is granted then the front page of the application MUST be signed for approval to be confirmed.

Ethics Committee Reviewer Decision

This form must be completed by each reviewer. Each application will be reviewed by two members of the ethics committee. Reviews may be completed electronically and sent to the Faculty ethics administrator (Jo Deeley) from a University of Nottingham email address, or may be completed in paper form and delivered to the Faculty of Engineering Research Office.

Applicant full name Wan Zaki Wan

Reviewed by:

Name M03

Signature (paper based only) .....

Date 28/11/2017

- ☐ Approval awarded - no changes required
- ☐ **Approval awarded - subject to required changes (see comments below)**
- ☐ Approval pending - further information & resubmission required (see comments)
- ☐ Approval declined – reasons given below

Comments:

Sorry for the delay in replying to this one. The research involves attaching electrodes to the chest of participants. I think this is an issue that has come up before, but the applicants need to come up with a way that wouldn't involve male researchers fiddling with electrodes on the chest of a female participant.

Otherwise I'm happy to approve the study.

Please note:

1. The approval only covers the participants and trials specified on the form and further approval must be requested for any repetition or extension to the investigation.
2. The approval covers the ethical requirements for the techniques and procedures described in the protocol but does not replace a safety or risk assessment.
3. Approval is not intended to convey any judgement on the quality of the research, experimental design or techniques.
4. Normally, all queries raised by reviewers should be addressed. In the case of conflicting or incomplete views, the ethics committee chair will review the comments and relay these to the applicant via email. All email correspondence related to the application must be copied to the Faculty research ethics administrator.

Any problems which arise during the course of the investigation must be reported to the Faculty Research Ethics Committee

Ethics Committee Reviewer Decision

This form must be completed by each reviewer. Each application will be reviewed by two members of the ethics committee. Reviews may be completed electronically and sent to the Faculty ethics administrator (Jo Deeley) from a University of Nottingham email address, or may be completed in paper form and delivered to the Faculty of Engineering Research Office.

Applicant full name Wan Zaki Wan

Reviewed by:

Name D13

Signature (paper based only) .....

Date 20 November 2017

- ☐ Approval awarded - no changes required
- ■ Approval awarded - subject to required changes (see comments below)
- ☐ Approval pending - further information & resubmission required (see comments)
- ☐ Approval declined – reasons given below

Comments:

The participant information sheet is written for the participant – therefore sentences like "In the beginning of the experiment, the participant will be asked to relax in a sitting position for 5 minutes." should probably be rewritten as "At the beginning of the experiment you will be asked to relax in a sitting position for 5 minutes."

Please note:

1. The approval only covers the participants and trials specified on the form and further approval must be requested for any repetition or extension to the investigation.
2. The approval covers the ethical requirements for the techniques and procedures described in the protocol but does not replace a safety or risk assessment.
3. Approval is not intended to convey any judgement on the quality of the research, experimental design or techniques.
4. Normally, all queries raised by reviewers should be addressed. In the case of conflicting or incomplete views, the ethics committee chair will review the comments and relay these to the applicant via email. All email correspondence related to the application must be copied to the Faculty research ethics administrator.

Any problems which arise during the course of the investigation must be reported to the Faculty Research Ethics Committee

The University of Nottingham
UNITED KINGDOM · CHINA · MALAYSIA

Experimental Study to Investigate Whether Blood Pressure Can Be Estimated Using Pulse Transit Time (PTT) Techniques

Participant Information Sheet

You are invited to take part in a study which will investigate blood pressure estimation based on pulse transit time (PTT) between Electrocardiogram (ECG) and Photopleythsmography (PPG) signals. Before you decide whether to take part it is important for you to understand why the research is being done and what it will involve. If you would like more information or have any questions, please contact Wan Suhaimizan, eexwswa@nottingham.ac.uk or Prof. Steve Morgan, steve.morgan@nottingham.ac.uk

Background

Continuous blood pressure measurement in 24 hours is beneficial for clinicians following up the reactions of the cardiovascular system in the presence of some drugs or after medical treatment. Continuous monitoring of blood pressure can also be very useful in many situations, such as in cardiovascular diseases (hypertension), or to prevent falling accidents related to orthostatic hypotension (low pressure). Currently, blood pressure is monitored continuously using a Noninvasive Blood Pressure monitor based on auscultatory method. This method widely used for monitoring blood pressure due to the accuracy of the measurement. However, over a long period continuous blood pressure monitoring, this method will give pain and discomfort to the patient due to the inflatable cuff pressure and the bulk of the device. Therefore, a lot of research focuses on developing a cuff less blood pressure monitoring system for patient comfort during 24 hour monitoring process.

One of the methods for cuff-less blood pressure monitoring is by measuring the pulse transit time (PTT) between Electrocardiogram (ECG) and Photopleythsmography (PPG) signals on the body. In this study, conductive fabrics based electrode will be used for ECG detection and fibre optic based system used for PPG detection. The delay time between ECG and PPG signals will be correlated with the blood pressure. All the measurements will be validate against a commercial sensor.

Who are the participants?

Up to 30 healthy volunteers will be recruited primarily from the Optics and Photonics Group including researchers/PhD students.

Procedure

In this experiment, ECG signals will be acquired using textile based electrodes (conductive fabrics) and commercial ECG sensors (surface electrode). Both types of electrodes will be placed on the participant's chest. For the PPG measurements, the Blood Volume Pulse Sensor (commercial sensor) will be attached on fingertip and Plastic Optical Fiber (POF) will be attach on body in two differents position (wrist and toe). PPG Box which consists of green LED as a light source to illuminate skin through POF and photodiode with amplifier to receive light back from the fiber for pulse detection. All the measurements were acquired by the Nexus 10 Mark II device and the data were send to computer for further analysis.

For validation of the PTT method, blood pressure will be recorded using a conventional blood pressure device (OSTAR blood pressure monitor) on the right arm. The sensors location and the measurement setup for the PTT measurement is shown in Figure 1.

For the ECG electrode attachment, you should be able to attach the ECG electrode in privacy yourself, however, assistance can be provided if needed. It should be noted that the study organisers are not medically qualified and cannot offer advice about your ECG waveform and blood pressure reading. If you have any concerns after participating in this study then you should contact your general practitioner.

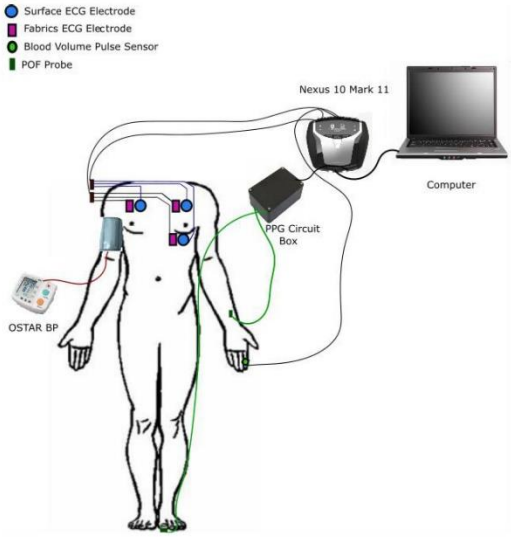


Figure 1: ECG and PPG measurement setup

For the first part, the participant will be asked to relax in a sitting position for 6 minutes. After that, ECG and PPG signals will be recorded for 30 seconds simultenously with the blood pressure measurement using the OSTAR system. Then, the participant will be asked to perform pedal exercise for 6 minutes. The PTT measurement and BP will be taken every two inutes interval.

Next, the participant will be asked to perform again pedal exercise for 6 minutes. Immediately after the exercise, the participant's blood pressure will be recorded and the PTT will be measured within two minutes interval (4 times).

Second part, the participant will be asked to relax on the tilt table for 6 minutes in supine position. Then, the tilt table will be move up to 70 degree and the participant will be in this position for 6 minutes. After that the tilt table will be moved to the initial position (0 degree) and the participant will be asked to stay in a supine position for 6 minutes. The PTT will be recorded continuously during this experiment and the BP will be recorded within two minutes interval.

The third part, the participant will be asked to move the left arm into four different levels during supine position on tilt table. For each level, the hand should be in still position for 2 minutes. The PTT will be recorded continuously during this experiment and at the ends of two minutes, PTT and blood pressure will be recorded for each levels.

This experiment should last approximately an hour for each participant.

Part 2: Further Information

1. Do I have to take part?

No. Participation in the study is entirely voluntary; it is up to you to decide whether or not to take part. If you do decide to take part you will be given this Participation Information Sheet to keep and be asked to complete a consent form. However, even if you complete the consent form you are still free to withdraw at any time and without giving a reason.

2. What will happen to me if I take part?

You will be asked to read through the Participant Information Sheet and then asked to complete the Participant Consent Form.

3. What will happen if I do not want to carry on with the study?

You can withdraw from the study at any time without having to provide a reason. If you do withdraw information that can be attributed to you will not be used in our analysis.

4. Will I be paid?

No.

5. Will my taking part in this study be kept confidential?

Yes. All information which is collected about you during the course of the research will be kept strictly confidential and our procedures for handling, processing, storage and destruction of your data are compliant with the Data Protection Act 1998. The data, including ECG signal, PPG signal, Pulse Transit Time (PTT) and blood pressure measurement will be retained for 7 years following any publication, after this time it will be destroyed. All of the data will be stored on password protected computers in the research laboratory of the Optics ans Photonics Group. Only members of the research group will have access to the data. It is not possible to identify any individuals because any data will be published anonymously.

6. What will happen to the results of the research study?

The results will be used in journal or any scientific conferences publications. The data will be used anonymously.

7. Who has reviewed the study?

The study has been reviewed and approved by the University of Nottingham, Faculty of Engineering Ethical Review Committee.

Appendix A

The University of Nottingham
UNITED KINGDOM · CHINA · MALAYSIA

Consent form

Experiment for the study of cuff-less blood pressure measurement

- I confirm that I have read the information sheet and have had the opportunity to ask questions. ☐
- I understand that the collected data will be used for journal publications. ☐
- I understand that I am free to withdraw at any time and that the any information will be destroyed and not used. ☐
- I understand that all information collected during the study will be kept strictly confidential. ☐
- I agree to take part in the above study. ☐

Print Name.....

Signature.....

Date.....

Participants information:

Question	Answer
Study case number	
Age	
Gender	
Height	
Weight	
Are you aware of any physical conditions that may affect your participation in this study?	

Appendix B1

Microcontroller Arduino code for trigger relay and generate pulse signal using tubular cardiovascular pulse delay time phantom system.

```
// the setup function runs once when you press reset or power the board
void setup() {
  // initialize digital pin 13 as an output.
  pinMode(13, OUTPUT);
  pinMode(12, OUTPUT);
}

// the loop function runs over and over again forever
// set duty cycle = 90%
void loop() {
  digitalWrite(13, HIGH);   // turn the LED on (HIGH is the voltage level)
  delay(900);
  digitalWrite(12, HIGH);
  delay(900);               // wait for a second
  digitalWrite(13, LOW);    // turn the LED off by making the voltage LOW
  delay(100);
  digitalWrite(12, LOW);    // turn the LED off by making the voltage LOW
  delay(100);               // wait for a second
}
```

The code to vary duty cycle

```
}

// set duty cycle = 80%
void loop() {
  digitalWrite(13, HIGH);   // turn the LED on (HIGH is the voltage level)
  delay(800);
```

```
  digitalWrite(13, LOW);    // turn the LED off by making the voltage LOW
  delay(200);

}
// set duty cycle = 60%
void loop() {
  digitalWrite(13, HIGH);   // turn the LED on (HIGH is the voltage level)
  delay(600);
  digitalWrite(13, LOW);    // turn the LED off by making the voltage LOW
  delay(400);

}
```

The code to vary pulse rate

```
}
// set pulse rate = 60pulse/min
void loop() {
  digitalWrite(13, HIGH);   // turn the LED on (HIGH is the voltage level)
  delay(900);
    digitalWrite(13, LOW);    // turn the LED off by making the voltage LOW
  delay(100);

}
}
// set pulse rate = 80pulse/min
void loop() {
  digitalWrite(13, HIGH);   // turn the LED on (HIGH is the voltage level)
  delay(650);
    digitalWrite(13, LOW);    // turn the LED off by making the voltage LOW
  delay(100);

}
}
// set pulse rate = 100pulse/min
```

```
void loop() {
  digitalWrite(13, HIGH);   // turn the LED on (HIGH is the voltage level)
  delay(500);
    digitalWrite(13, LOW);    // turn the LED off by making the voltage LOW
  delay(100);

}
}
// set pulse rate = 120pulse/min
void loop() {
  digitalWrite(13, HIGH);   // turn the LED on (HIGH is the voltage level)
  delay(400);
    digitalWrite(13, LOW);    // turn the LED off by making the voltage LOW
  delay(100);

}
}
// set pulse rate = 140pulse/min
void loop() {
  digitalWrite(13, HIGH);   // turn the LED on (HIGH is the voltage level)
  delay(430);
    digitalWrite(13, LOW);    // turn the LED off by making the voltage LOW
  delay(100);

}
}
// set pulse rate = 160pulse/min
void loop() {
  digitalWrite(13, HIGH);   // turn the LED on (HIGH is the voltage level)
  delay(370);
    digitalWrite(13, LOW);    // turn the LED off by making the voltage LOW
  delay(100);

}
```

Appendix B2

Matlab code for PAT calculation

Read data from file *.mat

```
clear;
s1=15% insert start time for cuff
e1=25;%insert end time for cuff
data = load('r1.mat');
data=data.Sessiondata(4:end,:);



time=cell2mat(data(:,1));
time1 =0: 1/256: (length(time)/256)-1/256;
start=s1*256;
ending=e1*256;% set time for pressure cuff (release pressure)
mi=start;
ma=ending;
%figure

timea=time1(start:ending);
time11=timea;
timea=timea';



ECG=cell2mat(data(:,3));%ECG Surface Electrode
ECGf=cell2mat(data(:,2));%ECG Fabrics Electrode
PPGpdf=cell2mat(data(:,5));%PPG from PD at toe
PPGpdw=cell2mat(data(:,4));%PPG from PD at wrist
PPGff=cell2mat(data(:,6));%PPG from fibre at foot
PPGnex=cell2mat(data(:,7));%PPG from nexus device
PPGfw=cell2mat(data(:,8));%PPG from fibre at wrist
Cuff=cell2mat(data(:,9));%Cuff Pressure
```

```
ECGfa=ECGf(start:ending);%ECG fabriks
ECGa=ECG(start:ending);%ECG nexus
plot(ECG);
figure
plot(PPGfw);
figure
plot(PPGnex)
```

Filter ECG and PPG signal using FIR filter

Filter ECG signal (Nexus)

```
% filter ECG signal
d1 = designfilt('bandpassfir','FilterOrder',20, ...
          'CutoffFrequency1',0.05,'CutoffFrequency2',40, ...
          'SampleRate',256);

ECG= filtfilt(d1,ECGa);
figure
%plot(timea,PPGnexaf);
% subplot(2,1,1)
plot(timea,ECGf,'b','LineWidth',3.0)
hold on
% subplot(2,1,2)
plot(timea,ECGa,'r','LineWidth',3.0)
%fvtool(d1)
set(gca,'FontSize',28);
h1title=title('ECG Measurement')
set(h1title,'FontSize',38)
xlabel('Time (s)')
ylabel('Voltage (uV)')
lgd =
legend({'Filter','Unfilter'},'FontSize',23,'TextColor','blue')
```

Filter ECG signal (Fabrics)

```
% filter ECG signal
d1 = designfilt('bandpassfir','FilterOrder',20, ...
         'CutoffFrequency1',0.05,'CutoffFrequency2',40, ...
         'SampleRate',256);

ECGf= filtfilt(d1,ECGfa);
```

Filter PPG signal at wrist

```
%filter cutt off 8 hz at PPG at wrist
%convert Hz to rad/s = xhz*2/256

      lpFilt =
designfilt('lowpassfir','PassbandFrequency',0.03125, ...
         'StopbandFrequency',0.125,'PassbandRipple',0.5, ...
         'StopbandAttenuation',65,'DesignMethod','equiripple');

Pcuffac= filtfilt(d1,PPGfwa);
figure
plot(timea,Pcuffac,'b','LineWidth',3.0);
```

Filter PPG signal at finger

```
%filter cutt off 8 hz at PPG nexus

%convert Hz to rad/s = xhz*2/256
%  d1 = designfilt('lowpassiir','FilterOrder',3, ...
%     'HalfPowerFrequency',0.0625,'DesignMethod','butter');

d1 = designfilt('lowpassiir','FilterOrder',8, ...
         'PassbandFrequency',8,'PassbandRipple',0.2, ...
         'SampleRate',256);
```

```
PPGnexaf= filtfilt(d1,PPGnexa);

plot(PPGnexaf);
hold on
plot(PPGnexa)

%%
```

Filter PPG signal underfoot

```
%filter cutt off 8 hz at PPG underfoot
%convert Hz to rad/s = xhz*2/256


%%filter cutt off 8 hz at PPG foot
 d1 = designfilt('lowpassiir','FilterOrder',3, ...
    'HalfPowerFrequency',0.0625,'DesignMethod','butter');

PPGffaf= filtfilt(d1,PPGffa);%filter PPG at foot

figure
plot(timea,PPGffaf);
```

Normalization of ECG and PPG signal using min-max method

Normalize ECG Nexus

```
%normalize ecg signal nexus device
figure
ECGn=ECGn_11;
maxV=max(ECGn);
minV=min(ECGn);
```

```
d=maxV-minV;
ECGn_1=(ECGn-minV)/d;
plot(timea,ECGn_1)



subplot(2,1,1)
plot(time1,ECGf,'b','LineWidth',3)
set(gca,'FontSize',24);
h1title=title('ECG Measurement')
set(h1title,'FontSize',34)
xlabel('Time (s)')
ylabel('Voltage (uV)')
xlim([3 8])
subplot(2,1,2)
plot(timea,ECGn_1,'r','LineWidth',3)
```

Normalize ECG fabrics

```
%normalize ecg fabrics
figure
ECGnf=ECGnf_11;
maxV=max(ECGnf);
minV=min(ECGnf);
d=maxV-minV;
ECGnf_1=(ECGnf-minV)/d;
plot(timea,ECGnf_1)
```

Normalize PPG signal at wrist

```
%normalize ppg at wrist
time11=time1(mi:ma);
PPGwafn=PPGwafn_11;
maxVp=max(PPGwafn);
minVp=min(PPGwafn);
dp=maxVp-minVp;
```

```
PPGwafn_1=(PPGwafn-minVp)/dp;


figure
plot(time11,PPGfwa);
figure
plot(time11,PPGwwafn_1);
```

Normalize PPG signal at finger

```
%normalize ppg signal nexus device
time11=time1(mi:ma);
PPGnex1n=PPGnexaf;
maxVp=max(PPGnex1n);
minVp=min(PPGnex1n);
dp=maxVp-minVp;
PPGnexn_1=(PPGnex1n-minVp)/dp;
```

Normalize PPG signal underfoot

```
%normalize ppg at toe
time11=time1(mi:ma);
PPGfafn=PPGffafn_11;
maxVp=max(PPGfafn);
minVp=min(PPGfafn);
dp=maxVp-minVp;
PPGfafn_1=(PPGfafn-minVp)/dp;
```

Thresholding and Peak detection using findpeak function

Find R-wave peak for ECG Nexus

```
%find peak for ECG nexus
[pksE,locsE] = findpeaks(ECGn_1,time11,'MinPeakDistance',0.35);
%[pksE,locsE] = findpeaks(ECGn_1,256);
m=1;
npeaks=[];
for i=1:length(pksE)
    if(pksE(i)>0.5)
        npeaks(m)=pksE(i);
        nlocsE(m)=locsE(i);

        m=m+1;
    end
end


plot(time11',ECGn_1,'b','LineWidth',3);

hold on;
plot(nlocsE,npeaks,'or','LineWidth',4);

hold on
plot(timea',PPGwafn_1,'r','LineWidth',3);
hold on;
plot(nlocsPw, PPGwpeaks,'or','LineWidth',4)

set(gca,'FontSize',30);
h1title=title('PAT Calculation')
set(h1title,'FontSize',40)
xlabel('Time (s)')
```

```
ylabel('Amplitude')
xlim([21 27])
```

Find R-wave peak for ECG fabrics

```
%%
%find peak for ECG fabrics
[pksEf,locsEf] =
findpeaks(ECGnf_1,time11,'MinPeakDistance',0.4);
%[pksE,locsE] = findpeaks(ECGn_1,256);
mf=1;
nfpeaks=[];
for ia=1:length(pksEf)
    if(pksEf(ia)>0.45)
        nfpeaks(mf)=pksEf(ia);
        nflocsE(mf)=locsEf(ia);

        mf=mf+1;
    end
end
plot(time11',ECGnf_1);
hold on;
plot(nflocsE,nfpeaks,'or');

%%
```

Find peak for PPG at finger

```
%find peak for PPGnex
% detrend PPG nexus



[pksPnex,locsPnex] =
findpeaks(PPGnexn_1,time11,'MinPeakDistance',0.3);
%[pksE,locsE] = findpeaks(ECGn_1,256);
m3=1;
```

```
nexpeaks=[];
for i3=1:length(pksPnex)
    if(pksPnex(i3) > 0.4)
        nexpeaks(m3)=pksPnex(i3);
        nlocsPnex(m3)=locsPnex(i3);
        m3=m3+1;
    end
end

plot(time11',PPGnexn_1);
hold on;
plot(nlocsPnex,nexpeaks,'or');
```

Find peak for PPG at wrist

```
%find peak for PPG at Wrist

[pksPw,locsPw] =
findpeaks(PPGwafn_1,timea,'MinPeakDistance',0.4);
%[pksE,locsE] = findpeaks(ECGn_1,256);
m4=1;
PPGwpeaks=[];
for i4=1:length(pksPw)
    if(pksPw(i4) > 0.5)
        PPGwpeaks(m4)=pksPw(i4);
        nlocsPw(m4)=locsPw(i4);
        m4=m4+1;
    end
end

figure
plot(timea',PPGwafn_1,'r','LineWidth',3);
hold on;
plot(nlocsPw, PPGwpeaks,'ob','LineWidth',3)

set(gca,'FontSize',30);
```

```
h1title=title('PPG Peak Detection')
set(h1title,'FontSize',40)
xlabel('Time (s)')
ylabel('Amplitude')
xlim([21 30])
 %%
```

Find peak for PPG underfoot

```
%find peak for PPG at toe


[pksPt,locsPt] =
findpeaks(PPGfafn_1,timea,'MinPeakDistance',0.4);
%[pksE,locsE] = findpeaks(ECGn_1,256);
m4=1;
PPGtpeaks=[];
for i4=1:length(pksPt)
    if(pksPt(i4) > 0.45)
        PPGtpeaks(m4)=pksPt(i4);
        nlocsPt(m4)=locsPt(i4);
        m4=m4+1;
    end
end
```

PAT Calculation

```
%calculate PTT
%determine amplitude for PPG nexus device

locpnex=locsPnex;
PnexAmp=[];
for i=1:length(locpnex)
```

```
    PnexAmp(i,1)=find(abs(timea-locpnex(i))< 0.0001);
   PnexAmp(i,2)=PPGnexaf(PnexAmp(i,1));
   PnexAmp(i,3)=locpnex(i);
end
    Pnexlocn=PnexAmp(:,3);
    PnexAmpn=PnexAmp(:,2);
%determine amplitude for PPG on wrist
%determine amplitude for PPG on toe
loccuff=nlocsPcuff;
CuffAmp=[];
for ic=1:length(loccuff)
     CuffAmp(ic,1)=find(abs(timea-loccuff(ic))< 0.0001);
   CuffAmp(ic,2)=Pcuffa(CuffAmp(ic,1));
   CuffAmp(ic,3)=loccuff(ic);
    end
   Pcufflocn=CuffAmp(:,2);%amplitude cuff
   Pcuffamp=CuffAmp(:,3);%location cuff


 %%
%save data to excell format

A1=nflocsE';%ECG fabrics peak location
A2=nlocsE;%ECG Nexus peak location
A3=Pnexlocn;%PPG Nexus peak location
A4=PnexAmpn;%PPG Nexus amplitude
A5=nlocsPw';%PPG location at wrist
A6=nlocsPt';%PPG location at toe
A7=Pcufflocn;%cuff pressure location
A8=Pcuffamp;%cuff amplitude value
A9=nflocspdf';%PPG PD location at toe
A10=nflocspdw';%PPG PD location at wrist



da = cell(30, 10);

da{1,1} = 'ECG Fabrics';
da{1,2} = 'ECG Nexus';
```

```
da{1,3} = 'PPG Nex loc';
da{1,4} = 'PPG Nex Amp';
da{1,5} = 'PPG Wrist Loc';
da{1,6} = 'PPG Toe Loc';
da{1,7} = 'Cuff Pre Loc';
da{1,8} = 'Cuff Pre Amp';
da{1,9} = 'PPG PD Loc Toe';
da{1,10} = 'PPG PD Loc Wrist';

for k = 2:length(A1)
  da{k, 1} = A1(k-1);

end

for k = 2:length(A2)
  da{k, 2} = A2(k-1);

end

for k = 2:length(A3)
  da{k, 3} = A3(k-1);

end
for k = 2:length(A4)
  da{k, 4} = A4(k-1);

end
for k = 2:length(A5)
  da{k, 5} = A5(k-1);

end
for k = 2:length(A6)
  da{k, 6} = A6(k-1);

end
for k = 2:length(A7)
```

```
  da{k, 7} = A7(k-1);

end
for k = 2:length(A8)
  da{k, 8} = A8(k-1);

end
for k = 2:length(A9)
  da{k, 9} = A9(k-1);

end
for k = 2:length(A10)
  da{k, 10} = A10(k-1);

end
filename = savefile;

xlswrite(filename,da)

%%

%%
%calculate PTT
%check which signal is first before do substraction

n11=2;
PTT=[];% PTT for ECGnexus-PPGnexus
for k=2:length(A1)-1
    if A2(k)<A3(k)
        PTT(k)=A3(k)-A2(k);
        PTT=PTT';
    else
     n11=n11+1;
    PTT1(n11)=A3(n11)-A2(k);
     PTT=PTT1';
        end
```

```
end
stem((PTT))
PTTmean=mean(PTT(3:length(A2)-1))
PTTsig=std(PTT(3:length(A2)-1))
figure
plot(PTT)
```

ECG and BP Cuff Oscillation

```
%cuff pressure
%figure
%plot(time1',Cuff)
Pcuff=(((Cuff/1000)-0.236)/0.0024);

start=s1*256;
ending=e1*256;% set time for pressure cuff (release pressure)
mi=start;
ma=ending;
%figure

timea=time1(start:ending);
time11=timea;
timea=timea';

Pcuffa=Pcuff(start:ending);% BP cuff
figure
plot(time1',Cuff);

plot(time1',Cuff,'b.','LineWidth',5);%plot cuff pressure to
indicate start and ending time
set(gca,'FontSize',28);
h1title=title('BP Cuff Pressure Response')
set(h1title,'FontSize',38)
xlabel('Time (s)')
```

```
ylabel('Voltage (mV)')
   xlim([0 40]);

%figure
 %detrent Pcuff signal
Pcuffad=detrend(Pcuffa);
[pnc, Snc, mn1c] = polyfit(timea, Pcuffad, 5);
xpp1c = polyval(pnc, timea, [], mn1c);
%xpp1c=xpp1c';
Pcuffac=Pcuffad-xpp1c;

%%
%Normalised Pcuff signal
Pcuffamn=Pcuffac;
maxVc=max(Pcuffamn);
minVc=min(Pcuffamn);
dcc=maxVc-minVc;
Pcuff_1=(Pcuffamn-minVc)/dcc;
%figure
%plot(timea,dataLn_1)
%Pcuff_11=Pcuff_1-mean(Pcuff_1)
Pcuff_11=Pcuff_1;



%%
%plot normalise signal for cuff pressure

%first plot
figure % first
yyaxis left
plot(timea,Pcuffa,'b','LineWidth',1);hold on;

%second plot
yyaxis right
% plot(timea,Pcuff_11,'r','LineWidth',2)
hold on
```

```
plot(time11,ECGn_1,'r','LineWidth',1.5)
hold on
plot(time11,PPGnexn_1,'g','LineWidth',1.5)
%add title and axis labels

set(gca,'FontSize',25);
h1title=title('BP Cuff Oscillation Waveform')
set(h1title,'FontSize',25)

yyaxis left

xlabel('Time (s)')
ylabel('Cuff pressure (mmHg)')

yyaxis right
ylabel('Normalise Signal')
lgd = legend({'BP Cuff Pressure','Cuff
Oscillation'},'FontSize',15,'TextColor','blue')
xlim([s1 e1]);
hold off
%%
%plot ECG and BP Cuff
figure
p1=plot(timea',Pcuff_11);
hold on;
p2=plot(nlocsPcuff,cuffpeaks,'or');
p3=plot(time11',ECGn_1);
%hold on;
p4=plot(nlocsE,npeaks,'or');
set(gca,'FontSize',25);
h1title=title('BP Cuff Pressure and ECG Measurement (v1)')
set(h1title,'FontSize',28)
xlabel('Time (s)')
ylabel('Normalised Signal')
lgd = legend([p1 p3],{'BP Cuff','ECG
Nex'},'FontSize',20,'TextColor','blue')
xlim([16 27]);
```

Appendix B3

Labview software interface for recording pulse signal from PendoTech pressure sensor (Phantom System)

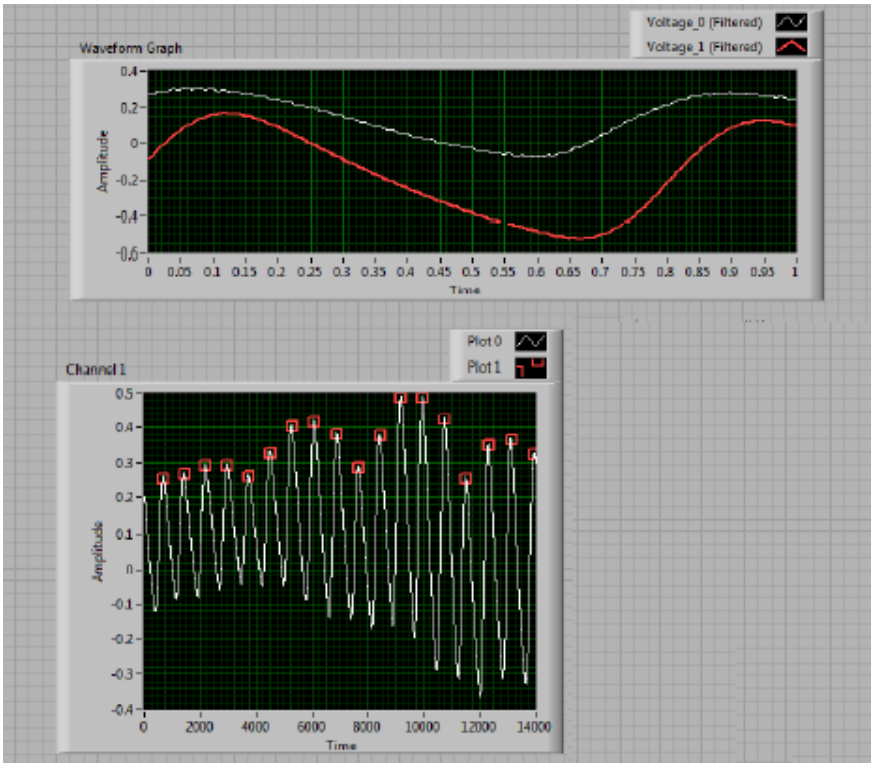


Figure1: Front panel of Labview software

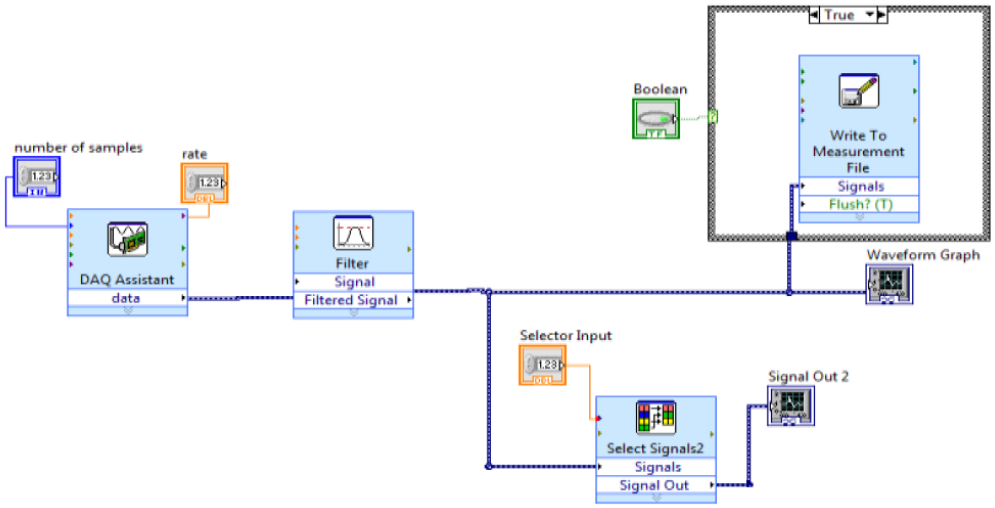


Figure 2: Block diagram of front panel